Solid state NMR of acid anhydride/hydroxyl crosslinking systems

Findlay, Anita

Solid state NMR of Acid anhydride/hydroxyl crosslinking systems

by

Anita Findlay

A thesis submitted in partial fulfilment
of the requirements for the degree of
Doctor of Philosophy

Department of Chemistry
The University of Durham
1991

To my Parents

The research in this thesis has been carried out at the Department of Chemistry of the University of Durham between October 1987 and September 1990. It is the original work of the Author unless stated otherwise. None of this work has been submitted for any other degree.

Acknowledgements

There are a number of people I wish to mention who have contributed either directly or indirectly to the work in this thesis.

First, I would like to express my gratitude to Professor Robin Harris for his supervision and encouragement throughout the last three years.

I would also like to convey my appreciation to Courtaulds Coatings for their support of my work, especially to Dr. A. Port and Dr. A. Marrion for many helpful discussions and suggestions, and without whose assistance much of this work would not have been possible.

I would like to mention other members of the group, both past and present who contributed towards this thesis. My thanks go to Alan for useful discussions, and to David and Nicola for the VXR300 spectra. Amongst my friends, I wish to especially mention Matthew Leach and Xiao Ping for their friendship and for the many enjoyable times we had together.

Lastly, I would like to thank Michael for his encouragement throughout the past three years, and for his patience and understanding whilst this thesis was being written.

Abstract

This thesis is concerned with the study by solid–state NMR of the polymers formed by acid anhydride/hydroxyl cross–linking systems. The polymers studied in this thesis are based on a copolymer containing either itaconic or maleic anhydride which cross–links with a polyester tipped with triethanolamine.

The mobility of the polyester chains in the cross–linked films is probed by solid–state NMR, and the kinetics of the cure between acid anhydride/hydroxyl systems is discussed.

The degradation of the cross–linked films is studied by ^{13}C solid–state NMR. The films are shown to undergo hydrolysis when subjected to their exposure environment.

The theory behind transient nuclear Overhauser effects in the solid state is discussed, and comparisons are made between the theoretical simulations and the experimental data for the cross–linked films.

Lastly, a solid–state heteronuclear NOESY experiment is presented for a $^{13}C_2$–enriched acid anhydride/hydroxyl cross–linked film.

Table of contents

Chapter Four

Experimental

Chapter Five

Spectral assignment and kinetics

CHAPTER 1

Introduction

1.1 Introduction

Polymers play a very important role in life today. They may be found in a wide range of applications from industrial situations through to domestic appliances. In systems where polymers are used, the polymers usually occur as solids or as highly viscous liquids. It is therefore of great interest to apply a suitable technique to the study of polymers in these states of matter. Solid–state NMR provides such a technique. The chemical shifts are sensitive to chemical structure: Thus NMR may be used for the structural determination of polymers. NMR is a technique which is also sensitive to motion: Therefore the mobility of polymers may be assessed by NMR. High–resolution, solid–state NMR, via both chemical shifts and relaxation times, provides a direct link between polymer physical properties and the details of molecular structure. Thus solid–state NMR may provide information of a similar quality to that obtained via mechanical loss and dielectric relaxation methods.

The polymers studied in this thesis are based on a copolymer of styrene, methyl methacrylate and either itaconic or maleic anhydride which cross–links with a polyester tipped with triethanolamine. The cross–linked film which results is intended for use as a yacht paint. The cross–linked film must therefore possess certain properties such as good adhesion and resistance to hydrolysis.

This thesis describes the application of high–resolution solid–state NMR techniques to the study of acid anhydride/hydroxyl cross–linking systems. Solid–state NMR is a very versatile technique which has many applications in the study of polymers. NMR offers the ability to study insoluble materials in their natural environment: Thus the degradation of the polymer films may be studied directly by solid–state NMR. NMR can also provide information about the mobilities of the two components of the cross–linked films from measurements of nuclear Overhauser enhancements and relaxation times. A short description of the contents of each chapter is presented below.

A brief overview of protective coatings and network polymers is given in Chapter Two. The chapter covers the composition and uses of industrial coatings, the classification of polymerisation reactions, as well as polymer network formation and cross–linking.

Chapter Three describes the theory and principles behind the NMR experiment. The aim of this chapter is to provide the background knowledge of NMR necessary to follow the experimental results covered in chapters Five to Eight.

Details of the spectrometer hardware, software and other equipment are given in Chapter Four. The pulse sequences used in this thesis are also discussed, and descriptions of the synthesis of the polymers used in the research are given.

Chapters Five, Six, Seven and Eight cover the experimental results and conclusions drawn. In Chapter Five assignments of the cross–polarisation spectra of the polymers are made. The polymers are

probed for regions of differing mobility using discriminating techniques and variable temperature, variable contact time experiments. A new experiment is presented which can be used to determine carbon T_1 values which are less than one second. Lastly, a study of the kinetics of the cure between acid anhydride/hydroxyl systems is discussed.

The potential application of the acid anhydride/hydroxyl cross–linked film is as a yacht paint. Chapter Six is concerned with the performance of the films when subjected to their expected exposure environment. The films are shown to undergo hydrolysis, and therefore fail to meet the requirements of a yacht paint.

Transient nuclear Overhauser effects (NOE) are a well–known phenomenon in the solution–state. However, a detailed study of transient NOE in the solid–state does not appear to have been made previously. Chapter Seven covers the theory behind such effects in the solid–state, and comparisons are made between the theoretical simulations and the experimental data for the cross–linked films. A new pulse program is presented in this chapter which determines the nuclear Overhauser enhancement factor in the solid–state using a saturation chain of pulses at the proton frequency to achieve build–up of the NOE.

Chapter Eight takes the theme of the nuclear Overhauser effect in the solid–state one step further. In Chapter Eight the first solid–state heteronuclear NOESY experiment is presented for a ^{13}C–enriched acid anhydride/hydroxyl cross–linked film. The 2–dimensional heteronuclear NOESY experiment is a well–known technique in solution–state NMR. However, the use of such an experiment for structural correlation in the

solid–state does not appear to have been made.

Finally, Chapter Nine summarises the general conclusions made from the work in this thesis, and suggestions for further research are made.

CHAPTER 2

Industrial cross–linked coatings and polymer networks

2.1 Introduction

The various paints currently on the market may be classified into two main categories: a) decorative paints and b) industrial protective coatings. The paints belonging to the two groups differ mainly in end applications and property requirements. Decorative paints are used mainly for interior and exterior house paints, whereas industrial paints are used for marine coatings, coatings for metal containers, wood and aircraft finishes, to name but a few.

The property requirements of the two categories of paints differ greatly. Decorative paints need to be fast drying, to have good adhesion to old paints and have a good appearance. In addition to this, exterior paints must possess outdoor durability properties. On the other hand, the main criteria for industrial coatings are mechanical properties, chemical resistance, adhesion, flexibility and corrosion and impact resistance properties. In this chapter only industrial coatings are considered.

2.2 Industrial coatings

2.2.1 Coating composition

The category consisting of industrial paints can be subdivided into atmospheric temperature–curing and heat–curing (stoving) systems. We

shall limit our discussion to atmospheric temperature–curing systems only. The large number of resins and curing agents available makes it possible to obtain coatings with a wide spectrum of properties. Rigid or flexible castings may be combined with outstanding adhesion, mechanical strength, and electrical insulation coupled with stability in widely differing environments. This range of behaviour can be extended even further by the incorporation of fillers, extenders, flexibilisers, plasticisers etc. into the basic resin mixture before curing. A paint consists of a polymeric binder plus pigments, extenders, solvent mixture and other materials where necessary.[1]

a). The binder is often a polyfunctional resin or high molecular weight polymer which reacts, either with itself or with another polymer, to form a cross–linked polymer network. The binder gives the film many of its protective properties such as its resistance to chemicals and abrasion as well as other properties of adhesion, flexibility and durability.

b). Pigments are used to colour the film and give it opacity. They may also enhance some of the properties of the coating, for example durability, adhesion and toughness. Sometimes pigments such as barium chromate may also be incorporated into the film to enhance the anti–corrosive properties of the coating.

c). Extenders are often incorporated into a paint system. Extenders are sometimes used to replace some of the pigments, thus making the manufacture of the paint more economical.

d). Solvents are added to the paint to facilitate the handling and mixing with materials. They are used to lower the viscosity of the paint,

making the application of the paint easier.

2.2.2 Reasons for interest in cross–linking coating systems

The curing mechanism and the type of binder system selected for each paint system vary depending on the end application and the property requirements of the paint. The curing mechanism is independent of the state in which the binder exists, whether in solution, dispersion, emulsion or as a solid. From a properties point of view, resins which are used as paint binders should have as high a molecular weight as possible. However, the use of very high molecular weight resins in paint formulations is restricted by both the polymerisation techniques used for polymer synthesis and the solution viscosities necessary for paint–application.

In order to overcome the problems associated with the molecular weight of resins, a method is used in which low molecular weight resins containing functional groups as binders are cross–linked in situ. The cross–linking may involve either intra– or inter–molecular bond formation. In order for inter–molecular cross–linking to take place, it is customary to add a different type of external cross–linking agent to the system. Curing catalysts are also often added to the system, either to lower the reaction temperature or to speed up the curing rate or both.

2.3 Cross–linking resins

In this thesis, the reaction of acid anhydride/hydroxyl cross–linking systems is considered specifically. For this reason only polyester resins and

acrylic resins are discussed in this chapter.

2.3.1 Polyester resins

Polyesters belong to a general category of resins obtained by reacting together a suitable polybasic acid with a suitable polyhydric alcohol.[2] The functional groups which are generally used to bring about *in situ* curing are carboxyl, hydroxyl or unsaturated groups in the resins. Polyesters almost inevitably contain hydroxyl and/or carbonyl end groups according to formulation and manufacture, and such groups can very conveniently be used for cross–linking. A hydroxylated polyester resin is often used in industrial paints. This type of resin is discussed in more detail later in this chapter.

Resins generally used to cure and modify the properties of polyester cross–linkers include amino resins, phenolic resins, polyisocyanates, epoxy resins, silicone resins, vinyl and acrylic resins with suitable functionality. The latter is also covered in more detail later in this chapter.

2.3.2 Acrylic resins

Acrylic resin is a term generally applied to the polymers and copolymers of methacrylic and acrylic acid derivatives.[2] The copolymers of one or more of these esters with non–acrylic monomers such as styrene, butadiene or vinyl acetate are also often referred to as acrylic resins. The main properties of an acrylic resin are: outstanding outdoor durability, good flexibility and toughness, resistance to chemicals such as acids, alkalis and water and minimum pigment reactivity.

The work in this thesis is concerned with the cross–linking between an acrylic resin of itaconic or maleic anhydride, styrene and methyl methacrylate and a triethanolamine tipped polyester resin of adipic acid, butane 1,4 diol and ethylene glycol. Figure 2.1 shows the cross–linking reaction between the itaconic anhydride resin and the triethanolamine tipped polyester resin. The product is a three–dimensional network of acrylic resin molecules cross–linked via ester linkages to the polyester chains.

2.4 Classification of polymerisation reactions

The formation of a polymer from monomer or monomers is traditionally divided into two broad reaction classes: step growth and chain growth. The distinction between these two processes can be made on mechanistic grounds as they exhibit quite dissimilar reaction kinetics which lead to different distributions of species as a function of the extent of reaction, and, depending on the detailed mechanism, the molecular weight distributions of the polymers formed. With both the step and chain mechanism, the polymerisation processes can be based on either one or two types of propagation reaction: condensation or addition[3,4] (i.e. with or without elimination of various by–products, respectively).

2.4.1 Step–growth polymerisations

Step–growth polymerisations[5] proceed via a step–by–step succession of elementary reactions between reactive sites, which are usually functional groups, but may also be ions or complexes. Each independent step causes

the disappearance of two co–reacting centres and creates a new linking unit between a pair of molecules. In order to obtain high polymers, the reactants must be at least difunctional; monofunctional ones act as chain stoppers.

The features of step–growth processes from a general point of view have been described by Lenz[3] and Sakolov.[6]

$$n\ A{-}Y{-}A + n\ B{-}Z{-}B \longrightarrow A{-}(-Y{-}E{-}Z{-}E{-})_n{-}Y{-}E{-}Z{-}B + \text{by–products}$$

$$n\ A{-}Y{-}A \longrightarrow A{-}(-Y{-}E{-})_{n-1}{-}Y{-}B + \text{by–products}$$

Each reaction step causes the disappearance of two reaction sites A and B, and converts them into a linking unit E. Two reactive sites remain at the end of any growing molecule, irrespective of its size. Throughout the reaction, the polymerisation process has the characteristics of a statistical combination of fragments. In the initial stages of the reaction dimer formation will be largely predominant; in subsequent stages trimers, tetramers and so on will be preferentially produced. Molecular weight distributions follow this random scheme. The increase in molecular weight becomes increasingly rapid as conversion increases, but the reaction rate becomes lower owing to the increasing difficulty of assembling fewer, larger fragments. In order to get the highest molecular weights there is a need for equimolecularity of reactive sites as close as possible to the theoretical value.

2.4.1.1 Condensation reactions

An example of a step–growth condensation polymerisation reaction is the formation of a polyester from a dicarboxylic acid and a diol.

2.4.1.2 Addition reactions

An example of a reaction which proceeds via a step–growth addition mechanism is the cross–linking between an acrylic resin and a hydroxyl–amine tipped polyester as shown in figure 2.1.

2.4.2 Chain–growth polymerisations

Addition polymerisations are known to take place via a chain reaction[5] which is a self–sustaining molecular reaction maintained by the fact that the product of one stage initiates a further reaction step which in turn regenerates more product capable of causing further reactions. The polymerisation thus involves a large number of identical and successive events, initiated by some triggering mechanism, which eventually lead to the production of long chain–like molecules.

For a successful polymerisation, the chain reaction must be started by first providing a suitable active centre capable of reacting with the monomers present and in doing so regenerate the active centre during each addition step, thereby allowing the reaction to continue. Addition polymerisation can be regulated by the controlled production of initiating active centres which only regenerate themselves singly at each step and are susceptible to deactivation in a variety of ways. Thus an addition

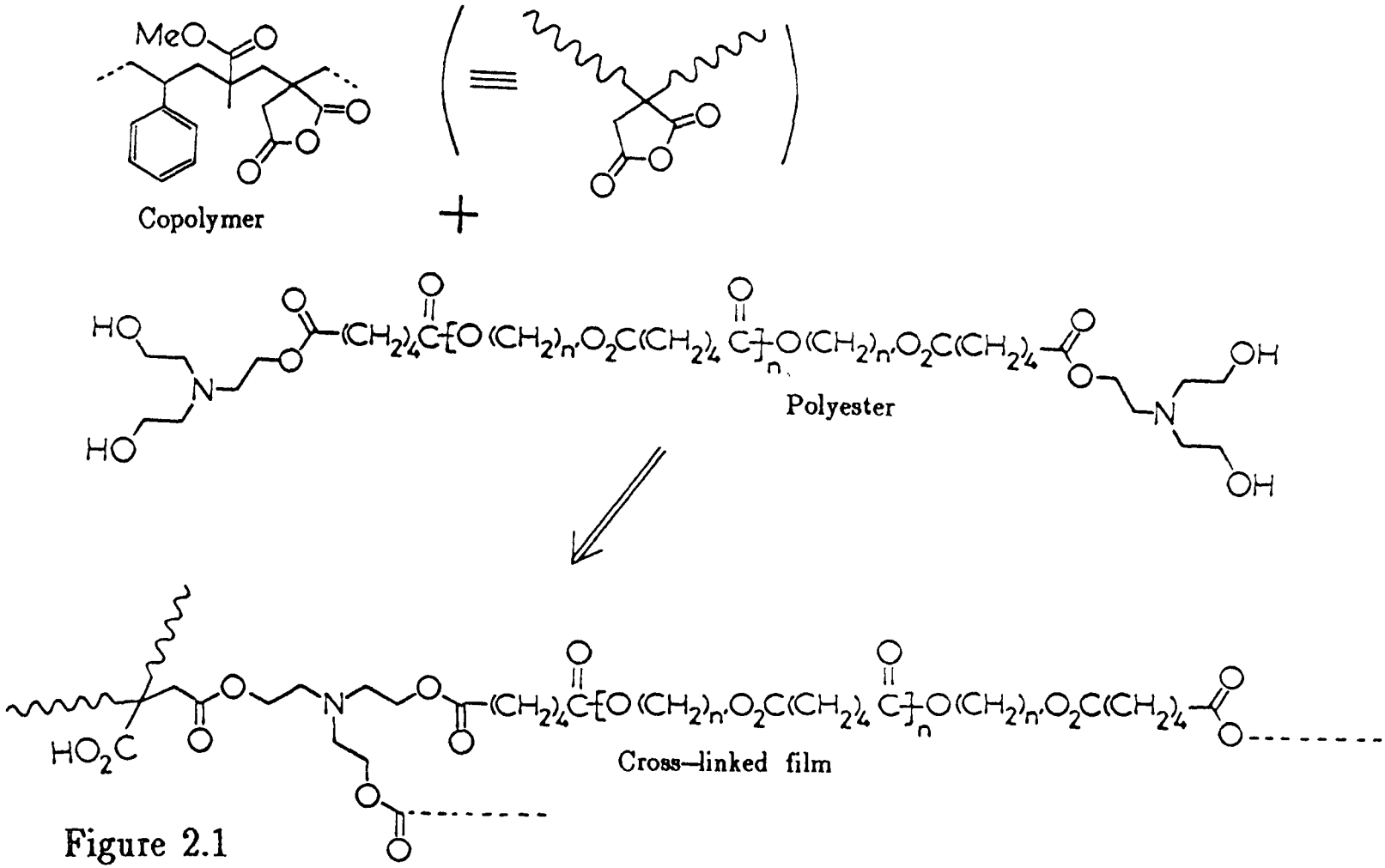

Figure 2.1

The cross–linking reaction between a random copolymer of itaconic anhydride, styrene and methyl methacrylate, and a polyester tipped with triethanolamine. The itaconic anhydride ring–opens during the reaction to form a half–ester cross–link.

polymerisation has three clearly defined reaction stages: i) initiation of the reaction ii) propagation and chain–growth by means of a chain reaction, and iii) termination of the growing chain.

2.4.2.1 Initiation

The active centre which initiates and propagates the chain can be either a free radical, an ion or a radical ion. The free radical is perhaps the most commonly used type of initiator and is produced by decomposition of a suitable material either thermally or by irradiation. In general the active species is produced by homolytic fission of a σ bond to produce two free radicals.

2.4.2.2 Propagation

Once initiation has taken place, growth of the polymer chain is effected by the repetitive addition of a monomer to the active centre with regeneration of that centre. Although the lifetime of an individual radical centre is short, the propagation steps occur many times in rapid succession to build a polymer chain comprising 10^2 to 10^5 monomer units before termination takes place.

2.4.2.3 Termination

In free–radical–initiated polymerisations, chain termination occurs by reaction with other free radicals in the system, or abstraction of a moiety, usually $H^{\cdot}$, from a molecule to produce a new radical. The

growing chain can be terminated by interaction with initiator fragments, but a more likely process is the bimolecular reaction between two active chains. This can occur either by combination or disproportionation.

An example of a chain addition polymerisation is the reaction between styrene, itaconic anhydride and methyl methacrylate to form an acrylic resin.

2.4.3 Non–linear polymerisations

When a difunctional monomer is polymerised, the product consists of linear polymer chains. Linear polymers remain soluble in suitable solvents, regardless of the extent of reaction. Non–linear condensation polymers, on the other hand, are not restricted to growth in only two directions.

When polymers have a functionality of three or more, the polymer molecules grow in three dimensions rather than one dimension as for difunctional monomers.[7] This results in branching and ultimately in the formation of polymer networks. Polymer networks are discussed more fully in the following section.

2.5 Polymer network formation

2.5.1 Cure and cure mechanism

In order to achieve the required mechanical and resistance properties required in most of their applications, low molecular weight

acrylic resins need to be converted by means of cross–linking reactions into a three dimensional infusible network held together by covalent bonds. In acid anhydride acrylic resin technology, this conversion from a liquid into a tough cross–linked polymer is called curing, and is achieved by the addition of a curing agent. Curing agents in general fall broadly into two types: catalytic and polyfunctional We consider only polyfunctional curing agents here. Cross–linking between the resin molecules is achieved through the anhydride groups of the acrylic resin and the hydroxyl groups of the polyester curing agent, leading to the formation of a three–dimensional network composed of acrylic resin units cross–linked via the polyester curing agent. The cure reactions are exothermic and the rates of reaction are increased by increases in temperature.

The acid anhydride acrylic resin reacts with the polyester curing agent at room temperature. Thus the mixing of the resin and curing agent is a point of no return; cure begins and proceeds at a rate determined by reactivity, concentration and temperature. The mixture of resin has a finite pot life beyond which the viscosity of the system has so increased as to render the materials unusable. It will subsequently gel when viscosity becomes infinite and ultimately reach a satisfactory level of cure.

To obtain a three–dimensional meshed network on curing, the functionality of the resin and curing agent combination must accord with Kienle's principle that one component must have an average functionality greater than two and the other a functionality not less than two, their

sum therefore not being less than five. In practice, the functionality of groups can depend upon the particular set of reaction conditions being considered. Thus although the anhydride group is regarded as having a functionality of two, only one of these is involved when it reacts with the hydroxyl group of the polyester, the acid group not entering into any significant reaction under these conditions. This is illustrated in figure 2.2.

Also the total environment of the acid anhydride group has a great influence on the curing process. Steric factors can play an overriding part in determining the ease with which cross–linking can take place.

2.5.2 The gel point

Among the physical characteristics of non–linear condensation polymerisations, the occurrence of a gel point[8] is of foremost significance. Before the reaction starts, the polymer mixture consists of a fluid of low molecular weight molecules. As the reaction proceeds, larger and larger molecules are formed. Eventually a stage is reached where an infinitely large molecule extends throughout the volume of the sample. This is known as the gel point.[4] At the gel point, which occurs at a well–defined stage in the course of the polymerisation, the polymer transforms suddenly from a viscous liquid to an elastic gel. Prior to the gel point, all of the polymer is soluble in suitable solvents, however beyond the gel point, the polymer is not entirely soluble in solvents.

The gel point occurs at a particular extent of reaction, independent of temperature or solvent. Gelation also occurs before all of the monomer has reacted to form one infinite molecule. This indicates that there are

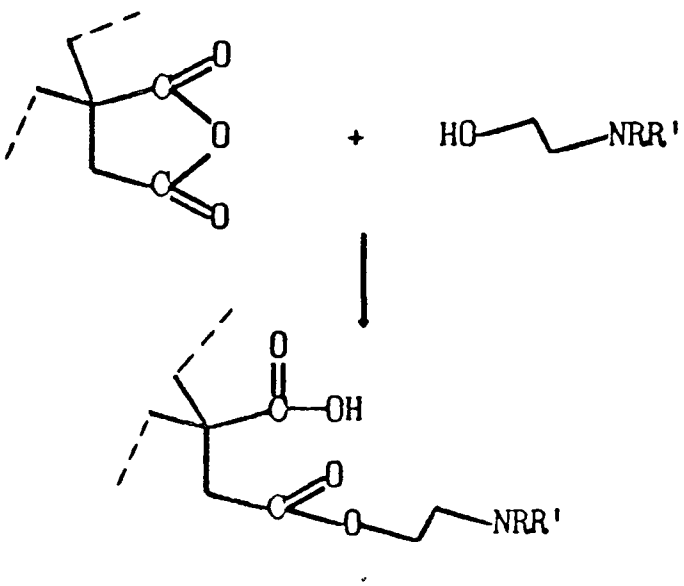

Figure 2.2

A diagram to show the cross–link formation between an acid anhydride resin and an hydroxy–amine tipped polyester resin.

other molecules of varying size distributed throughout the gel. These other molecules are known as the sol fraction, and may be extracted by solvent.

Carothers'[9] work on step–growth condensation polymerisation reactions lead him to derive an expression to relate the extent of reaction of functional groups, P, to the degree of polymerisation of the polymer produced, $\overline{DP}_n$, and to the functionality of the monomer, f.

$$P = \frac{2}{f} - \frac{2}{\overline{DP}_n \cdot f} \qquad (2.1)$$

It was assumed in the derivation of equation 2.1 that only intermolecular reaction takes place. As the network becomes infinitely large, the $\overline{DP}_n$ approaches an infinite value, and thus $\frac{2}{\overline{DP}_n \cdot f} \rightarrow 0$.

By substituting this in equation 2.1, Carothers was able to predict a value of the extent of reaction at the gel point, P_c.

$$P_c = \frac{2}{f} \qquad (2.2)$$

Carothers stated that this value of P was the maximum value for gelation to occur. Flory[10] later showed that the $\overline{DP}_n$ is not infinite at the gel point, and some modifications were made to the theory of Carothers by both Flory[10,11] and Stockmayer.[12]

2.5.3 Cross–linking

The changes in polymer structure during cross–linking of long polymer chains are indicated schematically in figure 2.3. Regardless of the chemical method employed, the formation of cross–linkages consists of the joining together of pairs of structural units belonging to different molecules. Each pair of units participating in the formation of a cross–linkage will be selected at random; it is required merely that the partners be in suitable proximity at the instant of formation of the linkage. From a chemical point of view, cross–linkages are scattered throughout the bulk of the polymer at random points where pairs of polymer units were properly situated with respect to each other before gelation.

2.6 The molecular network

2.6.1 Importance of cross–linking

Both the curing rate and the degree of cross–linking influence the final properties of paint films.[5] The curing rate affects the rate of surface and through drying of the coating, while increasing the degree of cross–linking increases the modulus (stiffness and surface hardness) and the mechanical properties of the films. The glass–transition temperature of a film also increases as the degree of cross–linking is increased.

2.6.2 Elastic properties of networks

In order to obtain a more precise understanding of the properties of a network, consideration must be given to the way in which the molecules are arranged in relation to one another and to the forces by which they are held together. For a network to possess elastic properties there are three main criteria which must be satisfied:[13]

i) The network must contain long–chain units which possess freely rotating links

ii) The forces between the molecules as segments must be weak, as in a liquid

iii) The molecules must be joined together or 'cross–linked' at certain points along their lengths.

The first of these criteria is self–explanatory and need not be discussed any further. The second is essential if the molecules are to have the freedom of motion and the ability to change their conformations necessary for the network to possess elastic properties. The materials of which networks are composed are of such a chemical nature that the forces between their molecules are of the same order of magnitude as the forces between the molecules of an ordinary liquid. In a liquid the inter–molecular forces are not too strong, and individual molecules possess sufficient kinetic energy to break away from neighbouring molecules and form other attachments. It is this repeated breaking away of individual molecules which gives the liquid its fluidity. For a material to possess elastic properties, it must have the same kind of loose structure which enables the molecules to rearrange themselves.

Although the forces between the molecules of a network are sufficiently weak for them to be able to move freely with respect to one another, like the molecules of a liquid, the network is in fact a solid rather than a liquid. It is the presence of cross–links at certain points along the length of the molecules which causes the network to be a solid. Owing to the great length of the chains, quite a small number of cross–linkages is sufficient to ensure that each molecule is connected to at least two other molecules so that the whole assembly of chains becomes one single structure as shown in figure 2.3.

These cross–linkages do not interfere appreciably with the local freedom of motion of the molecules with respect to neighbouring chains, but they do eliminate the possibility of bulk slippage of one molecule past another, which is the necessary condition for flow to take place. Network polymers exhibit no viscoelastic flow even up to the point of decomposition. The combination of the second and third criteria thus enables the two opposing requirements to be satisfied; the requirement of freedom of local molecular motion and the requirement of suppression of flow, and hence to combine in a single material certain of the properties of both the liquid and solid states.

2.7 Why study networks by NMR ?

Network polymers have many unique characteristics. Depending on the degree of cross–linking, they tend to be virtually insoluble in all solvents. For this reason solid–state NMR is an excellent tool for the study of cross–linked networks. Cross–linking reactions start from the

a).

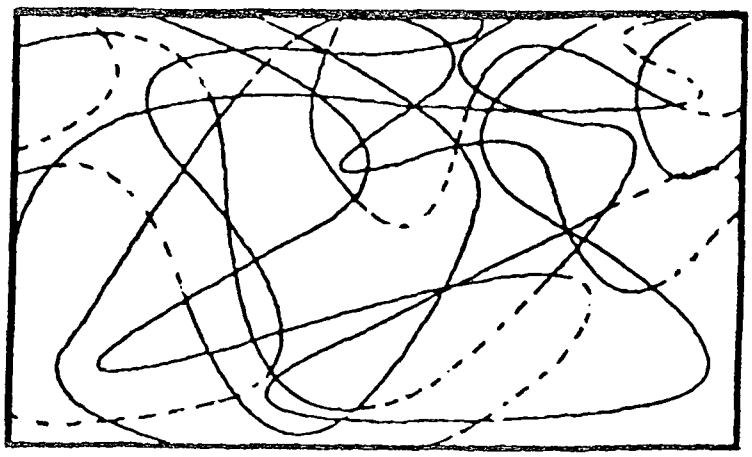

b).

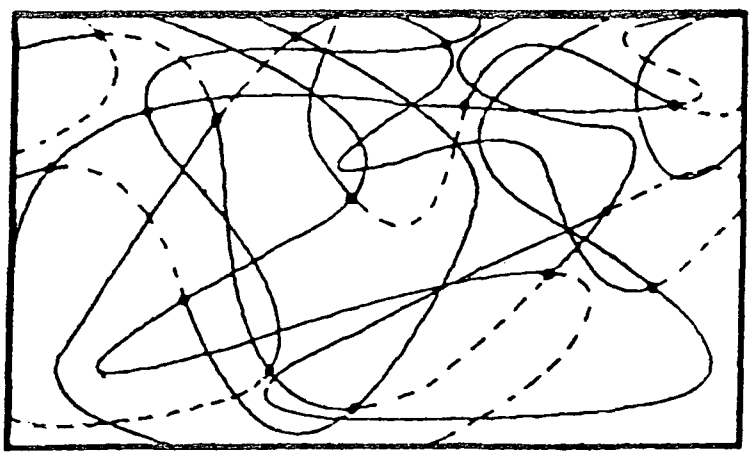

● = cross–link

Figure 2.3

a). An entangled network of copolymer and polyester chains immediately after mixing.

b). The same network at a later time in the cure. The cross–links form where two suitable reactive centres find themselves placed near enough to each other in space.

solution state and proceed through to the solid state. Since nuclear magnetic resonance can be applied to both the solution and solid states, it is an ideal technique for the study of such reactions.

CHAPTER 3

Theory

3.1 General theory

Isotopes with an odd atomic number or an odd atomic mass possess spin angular momentum. The nuclear magnetic moment (μ)[1] which arises from the motion of a charged particle, is colinear with the axis of spin and is usually described in terms of the gyromagnetic ratio,[2] γ, where I is the nuclear spin quantum number.

$$\mu = \gamma\hbar[I(I+1)]^{\frac{1}{2}} \qquad (3.1)$$

Throughout this thesis, only nuclei with spin $I = \frac{1}{2}$ are discussed. Therefore, the theory in this chapter will concentrate only on the spin $I = \frac{1}{2}$ case.

3.2 The classical case[2,3]

Consider the case when a nucleus of spin $I = \frac{1}{2}$ is placed in a static magnetic field (B_0). A torque is exerted upon the magnetic moment by the magnetic field which causes it to precess about B_0 with a precession frequency (ω).

$$\omega = -\gamma B_0 \qquad (3.2)$$

The motion of the magnetic moment is expressed by equation 3.3.

$$\frac{d\bar{\mu}}{dt} = \gamma\bar{\mu}\times\bar{B}_0 \tag{3.3}$$

Defining the static magnetic field B_0 to be along the z axis in the laboratory frame of reference, the magnetic moment, μ, may be resolved into three components, μ_x, μ_y and μ_z.

In a static field, B_0, the component of the magnetic moment in the direction of the field is constant. However the two components perpendicular to the magnetic field, μ_x and μ_y, oscillate so that the magnitude of the transverse component remains constant.

i.e. $$\mu_x^2(t) + \mu_y^2(t) = \mu_x^2(0) + \mu_y^2(0) \tag{3.4}$$

The net result corresponds to a rotation of the direction of μ in a cone with the axis along B_0. Such a motion is known as Larmor precession. The angular velocity of the precession is given by $\omega_i = -\gamma B_0$, and thus the Larmor frequency, ω_0 is

$$\omega_0 = -\gamma B_0 \tag{3.5}$$

So far only the motion of individual nuclear magnetic moments has been considered. A typical macroscopic sample will contain an ensemble of many such magnetic moments, which will be distributed at random around the precessional cone.

The total magnetic moment or magnetisation M of the sample is the resultant of the individual magnetic moments μ.

$$\mathbf{M} = \sum_i \mu_i \tag{3.6}$$

The effects of the individual magnetic fields upon each other are negligible compared to B_0. Therefore, as the individual magnetic moments are identical, the equation of motion for the net magnetic moment is

$$\frac{d\mathbf{M}}{dt} = \sum_i \frac{d\mu_i}{dt} = \sum_i +\gamma_i \bar{\mu}_i \times \bar{B}_0 = \gamma \bar{\mathbf{M}} \times \bar{B}_0 \tag{3.7}$$

Equation 3.7 holds provided that all the magnetic moments started at time zero with identical positions. However, in any one sample, there will be a random distribution of initial orientations, and therefore a random orientation of the x and y components of the individual magnetic moments. The net result is that the sum of the x and y components of the magnetic moments average to zero. Thus the only observable magnetic moment is the z component, which lies along the direction of the field B_0.

3.3 Population of the spin states

For a spin $I = \frac{1}{2}$ nucleus with a positive gyromagnetic ratio, the two possible orientations of the nuclear spin define a high (β) and a low (α) energy state.

When the system is at thermal equilibrium, the spins will be distributed among the two energy levels according to the Boltzmann law. Thus, for spin $I = \frac{1}{2}$ nuclei, the ratio of nuclei in the upper energy level (n_β) to the number in the lower level (n_α) as a function of absolute temperature is given by

$$\frac{n_\beta}{n_\alpha} = \exp\left[\frac{-\gamma\hbar B_0}{kt}\right] \tag{3.8}$$

where k is the Boltzmann constant, and $\frac{\Delta E}{kt} \ll 1$

At ordinary temperatures the populations of the spin states are almost equal, with n_α slightly more populated than n_β. Therefore net absorption can occur at the resonance condition which will produce a corresponding signal.

3.4 Relaxation

The excitation and detection of a signal will affect the equilibrium Boltzmann populations of the spin states. Just as excitation transfers population from the lower to the higher energy level, so there is an opposing phenomenon which tries to re–establish thermal equilibrium by transferring population from the higher energy level to the lower. This phenomenon is known as relaxation.

Two types of relaxation describe the re–establishment of thermal equilibrium

a). Spin–lattice or longitudinal relaxation is characterised by a time constant T_1. This governs the return to equilibrium along the z axis after some perturbation.

b). Spin–spin or transverse relaxation is characterised by a time constant T_2. Spin–spin relaxation is the relaxation of the M_x and M_y components of the magnetisation in the xy plane.

3.5 The Bloch equations

One of the most convenient treatments of the magnetic resonance phenomenon is that described by Bloch. His classical approach was to use a vector model and treat the assembly of nuclear spins in macroscopic terms.

The magnetisation M may be resolved into three components along the x, y and z axes. Bloch derived the combined relaxation/equation of motion with first order kinetics[4] so that

$$\frac{d\mathbf{M}}{dt} = \gamma \mathbf{M} \times \mathbf{B}_0 - \frac{\mathbf{M}_{xi}}{T_2} - \frac{\mathbf{M}_{yj}}{T_2} - \frac{(\mathbf{M}_z - \mathbf{M}_{eq})_k}{T_1} \qquad (3.9)$$

The z component of the Bloch equation was modified by Solomon[5] for the case of coupled C–H spins.

$$\frac{d\langle I_z\rangle}{dt} = -\frac{1}{T_1^{II}}\left[\langle I_z\rangle - I_0\right] - \frac{1}{T_1^{IS}}\left[\langle S_z\rangle - S_0\right] \qquad (3.10a)$$

$$\frac{d\langle S_z\rangle}{dt} = -\frac{1}{T_1^{SS}}\left[\langle S_z\rangle - S_0\right] - \frac{1}{T_1^{IS}}\left[\langle I_z\rangle - I_0\right] \qquad (3.10b)$$

These modified Bloch equations are known as the Solomon equations.

Although it is not possible to give an analytical solution to this set of differential equations, they may be solved under various limiting conditions. This is demonstrated in chapter 7.

3.6 The rotating frame of reference

Up until now all our descriptions of the NMR experiment have used a set of cartesian coordinates which are fixed with respect to the laboratory. Within this frame we have seen that the nuclei precess about the B_0 field at the Larmor frequency. Now let us consider a new set of cartesian axes (x', y' and z') which rotate about the static magnetic field, B_0 at $\omega = 2\pi\nu$.[6]

$$x' = x\cos 2\pi\nu t + y\sin 2\pi\nu t \qquad (3.11a)$$

$$y' = -x\sin 2\pi\nu t + y\cos 2\pi\nu t \qquad (3.11b)$$

$$z' = z \qquad (3.11c)$$

The mathematics of the system becomes substantially simpler when the axes are transformed from the laboratory frame into the rotating frame of reference.

In the rotating frame of reference the nuclei precess about the effective field, B_{eff} (illustrated in figure 3.1)

where $$B_{eff} = \left[\left[B_0 - \frac{\omega}{\gamma} \right]^2 + B_1^2 \right]^{\frac{1}{2}} \tag{3.12}$$

The resonance condition occurs when $\omega = \omega_0$.

In equation 3.12, when $\omega = \omega_0$ then

$$B_0 - \frac{\omega}{\gamma} = 0 \tag{3.13}$$

$$\text{and } B_{eff} = B_1$$

The effective field, B_{eff} now lies in the x' direction along B_1. The magnetisation, M, precesses about B_1 in a circle in the $y'z$ plane at a rate $-\gamma B_1$.

Let us now consider the effect of an RF pulse applied at a frequency ω_0 and in the direction of the x axis in the rotating frame. When the field is first turned on the magnetisation precesses from the z axis through an angle θ in the $y'z$ plane.

$$\theta = \gamma B_1 t \tag{3.14}$$

where t is the length of time the RF pulse is turned on (see figure 3.2). It is this property of rotating the magnetisation that is utilised in pulsed NMR experiments.

There are two angles of particular interest which are worth our consideration.

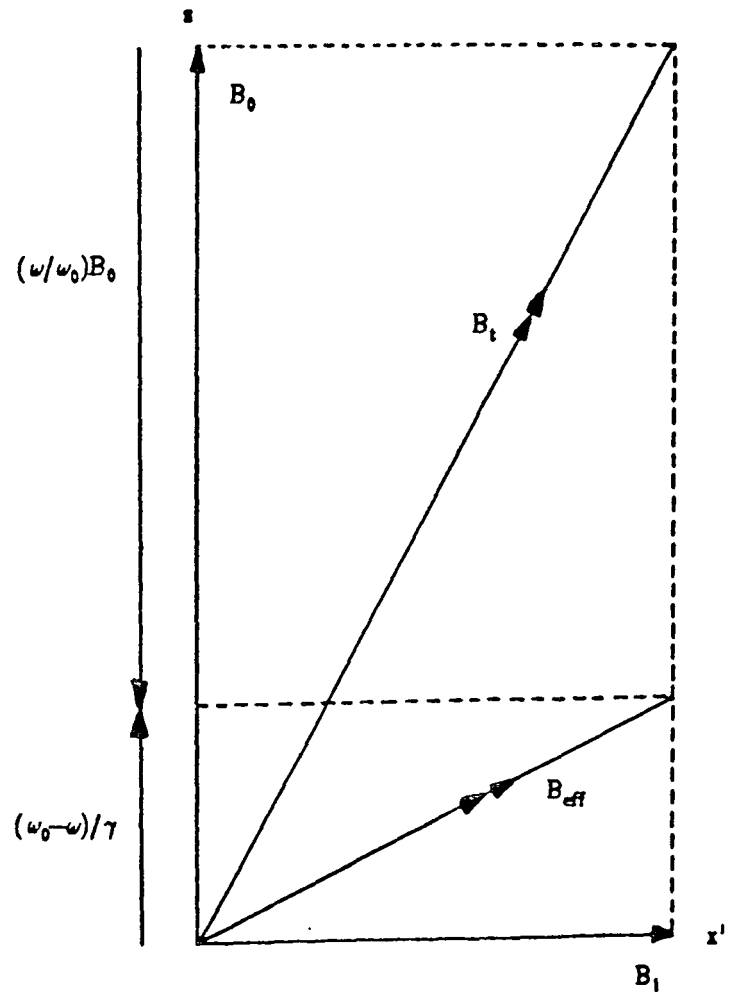

Figure 3.1

The magnetic fields in the rotating frame of reference. The magnitude of the rotating field (B_1) is exaggerated with respect to B_0, the static field.

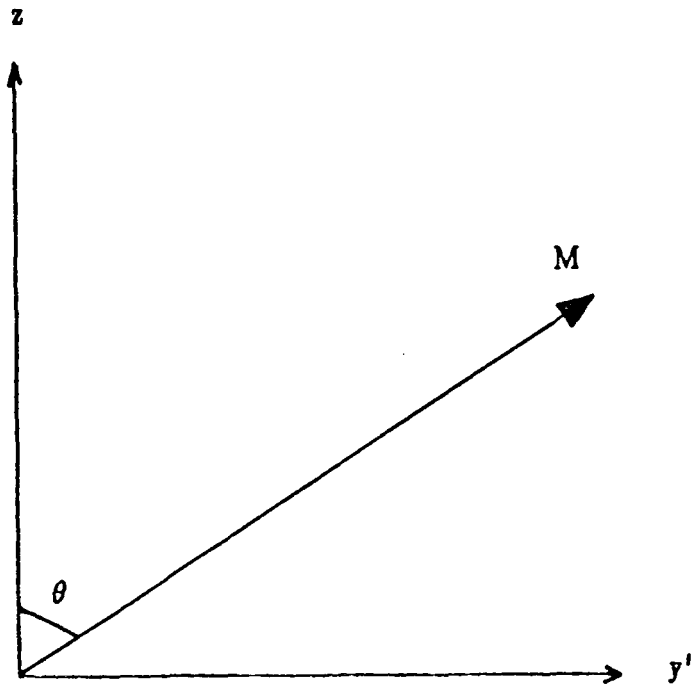

Figure 3.2

Precession of the magnetisation M occurs in the y'z plane after the B_1 field is turned on. θ, the angle through which precession occurs, is equal to $\gamma B_1 t$, where t is the length of time for which the B_1 field is turned on.

3.6.1 Case 1

When $\theta = \pi$ the magnetisation is flipped into the $-z$ direction. A 180° or π pulse may be seen schematically as the inversion of the α and the β states, thus inverting the magnetisation. Following the pulse, the Boltzmann equilibrium situation is restored by relaxation. A 180° (or π) pulse is succeeded by purely spin–lattice relaxation as in equation 3.15.

$$M_z(t) - M_0 = [M_z(0) - M_0]\exp(-t/T_1) \tag{3.15}$$

3.6.2 Case 2

When $\theta = \frac{\pi}{2}$ the magnetisation is flipped into the $x'y'$ plane along the y' direction. The 90° pulse causes phase coherence of the spins. Following a 90° (or $\frac{\pi}{2}$) pulse, two types of relaxation occur; spin–lattice relaxation and transverse relaxation. Spin–lattice relaxation is given by equation 3.15, whereas transverse relaxation, which governs the rate at which the spins dephase in the rotating frame of reference is given by

$$M_y(t) = M_y(0)\exp(-t/T_2) \tag{3.16}$$

3.6.3 Relaxation in the rotating frame of reference

As has been discussed in section 3.6.2, a 90° pulse is followed by transverse relaxation. However if the radiofrequency field is not switched off following the pulse, but is phase–adjusted by 90°, as shown in figure

3.3, a different situation is obtained. In this case the magnetisation is aligned with the RF field, which is the only effective field in the rotating frame of reference when on resonance. The magnetisation does not precess in the rotating frame, and is said to be spin–locked. But the magnetisation is much greater than can be maintained by B_1, since it was developed in B_0, which is several orders of magnitude larger than B_1. Consequently the M_y magnetisation will decay with time to its equilibrium value $(B_1/B_0)M_0$ at a rate governed by the exponential time constant $T_{1\rho}$.

$$M_y(\tau) = M_0 \exp(-\tau/T_{1\rho}) \tag{3.17}$$

3.7 Spin diffusion

Spin diffusion is not an actual molecular diffusion, but is the transport of spin energy within the system by mutual, energy–conserving spin flips. Consider two adjacent protons in a solid coupled by the dipolar interaction. If the two protons have antiparallel magnetic moments, it is an entropy–favourable process for both of them to change orientations simultaneously or 'flip', again yielding an antiparallel pair, but with moments reversed. Such flips can occur rapidly among neighbouring coupled protons in a solid, and serve to distribute excess energy or magnetisation among all the coupled spins. The process, like any diffusion process, is driven by a concentration gradient, in this case the spatial gradient in the magnetisation. It is spin diffusion that ensures that the ^1H linewidth is homogeneous. However, spin diffusion between dilute spins

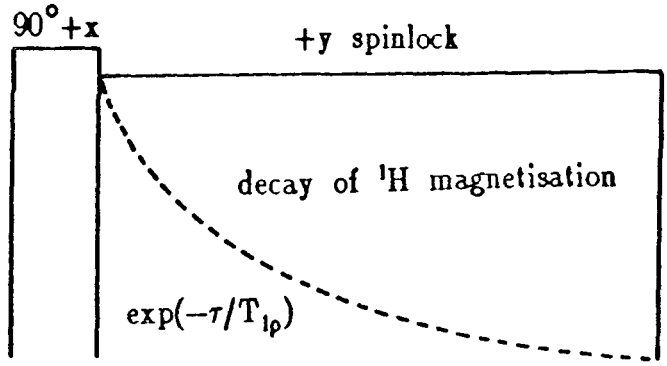

Figure 3.3

The decay of M_y, the magnetisation in the y direction, to its equilibrium value occurs at a rate characterised by the exponential time constant $T_{1\rho}$.

such as ^{13}C is slow. This means that whereas a single value of T_1 will be obtained for all protons in a solid sample unless there is substantial heterogeneity (domain sizes > hundreds of Angstroms), ^{13}C nuclei in a homogeneous sample will have separate values of T_1. Such differences between ^1H and ^{13}C also correlate with the lack of resolution in proton spectra.

3.8 The quantum mechanical approach[3,7]

In order to fully understand the behaviour of spins in pulsed NMR experiments, it is necessary to consider the quantum mechanical approach.

Spin interactions can be described quantum mechanically in terms of the appropriate Hamiltonians. The total Hamiltonian, $\mathcal{H}$, which completely describes the spin interactions of a system is given by

$$\mathcal{H} = \mathcal{H}_{int} + \mathcal{H}_{ext} \tag{3.18}$$

$$\mathcal{H}_{ext} = \mathcal{H}_z + \mathcal{H}_{RF} \tag{3.18a}$$

$$\mathcal{H}_{int} = \mathcal{H}_{II} + \mathcal{H}_{SS} + \mathcal{H}_{IS} + \mathcal{H}_S + \mathcal{H}_J + \mathcal{H}_{SR} + \mathcal{H}_Q \tag{3.18b}$$

$\mathcal{H}_{ext}$ is the external hamiltonian. The name arises from the fact that the terms in $\mathcal{H}_{ext}$ depend on external parameters which are controlled by the experiment.

$\mathcal{H}_{int}$ is the internal hamiltonian. $\mathcal{H}_{int}$ comprises of terms which depend upon the sample, and therefore it is these terms in the Hamiltonian which provide information of chemical interest.

3.8.1 The external Hamiltonian $\mathscr{H}_{ext}$

The external Hamiltonian, $\mathscr{H}_{ext}$, consists of the sum of the zeeman and radiofrequency terms.

3.8.1.1 Zeeman Hamiltonian $\mathscr{H}_z$

The zeeman term describes the interaction between the nuclear spins and the magnetic field, B_0.

For a single nuclear spin,

$$\mathscr{H}_z = \hbar\gamma B_0 \hat{I}_z \tag{3.19}$$

$$= -\hbar\omega_0 \hat{I}_z \tag{3.19a}$$

For an ensemble of nuclear spins, equation 3.19a may be modified to

$$\mathscr{H}_z = -\hbar \sum_i \omega_0{}^i I_{zi} \tag{3.20}$$

where I_{zi} is the i^{th} nuclear spin with Larmor frequency $\omega_0{}^i$.

3.8.1.2 Radiofrequency Hamiltonian $\mathscr{H}_{RF}$

The radiofrequency term, $\mathscr{H}_{RF}$, of the external Hamiltonian describes the interaction between the spins and the perturbing radiofrequency field.

The perturbing radiofrequency field (RF) is applied perpendicular to the static magnetic field B_0 , and is aligned parallel to the x axis by convention.

$$\mathcal{H}_{RF} = \hbar\gamma I_x B_1 \cos(\omega t + \phi) \qquad (3.21)$$

where ωt and ϕ are the frequency and phase respectively of the perturbing field.

3.8.2 The internal Hamiltonian

$$\mathcal{H}_{int} = \mathcal{H}_D + \mathcal{H}_S + \mathcal{H}_{SR} + \mathcal{H}_Q + \mathcal{H}_J \qquad (3.22)$$

The internal Hamiltonian consists of the sum of the dipolar ($\mathcal{H}_D$), J–coupling ($\mathcal{H}_J$), spin–rotation ($\mathcal{H}_{SR}$), shielding ($\mathcal{H}_S$) and quadrupolar ($\mathcal{H}_Q$) Hamiltonian terms. The spin–rotation and the quadrupolar Hamiltonian terms are not relevant to the work presented in this thesis, and for this reason are omitted.

3.8.2.1 The principal axis system

The above spin interactions may be written in compact form using second–rank tensors. Any Hamiltonian involving spin interactions may be expressed in the form

$$\mathcal{H}_\lambda = K^\lambda I^\lambda R^\lambda Y^\lambda \qquad (3.23)$$

R^λ is a second–rank cartesian tensor (3×3 matrix), I^λ and Y^λ are vectors, and K^λ is a typical constant for each interaction mechanism.

All the tensors are molecular properties, and for this reason are

best described in a molecule–fixed axis system. The cartesian tensor consists of 9 components. A sensible choice of molecule–fixed axes (say XYZ) puts a tensor into a diagonal form.

$$\begin{bmatrix} R_{xx} & R_{xy} & R_{xz} \\ R_{yx} & R_{yy} & R_{yz} \\ R_{zx} & R_{zy} & R_{zz} \end{bmatrix} \longrightarrow \begin{bmatrix} R_{xx} & 0 & 0 \\ 0 & R_{yy} & 0 \\ 0 & 0 & R_{zz} \end{bmatrix} \qquad (2.24)$$

This choice of axes is called the principal axis system (PAS), and the diagonal elements R_{xx}, R_{yy} and R_{zz} are known as the principal components of the tensor R.

The principal axes are usually defined so that:

$$|R_{zz} - \tfrac{1}{3}TrR| \geq |R_{xx} - \tfrac{1}{3}TrR| \geq |R_{yy} - \tfrac{1}{3}TrR| \qquad (3.25)$$

where
$$TrR = R_{xx} + R_{yy} + R_{zz} \qquad (3.25a)$$

Each tensor R may be divided into the sum of the isotropic, R_{iso}, antisymmetric R_{asym} and symmetric, R_{sym} parts.

These are given by

$$R_{iso} = \tfrac{1}{3}TrR$$
$$= \tfrac{1}{3}(R_{xx} + R_{yy} + R_{zz}) \qquad (3.26a)$$

$$\text{anisotropy } \Delta R = R_{zz} - \tfrac{1}{2}(R_{xx} + R_{yy}) \qquad (3.26b)$$

$$\text{asymmetry } \eta = \frac{(R_{yy} - R_{xx})}{R_{zz} - R_{iso}} \qquad (3.26c)$$

where $0 \leq \eta \geq 1$

If the tensor is axially symmetric (i.e. $R_{zz} = R_{\parallel}$ and $R_{xx} = R_{yy} = R_{\perp}$)

Table 3.1

Values of K^{λ}, R^{λ} and Y^{λ} for the interactions.

$\hbar\mathcal{H}$	K^{λ}	R^{λ}	Y^{λ}	units	Interaction
$\hbar\mathcal{H}_S$	1	σ	B_0	None	Shielding Tensor
$\hbar\mathcal{H}_J$	2π	J	S	Hz	Indirect Coupling Tensor
$\hbar\mathcal{H}_D$	$\frac{\mu_0\gamma_i\gamma_j\hbar}{4\pi\ r^3_{ij}}$	D	S	None	Dipolar Tensor
$\hbar\mathcal{H}_{SR}$	2π	C	J	None	Spin Rotation Tensor

then $\eta = 0$.

$$R\ (PAS) = \begin{bmatrix} R_{xx} & R_{xy} & R_{xz} \\ R_{yx} & R_{yy} & R_{yz} \\ R_{zx} & R_{zy} & R_{zz} \end{bmatrix} = R_{iso} + \delta \begin{bmatrix} -\frac{1}{2}(1+\eta) & 0 & 0 \\ 0 & -\frac{1}{2}(1-\eta) & 0 \\ 0 & 0 & 1 \end{bmatrix} \quad (3.27)$$

The values of K^{λ}, R^{λ} and Y^{λ} for the various interactions are listed in table 3.1.

3.8.2.2 The shielding Hamiltonian $\mathcal{H}_S$

The shielding Hamiltonian describes the coupling between a spin I and the static magnetic field B_0

$$\mathcal{H}_S = \hbar \sum_i \gamma^i \hat{I}^i . \sigma^i B_0 \quad (3.28)$$

where σ is the shielding tensor in the principle axis system.

$$\sigma = \begin{bmatrix} \sigma_{xx} & 0 & 0 \\ 0 & \sigma_{yy} & 0 \\ 0 & 0 & \sigma_{zz} \end{bmatrix} \quad (3.29)$$

$\mathcal{H}_S$ may be expanded as

$$\mathcal{H}_S = \hbar \gamma I_z \left[\sigma_{iso} + \bar{\sigma} \begin{bmatrix} -\frac{1}{2}(1+\eta) & 0 & 0 \\ 0 & -\frac{1}{2}(1-\eta) & 0 \\ 0 & 0 & 1 \end{bmatrix} \right] B_0 \quad (3.30)$$

where $\sigma_{iso} = \frac{1}{3} Tr \underline{\sigma}$

3.8.2.3 The indirect spin–spin coupling interaction $\mathcal{H}_J$

The indirect spin–spin coupling Hamiltonian $\mathcal{H}_J$ describes the coupling between two nuclei (i,k) via their associated electron spins.

$$\mathcal{H}_J = h\sum_{i<k} \hat{\underline{I}}_i \cdot \underline{J}_{ik} \cdot \hat{\underline{I}}_k \qquad (3.31)$$

The magnitude of the indirect spin–spin coupling is small compared to the dipolar coupling and therefore is not discussed further in this thesis.

3.8.2.4 The dipole–dipole interaction $\mathcal{H}_D$

Classically, the energy of interaction between two magnetic point dipoles, μ_I and μ_S , is given by

$$U = \left[\frac{\mu_I \cdot \mu_S}{r_{IS}^3} - \frac{3(\mu_I \cdot \underline{r}')(\mu_S \cdot \underline{r}')}{r_{IS}^5} \right] \frac{\mu_0}{4\pi} \qquad (3.32)$$

where r_{IS} is the internuclear distance, and $\underline{r}'$ is the internuclear vector common to the dipoles.

The appropriate quantum mechanical expression equation 3.33 is obtained by substituting the expression for the magnetic moment $\mu = \gamma\hbar\mathbf{I}$ into equation 3.32.

$$\mathcal{H}_D = \hbar\gamma_I\gamma_S \left[\frac{\hat{I}_I \cdot \hat{I}_S}{r_{IS}^3} - \frac{3(\hat{I}_I \cdot \underline{r}')(\hat{I}_S \cdot \underline{r}')}{r_{IS}^5} \right] \frac{\mu_0}{4\pi} \qquad (3.33)$$

The dipolar Hamiltonian may be written in tensor form

$$\mathcal{H}_D = K^{\lambda} I_{\tilde{I}} \underset{\sim}{D} I_S \tag{3.34}$$

where $\underset{\sim}{D}$ is the dipole tensor.

The tensor $\underset{\sim}{D}$ is not diagonal if the orientation of the internuclear vector, $\underline{r}'$, is given relative to the x, y, z axes of the laboratory frame of reference.

However if the principal axis system is used, where r is parallel to the z axis, then the tensor $\underset{\sim}{D}$ is diagonalised.

i.e

$$\mathcal{H}_D = \left[\frac{\mu_0}{4\pi} \right] \frac{\gamma_I \gamma_S \hbar^2}{r_{IS}^3} \begin{bmatrix} I_{Ix} I_{Iy} I_{Iz} \end{bmatrix} \begin{bmatrix} 1 & 0 & 0 \\ 0 & 1 & 0 \\ 0 & 0 & -2 \end{bmatrix} \begin{bmatrix} I_{Sx} \\ I_{Sy} \\ I_{Sz} \end{bmatrix} \tag{3.35}$$

It is possible to describe the dipolar interaction in terms of polar coordinates, which define the orientation of the principal axis system to the laboratory frame of reference. The common factor $\frac{\hbar}{2\pi}\left[\frac{\mu_0}{4\pi}\right] r_{IS}^{-3} \gamma_I \gamma_S$ (in frequency units) is known as the dipolar coupling constant. Polar angles θ and ϕ may be used to describe the position of the internuclear vector $\underline{r}'$ in the laboratory frame of reference.

The dipolar Hamiltonian may be expanded into the dipolar alphabet, and may be expressed as

$$H_D = \frac{\mu_0}{4\pi} \frac{\gamma_I \gamma_S \hbar}{r_{IS}^3} \left[A + B + C + D + E + F \right] \tag{3.36}$$

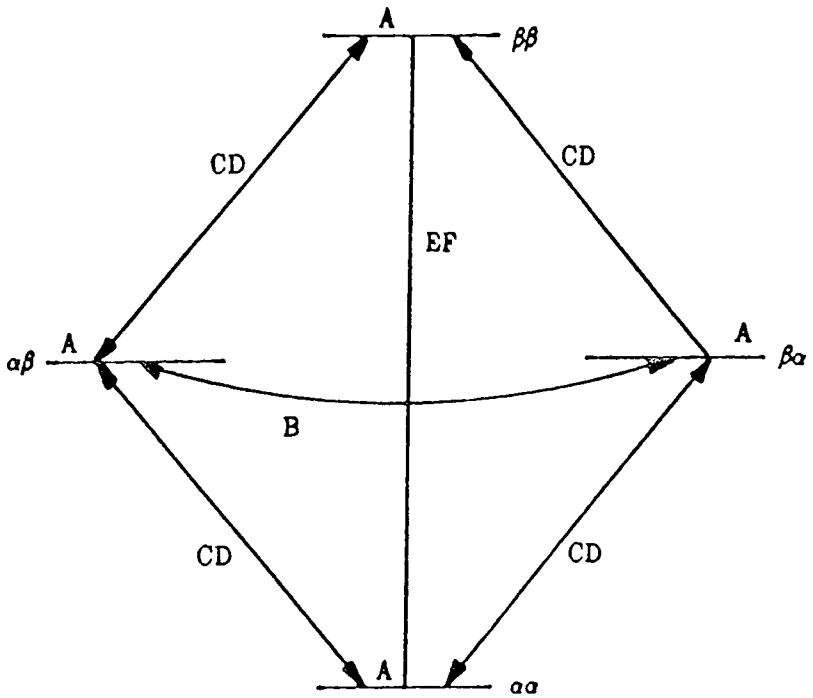

Figure 3.4

States joined by the terms A to F in the alphabet expansion.

where

$$A = (1-3\cos^2\theta)I_{Iz}I_{Sz} \tag{3.36a}$$

$$B = -\tfrac{1}{4}(1-3\cos^2\theta)\left[I_{I+}.I_{S-} + I_{I-}.I_{S+}\right] \tag{3.36b}$$

$$C = -\tfrac{3}{2}\sin\theta\cos\theta\exp(-i\phi)\left[I_{Iz}.I_{S+} + I_{I+}.I_{Sz}\right] \tag{3.36c}$$

$$D = -\tfrac{3}{2}\sin\theta\cos\theta\exp(+i\phi)\left[I_{Iz}.I_{S-} + I_{I-}.I_{Sz}\right] \tag{3.36d}$$

$$E = -\tfrac{3}{4}\sin^2\theta\exp(-2i\phi)\left[I_{I+}.I_{S+}\right] \tag{3.36e}$$

$$F = -\tfrac{3}{4}\sin^2\theta\exp(2i\phi)\left[I_{I-}I_{S-}\right] \tag{3.36f}$$

Each of the terms A to F contains a spin factor and a geometrical factor[8]. The effects of these spin and geometrical factors may be appreciated separately. Term B simultaneously flips one spin down and one spin up, that is to say term B links the $\alpha\beta$ and $\beta\alpha$ states only. The terms C and D each flip one spin only, and the terms E and F flip both spins up or both spins down. The states joined by the terms A to F are shown in figure 3.4.

3.9 Relaxation

In order for relaxation to take place, it is necessary that local fields fluctuating at the appropriate frequency are present in order to bring about transitions between the various energy levels. These fluctuating local fields originate from the various interactions already mentioned in section 3.8 and from molecular motion[6].

3.9.1 The effect of molecular motion on relaxation

One of the most important properties of NMR is its sensitivity to

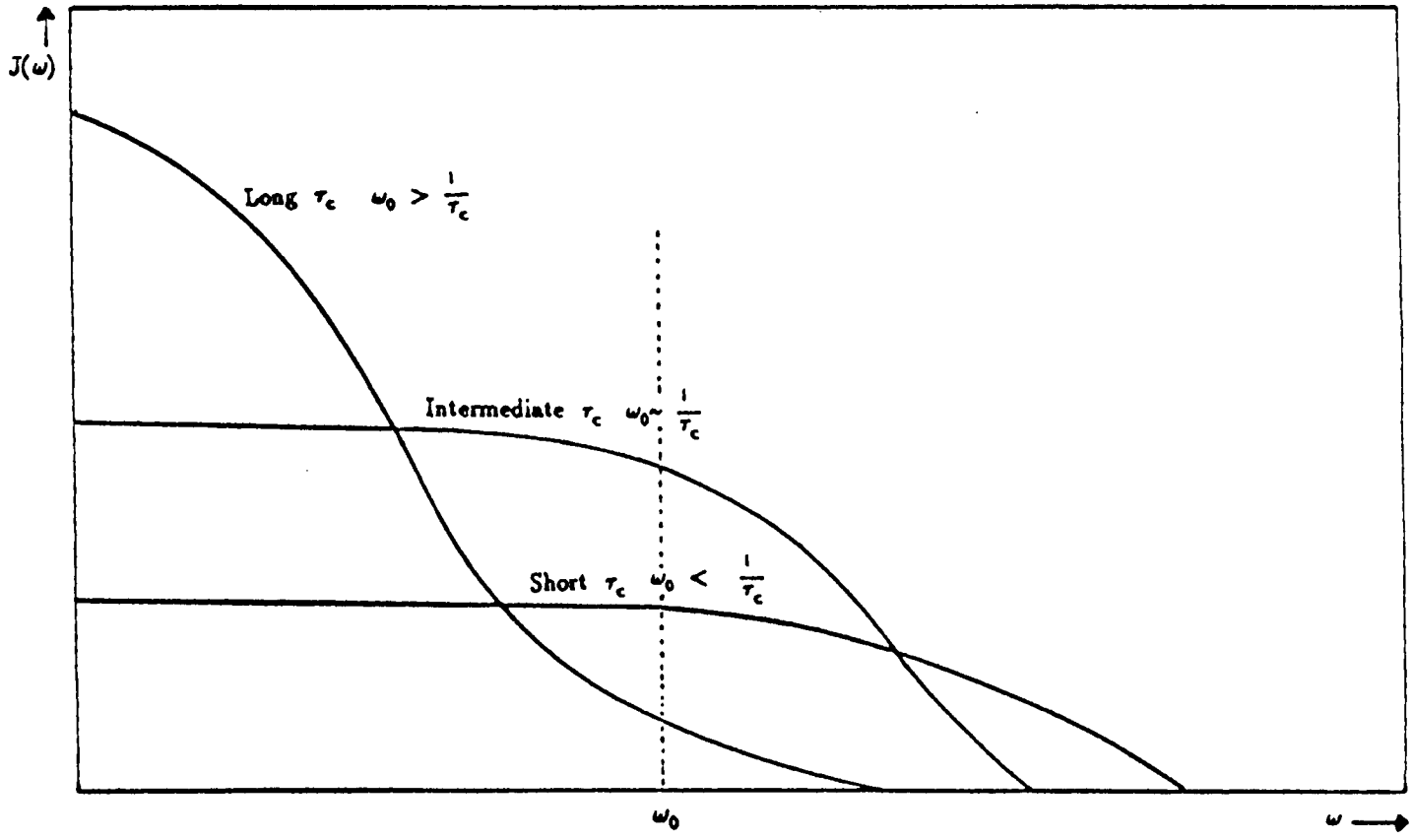

Figure 3.5

A plot which illustrates the change in the spectral density as a function of frequency for fast, intermediate and slow molecular motion.

the types of molecular motion. The power available from the fluctuations in the local fields at the relevant transition frequency, ω, may be expressed in terms of the spectral density $J(\omega)$. If $J(\omega)$ is known, then it is possible to work out the magnitude of the fluctuating fields at the Larmor frequency, which is what is required to study relaxation processes.[2]

A useful property in describing random molecular motion is that of a correlation time, τ_c. Roughly τ_c is the average time for a molecule to rotate by one radian. Figure 3.5 shows a plot of spectral density as a function of frequency.

It is informative to look at the shape of the plot. There is a flat portion, and then a sudden drop at $\omega\tau_c \sim 1$. The flat portion occurs when $\omega^2\tau_c^2 \ll 1$. This is known as the extreme narrowing condition. If τ_c is short, then the molecular motion is distributed over a wide range, and all motional frequencies within that range have an equally probable chance of occurring. If τ_c is long, then low motional frequencies have a higher chance of happening while high frequency has an almost zero probability.

The expression for $J(\omega)$ is

$$J(\omega) = \frac{2\tau_c}{(1+\omega^2\tau_c^2)} \qquad (3.37)$$

The expression predicts a maximum in T_1^{-1} (a minimum in T_1) as a function of τ_c. This is shown in figure 3.6. Figure 3.6 shows the dependence of T_1 T_2 and $T_{1\rho}$ on the correlation time τ_c[9]. The T_1 minimum occurs when the sudden drop in $J(\omega)$ as a function of $\log(\omega)$

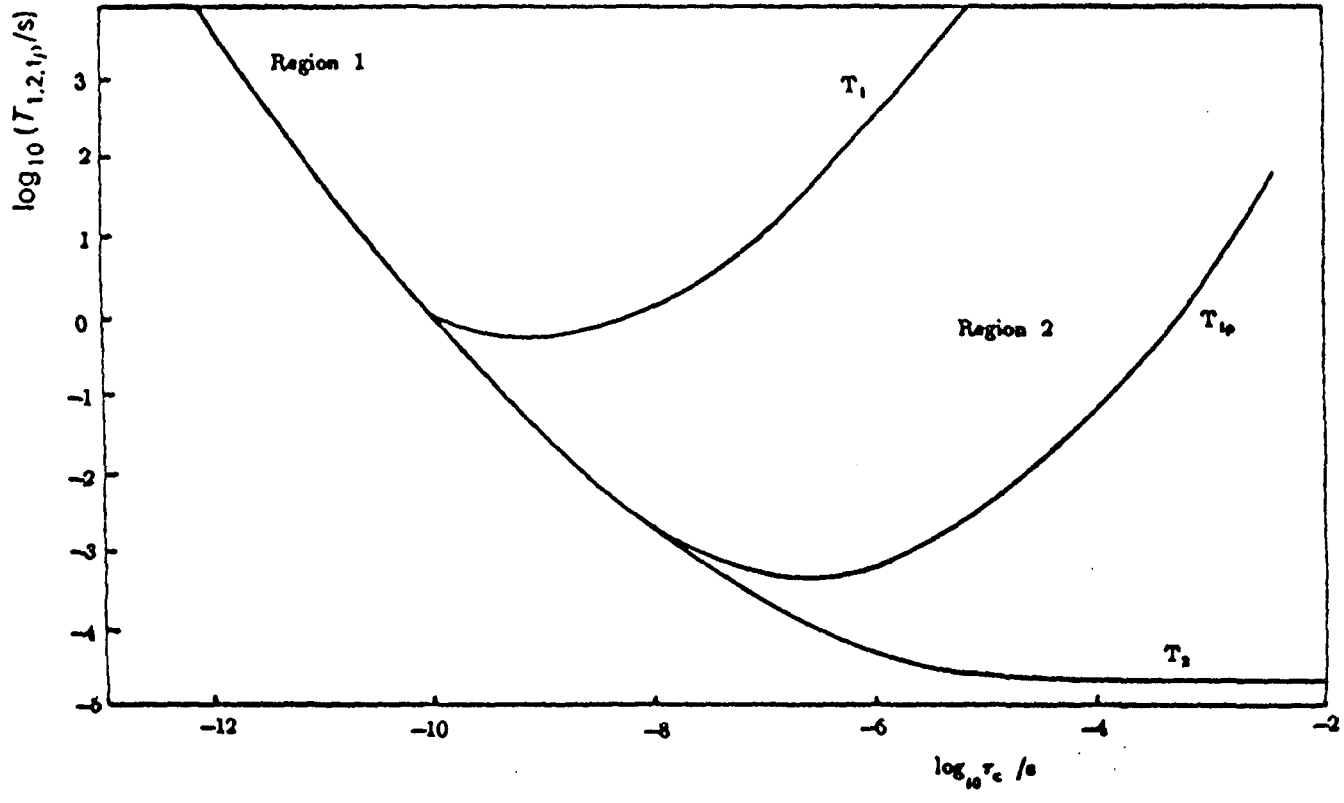

Figure 3.6

The effect of correlation time on T_1, $T_{1\rho}$ and T_2. for an isolated CH vector rotating isotropically in a field of 63kG. The bond length, r_{CH} is 1.09 Å.

corresponds to the resonance frequency, i.e. when $\tau_c = \omega_0^{-1}$.

For very short values of the correlation time, the molecule undergoes rapid isotropic molecular motion which causes averaging of the anisotropic interactions to such an extent that $T_1 = T_{1\rho} = T_2$. This is the extreme narrowing limit. As τ_c decreases the anisotropic interactions are averaged to an even greater extent. This leads to an increase in T_1, $T_{1\rho}$ and T_2 (region 1 in fig 3.6).

As the correlation time is increased, the T_1 passes through a minimum value as already described. As τ_c is increased even further, the degree to which the isotropic interactions are averaged decreases. This causes the amplitudes of the local fields produced by the anisotropic interactions to increase, but the fields fluctuate at a slower rate. The overall result is that there are fewer local fields which fluctuate at an appropriate frequency to introduce transitions between the β and α energy states in either the laboratory or the rotating frame of reference. This results in an increase in T_1 as τ_c increases (region 2, figure 3.6). T_2 is governed by spin–spin flip–flop transitions. These transitions are energy–conserving, and therefore T_2 decreases as τ_c increases.

3.10 The nuclear Overhauser effect

Solid–state single pulse ^{13}C spectra are obtained routinely under conditions of dipolar decoupling. Saturation of the proton energy levels results in a non–Boltzmann distribution of the ^{13}C spins in their own energy levels. This phenomenon, known as the nuclear Overhauser enhancement (NOE) depends on the extent to which C–H dipolar

relaxation is the operative mechanism.

The NOE may be calculated from the ratio of the intensities of the decoupled resonance without saturation (I_{ns}) to the decoupled resonance with saturation (I_s).

$$NOE = \frac{I_s}{I_{ns}} = 1 + \eta \qquad (3.38)$$

where η is the nuclear Overhauser enhancement factor (NOEF).

In the extreme narrowing case, η may be expressed by

$$\eta = \frac{\gamma_H}{2\gamma_S} \frac{(T_1^D)^{-1}}{(T_1^D)^{-1} + (T_1^0)^{-1}} \qquad (3.39)$$

where T_1^D is the longitudinal relaxation time for the dipolar mechanism, and T_1^0 is the longitudinal relaxation time for other relaxation mechanisms.

The maximum value for the NOEF for carbon is 2.99 under extreme narrowing conditions to 1.15 for $\omega^2\tau_c^2 \gg 1$.

3.10.1 The nuclear Overhauser effect and molecular motion

For bulk polymers above T_g, the magnetic resonance parameters that primarily relate to molecular dynamics are the spin–relaxation times T_1 and the nuclear overhauser enhancement (NOE). Spin–lattice processes are sensitive to motions at or near the nuclear Larmor frequencies,

typically 5–500 MHz. There are several mechanisms that contribute to the spin relaxation of ^{13}C nuclei. The ^{13}C dipolar relaxation mechanism is the most useful to analyse molecular rotational motions in polymers. Other mechanisms may be ignored as their contributions to relaxation are usually small.

The NOE depends on motions near the Larmor frequency, but in a manner different from that of T_1[10]. For a carbon that is fully relaxed by the C–H dipolar mechanism, up to a threefold enhancement of intensity can be obtained.

It can be shown that the ^{13}C T_1 and NOE are given by

$$\frac{1}{T_1} = \frac{1}{10}\gamma_C^2\gamma_H^2\hbar^2\sum_i r_i^{-6}\left[f(\omega_H-\omega_C)+3f(\omega_C)+6f(\omega_H+\omega_C)\right] \qquad (3.40)$$

$$NOE = 1 + (\gamma_H/\gamma_C)\,\frac{\left[6f(\omega_H+\omega_C)-f(\omega_H-\omega_C)\right]}{\left[f(\omega_H-\omega_C)+3f(\omega_C)+6f(\omega_H+\omega_C)\right]} \qquad (3.41)$$

where ω_C and ω_H are the carbon and proton resonance frequencies respectively and r_i is the distance between the ^{13}C nucleus of interest and the ith relaxing proton.

The spectral density functions $f(\omega_i)$ are the Fourier transforms of the autocorrelation functions of second–order spherical harmonics. They describe the power available at angular frequency ω_i from the fluctuating interaction. The form of $f(\omega_i)$ depends on the model used to describe the molecular motion. The simplest model available is that of isotropic rotational diffusion. In this case the $f(\omega)$ have the form

Figure 3.7

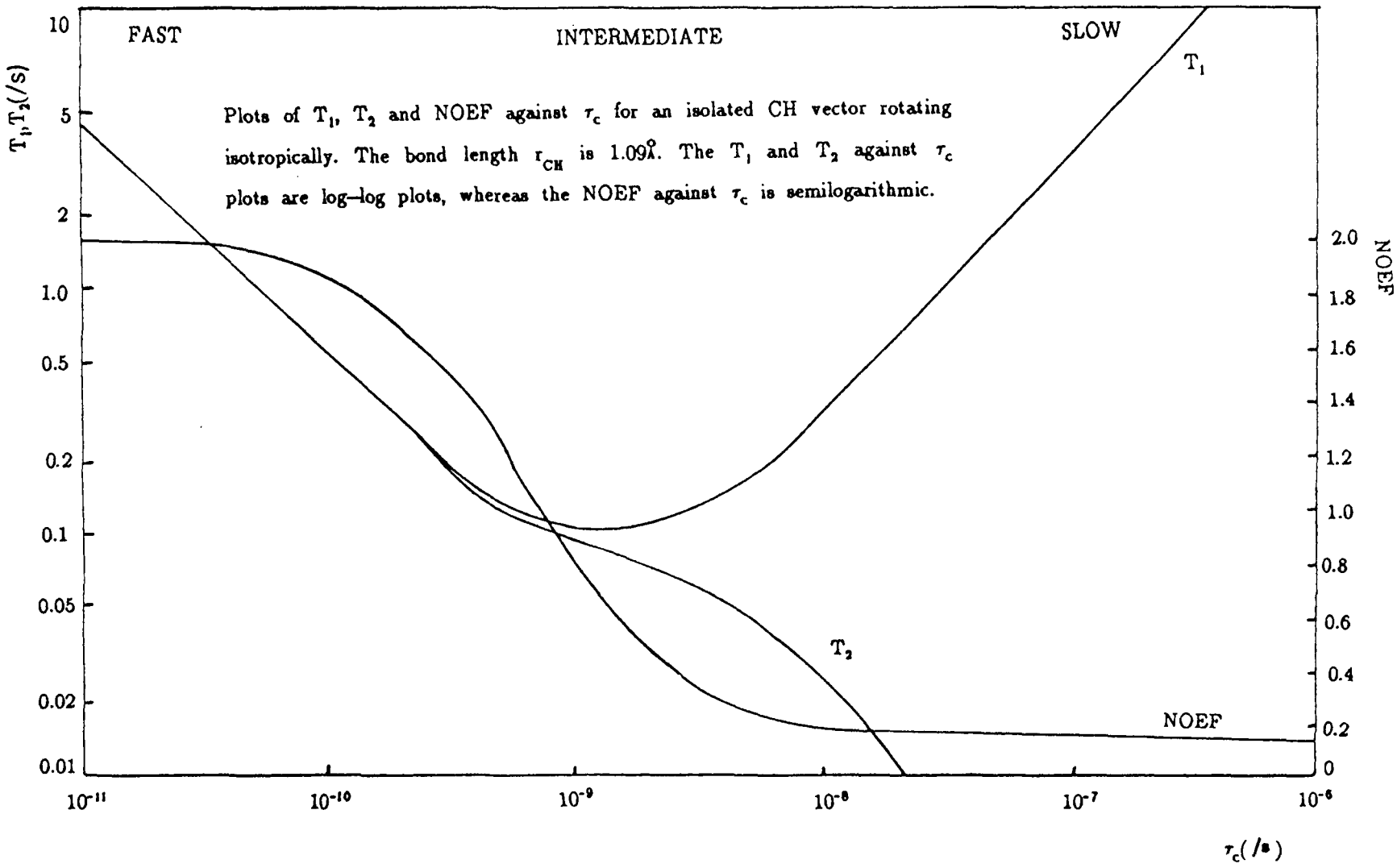
FAST
INTERMEDIATE
SLOW
Plots of T_1, T_2 and NOEF against τ_c for an isolated CH vector rotating isotropically. The bond length r_{CH} is 1.09Å. The T_1 and T_2 against τ_c plots are log–log plots, whereas the NOEF against τ_c is semilogarithmic.
$T_1, T_2 (/s)$
10
5
2
1.0
0.5
0.2
0.1
0.05
0.02
0.01
T_1
T_2
NOEF
2.0
1.8
1.6
1.4
1.2
1.0
0.8
0.6
0.4
0.2
0
10^{-11}
10^{-10}
10^{-9}
10^{-8}
10^{-7}
10^{-6}
$\tau_c (/s)$

$$f(\omega) = \tau_c(1+\omega^2\tau_c^2) \qquad (3.42)$$

where τ_c is the rotational correlation time.

Figure 3.7 shows the behaviour of T_1 and the NOE as a function of correlation time for a C–H vector rotating isotropically. A given value of T_1 corresponds to two values of the correlation time, except at the minimum. These correspond to the so–called 'fast' and 'slow' solutions for T_1, depending on the value of T_c. The NOE decreases monotonically with increasing τ_c. Since for slower motion the dipolar mechanism becomes less efficient, the NOE decreases as illustrated in figure 3.7. When τ_c is small, as is the case in the extreme narrowing region, the NOE = 3. As τ_c increases, the value of the NOE decreases.

For high molecular weight polymer chains in bulk, overall reorientation does not occur. The predominant motional feature is segmental mobility, either of the backbone or of the side chains. Thus the T_1 and NOE parameters of such polymers do not adhere to the simple isotropic model outlined here. Often more complicated models for segmental motion involving several or a distribution of correlation times are invoked. An important feature of these distributions is the inclusion of longer correlation times to account for the reduced NOE's observed in polymers.

3.11 Selective averaging techniques

In solution state NMR, high resolution NMR spectra are obtained. Rapid isotropic molecular tumbling averages the geometric factor

$(3\cos^2\theta-1)$ to zero, and hence the anisotropic spin interactions discussed in section 3.8 are averaged out. However, in solids, the molecules are generally held rather rigidly. The anisotropic spin interactions are not averaged out by molecular motion, and so contribute to the linewidth in the NMR spectra. These interactions lead to very broad lines in the solid state which obscure valuable high–resolution information. There are two types of broadening which contribute to the linewidth in the solid state.

a). Homogeneous broadening arises from the dipolar interactions between abundant spins, where each spin is coupled to every other spin. All nuclei in the sample give rise to the entire line, which is broad because of spin–relaxation or spin–diffusion effects.

b). Inhomogeneous broadening of lineshapes arises from the dipolar interactions between abundant and rare spins and shielding anisotropy. The resonance frequency for a particular spin depends on the orientation of the principal axis system with respect to the magnetic field B_0. In a powder, all orientations of PAS with respect to B_0 are possible. Therefore the lineshape results from the summation of many individual lines tending towards a gaussian shape.

In order to obtain 'solution–state' type spectra in the solid state, the interactions discussed in section 3.8 must be averaged to zero.

Several techniques have been developed which selectively average these interactions. This results in line–narrowing, and hence high resolution spectra may be obtained for solids.

3.11.1 Magic angle spinning

It is possible to reduce the effect of the direct dipolar interactions and the shielding anisotropy in solids using a technique called magic angle spinning (MAS). Manipulation of the spin interactions can be achieved by rotating the sample at a rate ω_r about an axis which is tilted by an angle θ with respect to the magnetic field B_0. This technique simulates the isotropic molecular tumbling found in liquids.

Inspection of the dipolar Hamiltonian $\mathcal{H}_D$ and the shielding Hamiltonian $\mathcal{H}_S$ (equations 3.33 and 3.28 respectively) shows that there exists the option of averaging the spatial term to zero. Both these Hamiltonians contain the common term $(1-3\cos^2\theta)$. The angle θ describes the orientation of the principal axis system of those interactions with respect to B_0.

Rotation of the sample at an angle β which is fixed relative to B_0 causes orientation dependent interactions to have a time dependence[11]. As long as the rate of sample rotation is greater than the static linewidth, the average angle of θ is such that

$$\langle 3\cos^2\theta-1\rangle = \tfrac{1}{2}(3\cos^2\beta-1)(3\cos^2\aleph-1) \qquad (3.43)$$

The parameter $\aleph$ is fixed for a rigid solid, and it takes all possible values for a powder sample. The term $\frac{1}{2}(3\cos^2\beta-1)$ acts as a scaling factor on a dipolar powder pattern. The angle β is at the control of the experimentalist. The case of most interest is that when $\beta = 54^\circ44'$. At

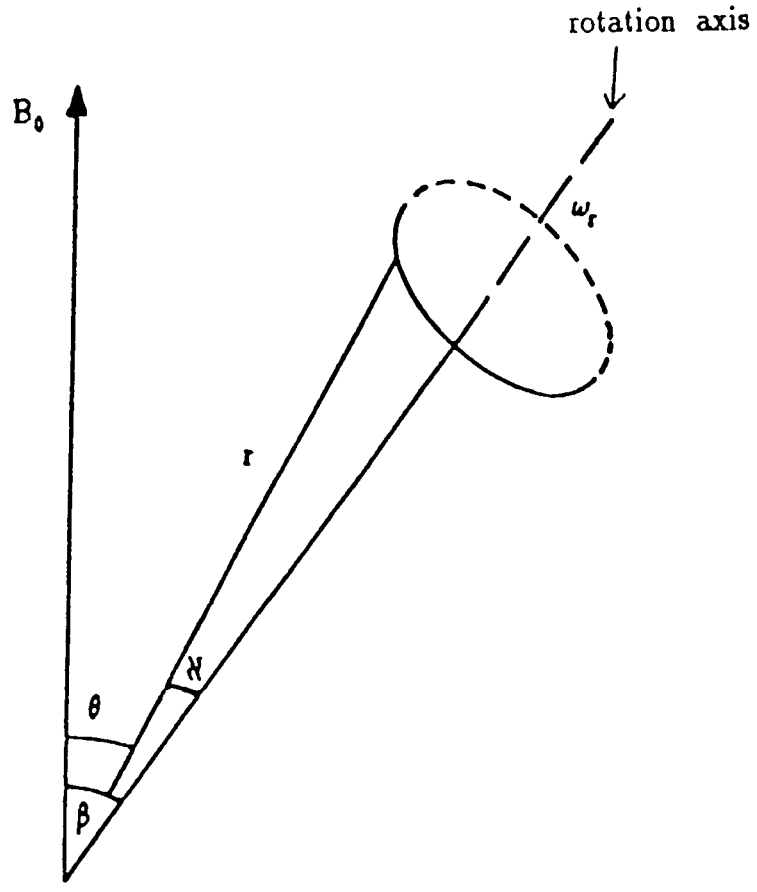

Figure 3.8

Magic–angle spinning. The sample is rotated at an angle β with respect to B_0 at a rate ω_r. r is the internuclear vector.

this angle the term $(3\cos^2\beta-1) = 0$, and therefore the term $\langle 3\cos^2\theta-1\rangle=0$. This is the spatial term in the dipolar Hamiltonian. Hence, just as for isotropic tumbling, the dipolar interaction is averaged to zero. This eliminates dipolar broadening, thus giving high resolution spectra.

Any solid–state interaction that displays the $(3\cos^2\theta-1)$ dependence can be removed, in principle, by MAS. The special requirements are different for homogeneous and inhomogeneous interactions, however. In the homogeneous case, as for H–H dipolar interactions in a solid, ω_r must exceed the full strength of the interaction for complete narrowing to take place. However, some narrowing may be accomplished by using slower spinning speeds. For inhomogeneous interactions such as the chemical shift anisotropy, MAS at less than the full width of the interaction yields a relatively narrow centre band and a spectrum of side bands separated by the spinning frequency.

3.11.2 High Power dipolar decoupling

As a result of the dipolar interactions with protons, the ^{13}C NMR linewidth in an organic solid is of the order of 20 KHz. The fine structure associated with the various chemically shifted resonances occurs over a range much less than this. Therefore, in order for high–resolution NMR spectra to be obtained in the solid state, it is necessary to remove the effects of this dipolar interaction. The dipolar interactions are often so large that they cannot be averaged completely by MAS. Dipolar decoupling averages I_zS_z , the spin part of $\mathcal{H}_{IS}$ rather than the spatial part. The ^{13}C magnetic moments experience the z component of the local

field from the proton moments. If this local field can be averaged to zero, the ^{13}C spin sees zero net field from the protons, and the effect of heteronuclear dipolar coupling is removed.

In a typical ^{13}C solid state experiment, RF radiation of sufficient power applied at the proton frequency forces the proton spins to precess rapidly. This averages the effective field from ^{1}H that is seen by the ^{13}C nucleus. For the averaging to be effective, the dipolar irradiation must be powerful enough to average $\mathscr{H}_{IS}$, the C–H dipolar coupling.

Dipolar decoupling is analogous to the proton decoupling normally done in ^{13}C NMR of liquids to remove ^{13}C spin–spin (scalar) couplings. For solids, decoupling fields at least an order of magnitude larger than those used in the solution state are necessary to reduce the much stronger dipolar coupling.

3.12 Spin temperature

In a static magnetic field B_0 the ^{1}H spins populate their set of zeeman levels separated by $\Delta E = \gamma\hbar B_0$ according to the Boltzmann distribution.

$$\frac{n_u}{n_l} = \exp\left[-\frac{\Delta E}{k T_s}\right] \tag{3.44}$$

where T_s is the temperature of the spin system, and n_u and n_l are the populations of the upper and lower energy states respectively.

A schematic diagram of the carbon and proton spin systems in a typical polymer is illustrated in figure 3.9.

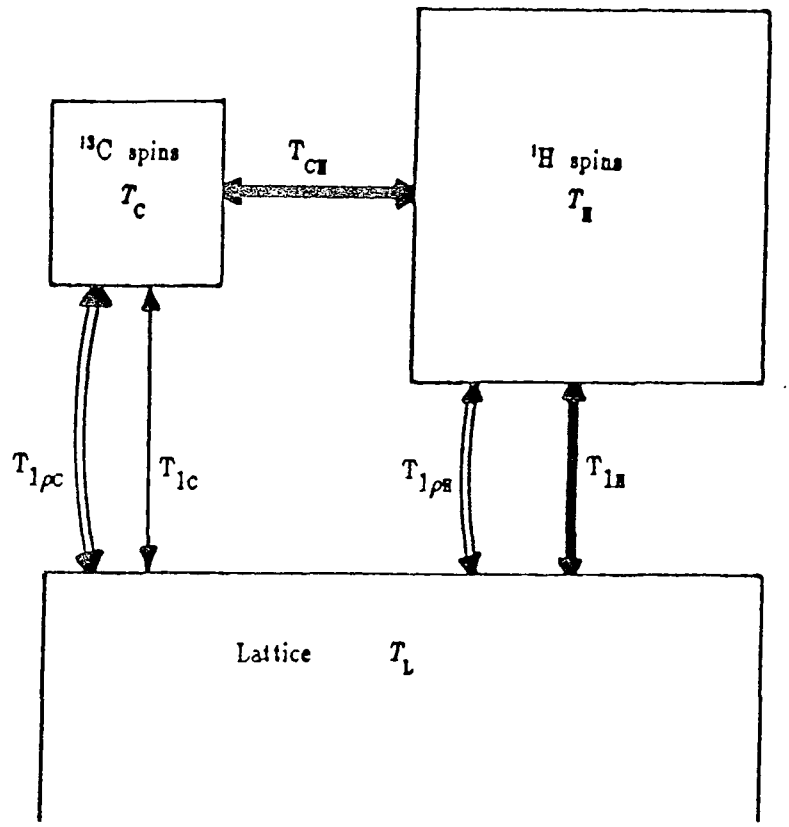

Figure 3.9

A schematic diagram to illustrate the carbon and proton spin systems in a typical polymer. The T indicate spin temperatures, the T indicate the relaxation processes which occur between the carbons, protons and the lattice.

From equation 3.44 it may be seen that a larger polarisation (greater population difference) corresponds to a lower spin temperature. Via spin diffusion the proton spin system equilibrates at a single T_S in a very short time, and may be considered as an isolated spin reservoir.

After a much longer time the proton system equilibrates with the surroundings (the lattice), and T_S equals T_L, the lattice temperature.

The proton magnetisation may be expressed by the Curie law.

$$M_H = \frac{C_H B_0}{T_L} \tag{3.45}$$

where

$$C_H = \frac{N_H \gamma_H^2 \hbar^2}{4k} \tag{3.46}$$

The carbon spins also equilibrate among their levels in the same manner. The carbon levels have only about $\frac{1}{4}$ the separation of the proton levels at the same temperature because $\gamma_H \sim 4\gamma_C$. Because of the different relaxation processes involved and the larger internuclear distances, the equilibrium times for the ^{13}C spin reservoir are longer than for the protons. The fact that the separation of the carbon levels is greatly different from the separation of the proton levels (i.e. the nuclei have greatly different resonance frequencies) means that these two sets of nuclei cannot undergo mutual energy–conserving spin flips efficiently, and are therefore isolated from each other. This enables them to possess different relaxation times.

3.13 Cross–polarisation

A common problem that is encountered when attempting to obtain high–resolution NMR spectra of solids is the low sensitivity of the nucleus under observation. The sensitivity of a particular nucleus is dependent upon several factors:

1). The natural abundance of the isotope

2). The size of the magnetic moment which results from the interaction of the nuclear magnetic moment with the static field B_0

3). The length of the spin–lattice relaxation times (relative to the proton T_1 values).

The last factor limits the rate at which experiments may be repeated, and therefore reduces the sensitivity. The sensitivity may be enhanced by using the cross–polarisation (CP) technique. The pulse sequence used in the cross–polarisation experiment is shown in figure 3.10.

As has already been stated in the last section, the equilibrium magnetisation for the abundant proton spins is given by

$$M_H = \frac{C_H B_0}{T_L} \qquad (3.47)$$

This proton magnetisation is tipped to lie along the y axis in the rotating frame of reference by a 90° $+x$ pulse applied at the proton frequency. This magnetisation is then spin–locked along the y axis by a field B_{1H} applied along the y axis at the proton frequency. The proton

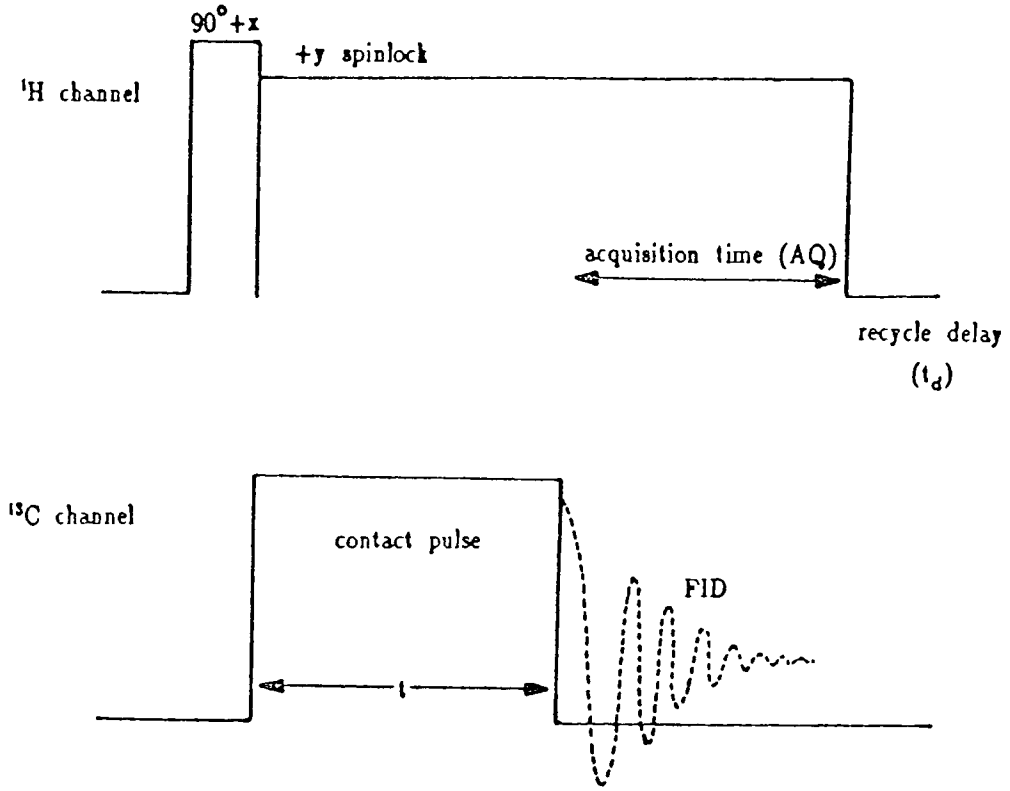

Figure 3.10

The cross–polarisation pulse sequence.

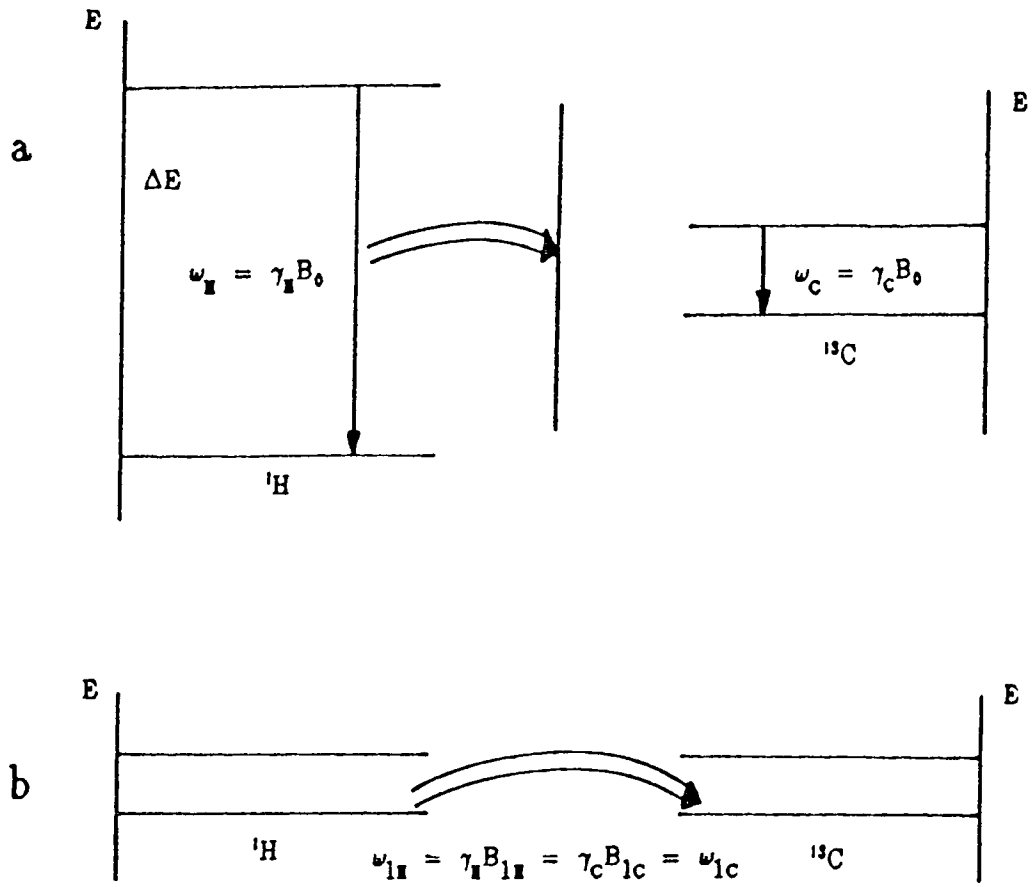

Figure 3.11

A schematic diagram to illustrate the cross–polarisation process.

In figure a). The proton levels have four times the separation of the carbon levels. This makes transfer from proton to carbon an unfavourable process.

In figure b). The Hartmann–Hahn condition is satisfied and both ^1H and ^{13}C spin systems are in frames rotating at the same rate. Energy transfer can now take place.

magnetisation is no longer at thermal equilibrium. At this stage

$$M_H = \frac{C_H B_0}{T_L} = \frac{C_H B_{1H}}{T_H} \tag{3.48}$$

From the above equation, it may be deduced that

$$T_H = \frac{B_{1H}}{B_0} T_L \tag{3.49}$$

B_{1H} is much less than B_0 , therefore $T_H \ll T_L$. Thus the effect of the spin–locking field B_{1H} is to effectively cool the spins. This was brought about not by an actual lowering of temperature, but by a lowering of the effective field seen by the protons.

The cross–polarisation process occurs when the smaller, hotter ^{13}C reservoir is brought into contact with the larger, cooler ^{1}H reservoir. This is accomplished by irradiating the carbons with an RF field B_{1C} of a strength such that the Hartmann–Hahn condition is satisfied:

$$\gamma_H B_{1H} = \gamma_C B_{1C} \tag{3.50}$$

When this condition is met the original proton and carbon levels which did not match, are brought to lower matching levels. This is illustrated in figure 3.11. The energy–conserving spin flips can now occur between the carbon and the proton spins instead of just within the individual reservoirs. The rotating frames of both the carbon and proton

spins precess at the same rate and with equal energies.

At this point, before transfer of magnetisation, the carbon magnetisation in the *xy* plane of the rotating frame is considered to be zero, and the carbon is said to have an infinite spin temperature.

$$T_C = \infty \tag{3.51}$$

During the transfer of magnetisation, the larger, cooler proton reservoir cools the carbon reservoir; that is, a carbon signal is created along B_{1C}. The spin energy is redistributed between the two spin systems to give a common spin temperature T_M.

Assuming energy conservation in the rotating frame

$$\frac{C_H B_{1H}^2}{f_H} + \frac{C_C B_{1C}^2}{f_C} = \frac{1}{f_M}\left[C_H B_{1H}^2 + C_C B_{1C}^2 \right] \tag{3.52}$$

But $T_C = \infty$,

So
$$\frac{f_H}{f_m} = \frac{1}{1 + \epsilon a^2} \tag{3.53}$$

where
$$\epsilon = \frac{N_C}{N_H} \tag{3.54}$$

and
$$a = \frac{\gamma_C B_{1C}}{\gamma_H B_{1H}} \tag{3.55}$$

Following cross–polarisation, the carbon magnetisation is

$$M_C = \frac{M_C(0)\, B_{1C} T_L}{B_0 T_M} \qquad (3.56)$$

Therefore,
$$M_C = \frac{\gamma_H}{\gamma_C} \frac{\sigma M_C(0)}{1+\epsilon\sigma^2} \qquad (3.56a)$$

Since $\gamma_H/\gamma_C > 1$, the intensity of the carbon magnetisation has been enhanced. $M_C(0)$ is the intensity of the carbon spin magnetisation observed in a single pulse experiment.

3.13.1 Cross–polarisation dynamics[12]

The description of the cross–polarisation experiment in the last section omitted the effects of the various types of relaxation on the observed carbon intensity at a particular contact time.

During the cross–polarisation experiment, the abundant proton spins undergo three types of relaxation.

1. During the cross–polarisation experiment, a 90° $+x$ proton pulse transfers S spin magnetisation to the y axis in the rotating frame of reference. When T_2^* for the S spins is comparable to the duration of the 90° pulse, spin–spin relaxation can occur during this period, which results in a reduction in the amount of S spin magnetisation which is transferred.
2. Immediately after the S spin magnetisation is spin–locked, the magnetisation decays at a rate characterised by the exponential time constant $T_{1\rho}^S$.
3. As a consequence of cross–relaxation with the carbon spins,

there is a loss of proton magnetisation. The rate at which cross–polarisation occurs is characterised by the exponential time constant T_{IS}.

The rare carbon spins (I) undergo two types of relaxation during the cross–polarisation experiment.

1. Loss of carbon magnetisation occurs as a result of relaxation in the rotating frame of reference. The rate of decay is characterised by the exponential time constant $T_{I\rho}^{I}$.
2. Whilst the proton spins are spin–locked, the I spin magnetisation grows as a consequence of cross–relaxation with the proton spins. The rate at which the growth of magnetisation occurs is characterised by the exponential time constant T_{IS}.

The following section assumes that $T_2^* \ll$ the 90° pulse length, and that $\frac{1}{T_{I\rho}^{I}} \approx 0$.

If energy conservation in the rotating frame of reference is invoked, it may be written

$$\frac{d\beta_I}{dt} + \epsilon a^2 \frac{d\beta_S}{dt} = 0 \qquad (3.57)$$

where β_I is the inverse spin temperature of spins I, and β_S is the inverse spin temperature of spins S.

The variation of the inverse spin temperature with contact time for both the I and S spins is given by

$$\frac{d\beta_I}{dt} = -\frac{1}{T_{IS}}\left[\beta_I - \beta_S\right] \tag{3.58a}$$

$$\frac{d\beta_S}{dt} = -\frac{\epsilon a^2}{T_{IS}}\left[\beta_S - \beta_I\right] - \frac{\beta_S}{T_{1\rho}^S} \tag{3.58b}$$

These coupled differential equations are straightforwardly solved under the initial conditions:

$$\beta_I(0) = 0 \quad \text{and} \quad \beta_S(0) = \beta_{S_0}$$

The solution for $\beta_I(t)$ is

$$\beta_I(t) = \beta_{S_0}\frac{1}{a_+ - a_-}\left[\exp(-a_- t/T_{IS}) - \exp(-a_+ t/T_{IS})\right] \tag{3.59}$$

where

$$a_\pm = \frac{1}{2}\left[1 + \epsilon a^2 + \frac{T_{IS}}{T_{1\rho}^S}\right]\left[1 \pm \left[1 - \frac{4T_{IS}/T_{1\rho}^S}{1 + \epsilon a^2 + T_{IS}/T_{1\rho}^S}\right]^{\frac{1}{2}}\right] \tag{3.60}$$

The variation of carbon magnetisation $M_I(t)$ with contact time is

$$\frac{M_I(t)}{M_{I0}} \propto \frac{\gamma_I}{\gamma_S}\frac{\beta_I(t)}{\beta_{S_0}} \tag{3.61}$$

After the carbon magnetisation has been developed, the spin–locking of the proton spins is continued. This decouples the proton spins from the carbon spins, allowing observation of the carbon spins during the

acquisition period. Since the carbon spin magnetisation is derived from the proton spins, the recycle delay between pulses is governed by the T_1 of the proton spins, and not the carbon spins. Proton T_1 values are usually considerably shorter than carbon T_1 values, therefore the delay between pulses is substantially reduced, and hence the experiment time is shortened.

The cross–polarisation experiment described so far is the "single–contact" cross–polarisation experiment. This is the pulse sequence which has been used in this thesis.

Two modifications have been made to this pulse sequence. They are known as spin–temperature inversion and flip–back.

3.13.2 Spin–temperature inversion[13]

Cross–polarisation experiments are susceptible to two different artifacts. These arise as a result of the long radiofrequency pulse on the proton channel. The first type of artifact arises from phase irregularities, or glitches. These result in some of the carbon spin magnetisation present at the start of the experiment being rotated by the glitch, and thus being spin–locked along the RF field. This carbon magnetisation is indistinguishable from the carbon magnetisation derived by cross–polarisation. The second artifact originates from transients generated by eddy currents in the aluminium probe housing. The characteristics of the pulse solely determine these artifacts, which may be removed by spin–temperature inversion.

3.13.3 Flip–back[14]

The second modified cross–polarisation experiment is called the flip–back experiment. It is designed to improve the efficiency with which spectra are acquired using cross–polarisation. In the ordinary single–contact experiment, the signal–to–noise is dependent upon the recycle delay during which the repolarisation of the spins occurs.

$$S/N \propto n^{1/2}(1 - B) \tag{3.62}$$

where n = number of transients acquired

and where $B = \exp\left[\frac{-RD}{T_1^S}\right]$. (3.63)

and RD = recycle delay.

when $T_1^S > T_{1\rho}^S > AQ$ (the acquisition time), then repolarisation of the proton spins may be effected by rotating the proton spin magnetisation so that it is aligned along the direction of B_0 following aquisition. This improves the efficiency of the experiment.

In the flip–back experiment,

$$S/N \propto \frac{n^{\frac{1}{2}}(1 - B)}{(1 - AB)} \tag{3.64}$$

where $A = \exp\left[\frac{-AQ}{T_{1\rho}^S}\right]$ (3.65)

CHAPTER 4

Experimental

4.1 Instrumentation

4.1.1 Bruker CXP200 NMR spectrometer

A Bruker CXP200 NMR spectrometer was used to acquire the majority of the solid–state spectra shown in this thesis. The spectrometer is equipped with an Oxford Instruments superconducting wide–bore (89.5 mm) solenoid magnet with an operating field of 4.7 Tesla. At this field the resonance frequencies of ^{1}H and ^{13}C are 200.13 MHz and 50.323 MHz respectively.

The CXP is a dual–channel spectrometer which is capable of simultaneous irradiation of both low and high frequency nuclei. The lower frequency channel can irradiate between 4 and 95 MHz, and the higher frequency channel can operate at either 200.13 MHz (^{1}H) or 188 MHz (^{19}F). For the research described in the following chapters, the high frequency channel is only used at the proton frequency. The NMR properties of the proton and carbon nuclei are listed in Table 4.1. The details of the spectrometer construction are well–known and a description may be found in reference one[1].

4.1.2 Other spectrometers utilised

Some of the work described in this thesis was obtained on a Varian VXR300 spectrometer equipped with a 7.1 Tesla narrow–bore

magnet. The operating frequencies are 75.431 MHz for carbon and 299.949 MHz for protons respectively.

The solution–state work described in this thesis was obtained using a Bruker AC–250 spectrometer equipped with a 5.9 Tesla narrow–bore magnet. The system was field/frequency locked by the ^{2}H resonance of deuterated DMSO.

Some proton work was carried out on a purpose–built static spectrometer operating at 60 MHz for protons. The spectrometer is equipped with an electromagnet, and is only suitable for static samples

4.1.3 The probes

During the course of this work two probes were routinely used on the CXP200 spectrometer. The two wide–bore (84.5 mm) broad–band, dual–channel, high–resolution commercial double–bearing probes covered a frequency range of 20–90 MHz. The double–bearing system allows samples in cylindrical–shaped zirconia rotors to be rotated at the magic angle, at rates between 100 Hz – 5 KHz, however the rotor had to be packed fully and homogeneously to obtain stable spinning rates.

The probe used for the VXR300 spectrometer was a narrow–bore double–bearing probe designed by Doty. The samples were packed in zirconia rotors for sample spinning.

The solution–state studies were made using a broad–band 10mm VSP probe.

Table 4.1

NMR properties of nuclei studied.

Isotope	% natural abundance	$\gamma/10^7 rad T^{-1} s^{-1}$	NMR ν/MHz at 4.7 T	Sensitivity rel to ^1H
^1H	99.99	26.75	200.13	1.000
^{13}C	1.11	6.73	50.32	1.76×10^{-4}

4.2 Experimental

4.2.1 Shimming the magnet

The homogeneity of the magnetic field is required to be maximised in order to obtain a good lineshape and narrow linewidths for signals. For the CXP200, the homogeneity of the field is maximised by adjusting the positions of the shim coils to minimise the linewidth of the proton signal observed from silicone gum. A recycle time of 3 seconds was used to acquire spectra. The linewidth at half–height of the silicone gum signal was typically between 6–10 Hz. The signal occurs at 0.2 ppm with respect to tetramethylsilane (TMS).

4.2.2 Setting the proton 90° pulse

In order to obtain a 90° proton pulse, the proton FID from silicone gum is first set on resonance. A 180° proton pulse is obtained by adjusting the gain until a null signal is observed after the pulse. To obtain the 90° proton pulse, the pulse duration is halved. 90° pulse durations of 4 μs were typically used for the double–bearing probe. This corresponds to a decoupling frequency of 62.5 kHz.

4.2.3 Setting the angle

In order to minimise the effects of dipolar coupling, it is necessary to adjust the angle at which the rotor spins to the magic angle (54°44'). This is achieved by maximising the sharpness of rotational echoes observed in the ^{127}I spectrum of potassium iodide. The nucleus ^{127}I has a

spin 5/2, and has a resonance frequency of 40.047 MHz on the CXP200 spectrometer. The sidebands observed arise from the spinning modulation of the first–order quadrupolar interaction resulting from imperfections in the crystal lattice. This technique is accurate to within $\pm 0.1^{\circ}$ of the magic angle.

4.2.4 ^{13}C referencing

The ^{13}C chemical shifts were obtained using adamantane as a reference. Adamantane exhibits shifts at 38.5 ppm and 29.5 ppm with respect to TMS for the CH and CH_2 carbons respectively.

4.2.5 ^{13}C matching for CP

The ^{13}C 90° pulse duration was established by adjustment of the gain setting on the low frequency amplifier until the Hartmann–Hahn matching condition was obtained, and the observed cross–polarisation signal maximised.

4.2.6 Setting ^{13}C 90° pulse for single pulse

For single pulse experiments, the 90° carbon pulse is set in a similar way to the 90° proton pulse. The gain on the low frequency amplifier is adjusted until a null signal is observed from adamantane. The pulse duration is then halved to obtain a 90° carbon pulse.

4.3 Pulse sequences

A number of pulse sequences have been used during the course of the work outlined in this thesis. The more common pulse sequences used are described in the following sections, whereas the new pulse sequences devised are described in more depth later in the thesis.

4.3.1 Single pulse excitation (SPE)

The single pulse excitation pulse sequence with high–power proton decoupling is shown in figure 4.1a. High–power proton decoupling is necessary when there are strong C–H dipolar interactions present such as in the case of polymers. The $\pi/2$ carbon pulse gives maximum signal provided the recycle delay is adequate for relaxation. Any inaccuracies in the pulse duration lead to a signal lower than the maximum. The intensities obtained are quantitative provided the recycle time is of sufficient length to allow the nuclei to relax back to equilibrium. The single pulse excitation experiment is of particular use when observing carbons which do not have long spin–lattice relaxation times. It is possible to discriminate between carbons in polymers which differ in mobility, and therefore differ in the length of the carbon T_1's.

4.3.2 INV1H

The INV1H pulse sequence is shown in figure 4.1b. The pulse sequence is used in the study of the transient nuclear Overhauser effect. At the start of the sequence there is a proton 180° inversion pulse. The

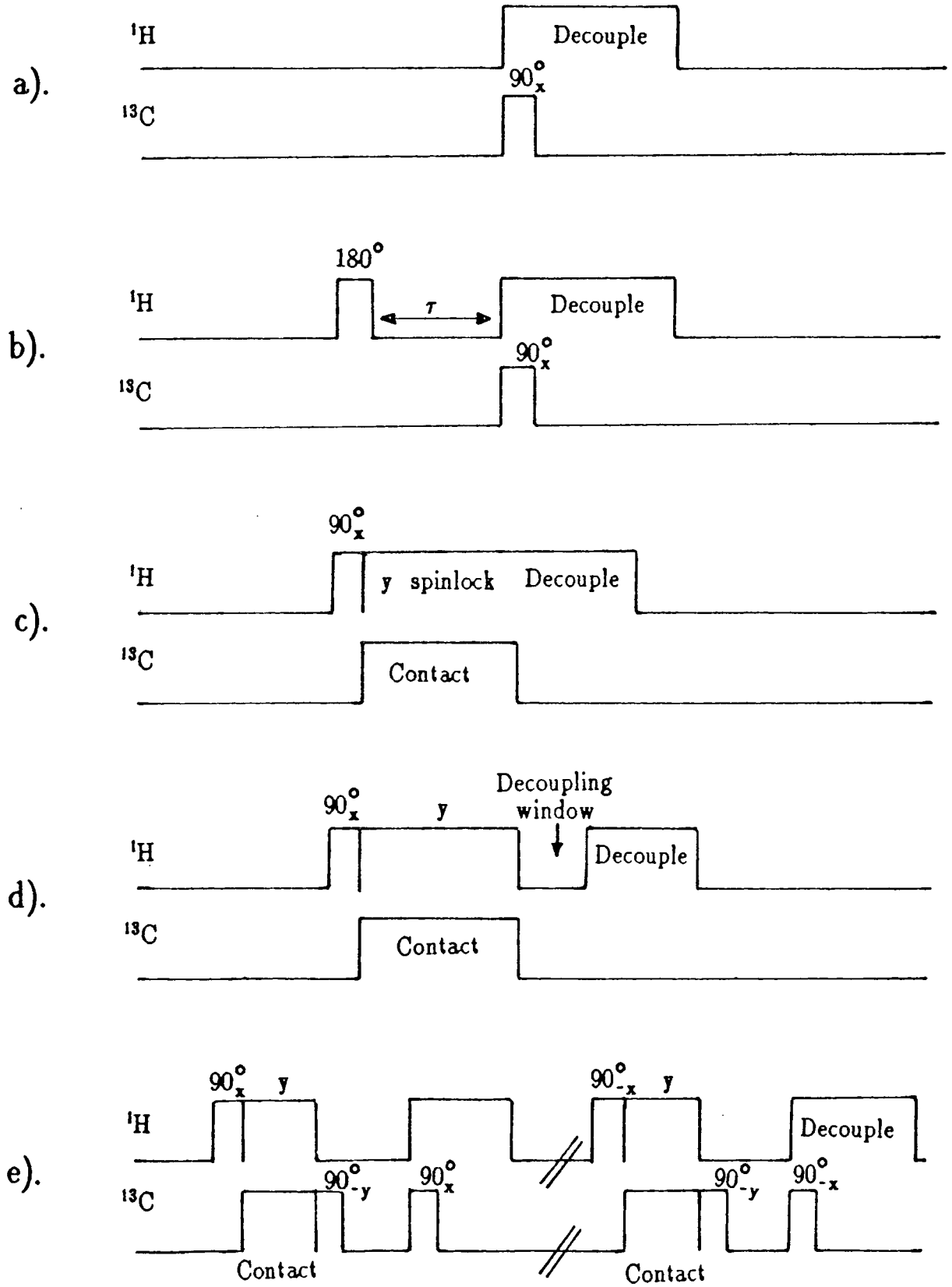

Figure 4.1

a). The pulse sequence for the Single–pulse–excitation experiment.

b). The pulse sequence for the INV1H experiment.

c). The pulse sequence for the Cross–polarisation experiment.

d). The pulse sequence for the NQS experiment.

e). The pulse sequence for the T1CP experiment.

protons are allowed to begin to relax back to equilibrium in delay time τ. The carbon signal is monitored as a function of τ, and thus the effect of the dipolar cross–relaxation between the protons and the carbons can be observed. During the acquisition time high–power proton decoupling is applied to average the strong C–H dipolar interactions to zero.

4.3.3 Cross–polarisation[2]

Often spins which are spatially or isotropically dilute have long T_1 values, whereas the abundant proton spins have T_1 values which are generally shorter than the T_1 values of the dilute spins. The cross–polarisation pulse sequence is shown in figure 4.1c. In this sequence the carbon signal is generated from the abundant spins. A $\pi/2$ proton pulse generates proton magnetisation. This is followed by a $\pi/2$ phase shift of the RF which spin–locks the proton magnetisation. The ^{13}C contact pulse is switched on immediately following the phase shift. If the Hartmann–Hahn condition is satisfied then transfer of polarisation takes place from the abundant proton spins to the dilute carbon spins. The dynamics of the cross–polarisation experiment have already been described in Chapter Three.

4.3.4 Non–quaternary suppression (NQS)[3]

The pulse sequence for the non–quaternary suppression pulse sequence is shown in figure 4.1d. The NQS pulse sequence differs from that of the cross–polarisation experiment only by the insertion of a window in the proton decoupling before acquisition of the FID. The

duration of this window is typically 40 μs. Protonated carbons have strong C–H interactions, and therefore give broad bands. This results in a rapid decay of transverse magnetisation, so that at the end of the decoupling window there is little signal left in the FID from such carbons. On the other hand, quaternary carbons give relatively narrow bands, so there is little decay of magnetisation during the decoupling window. This leaves a substantial signal from quaternary carbons during the carbon acquisition period.

4.3.5 T1CP[4]

The pulse sequence shown in figure 4.1e shows the experiment devised by Torchia for the measurement of the T_1 of dilute spins using cross–polarisation. The experiment consists of two similar but not identical pulse sequences. In the first pulse sequence, transverse carbon magnetisation is generated by CP. This magnetisation is then transferred to the z axis. This longitudinal magnetisation decays exponentially from an initial value $M_{CP}(0)$ to an equilibrium value M in a time characterised by the time constant T_1. This magnetisation is then detected. The second sequence differs from the first in that the proton spin temperature is inverted by a phase shift of π, giving rise to proton enhanced carbon signal of opposite sign to that obtained by the first sequence. Subtraction of the second sequence from the signal generated by the first sequence gives a signal equal to $M_{CP}(0)\exp(-t/T_1)$.

4.4 Fitting of variable contact time measurements

A program has been written on the mainframe computer which fits the data obtained from variable contact time measurements. The variation in the signal observed for the carbon spins with contact time in cross–polarisation experiments was fitted to equation 4.1.

$$M_I(t) = \frac{M_I(0)\gamma_S}{\gamma_I(1-\lambda)}\exp(-t/T_{1\rho}) - \frac{M_I(0)\gamma_S}{\gamma_I(1-\lambda)}\exp(-t/T_{IS}) \qquad (4.1)$$

where $\lambda = T_{IS}/T_{1\rho}$.

Equation 4.1 assumes single–exponential $T_{1\rho}$ behaviour for the peak in question.

The intensity of a particular carbon peak, and its corresponding contact time is read into the program for all the values of the contact time. The program notes the contact time at which the maximum signal intensity is observed (t_{opt}). A least squares fit on the data is then carried out, from which values of $T_{1\rho}$ and T_{IS} are determined. The least squares fit is done in two parts. Firstly the regime where the contact time t is greater than t_{opt} is fitted to a plot of ln $(M_I(t))$ against t to give a value for $T_{1\rho}$. Then, in the regime $t < t_{opt}$, T_{IS} is obtained from the slope of log M against time. The full theoretical curve is then plotted out, and an estimate of how well the parameters T_{IS} and $T_{1\rho}$ fit the curve is made by determining the sum of the squares of the error.

The variable contact time experiment may be used as a discriminating technique. The ^1H $T_{1\rho}$ values, and therefore the slopes of the plots, need not necessarily be the same in any one sample. It is possible for a sample to have more than one proton $T_{1\rho}$ value. This is usually an indication that either there is incomplete spin diffusion, or

that there is more than one proton reservoir in the system as can occur in heterogeneous systems. Variable contact measurements may also be used to obtain quantitative information about a sample. Comparison between two peaks at any individual contact time will not normally provide quantitative intensities. However, if a range of contact times are used, extrapolation back to zero contact time will result in quantitative intensity measurements.

4.5 Cross–linking chemistry

A surface coating may undergo a transition from a liquid or a solution to a film after application. One technique of achieving such films is to use coatings which undergo chemistry to form intractable films. The chemistry may be chain extension, polymerisation, or cross–linking between two polymers.

Many coatings are stoved at temperatures between 120°–250°C to form cross–links between the prepolymers. However there are many cases when such temperature conditions are impractical. For example, when the substrate is very large, such as a ship, coatings which require stoving are unsuitable.

For such cases as these, it is necessary to find an alternative surface coating which will cross–link at ambient temperatures. This is much more difficult. The functional groups of the prepolymers must be much more reactive than for stoving systems. Also ambient temperature and humidity vary according to the weather. Possibly the most successful ambient curing reactions are those undergone by two–pack systems

consisting of two components, each with reactive functional groups. The two components are mixed together. The coating has a finite time or 'pot life' within which it must be applied to the substrate.

One of the earliest types of ambient curing reactions was devised by Bayer during which an isocyanate functional curing agent reacts with an hydroxyl functional polymer forming a urethane linkage. Variations of this curing reaction were also used to form surface coatings with excellent mechanical properties. The one major drawback of chemistry based on these systems is the toxicity of the isocyanates. A substitute reaction of improved toxicity and similar mechanical properties would be extremely desirable.

Various reactions have been proposed for the formation of films with good mechanical properties at ambient temperatures.

4.5.1 Courtaulds Coatings cross–linking chemistry

Courtaulds have devised a cross–linking reaction which cures at ambient temperature. The reaction between an acid anhydride and an alcohol readily occurs at ambient temperature forming the half–ester (figure 4.2). It was found that polymers of either itaconic anhydride or maleic anhydride were the most suitable for this type of reaction[5]. The polymer used is a copolymer of styrene, methyl methacrylate and either itaconic or maleic anhydride. The styrene is included as it has a noticeable moderating effect on the cross–linking reaction. Methyl methacrylate is required in order that the copolymer is compatible with the curing polyester.

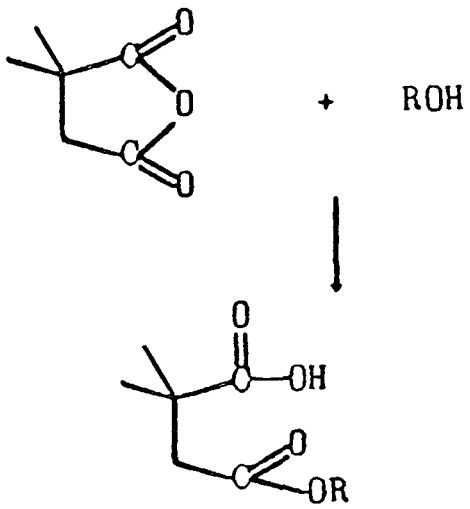

Figure 4.2

The reaction between an acid anhydride and an alcohol readily occurs at ambient temperature forming the half–ester.

Table 4.2

Monomers for the synthesis of the itaconic anhydride copolymer

monomer	% by weight
Itaconic anhydride	20
Styrene	65
Methyl methacrylate	15
Butyl acetate	+100
Vazo 67	+5

the curing polyester.

The curing polyester is formed from adipic acid and a 50/50 mixture of butane–1,4–diol and ethylene glycol. The polyester is tipped with triethanolamine. It has been found that primary alcohols react faster with acid anhydrides than secondary alcohols under the same conditions. It is also known that nitrogenous bases (e.g. tertiary amines) are effective catalysts for the cross–linking reaction. The tertiary amines, however, must be present in similar molar quantities as the reactants in order for the amine to have a noticeable catalytic effect on the rate of reaction. Courtaulds chemistry has incorporated the amine into the polyester chain orientated β to the reactive hydroxyl tip. An amine placed in such a position renders the hydroxyl tip highly reactive. A mechanism for the catalytic effect of amine positioned β to the hydroxyl tip has been suggested by Courtaulds. The mechanism is shown in figure 4.3[6]. It has been suggested that the enhanced reactivity of β–hydroxyamines may be explained in terms of 5–membered cyclic intermediates for nucleophilic catalysts (figure 4.4a) or general base catalysts (figure 4.4b).

4.6 Synthesis of the polymers[7,8]

4.6.1 Synthesis of itaconic anhydride copolymer

The recipe of the ingredients for the synthesis of the itaconic anhydride copolymer is listed in table 4.2. The percentage weight of the individual reactants is given as well as the mass of each reactant required to make up a standard–sized batch of copolymer. The itaconic anhydride was dissolved in some of the butyl acetate (340g). The itaconic

Table 4.3

Percentage weight and mass of monomers to make 1000g of polyester.

monomer	Molar ratio	Mass/g
Adipic acid	2.52	707.6
Ethylene glycol	1.00	119.3
Butane 1,4 diol	1.00	173.1

Figure 4.3

A general base mechanism has been proposed for the reaction between the triethanolamine–tipped polyester and the acid anhydride.

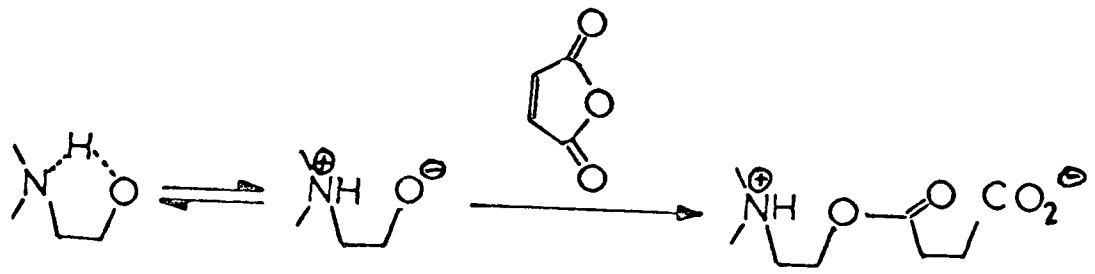

Figure 4.4

It is thought that the enhanced reactivity of β-hydroxyamines may be explained in terms of 5-membered cyclic intermediates for a). nucleophilic catalysts or b). general base catalysts.

a).

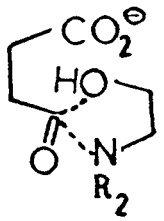

b).

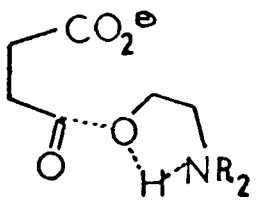

anhydride/butyl acetate solution was then filtered. 80g of the butyl acetate was charged into the reaction vessel. The styrene, methyl methacrylate and the initiator were dissolved in the remainder of the itaconic anhydride/butyl acetate solution. This mixture was then added dropwise to the reaction flask over a period of four hours with continual heating and stirring. The reaction was carried out under nitrogen. The average molecular weight of the itaconic anhydride film was 8000.

4.6.2 Synthesis of the maleic anhydride copolymer

The maleic anhydride copolymer was made in a similar way to the itaconic anhydride copolymer, with the itaconic anhydride replaced by an equivalent mass of maleic anhydride. The synthesis of the maleic anhydride copolymer was carried out according to the method described in the last section. The average molecular weight of the maleic anhydride film was 8000.

4.6.3 Synthesis of the polyester

Table 4.3 lists the percentage weight and the mass of the reactants required to make approximately 1000g of polyester. The quantities of monomers were such that the polymer formed was acid–tipped, and the alcohol component was a 50/50 mixture of ethylene glycol and butane–1,4–diol. The adipic acid, ethylene glycol and butane–1,4–diol were placed together in a reaction flask. The reaction was carried out under nitrogen, and the water was removed by the use of a dean and stark

trap. The reaction took place at a temperature between 160–190°C over a period of two days with continual heating and stirring. Towards the end of the reaction the temperature of the flask was raised by 20°C to drive off the excess water. A small quantity of xylene was added beforehand to prevent decomposition of the polyester. During the reaction, glycol loss was monitored by measuring the refractive index of the water collected by the dean and stark trap, and extra glycol was added to make up for glycol lost during water extraction. The average molecular weight of the polyester was 1000.

4.6.4 Characterisation of the polyester

The polyester was characterised by solution–state ^{13}C and ^{1}H NMR and IR.

4.6.4.1 Determination of the acid value

The acid value is a measure of how many of the polyester chains are acid–tipped. The higher the acid value, the greater is the number of polyester chains with acid end groups.

The amount of polyester used is dependent upon the expected acid value of the sample. Table 4.4 lists the weight of polymer required depending on the expected acid value.

The monomers used to form the polyester were reacted together with a ratio such that the polyester would be acid–tipped. Therefore the expected acid value is >50. Hence 1g of polyester was accurately weighed into a conical flask. This sample was then dissolved in 50ml of acid

Table 4.4

Weight of polymer required for the determination of the acid value.

Expected acid value	Weight of resin/g
<10	5
10–50	5–3
>50	1

value solvent. This solvent is a 3:1 v:v mixture of xylene:butanol containing phenolphthalein indicator (0.1g/litre). This mixture is titrated with 0.1M methanolic KOH until the end point is reached, when a faint pink colour is sustained for more than 10 seconds. The titration is repeated several times, and an average titre taken. A blank titration is also performed on the acid value solvent which may have an inherent acid value.

The acid value (AV) is calculated from equation 4.2.

$$AV = \frac{(A-B)\times M\times 56.1}{W} \qquad (4.2)$$

where W = weight of sample (g)

A = volume (ml) of 0.1M methanolic KOH used to titrate sample

B = volume (ml) of 0.1M methanolic KOH used to titrate blank

M = molarity of methanolic KOH.

The acid value of the polyester is in the region of 130.

The acid equivalent weight (AEW) is calculated by equation 4.3.

$$AEW = \frac{1000\times W}{(A-B)\times M} \qquad (4.3)$$

$$AEW = \frac{5610 0}{AV}$$

The AEW of the polyester is usually in the region of 420.

As the polyester is acid–tipped on both ends, the acid equivalent weight must be doubled.

4.6.5 Tipping of the polyester

The final stage in the formation of the polyester resin is to tip the ends with triethanolamine. The molecular weight of triethanolamine is 149.2. Therefore 149.2g of triethanolamine is equivalent to AEWg of

untipped polyester. To tip Zg of polyester, it is necessary to react the polyester with (149.2×Z)/AVg of triethanolamine.

Untipped polyester was added to an equivalent weight of triethanolamine in a reaction flask together with an equal amount of xylene. The system was refluxed under nitrogen for 2–3 hours. After the reaction was completed, most of the xylene was taken off under vacuum.

4.6.6 Characterisation of tipped polyester

The tipped polyester was characterised by IR, GPC, and ^{1}H and ^{13}C solution–state NMR.

4.6.6.1 Determination of the solids content

The ratio of tipped polyester:xylene was determined by weighing out accurately 1g of the tipped polyester. This sample was then placed in an oven, and the solvent allowed to evaporate. The sample was then reweighed. The percentage solid content of the tipped polyester was calculated by:

$$\% \text{ solid content} = \frac{\text{Mass of the sample after evaporation}}{\text{Mass of the sample before evaporation}} \times 100 \qquad (4.4)$$

This is repeated several times, and an average taken.

The solid content of the copolymers is usually in the region of 53%.

4.6.6.2 Determination of the amine equivalent weight

1g of tipped polyester was dissolved in 50ml of acetic acid. This was titrated against 0.1M $HClO_4$. The titration was repeated several

times, and an average titre taken.

The amine equivalent weight was calculated from equation 4.5.

$$\text{Amine equivalent weight} = \frac{1000 \times \text{Mass}}{0.1 \times \text{titre}} \qquad (4.5)$$

4.6.7 Preparation of the polymeric films

The polymeric films were prepared by mixing together stoichiometric amounts of either itaconic or maleic anhydride copolymer and the triethanolamine–tipped polyester in a 1:1 ratio of equivalent weights. The film was drawn evenly on a PTFE sheet and allowed to cure at room temperature for two weeks. For the solid–state NMR experiments, the film was powdered under liquid nitrogen, and then stored in a sample jar until required. Throughout this thesis, the film made with the itaconic anhydride copolymer will be referred to as itaconic anhydride film, and similarly the film made with the maleic anhydride copolymer will be referred to as maleic anhydride film.

4.6.8 Synthesis of polyester with ^{13}C enrichment

Polyester was made on a small scale with 90% $^{13}C_2$–enriched ethylene glycol. 1.9g of the enriched ethylene glycol was purchased from MSD Isotopes. Before making the enriched polyester, trial runs were carried out using scaled–down proportions of monomer.

4.6.8.1 The trial run

The amount of monomers required to react with 1.9g of ethylene glycol is shown in table 4.5. The monomers were placed together in a

Table 4.5

Mass of monomers required to form the polyester from 1.9g of $^{13}C_2$–enriched ethylene glycol.

Monomer	weight/g
Adipic acid	11.27
Butane 1,4 diol	2.76
Ethylene glycol	1.90

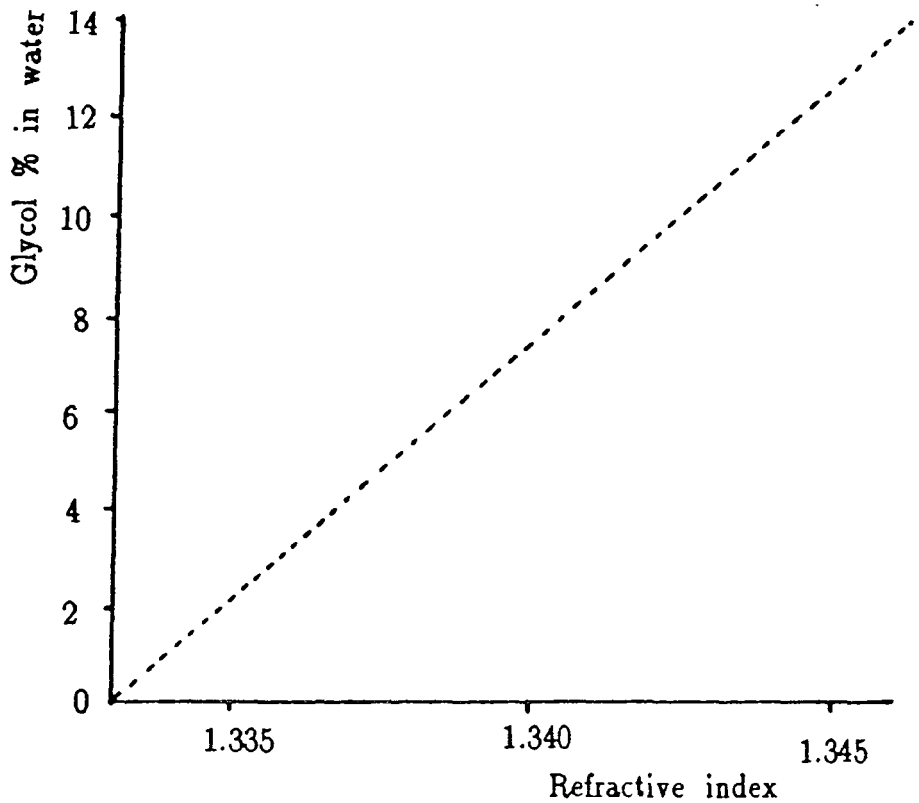

Figure 4.5

The determination of ethylene glycol content of distillate water using refractive index.

50ml flask. A small dean and stark trap was fitted, and the monomers were stirred and heated at 170°C for two days. The dean and stark trap was designed so that only water could collect at this temperature; the temperature in the flask was insufficient for ethylene glycol to be collected by the dean and stark trap. This would prevent expensive loss of ethylene glycol when enriching. The water collected by the dean and stark trap was monitored for glycol content by refractive index measurements. The refractive index of the water was measured at 1.34, which corresponds to 1% ethylene glycol content (figure 4.5). This loss was minimal. The polyester product was characterised by GPC, IR and ^{13}C and ^{1}H solution–state NMR.

4.6.8.2 Tipping of the polyester

A trial run of the final stage of the polyester formation was carried out on a similar scale. 4.76g of triethanolamine was added to 13.3g of polyester. An equivalent weight of xylene was added, and the mixture was refluxed at 160°C for 2–3 hours. After the reaction was completed, the flask was allowed to cool, and the xylene extracted under vacuum.

4.6.8.3 Characterisation of the polyester

The product was characterised by GPC, IR and ^{13}C and ^{1}H solution–state NMR. The product was found to be identical to the tipped polyester made using the standard bulk method as described in section

Figure 4.6

The ^{13}C solution–state spectrum of $^{13}C_2$–enriched polyester. The recycle delay was 3 seconds, the acquisition time 1.2 seconds and 256 transients were acquired.

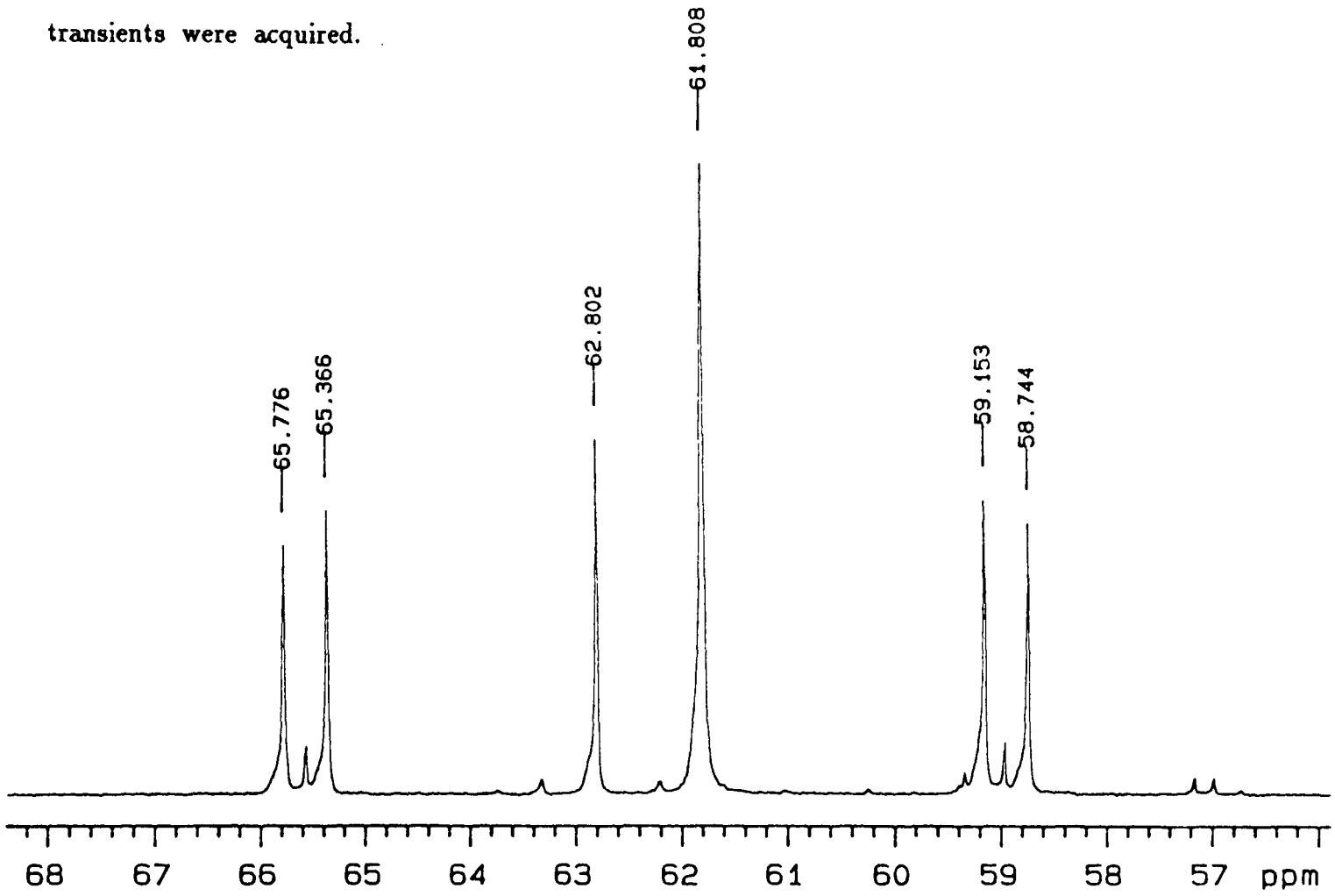

4.6.8.1. Both stages of this synthesis were each repeated several times to ensure that the enrichment would produce polyester.

4.6.8.4 The enrichment

1.9g of 90% $^{13}C_2$–enriched ethylene glycol, 2.76g of butane 1,4 diol and 11.27g of adipic acid were placed in a 50ml flask. The method used to make the enriched polyester follows that described for the trial run exactly.

4.6.8.5 Characterisation

The refractive index of the water was measured to be 1.34. this corresponds to 1% loss of enriched ethylene glycol during the synthesis. The enriched tipped polyester was checked by solution–state ^{13}C NMR. The solution–state ^{13}C spectrum obtained is shown in figure 4.6. The peak due to the expected product is present at 62.8ppm. The assignments of the other peaks can be, found in Chapter Eight.

CHAPTER 5

Spectral assignment and kinetics

5.1 Spectral assignment of the polymeric films

The solid–state ^{13}C cross–polarisation NMR spectra of both the maleic anhydride film and the itaconic anhydride film are complex. Figure 5.3a shows the CP spectrum of the itaconic anhydride film. With so many overlapping and obscured peaks, assignment of the spectra is not a straight–forward task. In order to fully assign the spectra, it is necessary to simplify the spectra as much as possible using discriminating techniques such as non–quaternary suppression (NQS)[1] and single pulse excitation (SPE) pulse sequences.

5.1.1 Assignment of the itaconic anhydride copolymer

The ^{13}C cross–polarisation spectrum of the itaconic anhydride copolymer is shown in figure 5.1a, together with the structure of the copolymer. The spectrum would be greatly simplified if the peaks due to the quaternary carbons could be identified and assigned. One method of achieving this is by using the non–quaternary suppression pulse sequence. Figure 5.1b shows the NQS spectrum of the itaconic anhydride copolymer with assignments. The assignments were made by searches for similar compounds in the ^{13}C NMR database at Daresbury and by comparing the solution–state shifts for similar carbons in a ^{13}C NMR databook[2]. By comparing the NQS spectrum with the CP spectrum of the itaconic

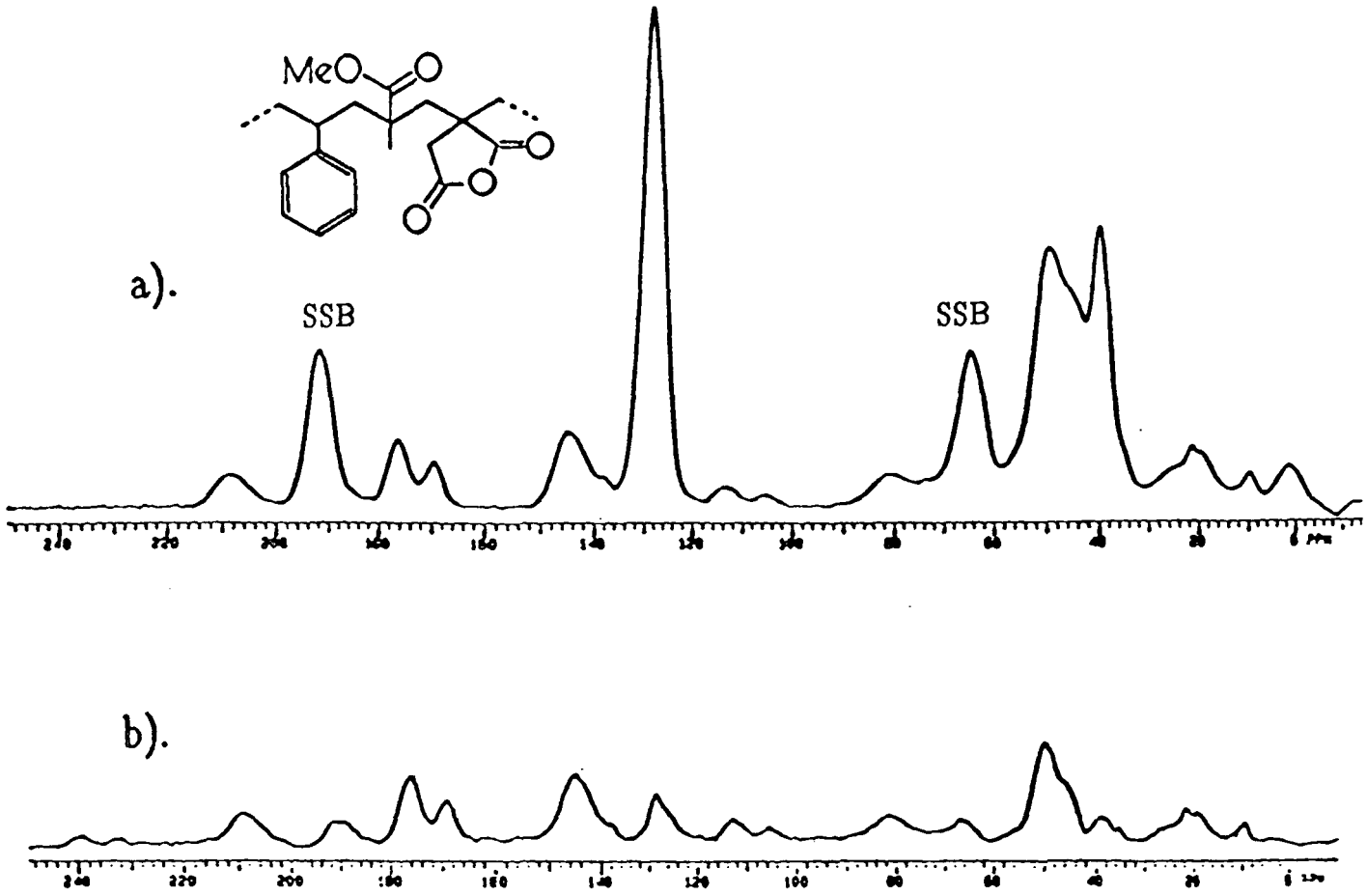

Figure 5.1

a). The ^{13}C cross–polarisation spectrum of the itaconic anhydride copolymer.

b). The NQS ^{13}C spectrum of the itaconic anhydride copolymer. A decoupling window of 40 μs was used.

parameters	contact time = 1.5 ms
	NT = 1000
	Recycle delay = 6 seconds
	Acquisition time = 26 ms.

Table 5.1

Assignment of the peaks in the itaconic anhydride copolymer spectrum.

Peak/ppm	Assignment
176	C=O of MMA
169.5	C=O of itaconic anhydride
144.8	Aromatic quaternary carbon of styrene
128.3	Aromatic C–H of styrene
49.6	CH_3O of MMA
49	Quaternary carbon of itaconic anhydride
45	Quaternary carbon of MMA
40–45	CH backbone carbons
41.5	CH of polystyrene
40.1	CH_2 'backbone' of copolymer
19.8	CH_3 of MMA

Table 5.2

Assignment of the peaks in the polyester spectrum.

Peak/ppm	Assignment
173	C=O in ester
64	$0{=}C{-}O{-}CH_2$
34	$O{-}C(=O){-}CH_2$
25	CH_2 'backbone'

Figure 5.2

The ^{13}C solution–state spectrum of the polyester. Deuterated acetone was used as a solvent.

Parameters: Recycle delay = 3 seconds

AQ = 1.2 seconds

NT = 1024

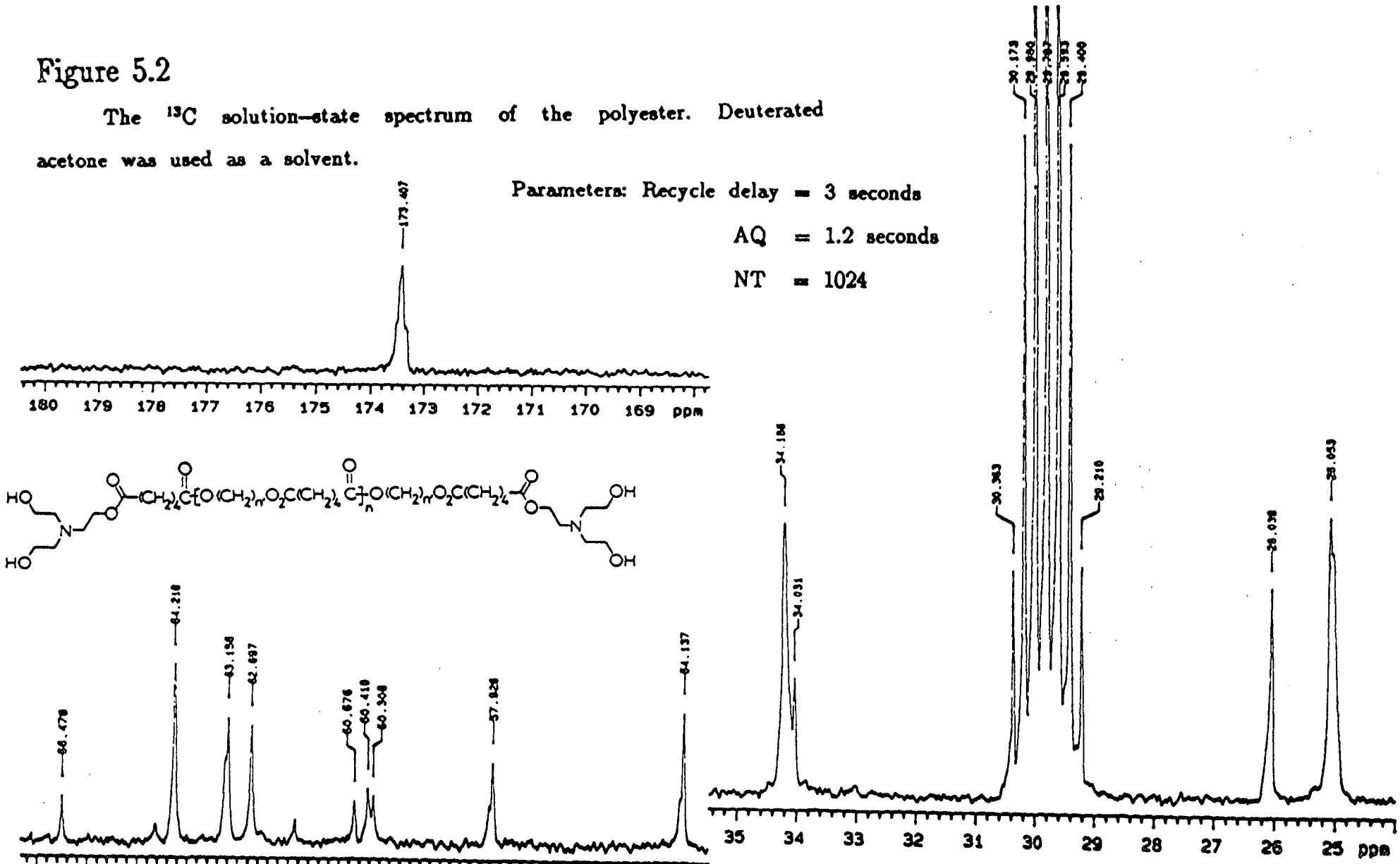

anhydride copolymer, it is possible to assign the remaining carbons in the itaconic anhydride copolymer. A full assignment of the itaconic anhydride copolymer is shown in Table 5.1.

5.1.2 Assignment of the polyester

The solution–state ^{13}C spectrum of the polyester tipped with triethanolamine is shown in figure 5.2 together with the structure of the polyester. The assignments were made on the basis of predicted chemical shifts in the ^{13}C NMR chemical shift data handbook[2]. An assignment of the peaks in the spectrum is shown in Table 5.2.

5.1.3 Assignment of the itaconic anhydride film

The ^{13}C cross–polarisation spectrum of the itaconic anhydride copolymer is shown together with the ^{13}C cross–polarisation spectrum of the itaconic anhydride film in figures 5.3a and 5.3b respectively. There are four main extra peaks at 25, 34, 64 and 173 ppm in the ^{13}C CP spectrum of the itaconic anhydride film which were not present in the ^{13}C CP spectrum of the itaconic anhydride copolymer. These peaks are due to the polyester component of the film. The assignments were made by looking–up the predicted chemical shift in the ^{13}C NMR chemical shift handbook[2], and comparing this predicted chemical shift with the four peaks observed. The chemical shifts and assignments of the peaks in the ^{13}C CP spectrum of the itaconic anhydride film are listed in Table 5.3.

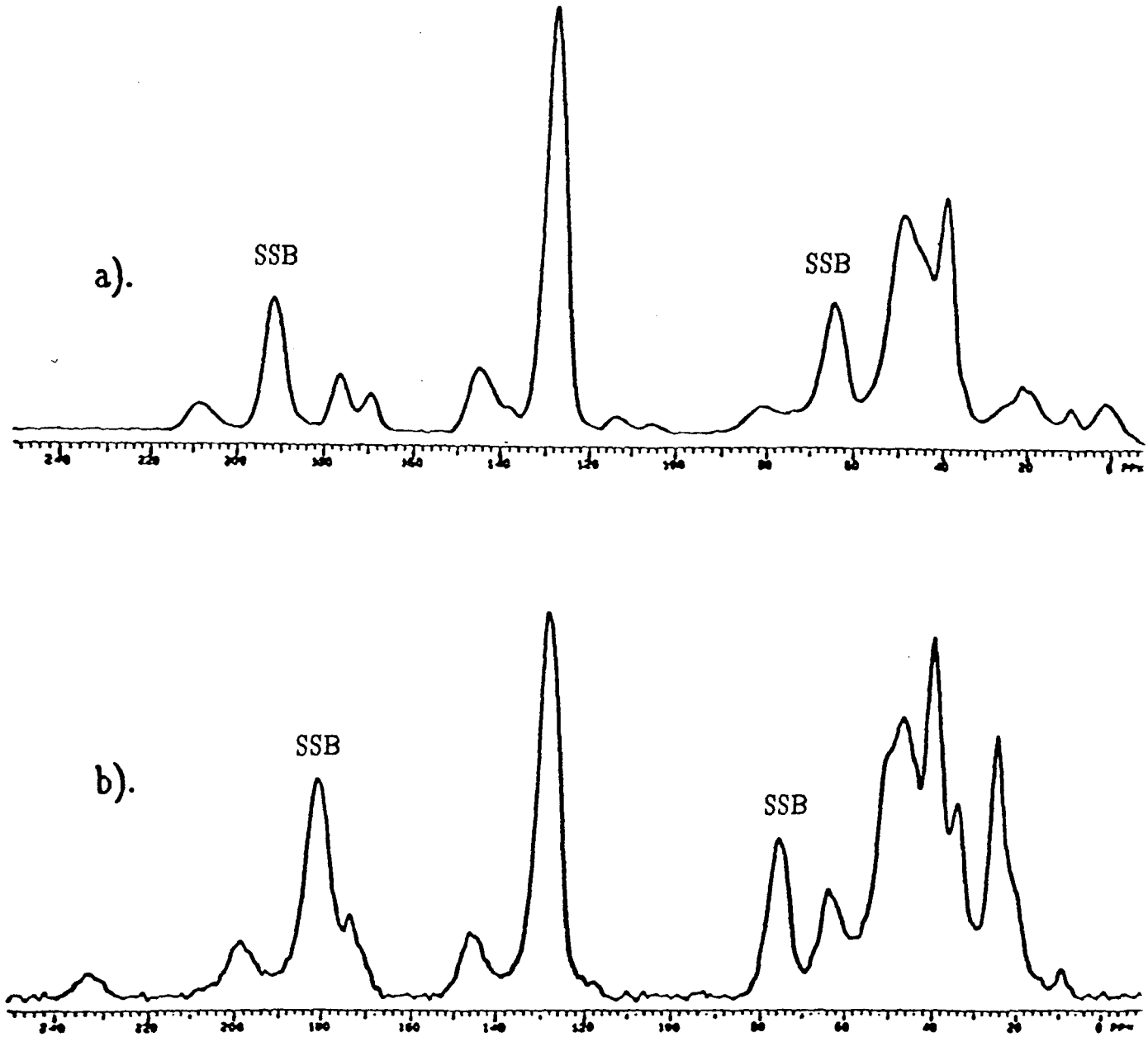

Figure 5.3

a). The ^{13}C CP spectrum of the itaconic anhydride copolymer.

b). The ^{13}C CP spectrum of the itaconic anhydride film.

Parameters

Contact time = 1.5 ms

NT = 1000

Recycle delay = 6 seconds

Acquisition time = 26 ms.

Table 5.3

Assignment of the peaks in the itaconic anhydride film spectrum.

Peak/ppm	Assignment
173.5	C=O of MMA, cross–link, and polyester
144.8	Aromatic quaternary carbon of styrene
128.3	Aromatic C–H of styrene
63	O=C–O–CH_2 in polyester chain
49.6	CH_3O of MMA
45	Quaternary carbon of MMA
40–45	CH backbone carbons
41.5	CH of polystyrene
40.1	CH_2 'backbone' of copolymer
33.5	O–C(=O)–CH_2 in polyester chain
25	CH_2 'backbone' of polyester
19.8	CH_3 of MMA

Table 5.4

Assignment of the peaks in the maleic anhydride copolymer spectrum.

Peak/ppm	Assignment
173	C=O composite peak of MMA and maleic anhydride
143	Aromatic quaternary carbon of styrene
128.4	Aromatic C–H of styrene
51.1	CH_3O of MMA
45.3	Quaternary carbon of MMA
40–45	CH backbone carbons
41.5	CH of polystyrene
40.9	CH_2 'backbone' of copolymer
19.7	CH_3 of MMA

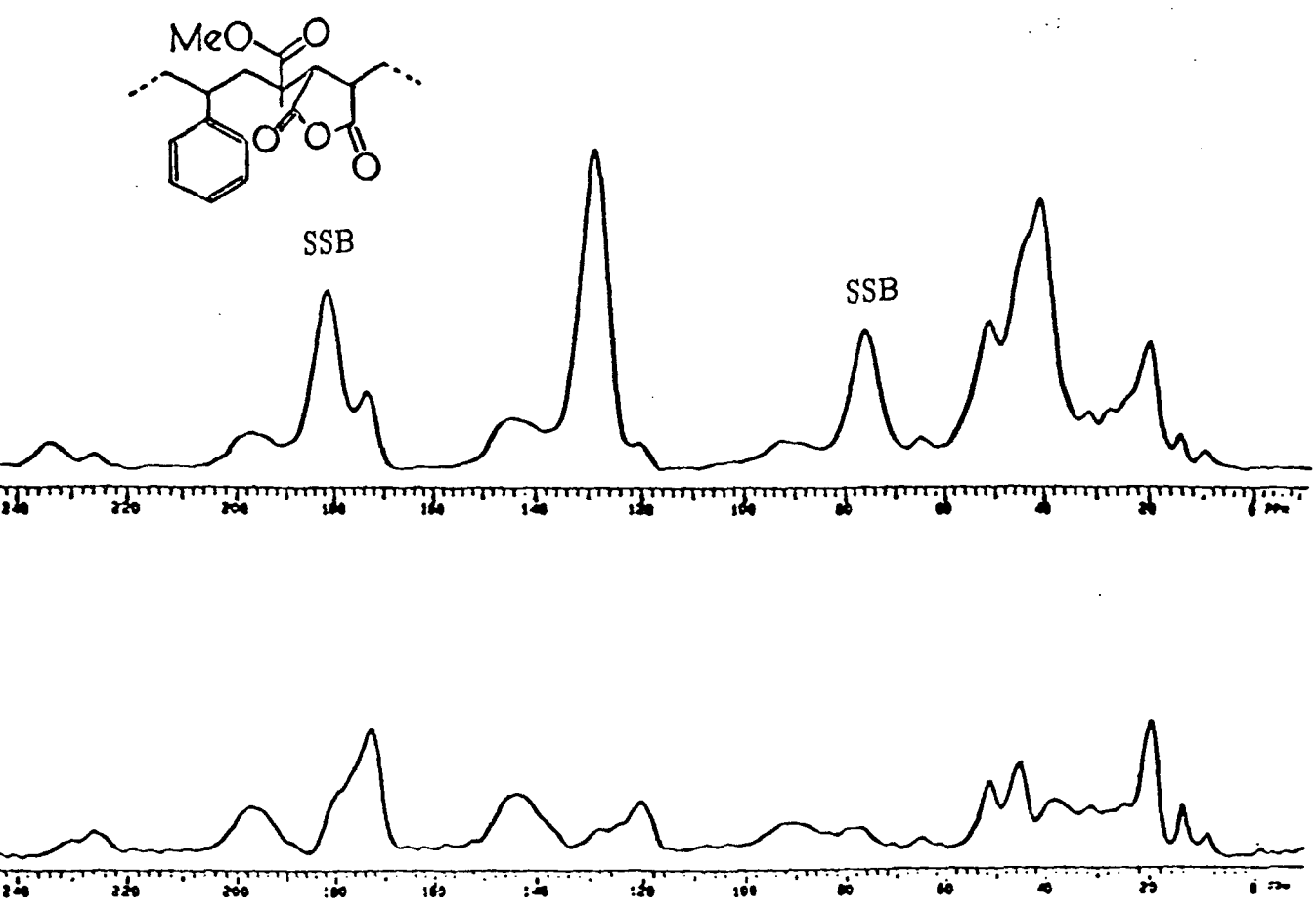

Figure 5.4

a). The ^{13}C cross–polarisation spectrum of the maleic anhydride copolymer.

b). The NQS ^{13}C spectrum of the maleic anhydride copolymer. A decoupling window of 40 μs was used.

parameters	contact time = 1.5 ms
	NT = 1000
	Recycle delay = 6 seconds
	Acquisition time = 26 ms.

5.1.4 Assignment of the maleic anhydride copolymer

The assignments of the peaks in the CP spectrum of the maleic anhydride copolymer were made in a similar way to those in the itaconic anhydride copolymer. Figure 5.4 shows the NQS spectrum of the maleic anhydride copolymer together with the CP spectrum of the same sample. The NQS spectrum shows peaks arising from quaternary carbons only. The assignments shown were made on the basis of the predictions of the chemical shifts of the quaternary carbons from the ^{13}C NMR chemical shift databook.[2] Comparison between the NQS spectrum and the CP spectrum of the maleic anhydride copolymer allows the non–quaternary peaks in the maleic anhydride copolymer to be assigned using the ^{13}C chemical shift databook. The full assignment of the maleic anhydride copolymer is shown in Table 5.4.

5.1.5 Assignment of the maleic anhydride film

The ^{13}C cross–polarisation spectrum of the maleic anhydride copolymer is shown together with the ^{13}C cross–polarisation spectrum of the maleic anhydride film in figure 5.5. In the same manner as for the itaconic anhydride film, comparison between these two spectra shows that there are four main additional peaks in the CP spectrum of the maleic anhydride film. These peaks at 25, 34, 64 and 173 ppm are assigned to the polyester regions of the maleic anhydride film. A full assignment of the peaks in the ^{13}C CP spectrum of the maleic anhydride film is shown in Table 5.5.

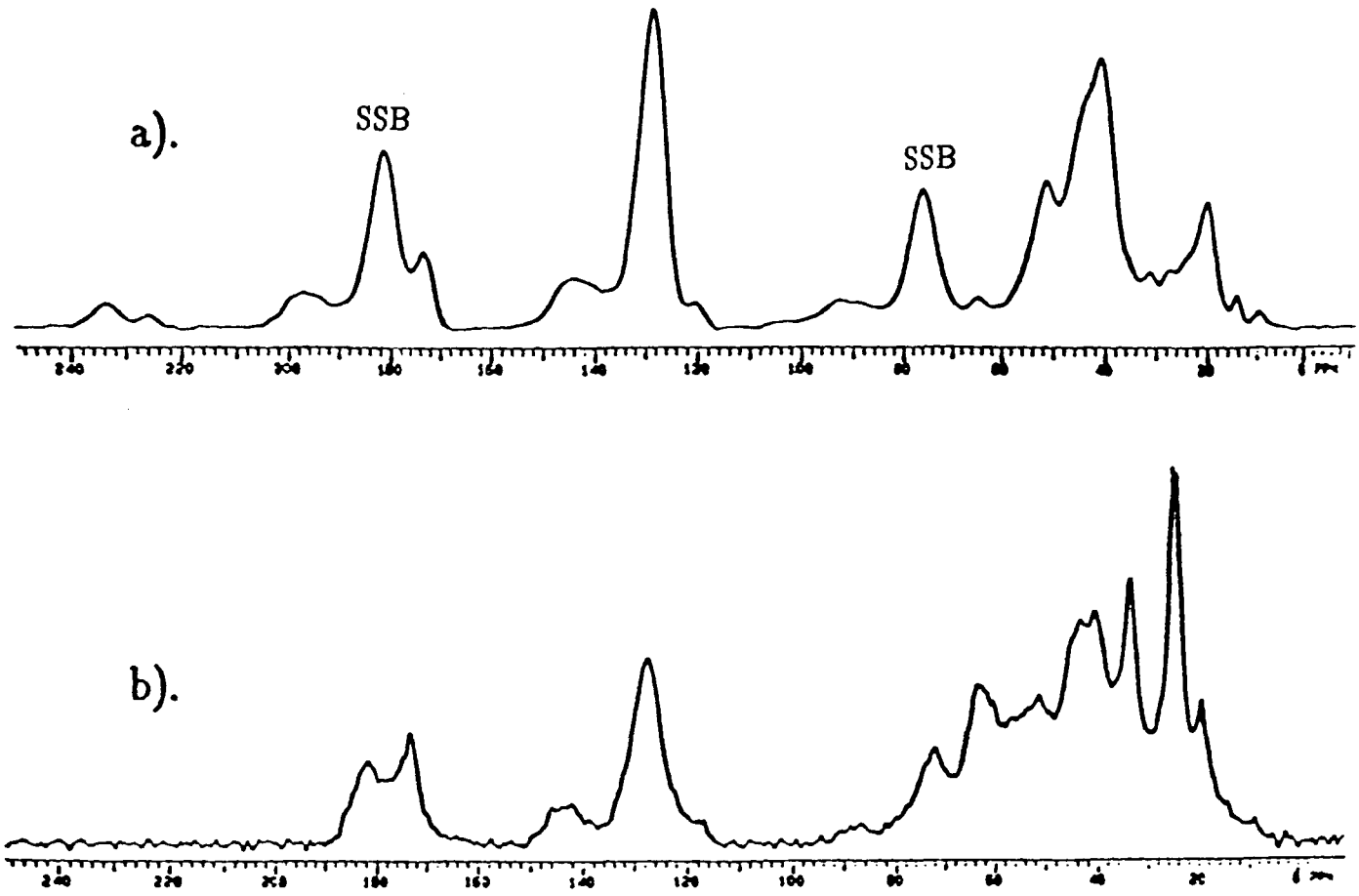

Figure 5.5

a). The ^{13}C CP spectrum of the maleic anhydride copolymer.

b). The ^{13}C CP spectrum of the maleic anhydride film.

Parameters	Contact time = 1.5 ms
	NT = 1000
	Recycle delay = 6 seconds
	Acquisition time = 26 ms.

Table 5.5

Assignment of the peaks in the maleic anhydride film spectrum.

Peak/ppm	Assignment
173.5	C=O of MMA, cross–link, and polyester
143	Aromatic quaternary carbon of styrene
127.8	Aromatic C–H of styrene
63.1	O=C–O–CH_2 in polyester chain
51.3	CH_3O of MMA
45	Quaternary carbon of MMA
40–45	CH backbone carbons
41.5	CH of polystyrene
40.8	CH_2 'backbone' of copolymer
33.8	O–C(=O)–CH_2 in polyester chain
24.9	CH_2 'backbone' of polyester
19.6	CH_3 of MMA

5.2 Polyester carbons of differing mobilities

The spectra of polymers will consist of a superposition of subspectra from carbons of different mobilities which may be in similar chemical environments and hence have overlapping resonances. It is of great interest to be able to discriminate between these mobilities and to be able to obtain spectra of carbons with different mobilities separately. To obtain spectra of the more mobile carbons, a simple 90° (^{13}C) repetitive (single–pulse–excitation) pulse sequence with high–power decoupling can be used. This experiment will discriminate in favour of carbons with short $T_1(^{13}C)$ if the repetition rate of the pulses is reasonably high. The pulse sequence for the single–pulse–excitation (SPE) experiment is shown in figure 5.6. The shorter the recycle delay, t_d, the more mobile are the carbons observed in the corresponding spectrum. A set of SPE spectra were acquired for the itaconic anhydride film. The recycle delay was varied between 0.05 and 10 seconds. Four of the spectra acquired with recycle times of 0.05, 0.2, 0.5 and 10 seconds are shown in figure 5.7a–d. Figure 5.7a with a recycle time of 0.05 seconds shows four peaks at 19, 25, 34 and 64 ppm. The peaks at 25, 34 and 64 ppm originate from the polyester chains in the film, and the peak at 19 ppm originates from the CH_3 in the copolymer chains. In general, the shorter the recycle time, the more mobile are the carbons shown in the spectrum. Thus the polyester chains in the film are much more mobile than the copolymer chains. As the recycle time is increased, peaks due to the more rigid copolymer chains begin to appear in the spectra. The apparent decrease in intensity of the peaks at 19, 25, 34 and 64 ppm

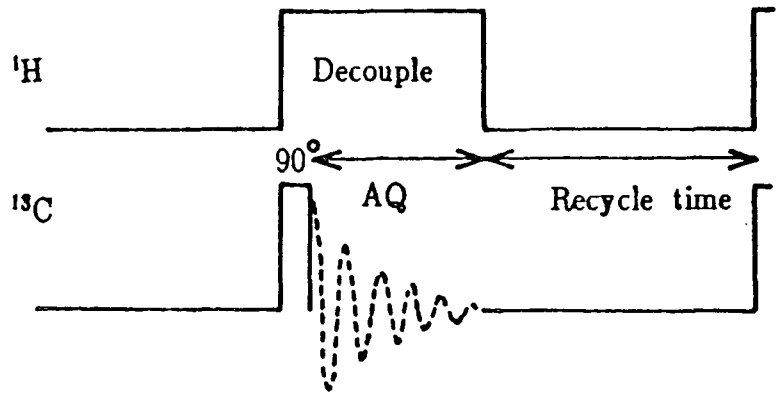

Figure 5.6

The pulse sequence for the single–pulse–excitation experiment.

between 0.5 and 10 seconds was thought to have arisen from transient nuclear Overhauser effects.[3] This suggestion is shown to be correct in Chapter Seven. Figure 5.8a–d shows similar SPE spectra of the maleic anhydride film for recycle times of 0.5, 0.75, 1.5 and 2 seconds. The peaks at 25, 34 and 64 ppm decrease substantially as the recycle time is increased. Again, this was thought to arise from transient nuclear Overhauser effects. The carbonyl peak of the polyester at 173 ppm increases as the recycle time increases. The carbonyl does not have any attached protons, thus the C–H interactions between the carbonyl and its neighbouring protons are a little weaker than for the carbons with protons directly bonded to them. Hence the carbonyl carbon, even though it is mobile, does not show transient nuclear Overhauser effects. One point of particular interest in figure 5.8 is that the peak at 64 ppm with a recycle time of 0.5 seconds shows fine structure, which is subsequently lost as the recycle time is increased. The fine structure of the peak at 64 ppm shows two peaks resolved at 62.1 ppm and 63.3 ppm. These peaks originate from the CH_2 in the alcohol component of the polyester next to the ester linkage in the polyester chain. The ethylene glycol component gives rise to the peak at 62.1 ppm, and the butane–1,4 diol component gives rise to the peak at 63.3 ppm. One possible explanation for this loss of structure is that there are two types of polyester present in the film, one slightly more mobile than the other. This would result in a two component carbon T_1 for the polyester peaks: a shorter T_1 component arising from the more mobile polyester chains, and a longer T_1

Figure 5.7

Single–pulse–excitation spectra of the itaconic anhydride film obtained with a recycle time of a). 0.05 seconds b). 0.2 seconds c). 0.5 seconds and d). 10 seconds.

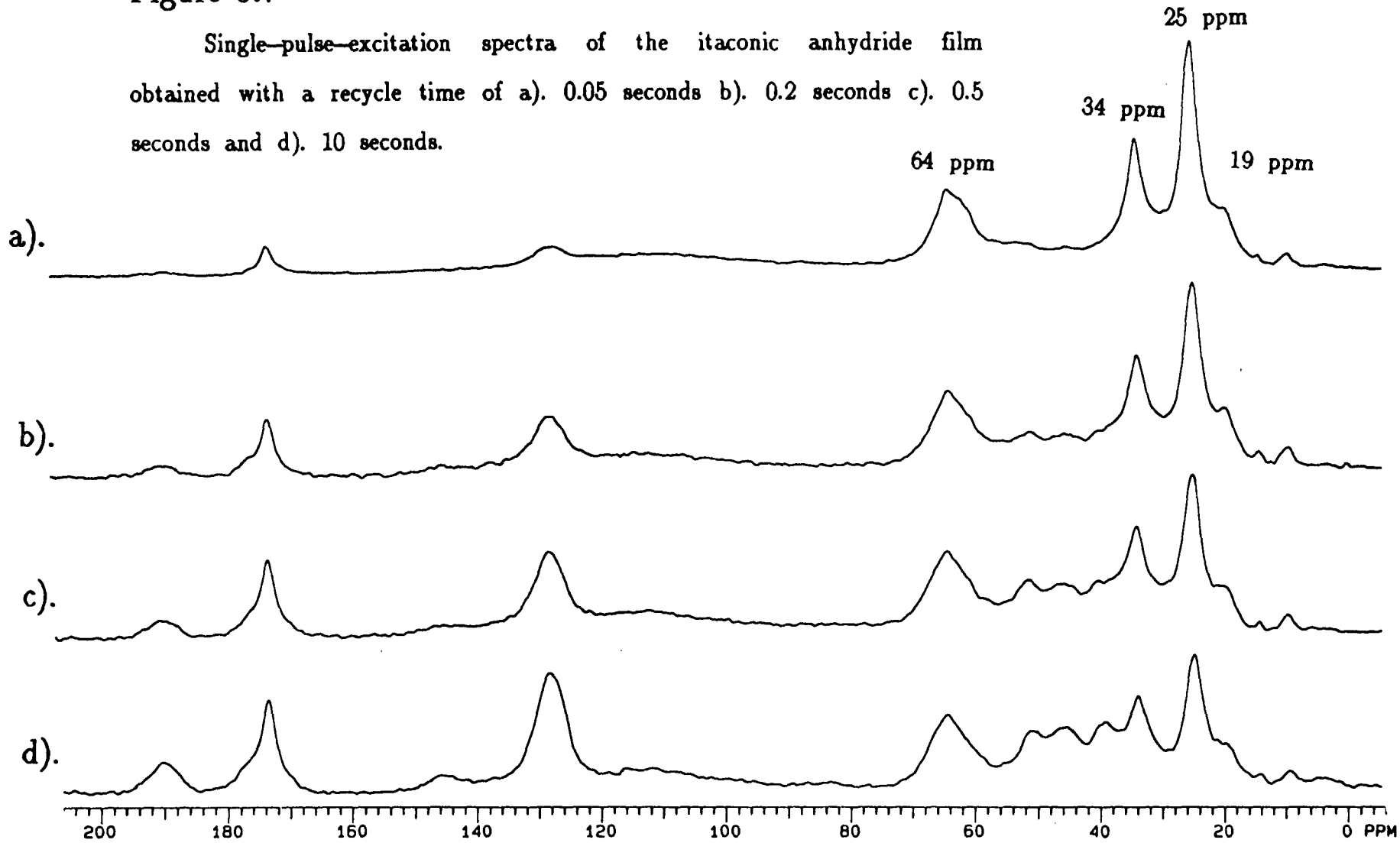

Parameters: NT = 1000

AQ = 20 ms

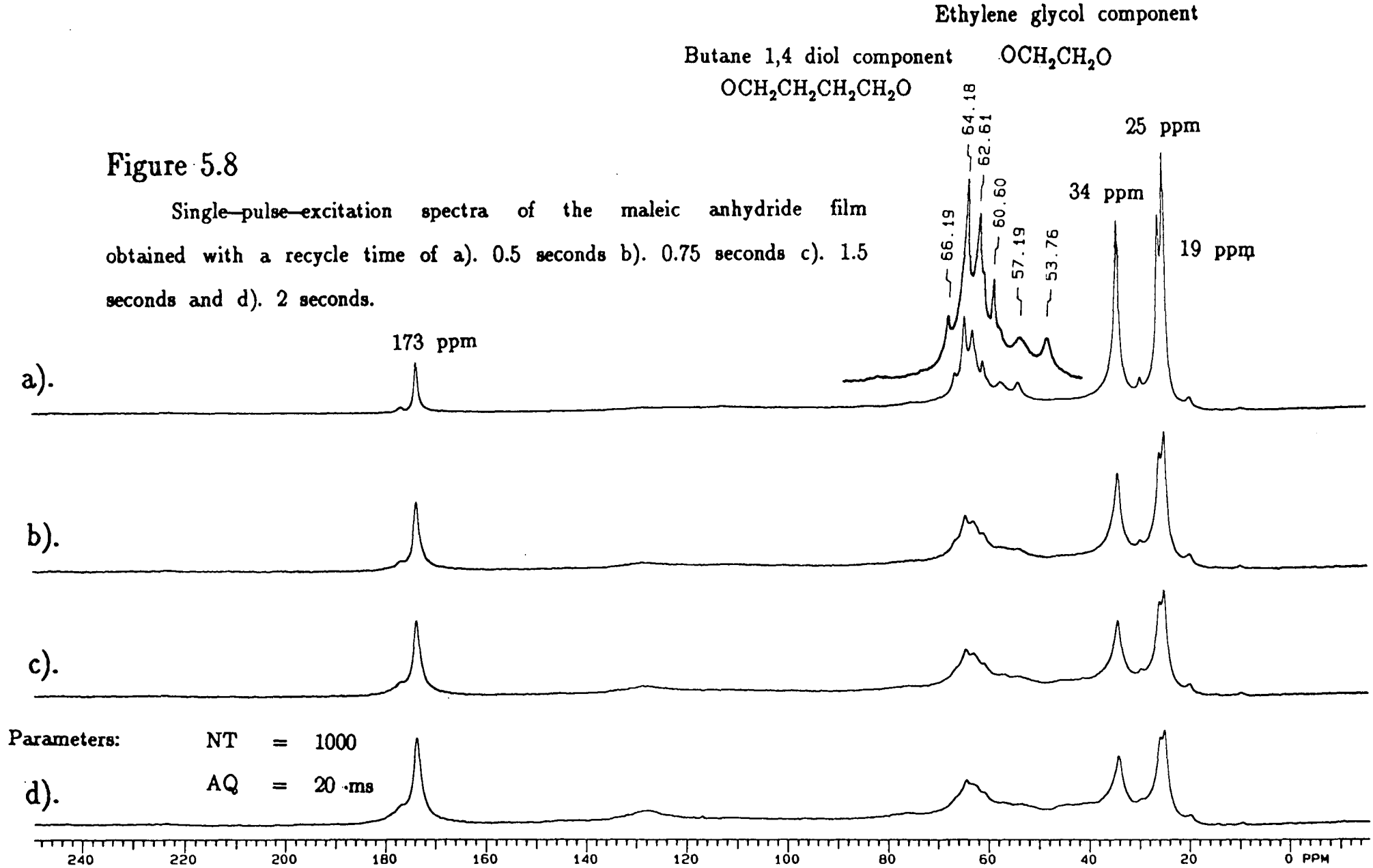

Figure 5.8

Single–pulse–excitation spectra of the maleic anhydride film obtained with a recycle time of a). 0.5 seconds b). 0.75 seconds c). 1.5 seconds and d). 2 seconds.

component arising from the less mobile polyester chains. It is not easy to distinguish a two component carbon T_1 from a single component carbon T_1 using conventional techniques to measure the T_1. This is because usually only a few datapoints are obtained for each peak on account of the large amount of time which a ^{13}C T_1 experiment takes. It is totally impractical to obtain enough datapoints to distinguish between a two component or a one component carbon T_1 via the inversion recovery method. Another well–known method of measuring carbon T_1's is by using the method proposed by Torchia[4] involving cross–polarisation. However this method is suitable for more rigid carbons because of the cross–polarisation stage in the pulse sequence.

5.2.1 Measurement of the shorter carbon T_1 component

A new pulse sequence has been devised which specifically measures short carbon T_1's. The pulse sequence for the measurement of short spin–lattice relaxation times for ^{13}C in solid polymers is presented in figure 5.9. The usual way to measure the carbon spin–lattice relaxation times in a sample in the solid–state is by using the inversion recovery pulse sequence. However in some cases it is not feasible to use this method. For example, when spectra are complex with overlapping peaks from carbons with short and long relaxation times, the inversion–recovery method will produce complicated recovery curves because of the requirement for a long recycle delay to allow full recovery between successive 180° pulses. The MOST pulse sequence was devised to measure the carbon T_1's of the mobile chains in a solid polymer. The mobile

Figure 5.9

MOST: The pulse sequence for the measurement of short carbon T_1 values.

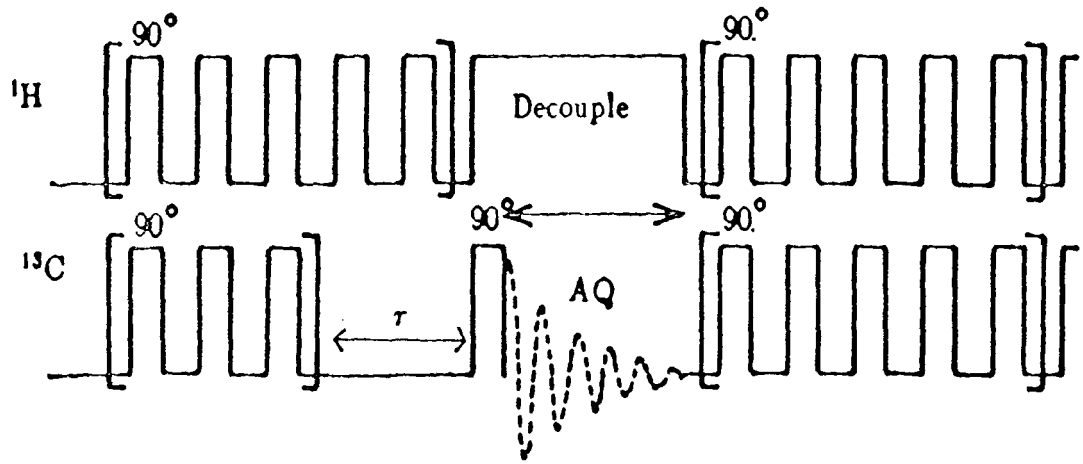

polymer chains of such a system tend to have short carbon T_1's, but more rigid polymer chains (with longer carbon T_1's) give peaks in the same part of the spectrum as the mobile carbons.

An $I=\frac{1}{2}$ spin is saturated when the populations of the two energy levels are equal. This situation occurs when the magnetisation is placed in the xy plane. Therefore a succession of 90° pulses at the proton frequency during the recycle delay saturates the proton spins. A similar saturation chain applied at the carbon frequency saturates the carbon spins. In practice 5 μs 90° proton and carbon pulses were applied alternately every 1ms during the saturation chain. During the recovery time, τ, only the proton saturation pulses are continued.

The aim of the pulse sequence is to monitor the recovery of the carbon signal from saturation whilst the proton spins remain saturated. One effect of saturating the proton spins is to increase the carbon signal by the nuclear Overhauser enhancement factor. The saturation–recovery method for determining T_1 for solutions is not generally applicable to the solid–state because of the risk that a large duty–cycle of high–power decoupling may damage the probe. The maximum ^1H duty–cycle used in the following experiments is 0.007, though obviously there is also ^{13}C irradiation to consider.

Solomon[5] derived equations through consideration of the population changes to describe the behaviour of macroscopic magnetisation with time. Consider a pair of coupled spins $^{13}C \equiv I=\frac{1}{2}$ and $^1H \equiv S=\frac{1}{2}$. These obey the coupled equations:

$$\frac{d\langle I_z\rangle}{dt} = -\frac{1}{T_1^{II}}\left[\langle I_z\rangle - I_0\right] - \frac{1}{T_1^{IS}}\left[\langle S_z\rangle - S_0\right] \qquad (5.1a)$$

$$\frac{d\langle S_z\rangle}{dt} = -\frac{1}{T_1^{SI}}\left[\langle I_z\rangle - I_0\right] - \frac{1}{T_1^{SS}}\left[\langle S_z\rangle - S_0\right] \qquad (5.1b)$$

where

$1/T_1^{SS}$ is the total direct relaxation rate of the protons

$1/T_1^{II}$ is the total direct relaxation rate of the carbons

$1/T_1^{IS}$ is the cross–relaxation rate,

and I_0, S_0 are the Boltzmann equilibrium values of I_z, S_z respectively. The intensity of the carbon magnetisation, $\langle I_z\rangle$, at any instant in a single–pulse experiment may be calculated by solving the above linear simultaneous differential equations under the appropriate boundary conditions.

These boundary conditions are:

$$\langle I_z\rangle(0)=0 \qquad (5.2a)$$

$$\langle S_z\rangle(0)=\langle S_z\rangle(\tau)=0 \qquad (5.2b)$$

This results in expression 5.3 for the intensity of the carbon signal at the end of the delay period τ.

$$\langle I_z\rangle_\tau = \left[\frac{S_0 T_1^{II}}{T_1^{IS}} + I_0\right]\left[1 - \exp(-\tau/T_1^{II})\right] \qquad (5.3)$$

Figure 5.10 shows the growth from saturation of the polyester carbons in the itaconic anhydride film with τ values ranging between 0.05 and 8 seconds (infinity measurement). By fitting the experimentally measured carbon intensities to equation 5.3, it is possible to obtain values for the carbon spin–lattice relaxation time, T_1^{II}. The fitted intensities are

Table 5.6

Short carbon T_1 values of the polyester chains in the itaconic anhydride film.

Peak/ppm	Assignment	Short $T_1(^{13}C)$/secs
64	O=C–O–CH_2	0.36
34	O–C(=O)–CH_2	0.29
25	CH_2 'backbone'	0.28
19	CH_3 of MMA	0.29

Table 5.7

Short carbon T_1 values of the polyester chains in the maleic anhydride film.

Peak/ppm	Assignment	Short $T_1(^{13}C)$/secs
64	O=C–O–CH_2	0.31
34	O–C(=O)–CH_2	0.33
25	CH_2 'backbone'	0.26
19	CH_3 of MMA	0.57

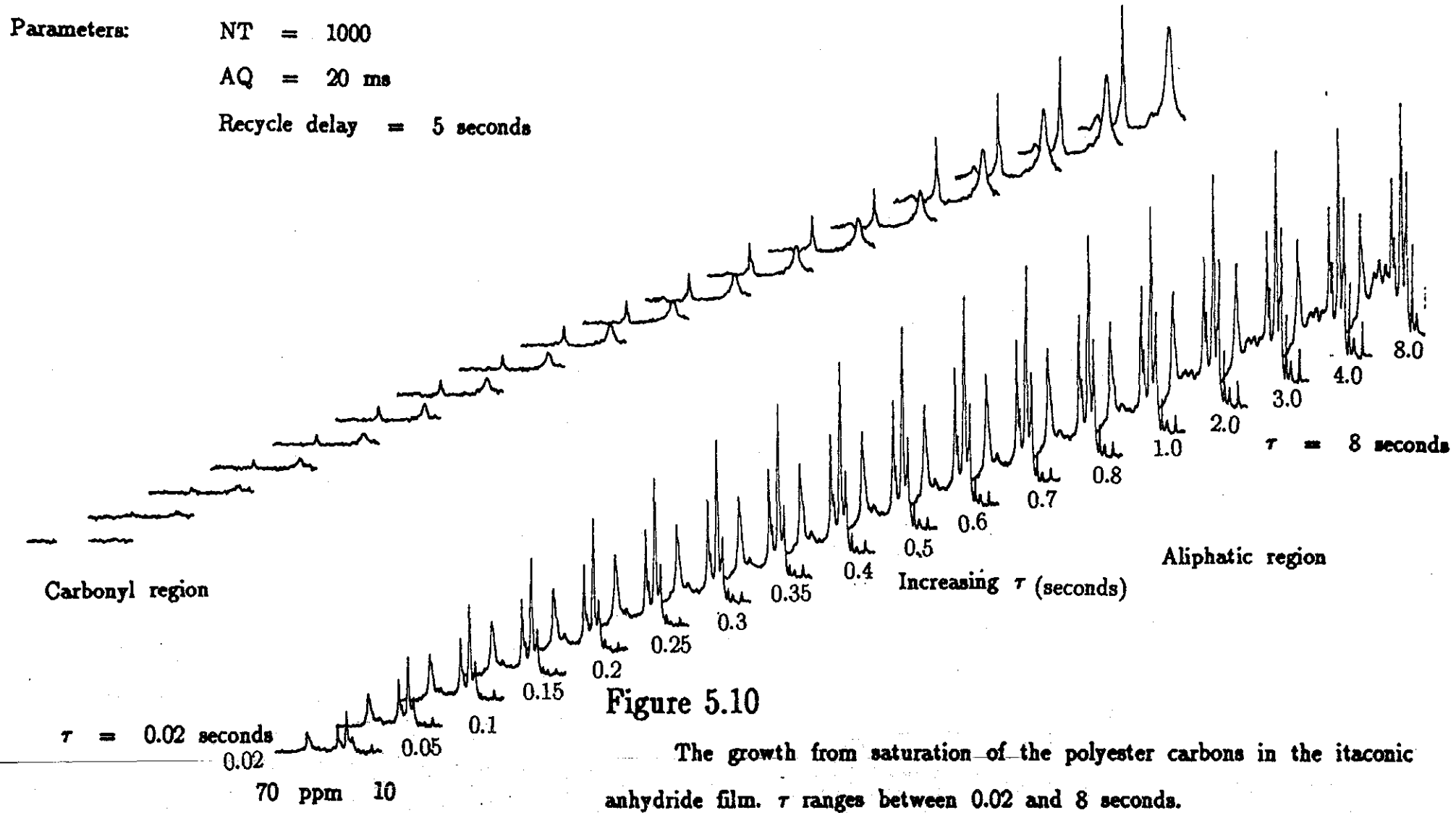

Figure 5.10

The growth from saturation of the polyester carbons in the itaconic anhydride film. τ ranges between 0.02 and 8 seconds.

Figure 5.11

The fitted MOST carbon intensities for the itaconic anhydride film.

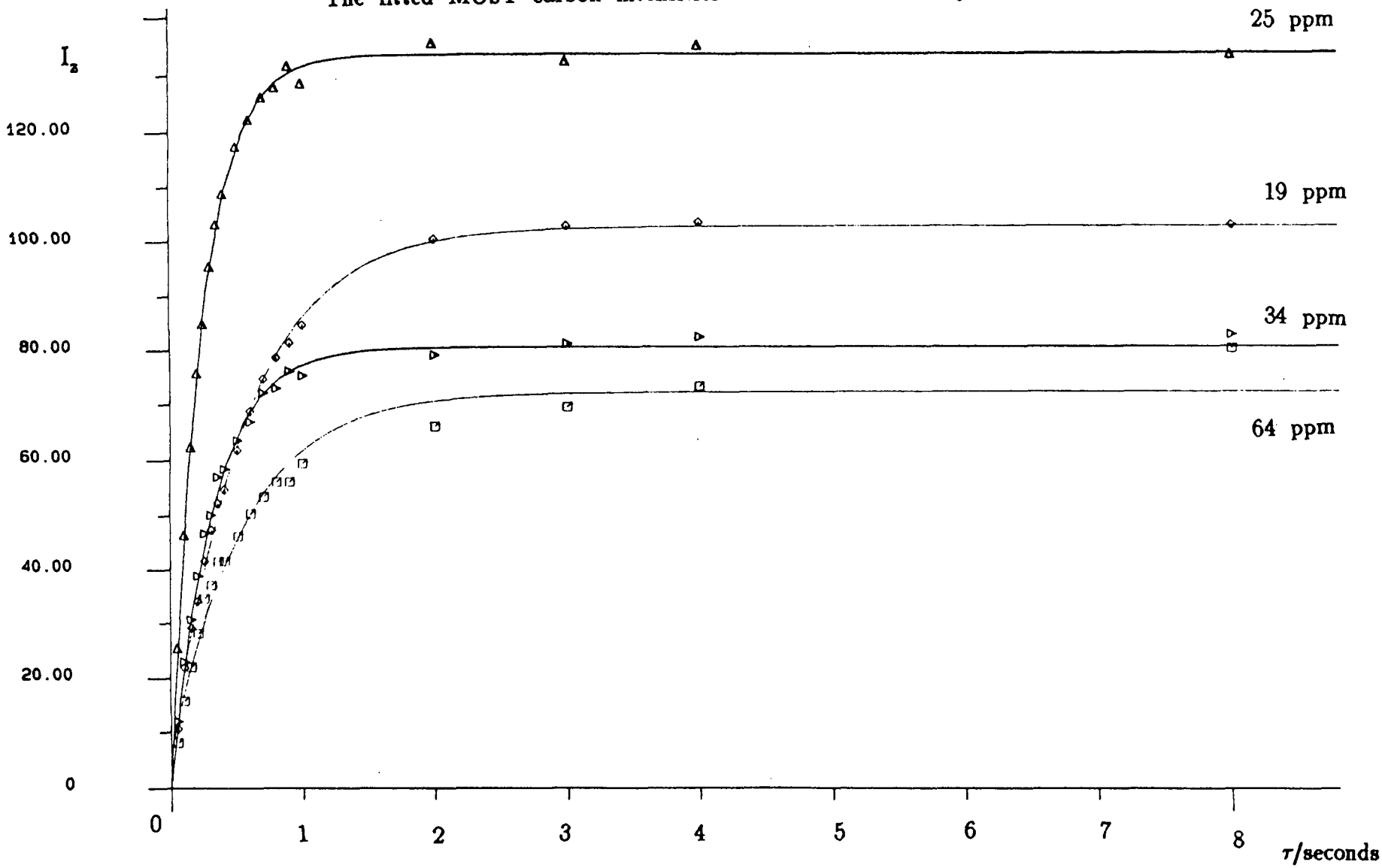

Figure 5.12

The growth from saturation of the polyester carbons in the maleic anhydride film. τ ranges between 0.02 and 8 seconds.

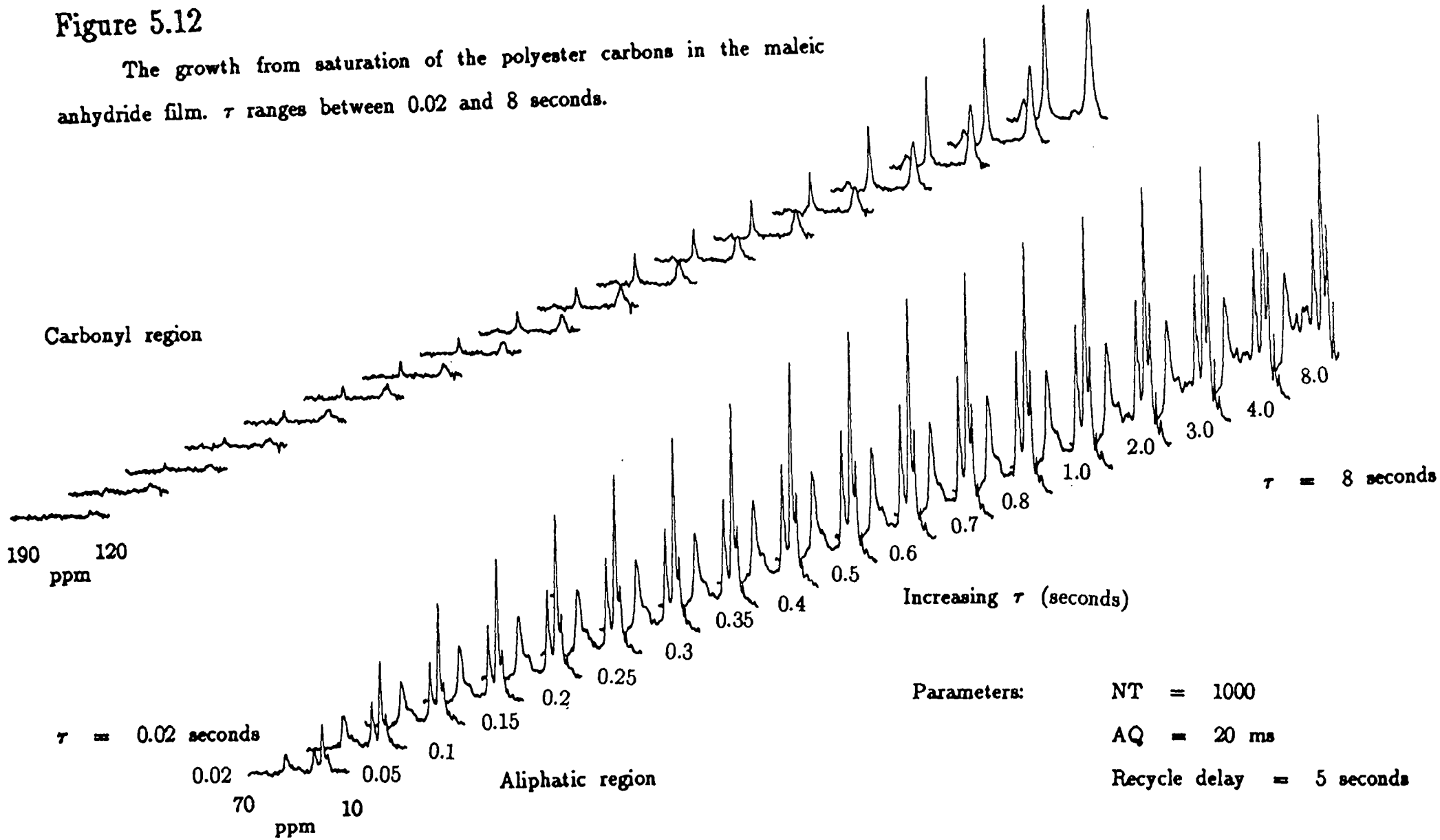

Figure 5.13

The fitted MOST carbon intensities for the maleic anhydride film.

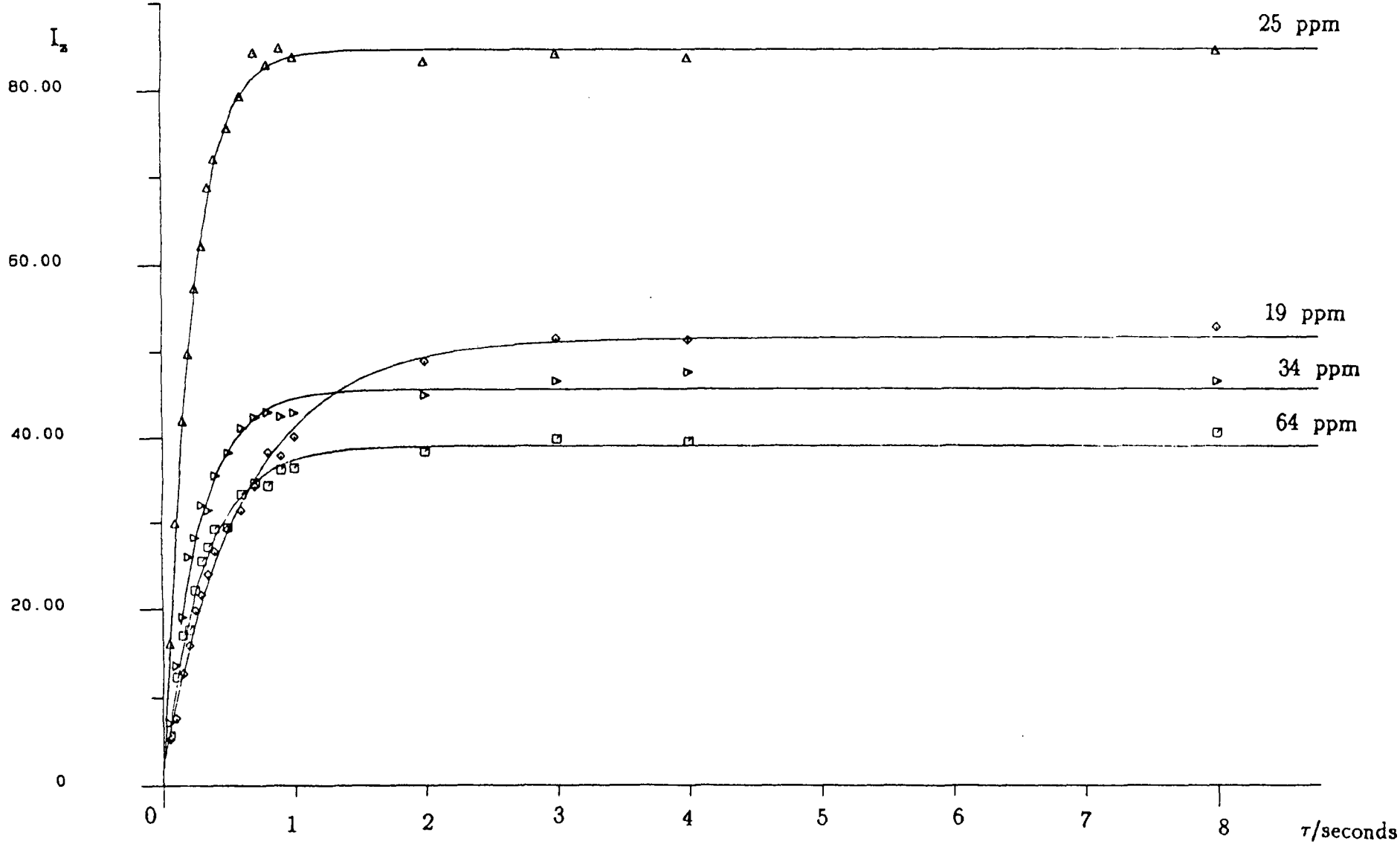

shown in figure 5.11, and the corresponding short component of the carbon T_1 values for the more mobile polyester chains in the itaconic anhydride film are shown in Table 5.6.

Figure 5.12 shows the growth from saturation of the polyester carbons in the maleic anhydride film with τ values ranging between 0.05 and 8 seconds. Figure 5.13 shows the fitted intensities of the spectra, and Table 5.7 lists the corresponding short component of the carbon T_1 values for the more mobile polyester chains in the maleic anhydride film.

In principle, each peak has a contribution from more rigid polyester chains of the sample as well as the more mobile polyester chains which have the short ^{13}C T_1 values. However, the longer component of the carbon T_1's was expected to be at least an order of magnitude larger than the short component of the carbon T_1's, and thus any error in the intensity at short τ is small.

5.2.2 Measurement of the longer T_1^{II} component

The carbon peaks arising from more rigid polyester chains are observable by the cross–polarisation technique. Cross–polarisation works best for rigid, protonated carbons. Thus the longer component of the carbon T_1 may be measured using cross–polarisation without complications arising from the contribution to the T_1 of the short component. The pulse sequence for the measurement of carbon T_1 values via cross–polarisation from the proton spins is shown in figure 5.14. The T1CP experiment, as the pulse sequence is known, was originally proposed

Figure 5.14

The T1CP pulse sequence.

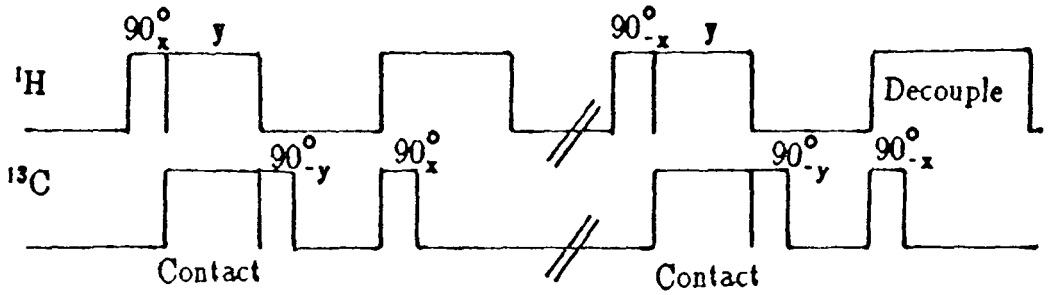

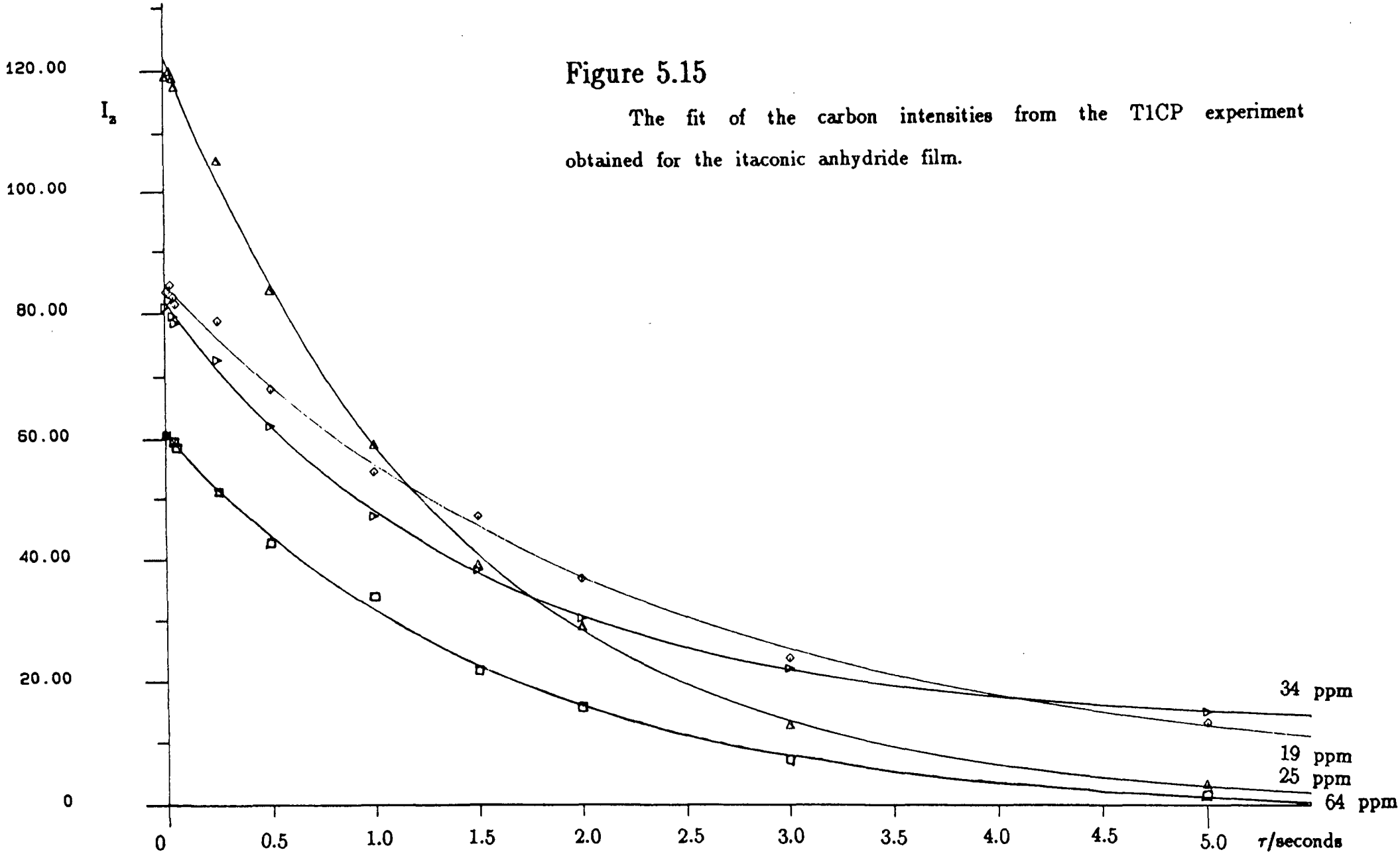

Figure 5.15

The fit of the carbon intensities from the T1CP experiment obtained for the itaconic anhydride film.

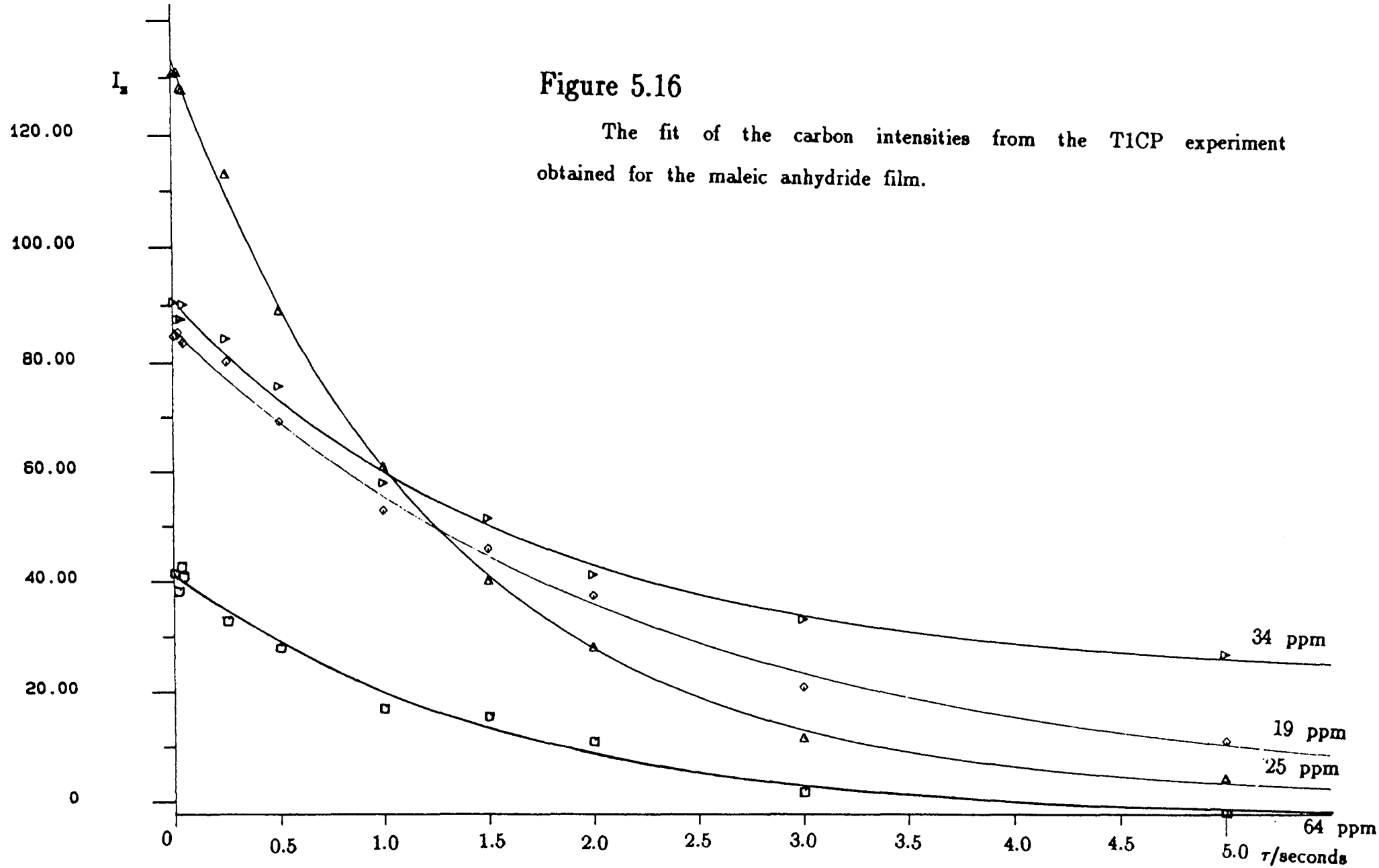

Figure 5.16

The fit of the carbon intensities from the T1CP experiment obtained for the maleic anhydride film.

Table 5.8

Long carbon T_1 values of the polyester chains in the itaconic anhydride film.

Peak/ppm	Assignment	Long $T_1(^{13}C)$/secs
64	O=C–O–CH_2	1.22
34	O–C(=O)–CH_2	3.32
25	CH_2 'backbone'	1.22
19	CH_3 of MMA	2.92

Table 5.9

Long carbon T_1 values of the polyester chains in the maleic anhydride film.

Peak/ppm	Assignment	Long $T_1(^{13}C)$/secs
64	O=C–O–CH_2	0.83
34	O–C(=O)–CH_2	3.87
25	CH_2 'backbone'	1.53
19	CH_3 of MMA	2.55

by Torchia.[4] The T1CP experiment consists of two pulse sequences. In the first sequence, a B_{1H} resonant field is applied to the proton spins, which causes the proton magnetisation to rotate until it lies along the $+y$ direction in the rotating frame of reference, and is then spin–locked along this direction. A B_{1C} field is then applied to the carbon spins, and the carbon magnetisation is then derived along the $+x$ axis. The proton spin–locking field is then switched off, and the carbon magnetisation is rotated from the x axis to the z axis by the B_{1C} field which has been phase–shifted to the $-y$ direction. In the absence of the B_1 field, the carbon magnetisation decays exponentially from its initial value $M_{CP}(0)$ to its equilibrium value M(0) with time τ. After the delay time τ, the remaining carbon magnetisation is measured from the intensity of the peaks in the spectrum obtained from the Fourier Transform of the resultant FID acquired.

The second part of the pulse sequence has spin–temperature inversion, thus inverting the sign of the proton–enhanced carbon signal compared to that obtained in the first pulse sequence. The carbon magnetisation is then rotated into the $-z$ direction, and then recovers from an initial value of $-M_{CP}(0)$ to an equilibrium value of M(0) with time τ. By subtracting one from the other, the change in the carbon intensity with delay τ may be described by equation 5.4.

$$M(\tau) = 2M_{CP}(0)\exp(-\tau/T_1^{H}) \qquad (5.4)$$

There are several advantages of using the T1CP experiment rather than the inversion–recovery pulse sequence to measure the longer component of the carbon T_1 values in the polyester chains in the films.

1). It is only necessary to leave a recycle delay of $5\times T_1(^1H)$ between experiments instead of $5\times T_1(^{13}C)$

2). The carbon signal is enhanced by cross–polarisation

3). Spectral artifacts are suppressed by spin–temperature inversion.

The T1CP experiment was used to measure the longer component of the carbon T_1 of the films which arises from the more rigid polyester chains in the films. The experimental plot used to determine the T_1 values of the less mobile polyester chains in the itaconic anhydride film is shown in figure 5.15. The long components of the T_1 values of the carbons in polyester chains are shown in Table 5.8 together with the assignments of the relevant peaks. A similar experimental plot is shown in figure 5.16 for the maleic anhydride film. the long T_1 components of the T_1 values of the polyester chains in the maleic anhydride film are shown in Table 5.9.

5.2.3 Origins of the two component T_1^{II}

It appears from the ^{13}C T_1 measurements that there are two distinct types of polyester chains in the cross–linked films, one more mobile than the other. In order to understand how this might arise, it is necessary to consider the cross–linking chemistry between the two components of the films. In the cross–linking reaction the acid anhydride in the copolymer reacts with the triethanolamine tip of the polyester, ring–opening to form an ester cross–link as shown in figure 5.17a. The

Figure 5.17

Origins of the two component carbon T_1.

a). The acid anhydride in the copolymer reacts with the triethanolamine tip of the polyester, ring–opening to form an ester cross–link.

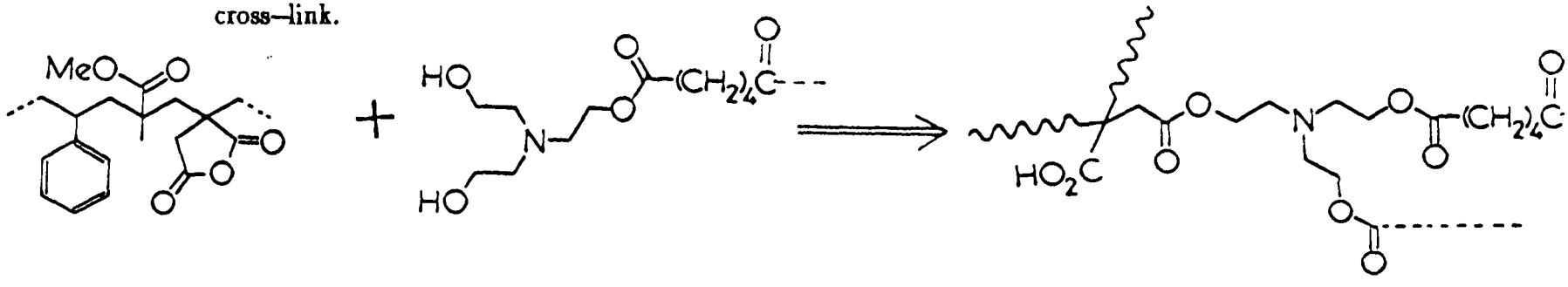

Figure 5.17

b). Some of the polyester chains will be cross–linked at both ends.

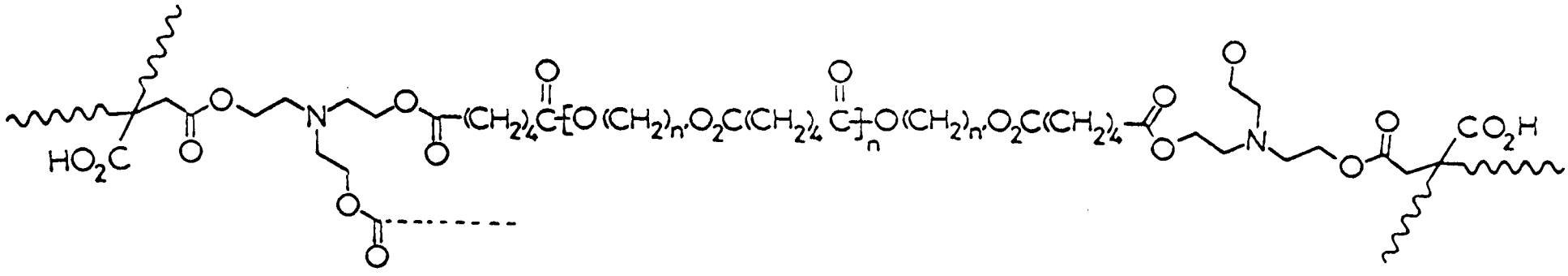

c). Some of the polyester chains will be cross–linked at only one end.

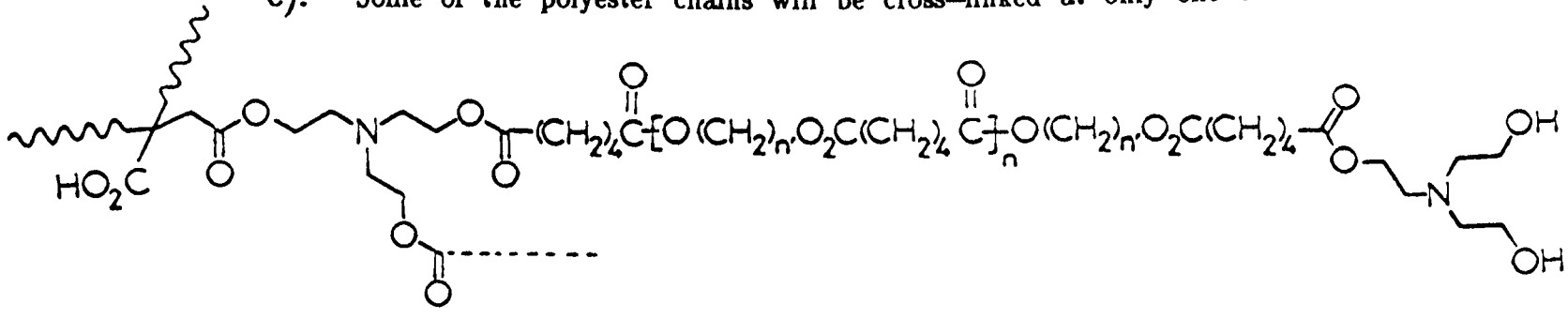

d). There will be some polyester chains which are not cross–linked at all.

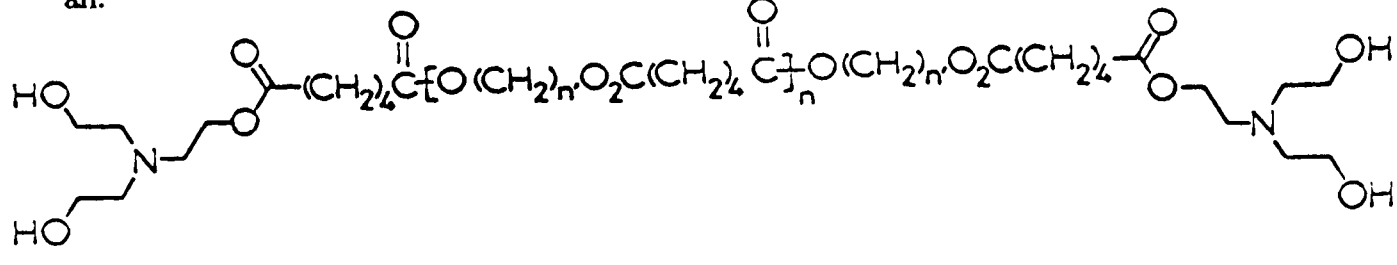

tip of the polyester can only react with the acid anhydride to form a cross–link if they are both close enough to each other in space. In a typical cross–linking system the polymer chains are entangled. There will be some acid anhydride groups which will be inaccessible to the polyester chains, and similarly, there will be some tips of the polyester chains which are not near enough to an acid anhydride group to react. Thus, some of the polyester chains will be cross–linked at both ends, as illustrated in figure 5.17b, and some of the polyester chains will be cross–linked at only one end, with the other end free, as shown in figure 5.17c. There may also be some polyester chains which are not cross–linked at all (figure 5.17d). There will be a difference in the mobility between these three polyester chains, the polyester chains shown in figure 5.17d being the more mobile. It could be this difference in mobility of the polyester chain depending on how the polyester is cross–linked which gives rise to a two–component carbon T_1 value.

5.3 Variable temperature studies

5.3.1 Cross–polarisation

In the last section it was seen that the polymer films contain polyester chains which differ in mobility. The polyester chains with a short ^{13}C T_1 were found to be much more mobile than the copolymer chains. This difference in mobility was detected using the SPE pulse sequence. It would be of interest if differences in mobility between polyester chains and copolymer chains could also be detected using cross–polarisation techniques. Cross–polarisation works best when a carbon

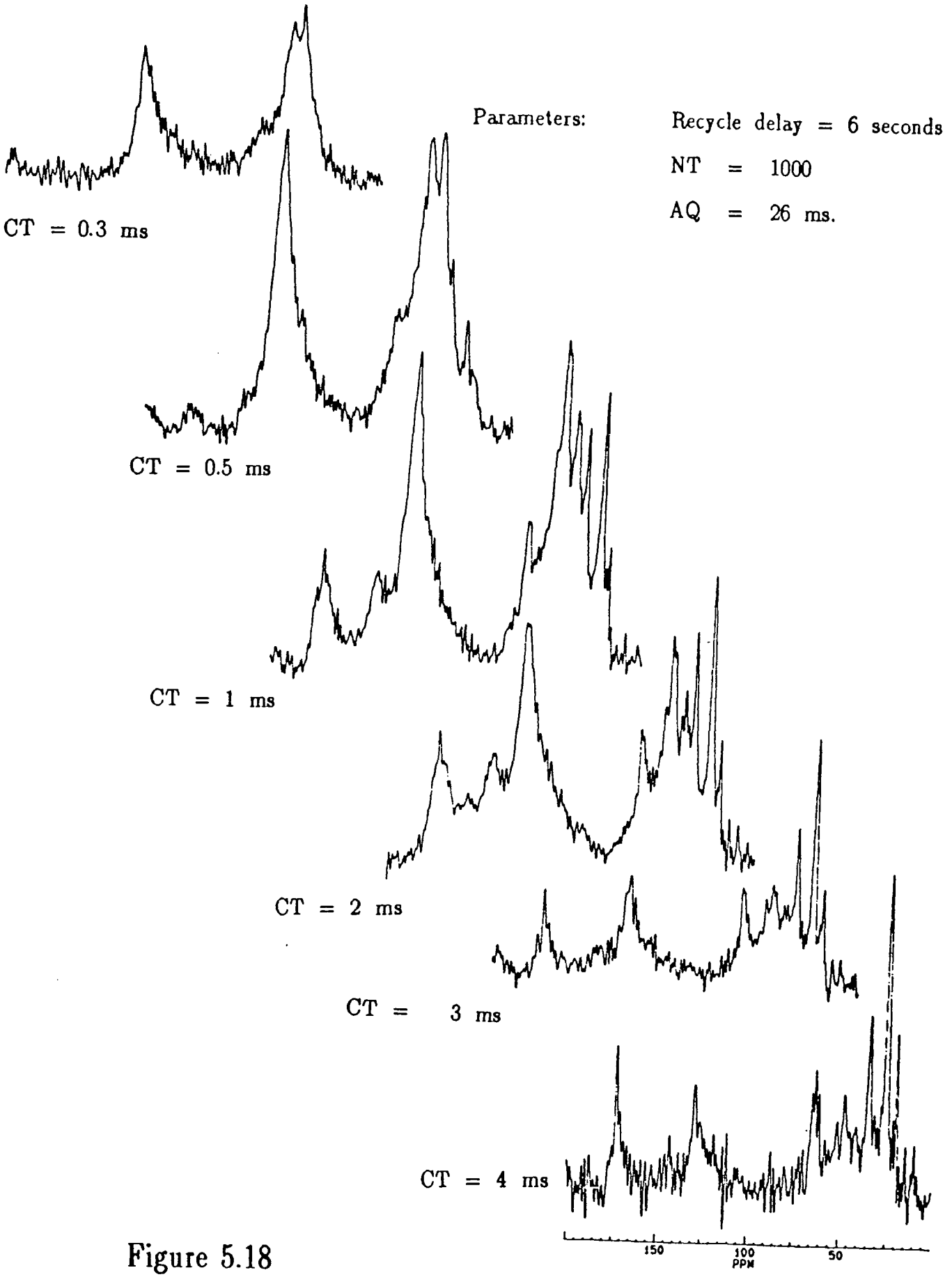

Figure 5.18

Variable contact time spectra of the maleic anhydride film at 60°C for a range of contact times.

is rigid, especially when that carbon is protonated. Variable contact time measurements were made for the itaconic and the maleic anhydride films both at room temperature (25°C) and at higher temperatures. The variable contact time experiment leads to values of T_{IS} and the $T_{1\rho}$ of the protons which cross–polarised the carbon in question.

5.3.1.1 The maleic anhydride film

Variable contact time measurements were obtained for the maleic anhydride film at room temperature (25°C), 60°C and 80°C. Figure 5.18 shows variable contact time spectra of the maleic anhydride film at 60°C for a range of contact times. Plots of peak intensity against contact time at room temperature (25°C), 60°C and 80°C are shown in figures 5.19 to 5.21 for the peaks at 25 ppm and 40 ppm. The assignments of these peaks and the values of T_{IS} and $T_{1\rho}$ obtained from these plots at room temperature (25°C), 60° and 80°C are shown in table 5.10. At room temperature (25°C) both copolymer and polyester peaks were present in the spectra at all values of the contact time. However, as the temperature was raised, spectra at short contact times were dominated by peaks due to the copolymer only, and spectra at long contact times were dominated by peaks due to the polyester only. The signal to noise of the cross–polarisation spectra becomes worse as the temperature is raised. This is because the overall mobility of the films increases as the temperature increases, and therefore CP efficiency decreases. It can be seen that at room temperature (25°C), the $T_{1\rho}$ and the T_{IS} values of the polyester peaks are identical within experimental error to those of the copolymer peaks. Therefore at room temperature (25°C) the copolymer and the

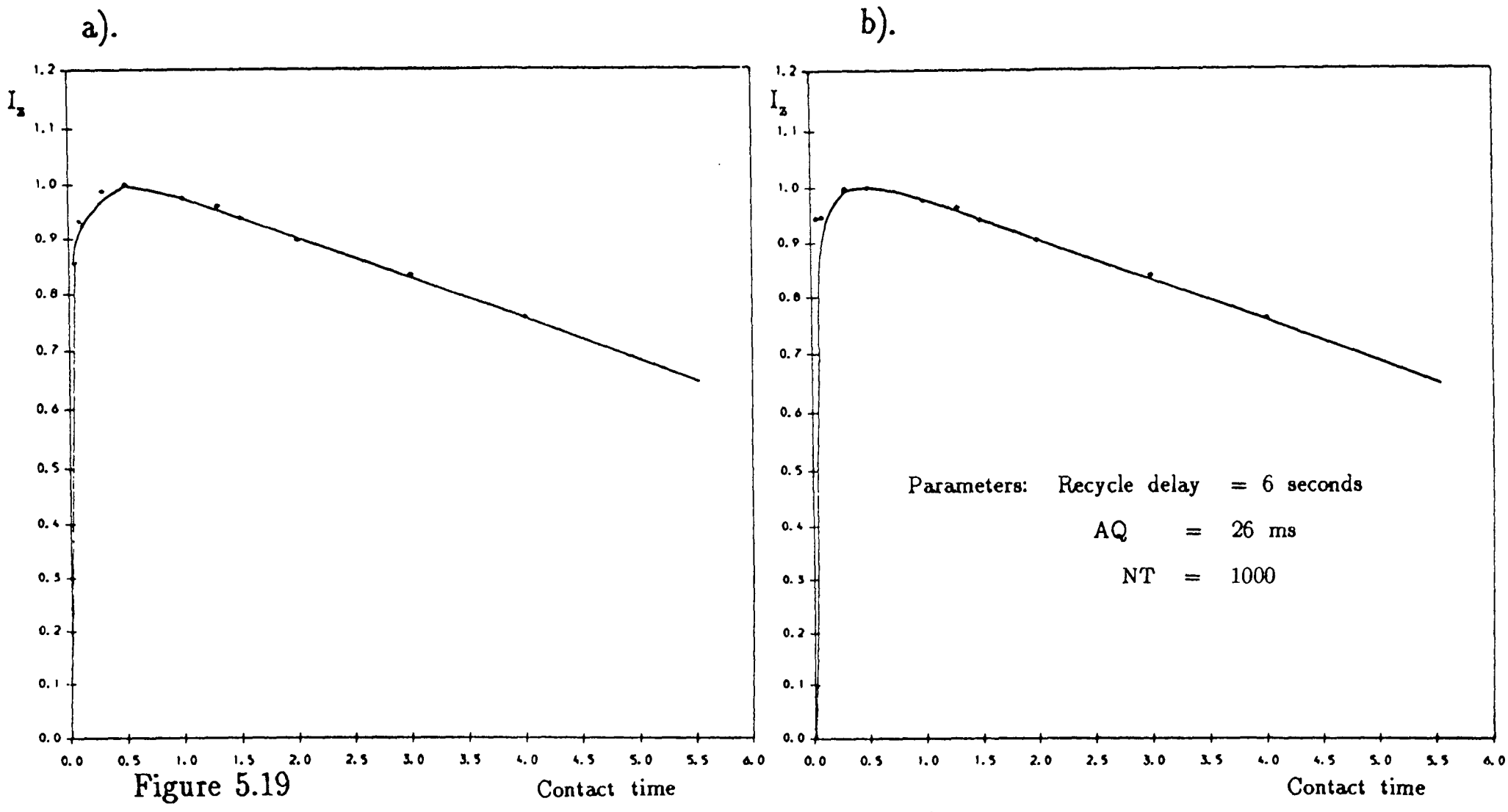

Figure 5.19

a). Plot of peak intensity against contact time at room temperature for the polyester peak at 25 ppm in the maleic anhydride film.

b). Plot of peak intensity against contact time at room temperature for the copolymer peak at 40 ppm in the maleic anhydride film.

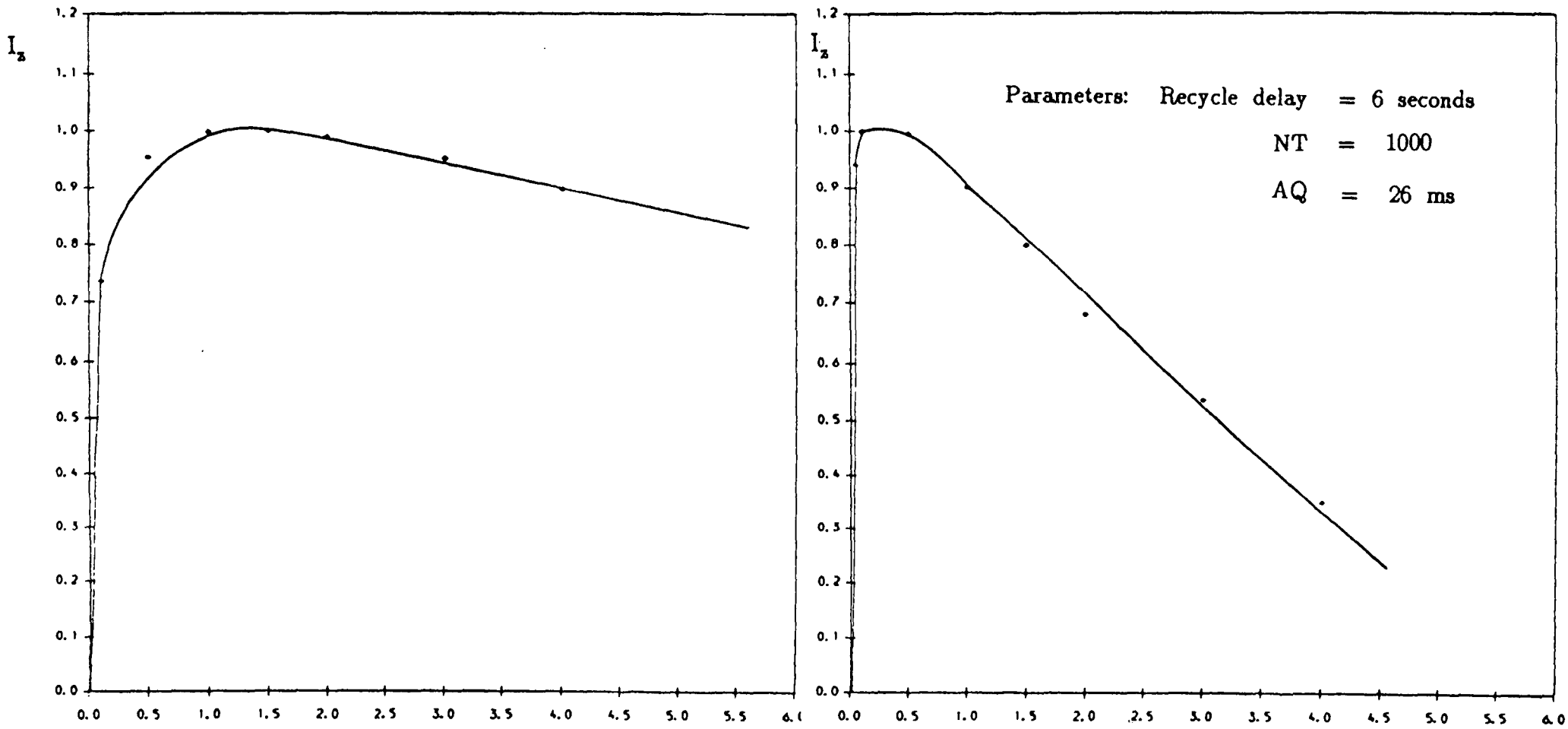

Figure 5.20

a). Plot of peak intensity against contact time at 60°C for the polyester peak at 25 ppm in the maleic anhydride film.

b). Plot of peak intensity against contact time at 60°C for the copolymer peak at 40 ppm in the maleic anhydride film.

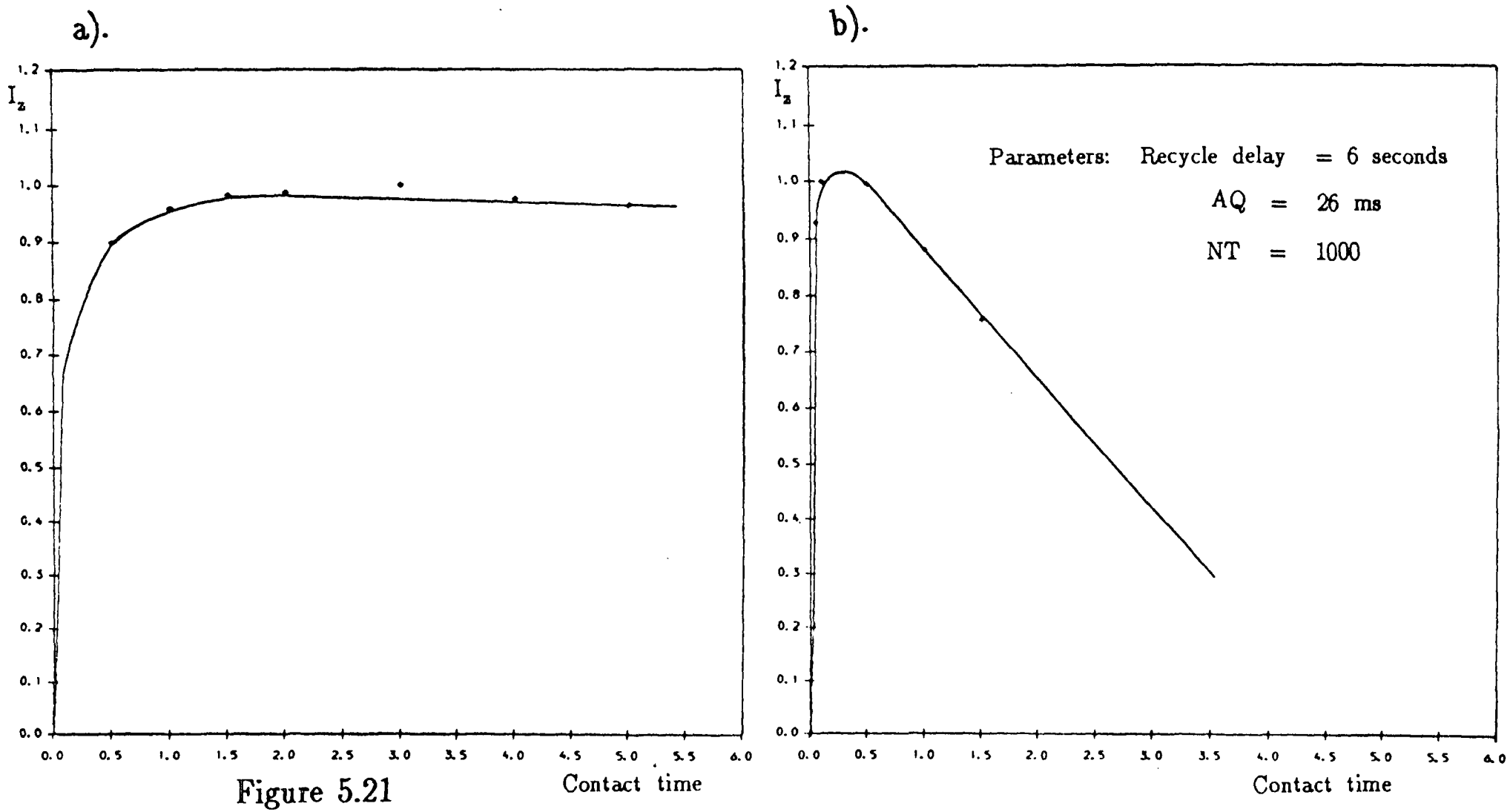

Figure 5.21

a). Plot of peak intensity against contact time at 80°C for the polyester peak at 25 ppm in the maleic anhydride film.

b). Plot of peak intensity against contact time at 80°C for the copolymer peak at 40 ppm in the maleic anhydride film.

Table 5.10

Values of $T_{1\rho}$ and T_{IS} obtained from Variable contact time measurements for the maleic anhydride film at room temperature, 60°C and 80°C.

Temperature/°C	Peak/ppm	T_{IS}/ms	$T_{1\rho}$/ms
RT	25	0.063	9.676
RT	40	0.054	10.07
60	25	0.084	12.346
60	40	0.031	2.706
80	25	0.110	57.519
80	40	0.015	1.430

polyester peaks in the film are not distinguishable by cross–polarisation. However, at temperatures of 60°C and 80°C, both the T_{IS} and the $T_{1\rho}$ of the copolymer peaks are different from those of the polyester peaks. It is interesting to note the general trend of the relaxation times. As the temperature is increased, T_{IS} and $T_{1\rho}$ of the copolymer peaks decrease but the T_{IS} and $T_{1\rho}$ of the polyester peaks increase.

At room temperature (25°C), the relaxation times of the copolymer and the polyester peaks are too similar to make it possible to distinguish between copolymer and polyester peaks using either cross–polarisation variable contact or delayed contact techniques. However, as the temperature is raised, the relaxation characteristics of the copolymer and the polyester peaks become different. It becomes possible to distinguish between copolymer and polyester peaks using CP techniques.

5.3.1.2 The itaconic anhydride film

Variable contact measurements were made on the itaconic anhydride film at room temperature (25°C), 60°C and 80°C. Plots of peak intensity against contact time at room temperature (25°C), 60°C and 80°C are shown in figures 5.22 to 5.24 for the peaks at 25 ppm and 40 ppm. The assignments of these peaks and the values of T_{IS} and $T_{1\rho}$ obtained from these plots at room temperature (25°C), 60°C and 80°C are listed in table 5.11. Again, as the temperature is increased, T_{IS} of the copolymer peaks decrease while the T_{IS} of the polyester peaks increase. Separate copolymer and polyester peaks cannot be distinguished by cross–polarisation techniques at room temperature (25°C). This is because at 25°C the relaxation times $T_{1\rho}$ and T_{IS} of the polyester and the

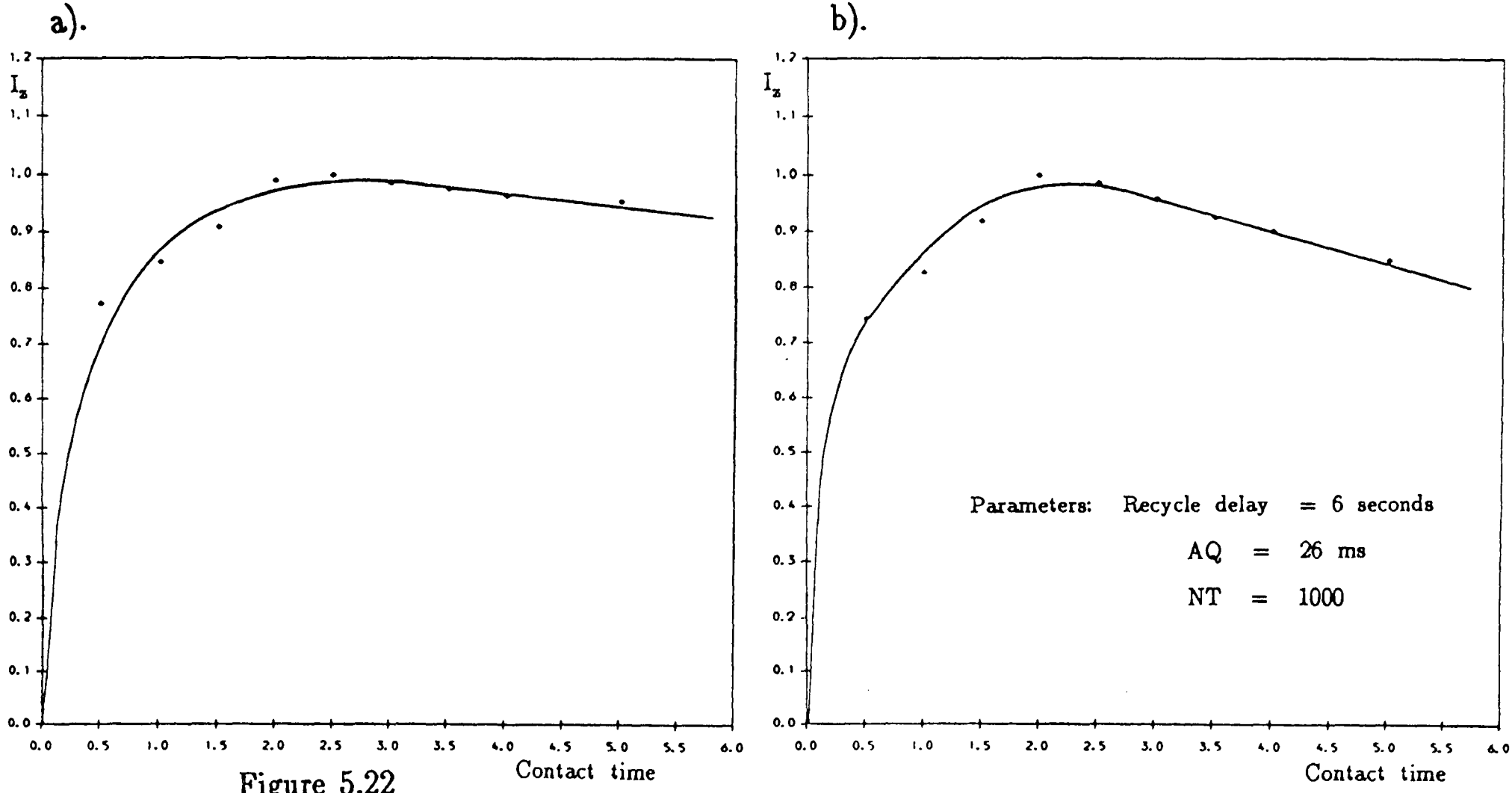

Figure 5.22

a). Plot of peak intensity against contact time at room temperature for the polyester peak at 25 ppm in the itaconic anhydride film.

b). Plot of peak intensity against contact time at room temperature for the copolymer peak at 40 ppm in the itaconic anhydride film.

a).

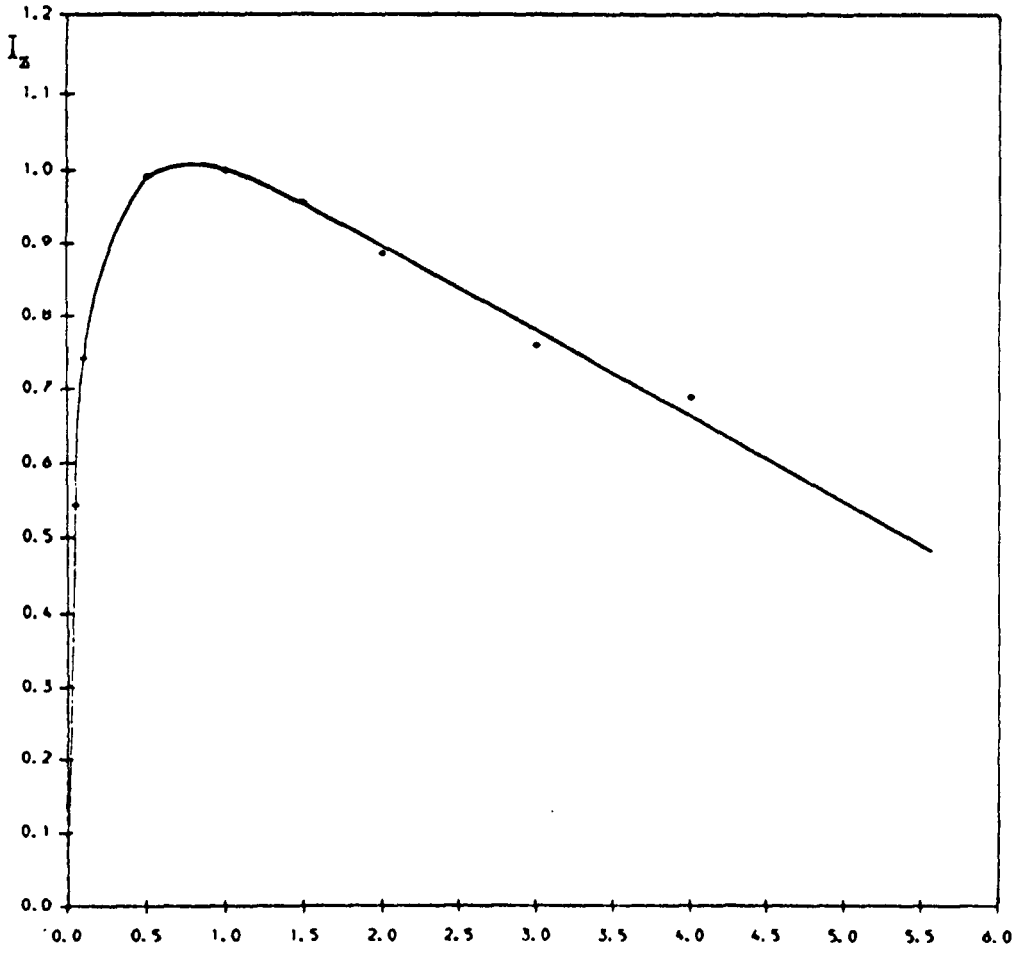

b).

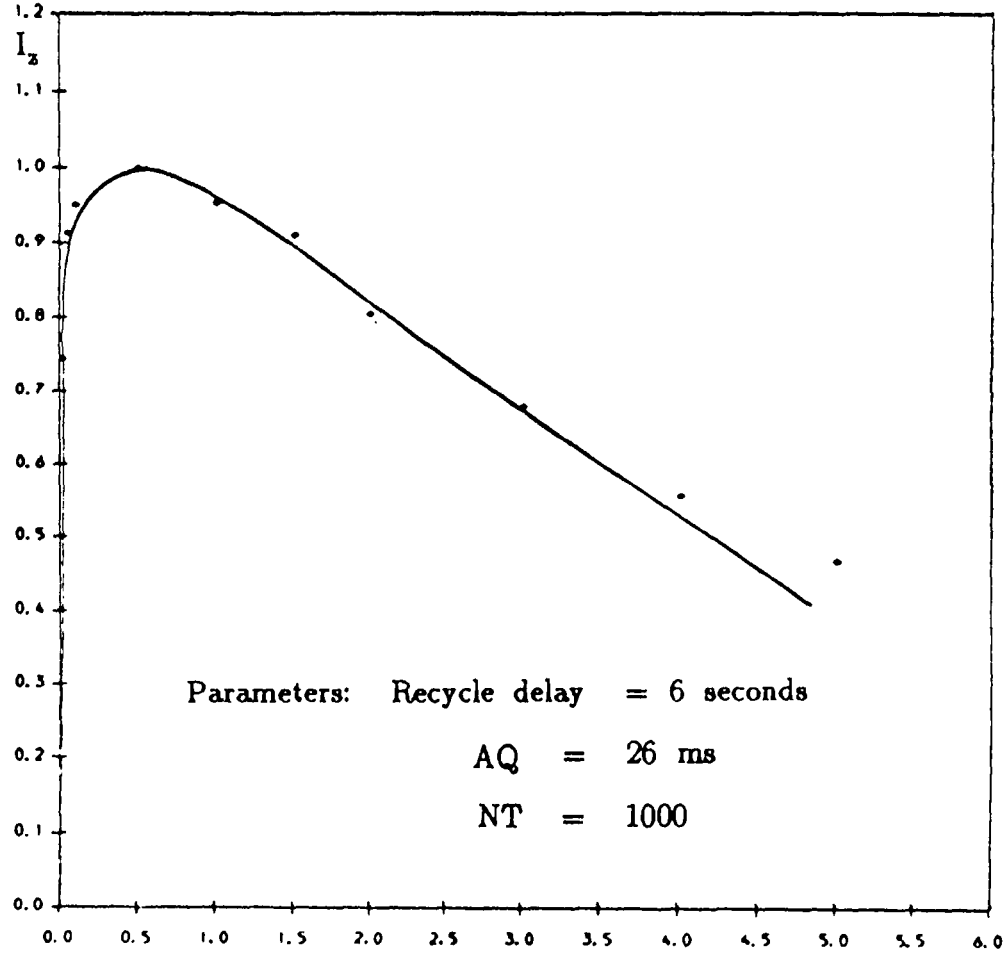

Figure 5.23

a). Plot of peak intensity against contact time at 60°C for the polyester peak at 25 ppm in the itaconic anhydride film.

b). Plot of peak intensity against contact time at 60°C for the copolymer peak at 40 ppm in the itaconic anhydride film.

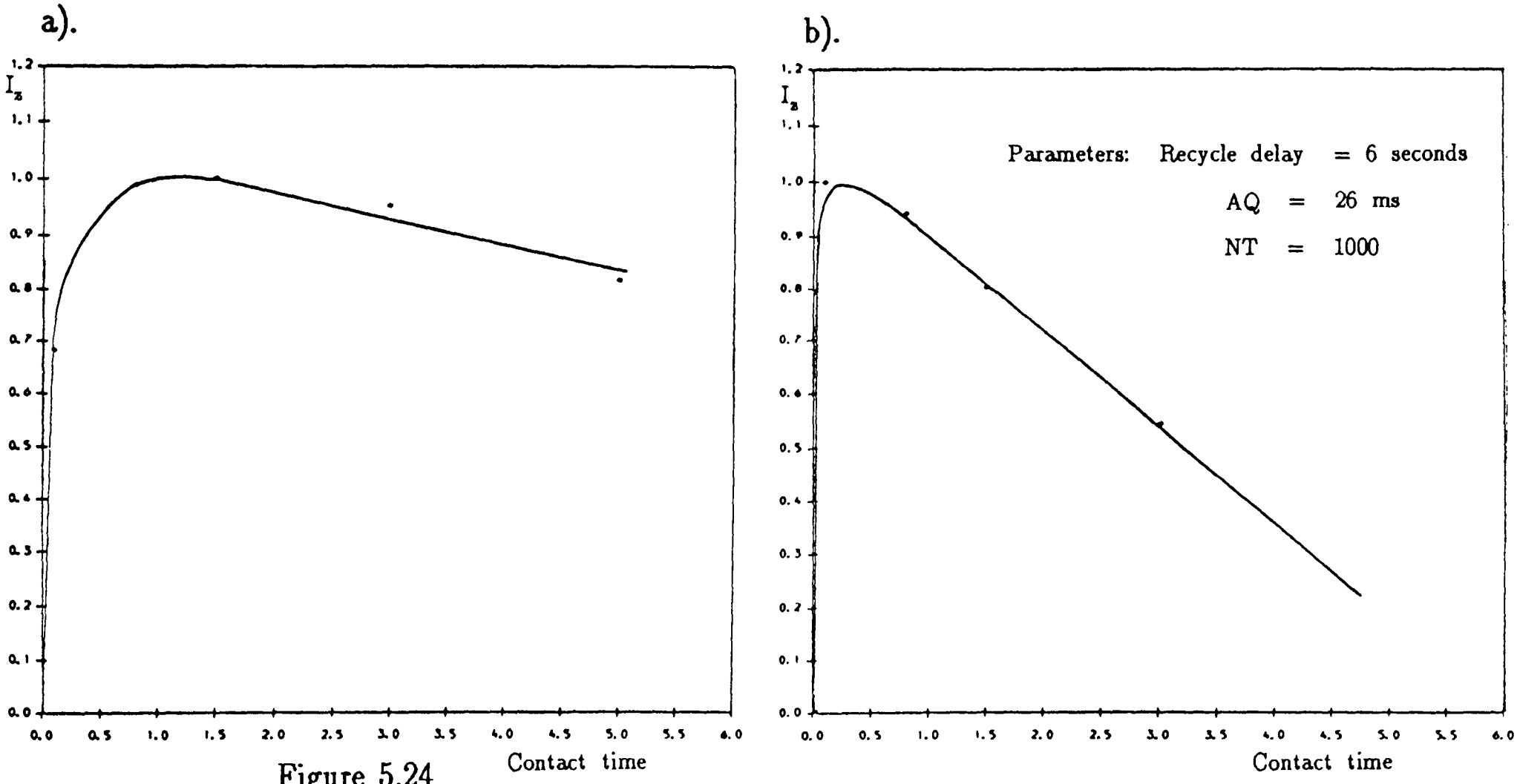

Figure 5.24

a). Plot of peak intensity against contact time at 80°C for the polyester peak at 25 ppm in the itaconic anhydride film.

b). Plot of peak intensity against contact time at 80°C for the copolymer peak at 40 ppm in the itaconic anhydride film.

Table 5.11

Values of $T_{1\rho}$ and T_{IS} obtained from Variable contact time measurements for the itaconic anhydride film at room temperature, 60°C and 80°C.

Temperature/°C	Peak/ppm	T_{IS}/ms	$T_{1\rho}$/ms
RT	25	0.063	9.676
RT	40	0.054	8.493
60	25	0.152	3.399
60	40	0.021	3.395
80	25	0.190	7.198
80	40	0.014	1.799

copolymer peaks are too similar to distinguish between the two types of peaks. However, at higher temperatures the relaxation times T_{IS} and $T_{I\rho}$ of the copolymer and the polyester peaks become sufficiently dissimilar to allow the two components to be observed separately.

5.3.1.3 Discussion

It is not an easy matter to decide on the reason why it is possible to distinguish between copolymer and polyester peaks at higher temperature, but not at 25°C. There are two possible explanations for this.

Firstly, it is known that carbons in the polyester chains have a two–component carbon T_1 arising from the difference in mobility of the various types of cross–linked polyester chains in the polymer films. If the carbon T_1 of the polyester chains are two–component, then it is very likely that the T_{IS} values of the polyester peaks will be complex, and not single–component. The theory used here assumes that both T_{IS} and $T_{I\rho}$ are single–component. Thus the separation of the spectrum for the film at higher temperatures into copolymer peaks only at short contact times and into polyester peaks only at longer contact times may be an apparent effect.

The second, and perhaps the more probable, explanation of why the copolymer and polyester peaks may be observed separately at higher temperatures is that there may be a genuine phase separation of copolymer and polyester regions. It is possible that after mixing there may still be regions of high polyester density and regions of high copolymer density in the films. At room temperature (25°C), the

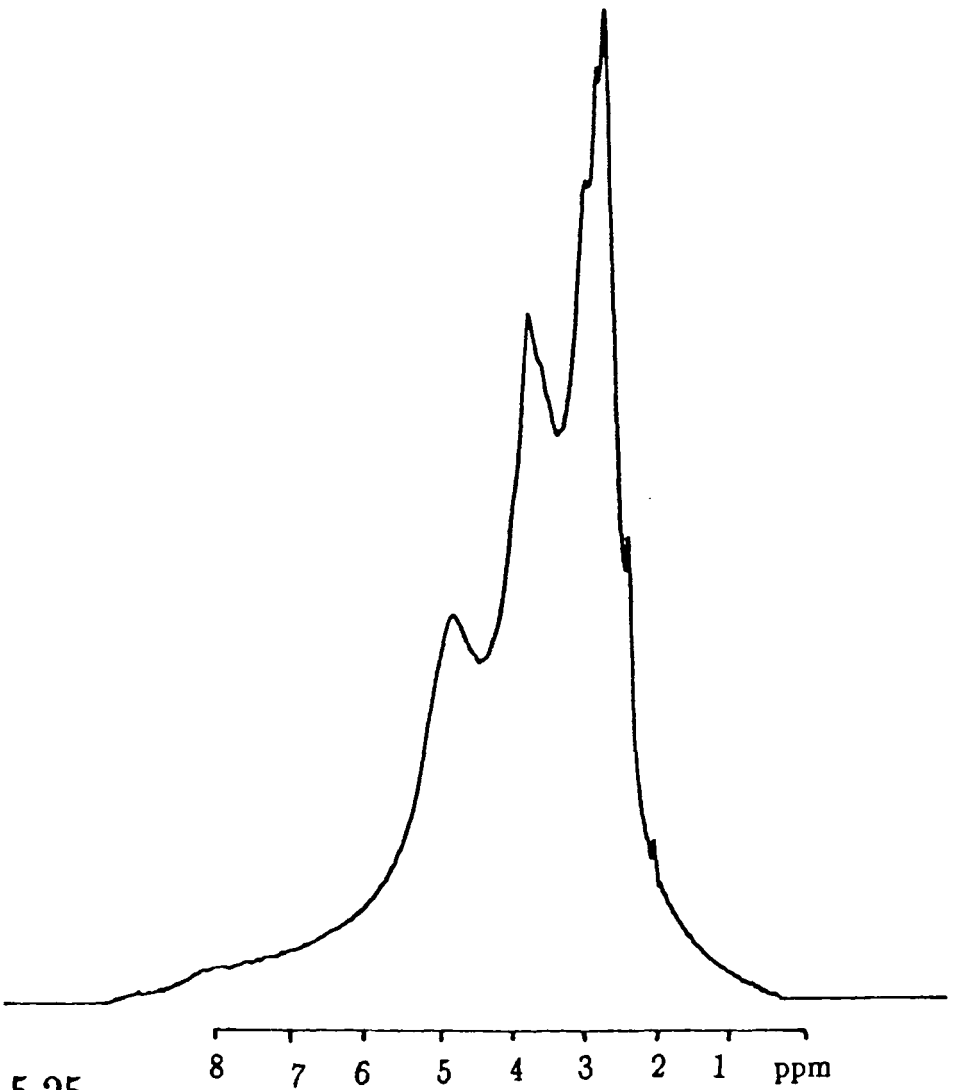

Figure 5.25

The proton single–pulse spectrum of the $^{13}C_2$–enriched itaconic anhydride film obtained at 363 K.

Parameters: NT = 32

AQ = 128 ms

Recycle time = 5 seconds

single–pulse proton spectrum of the film is a single broad band. This homogeneous lineshape indicates efficient spin diffusion over the whole film at room temperature. However, at higher temperatures the single–pulse proton spectrum shows partial resolution. The single–pulse proton spectrum of the itaconic anhydride film at 90°C is shown in figure 5.25. The partial resolution in the proton spectrum at higher temperatures may inhibit spin diffusion, thus allowing separate copolymer and polyester parts of the film to be resolved at higher temperature.

5.3.2 Single–pulse–excitation

Single–pulse spectra at recycle times of 1, 3 and 5 seconds have been obtained for both the itaconic anhydride and the maleic anhydride films at room temperature (25°C) and 80°C. The single–pulse spectra of the itaconic anhydride film at room temperature (25°C) and 80°C are shown in figures 5.26 and 5.27 respectively, and the single–pulse spectra of the maleic anhydride film at room temperature (25°C) and 80°C are shown in figures 5.28 and 5.29 respectively. There are some interesting points to note about the spectra obtained at 80°C. Firstly the linewidths of the spectra at 80°C are about 100 Hz less than the linewidths at room temperature (25°C). This is because the dispersion of the chemical shifts is averaged to a greater extent by molecular motion at higher temperatures. Secondly, the transient nuclear Overhauser effect observed is larger at higher temperature. This is as predicted: The nuclear Overhauser enhancement factor increases with increased mobility. In the spectra at 80°C with a recycle delay of 5 seconds (figures 5.27 and 5.29) peaks arising from the copolymer regions are of much lower intensity than the

Figure 5.26

Single–pulse spectra of the itaconic anhydride film at room temperature.

Parameters: AQ = 20 ms
NT = 3000

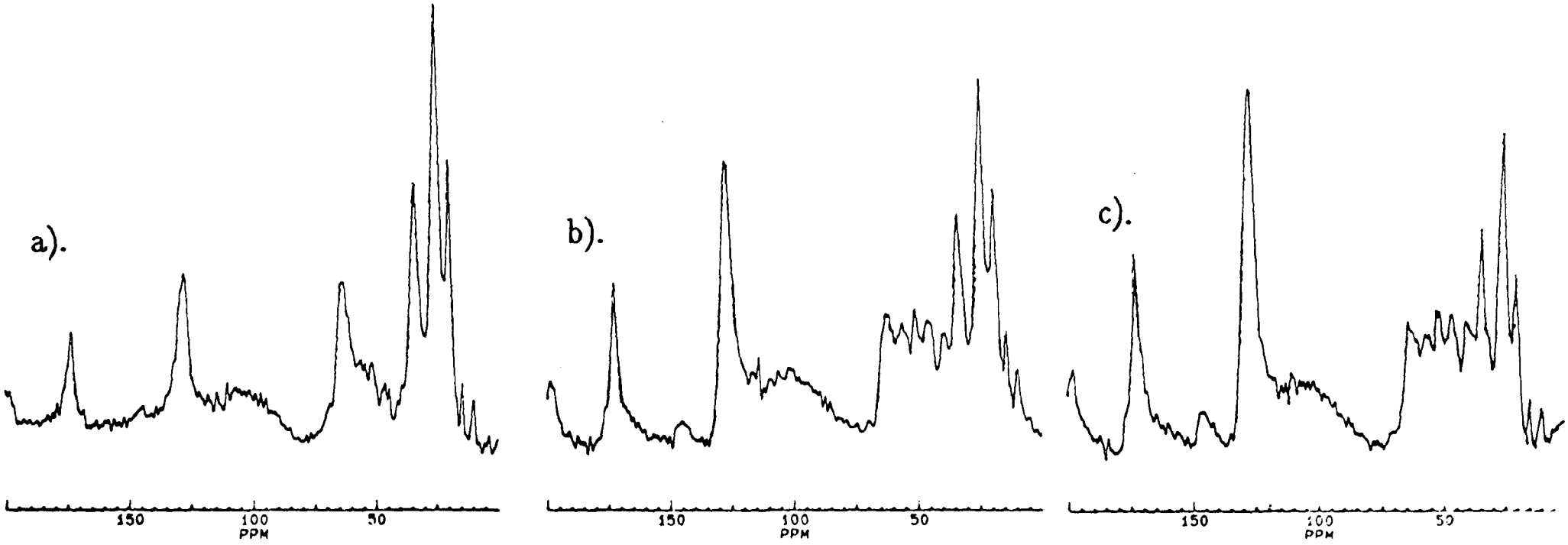

Recycle delay = 1 second

Recycle delay = 3 seconds

Recycle delay = 5 seconds.

Figure 5.27

Single–pulse spectra of the itaconic anhydride film at 80°C.

Parameters: AQ = 20 ms

NT = 3000

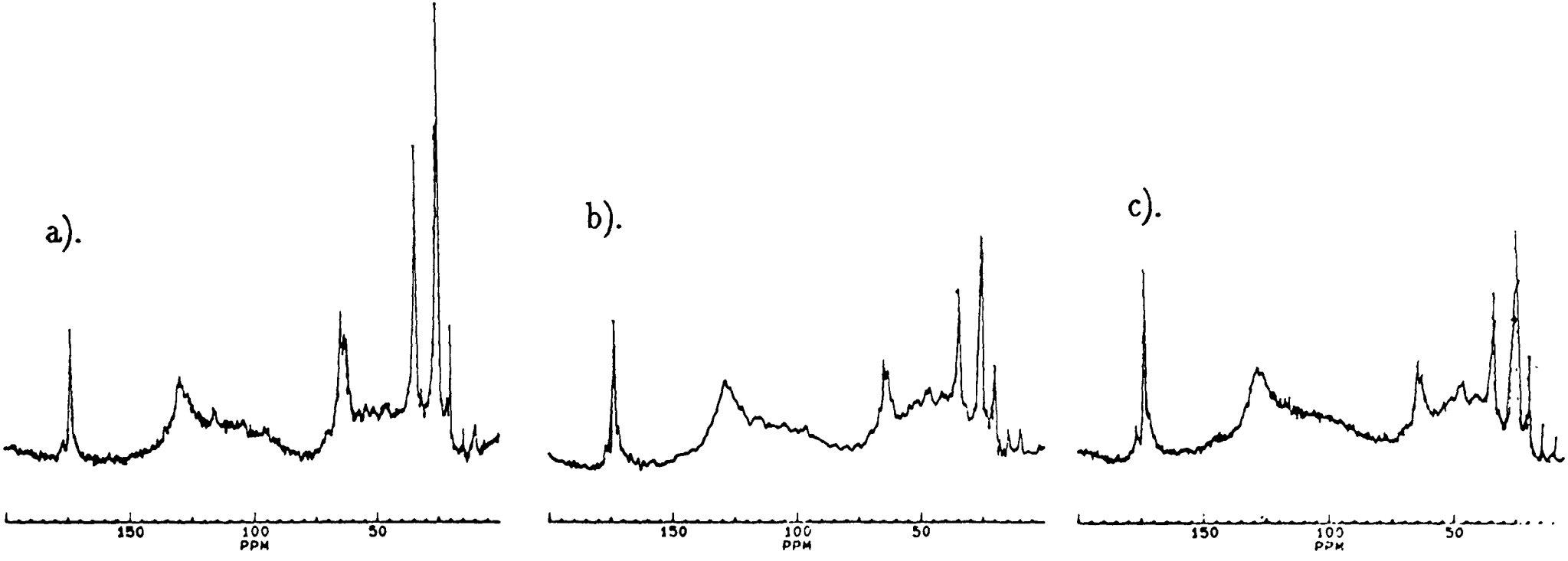

Recycle delay = 1 second

Recycle delay = 3 seconds

Recycle delay = 5 seconds.

Figure 5.28

Single–pulse spectra of the maleic anhydride film at room temperature.

Parameters: AQ = 20 ms

NT = 3000

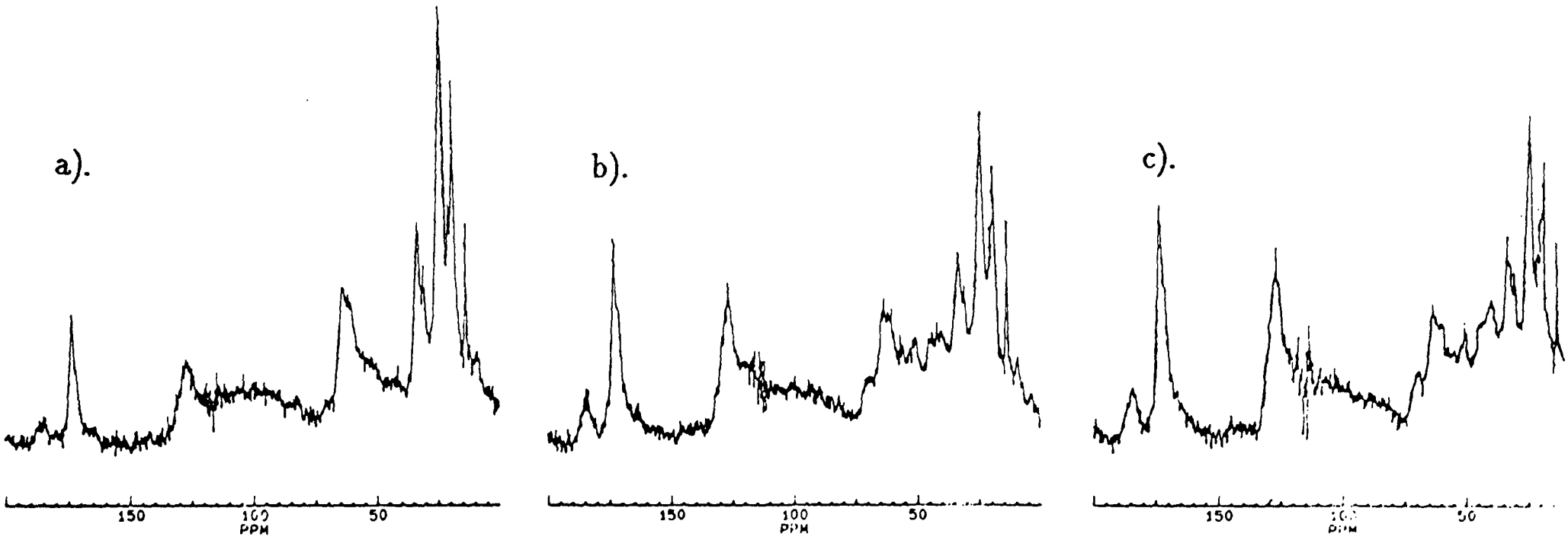

Recycle delay = 1 second

Recycle delay = 3 seconds

Recycle delay = 5 seconds.

Figure 5.29

Single–pulse spectra of the maleic anhydride film at 80°C.

Parameters: AQ = 20 ms

NT = 3000

a).

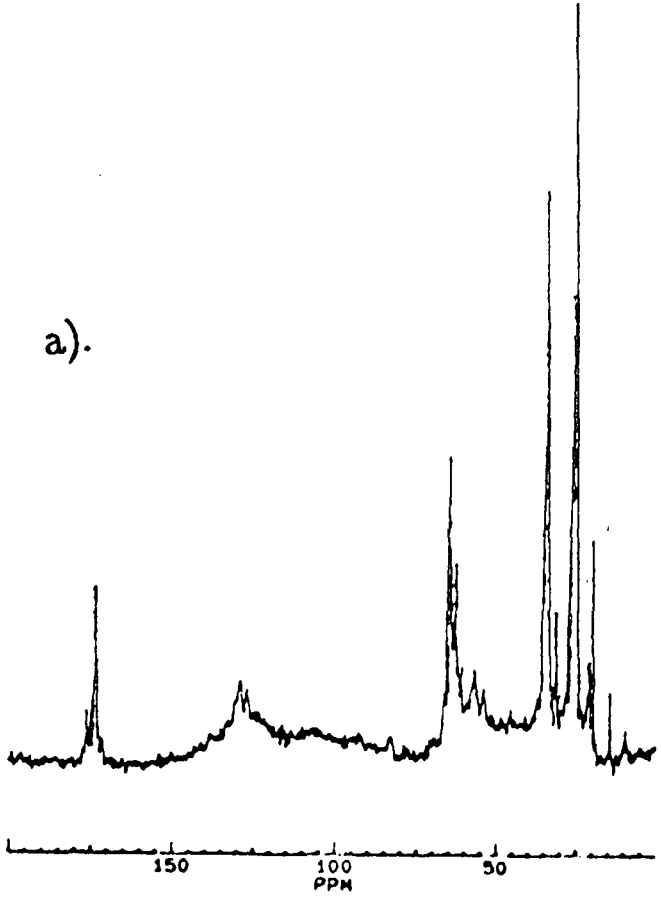

Recycle delay = 1 second

b).

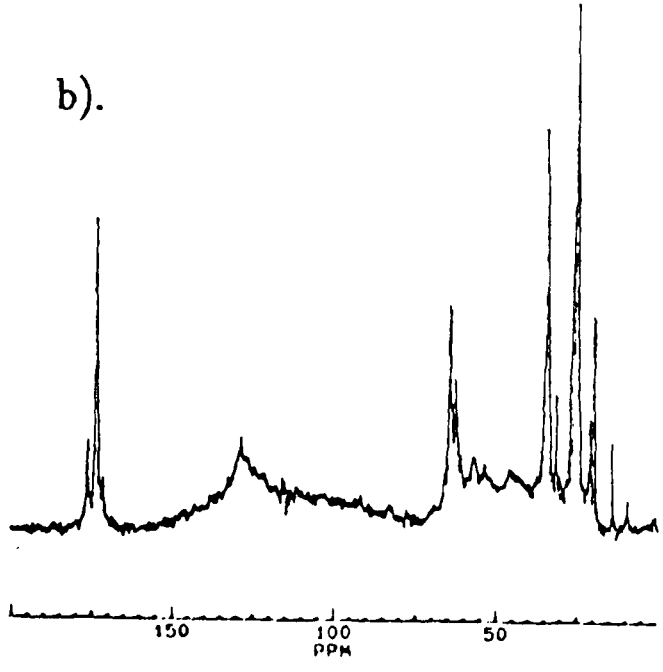

Recycle delay = 3 seconds

c).

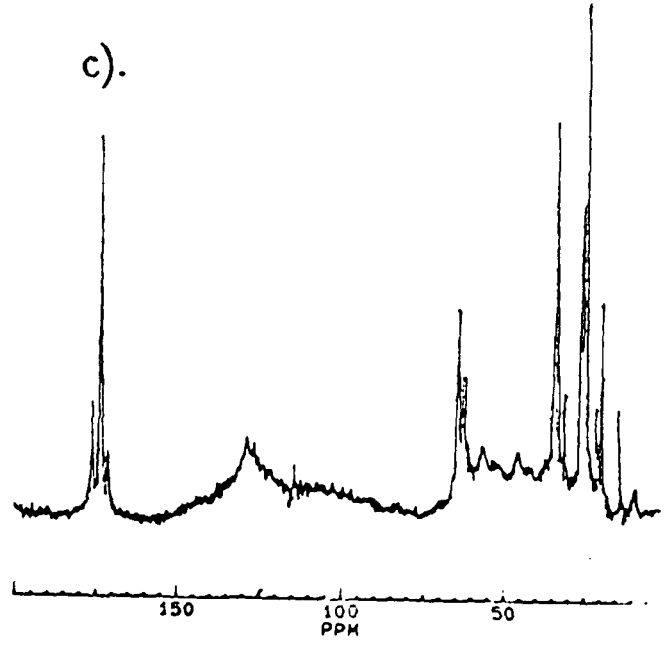

Recycle delay = 5 seconds.

same peaks in the room temperature (25°C) spectra with a recycle time of 5 seconds (figures 5.26 and 5.28). This indicates that the carbon T_1 values of the copolymer peaks increase with temperature. Figure 5.30 compares the 5 second recycle time spectrum at 80°C with the 5 second recycle time room temperature (25°C) SPE spectrum of the itaconic anhydride film. Figure 5.31 shows similar spectra for the maleic anhydride film. At 80°C the peaks have narrowed sufficiently to allow the carbonyl peak at 173 ppm to be resolved into three sharp lines and the CH_2 peak at 64 ppm to be resolved into two sharp lines. The carbonyl peak is split into three lines at 172.8, 173.3 and 175 ppm. The large peak at 173.3 ppm is known to arise from the carbonyl carbons in the polyester backbone, but the origin of the two smaller peaks at 172.8 and 175 ppm is a little less obvious. The two peaks are thought to originate from two different situations. The peak at 175 ppm probably arises from the carbonyl at the end of the polyester chain before the triethanolamine tip (figure 5.32a). Although the acid and the alcohols used to form the polyester were reacted together in such proportions so as to form an acid–tipped polyester, it is inevitable that some of the polyester will be formed with an alcohol tip. It is believed that the peak at 172.8 ppm originates from the carbonyl next to a terminal ethylene glycol unit (figure 5.32b). Although it is also possible that butane 1,4 diol could be the terminal unit, the chemical shift of the carbonyl next to this unit is too close to that of the carbonyl in the backbone of the polyester to be distinguished.

The broad peak at 64 ppm in the room temperature spectra is narrowed considerably in the spectra at 80°C. Two peaks are resolved at 62.1 ppm and 63.3 ppm. These peaks originate from the CH_2 in the

Figure 5.30

A comparison between the 5 second recycle delay SPE spectrum at room temperature and the 5 second recycle delay SPE spectrum at 80°C for the itaconic anhydride film.

Parameters: AQ = 20 ms
NT = 3000

a).
room temperature.

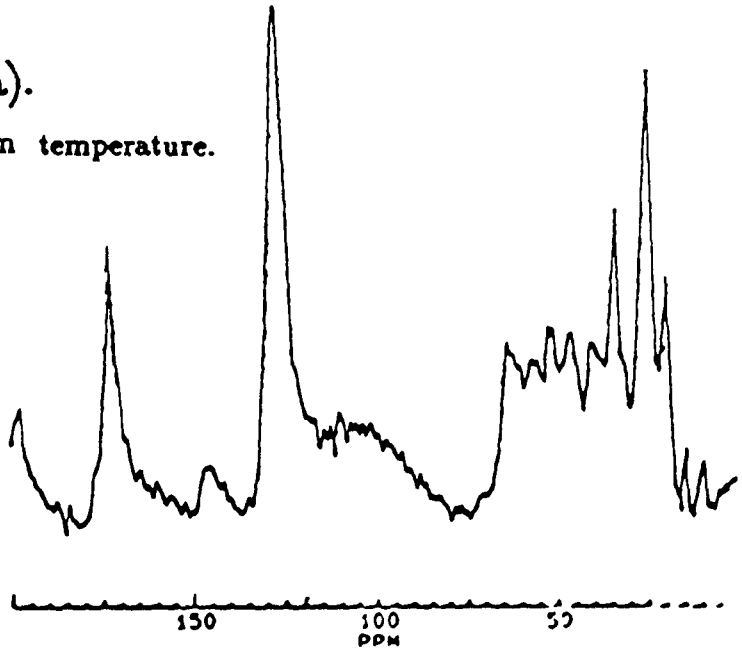

Recycle delay = 5 seconds

b). 80°C.

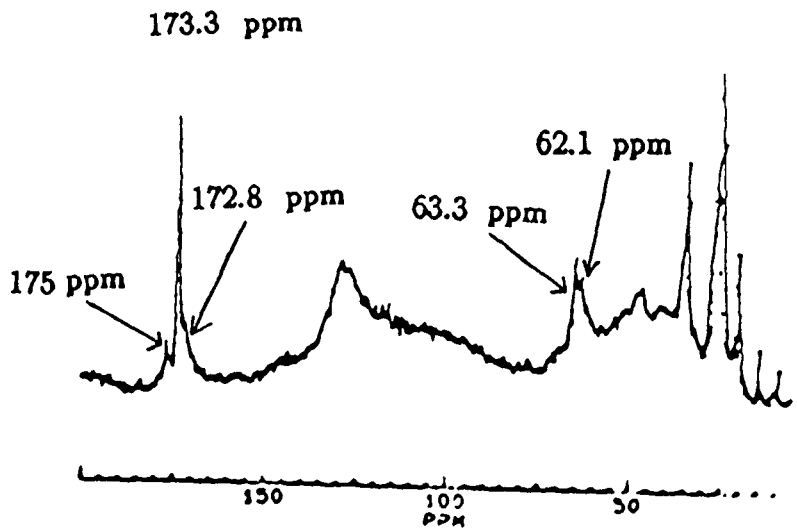

Recycle delay = 5 seconds

Figure 5.31

A comparison between the 5 second recycle delay SPE spectrum at room temperature and the 5 second recycle delay SPE spectrum at 80°C for the maleic anhydride film.

Parameters: AQ = 20 ms
NT = 3000

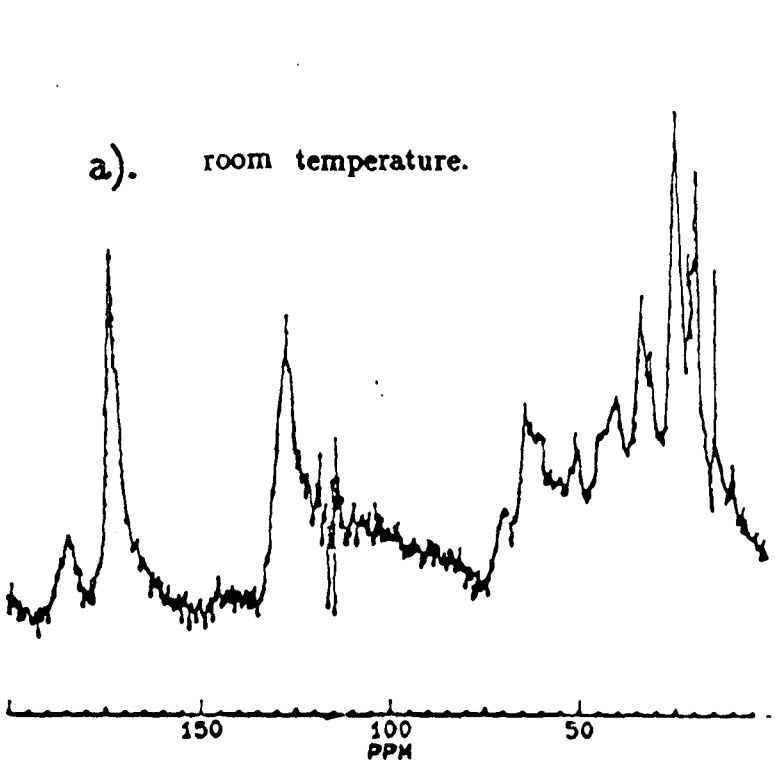

Recycle delay = 5 seconds

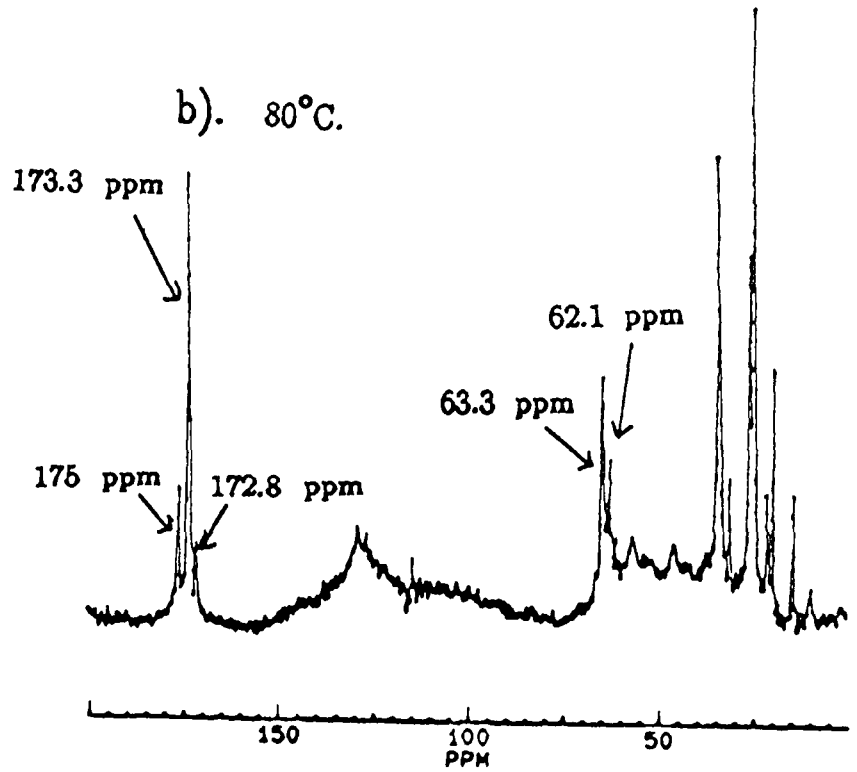

Recycle delay = 5 seconds

Figure 5.32

a). The peak at 175 ppm arises from the carbonyl at the end of the polyester chain before the triethanolamine tip.

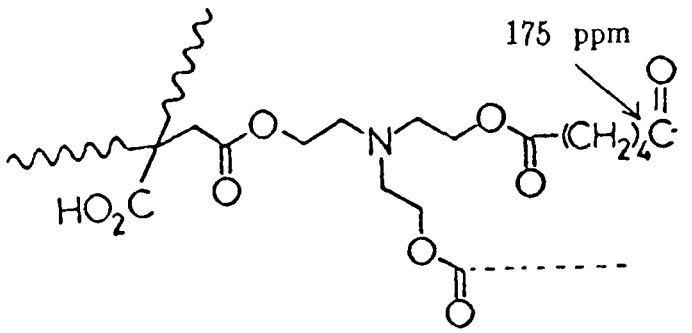

b). The peak at 172.8 ppm originates from the carbonyl next to a terminal ethylene glycol unit.

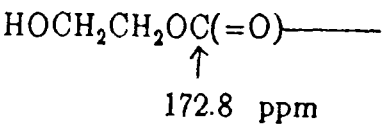

c). The peaks at 62.1 ppm and 63.3 ppm arise from the CH_2 in the alcohol component next to the ester linkage.

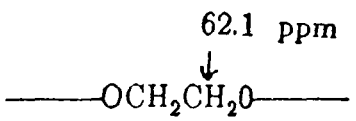

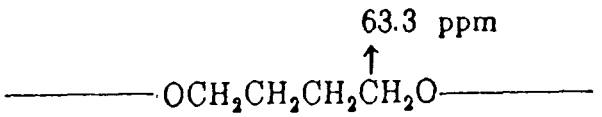

alcohol component next to the ester linkage as shown in figure 5.32c. The ethylene glycol component gives rise to the peak at 62.1 ppm, and the butane 1,4 diol component gives rise to the peak at 63.3 ppm.

5.4 Kinetics of the cure of the polymeric films[6,7]

It would be of great interest if the curing process between the acrylic copolymer and the triethanolamine–tipped polyester could be probed by solid–state NMR techniques. Unfortunately the cure is not very easy to follow by ^{13}C CP MAS techniques. The only regions of the spectra which changes during cure are the resonances arising from the formation of the cross–links. Due to a combination of the low intensity of the cross–link peaks and the broad resonances of other peaks, any changes in the intensity of old peaks and growth of new peaks are obscured by other resonances. Another method of monitoring the cure, therefore, had to be found.

It is predicted that as the cure progresses, the proton relaxation characteristics will change. It is well–known that the proton relaxation times change with both temperature and mobility. Initially, when the copolymer and the polyester are first mixed, both components are relatively mobile liquids. As the cure proceeds up until the gel point, the mixture becomes less and less liquid–like until at the gel point, a single three–dimensional network is formed. From then onwards, the film becomes less and less mobile as more cross–links are formed. The cure of the itaconic anhydride copolymer with the triethanolamine–tipped polyester was monitored by the proton spin–lattice relaxation times as a function of curing time. Stoichiometric amounts of itaconic anhydride copolymer

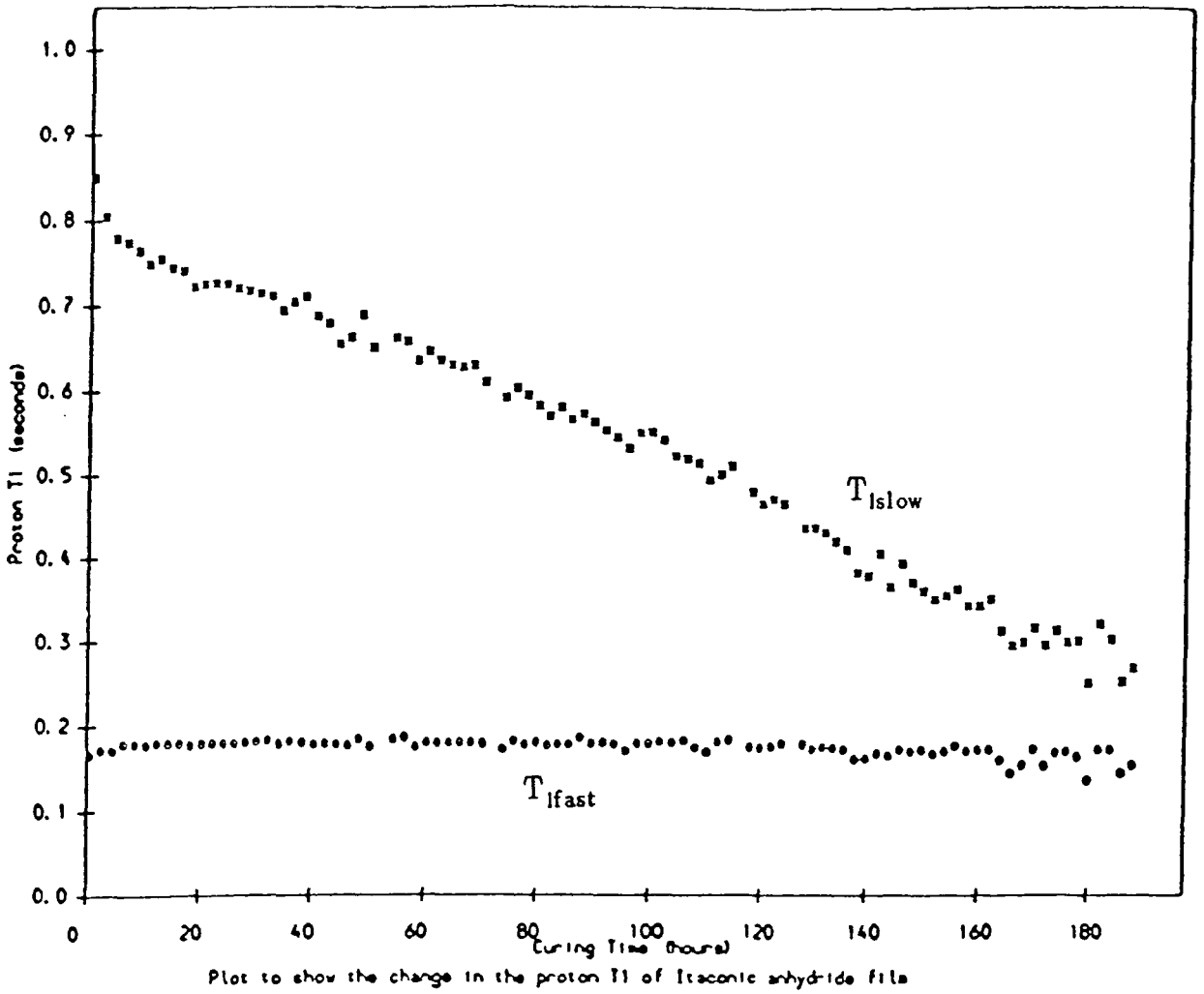

Figure 5.33

Plot to show the change in proton T_1 with curing time for the itaconic anhydride film. The recovery of the protons was biexponential, the two components of the proton T_1 were labelled T_{1fast} and T_{1slow} as shown in the figure.

and polyester were mixed thoroughly and placed in an NMR tube. Proton T_1 measurements were made using the inversion recovery pulse sequence at hourly intervals over a period of one week using a purpose–built proton/fluorine spectrometer operating at 60 MHz for protons. The plot of proton T_1 as a function of curing time is shown in figure 5.33. This study of the kinetics of the cure was carried out in a different situation to usual paint cure. The itaconic anhydride film network in this experiment was cured in the confined space of an NMR tube rather than in the usual environment of a thin cast film. One of the main differences between these two environments is the rate of loss of solvent. In a thin cast film solvent evaporation takes place much more rapidly than in a bulk network. The slow escape of solvent in the case of the bulk causes the cure to occur at a slower rate than for the cure of a thin film. The important factor in the rate of cure is the surface area:volume ratio. The larger this ratio, the faster the cure takes place. Therefore, not all the conclusions drawn from this experiment may be applicable to the kinetics of the cure of the itaconic anhydride network when cast as a film. There are several points of interest worth noting. The cure initially has a 2 component proton T_1 which gradually become closer together until finally, at the end of the cure, the two components are only separated by a factor of two and are therefore indistinguishable from each other. After seven days the cure is practically over; any changes in the proton T_1 are within the experimental error after this time. The copolymer before mixing has a proton T_1 of 0.85 seconds, and the polyester has a proton T_1 of 0.18 seconds. These times are close to the initial values of the proton T_1 after mixing, which suggests that the longer component of the proton T_1 arises from the copolymer in the network, and the shorter

component of the proton T_1 arises from the polyester in the network. It would appear that during the cure separate copolymer and polyester parts of the network can be resolved until approximately 140 hours into the cure when the two components become too close to be resolved. During the cure only the longer component of the proton T_1 changes significantly. It was expected that both components of the proton T_1 would change as cross–linking occurred. It is not at all clear why only the component arising from the copolymer parts of the network should change as the cure proceeds. It is possible that this is due to the effect of spin diffusion on the measured proton spin–lattice relaxation times. Another possibility is that there may be more than two components, but the components are too close together so that an average $T_1(^1H)$ is observed. During the cure the solvents evaporate. This loss of solvent is constrained to some extent by the conditions of the reaction. The solvent escapes from the system at a slower rate when the network is formed in bulk than when it is cast as a film. This loss of solvent will have an effect on the proton T_1 observed. The proton T_1 of butyl acetate, the comonomer solvent, was found to be 0.28 seconds at 60 MHz. This is close to the fast relaxing component of the proton T_1, although the proton T_1 for the solvent in the cross–linking medium is not necessarily the same as for the neat liquid. The fast relaxing component is apparently constant during the cure. This is a surprising observation as it would seem more logical if the fast relaxing component changed as solvent loss took place. However the fact that there is no apparent change in the value of the T_1 for the fast relaxing component during the cure may indicate that a balance is observed between the effects of solvent loss and curing.

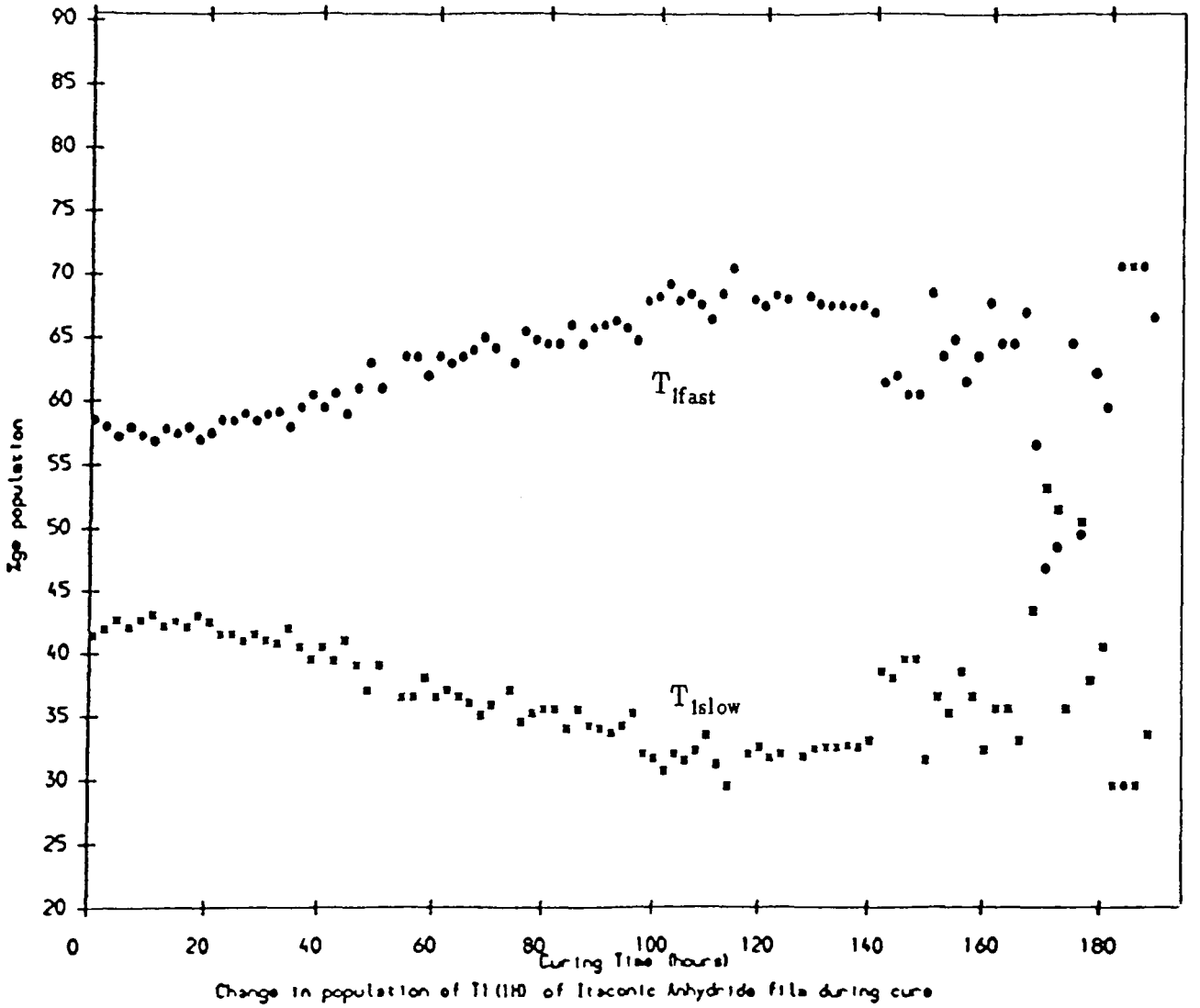

Figure 5.34

Plot to show the change in the populations of the two components with curing time for the itaconic anhydride film.

In order to clarify the effect of this loss of solvent on the proton T_1 observed during the cure, there are a number of possible experiments which could be carried out. If the loss of solvent from the polyester alone was monitored as a function of time by its proton T_1 value, then a direct comparison could be made between the proton T_1 of the polyester with time under conditions of loss of solvent but no cure, and the proton T_1 of the polyester component with time under conditions of loss of solvent and cure. Similar comparisons could be made for the copolymer component by monitoring the proton T_1 as a function of time for the copolymer as solvent evaporation takes place, and comparing this with the proton T_1 values observed for the copolymer component as the polymer system cures. A third experiment which would complement the last two suggested experiments is to monitor the proton T_1 as a function of time as the system cures in a sealed NMR tube. The sealed NMR tube would prevent loss of solvent during the cure, allowing a direct comparison between the cure observed with loss of solvent (figure 5.33) and the cure observed with no solvent loss.

It is interesting to determine on which side of the T_1 minimum the cure lies. As the cure proceeds, the network becomes more and more rigid. The proton T_1 decreases as the cure time increases. Therefore, an initial deduction would be that the cure lies to the left of the main T_1 minimum in the more mobile regime. However, on closer inspection, the more mobile polyester chains give the faster relaxing $T_1(^1H)$ component, and the more rigid copolymer chains give the slower relaxing $T_1(^1H)$ component. This would suggest that the cure actually lies to the right of the main T_1 minimum in the rigid regime. However, the proton T_1 values decrease as the cure proceeds, indicating that the cure occurs to the left

of a local minimum in the rigid regime.

The populations of these two components during the cure are shown in figure 5.34. The shorter T_1 component has the higher population, and the longer T_1 component has the lower population. Both the polyester and the copolymer are liquids before the cure takes place, and therefore initially neither component has any spin diffusion. Therefore, at curing time t=0, the populations should have their intrinsic values. As the cure proceeds, there is an apparent increase in the population of the fast relaxing component and an apparent decrease in the population of the slow relaxing component. The populations no longer have their intrinsic values, but are altered by the effect of spin diffusion. At a curing time of 140 hours to 190 hours almost total averaging is seen in the populations. It is in this part of the plot in figure 5.33 where the two components of the $T_1(^1H)$ are so close that they are within the experimental error of each other. Assuming that the two components of the T_1 arise from two distinct regions in the film, say A and B, then it is possible to state a few points about the relative sizes of the diffusion coefficients and the intrinsic T_1 values.

Using a one–dimensional two lamellar model it is possible to give some idea of the behaviour of the copolymer and polyester regions. Let the copolymer domains be called region A, and the polyester domains be region B. If L_A is half the lamellar thickness of region A and D_A is the spin diffusion coefficient of region A, then the time taken for magnetisation to diffuse out of a region is directly proportional to L_A^2/D_A. The relaxation of region A will be dominated by the intrinsic relaxation time of region A, T_A when $L_A^2/D_AT_A \gg 1$. However when $L_A^2/D_AT_A < 1$ then the relaxation in region A is dominated by spin diffusion to the faster

relaxing region B. It is unlikely that the parameters D_A, T_A, D_B and T_B remain constant during the cure. As the cure proceeds it can be expected that the spin diffusion coefficients and the intrinsic relaxation times will change. One prediction which is probably true is that the actual sizes of the regions L_A and L_B do not change appreciably after the gel point.

It is not possible from this data to gain a clearer indication of what is happening to the parameters D_A, D_B and T_A, T_B during the cure. There are an infinite number of solutions to explain the observed results. To summarise the conclusions drawn:

1). The cure in practically complete after one week

2). The values of the proton T_1 components are affected by spin diffusion during the cure

3). The domain sizes L_A and L_B of the polyester and the copolymer regions are unlikely to change appreciably after the gel point

4). The two T_1 components cannot be resolved at the end of the cure

5). The initial T_1 values at cure time t=0 are probably the intrinsic values at that stage

6). The faster relaxing polyester T_1 component has the higher population

7). D_A, D_B, T_A and T_B change during the cure.

5.5 Model studies of the cross–linking reaction

Because of the low intensity of the peaks arising from the cross–links and because of the complexity of the CP spectra obscuring

such peaks, it is not easy to study the curing process by ^{13}C CP NMR. The cross–linking reaction was studied using model compounds to simplify the spectra obtained. The copolymer was replaced by succinic anhydride, and the polyester replaced by various alcohol compounds. The aim was to observe the model cross–link formation, and to attempt to identify any intermediate and final compounds formed. The intention was to obtain an idea of the rates and mechanism of reaction.

5.5.1 Reaction between succinic anhydride and N,N dimethyl ethanolamine?

Excess N,N dimethyl ethanolamine was added to a 10mm NMR tube containing succinic anhydride dissolved in deuterated DMSO. The exothermic reaction was immediate, and by the time the first ^{13}C NMR spectrum was acquired, the reaction was complete. The reaction between succinic anhydride and N,N dimethyl ethanolamine was too fast to monitor the rate of reaction by NMR. Figure 5.35 shows the carbonyl region of the spectra obtained at 1, 3 and 5 minutes after the mixing of the reactants. The small peak at 176.8 ppm corresponds to unreacted carbonyl in succinic anhydride. The two large peaks belong to the carbonyls in the product. In the spectrum at three minutes two extra small peaks appear which subsequently disappear. The origin of these two peaks will be discussed a little later. Figure 5.36 shows the same three spectra, but this time the region between 35 to 60 ppm is shown. The assignments of the various peaks are shown on the diagram. Again, in the second spectrum 5 extra small peaks appear (indicated with arrows). These peaks disappear before the time reaches 5 minutes since the start of the reaction. Figure 5.37 again shows the same spectra, but this time

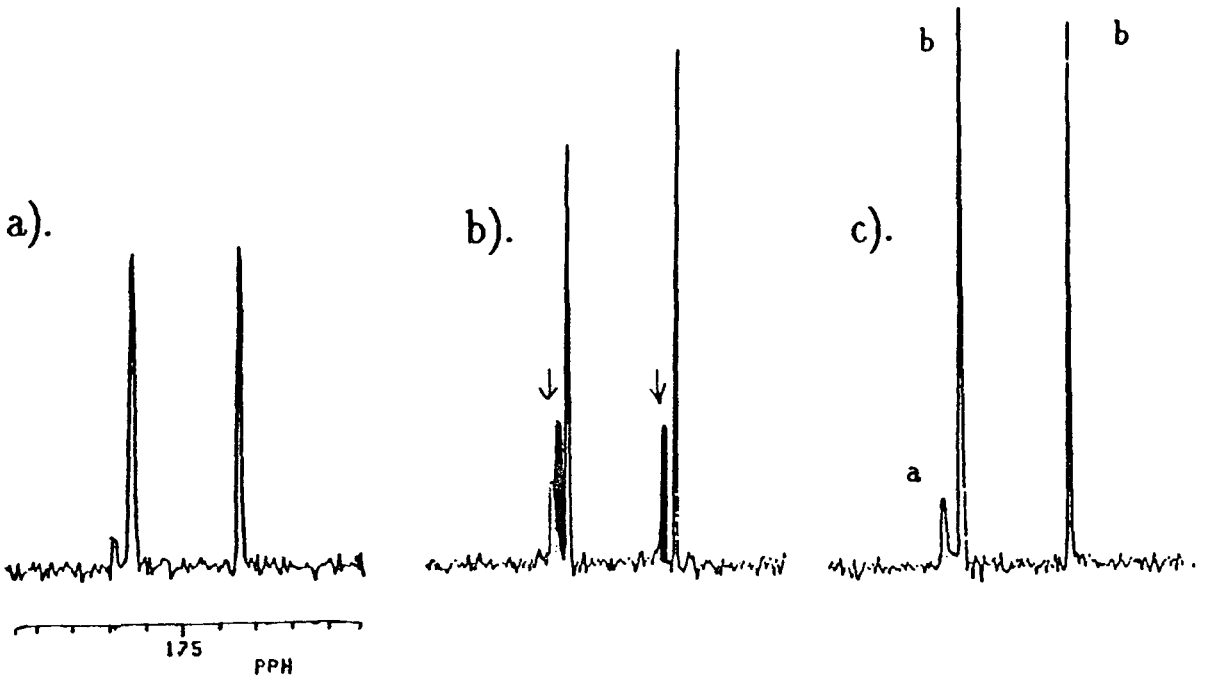

Time = 1 minute Time = 2 minutes Time = 3 minutes

Figure 5.35

The carbonyl region of the spectra obtained at 1, 3 and 5 minutes after the mixing of succinic anhydride and N,N dimethyl ethanolamine.

Parameters Recycle delay = 3 seconds

AQ = 0.2 seconds

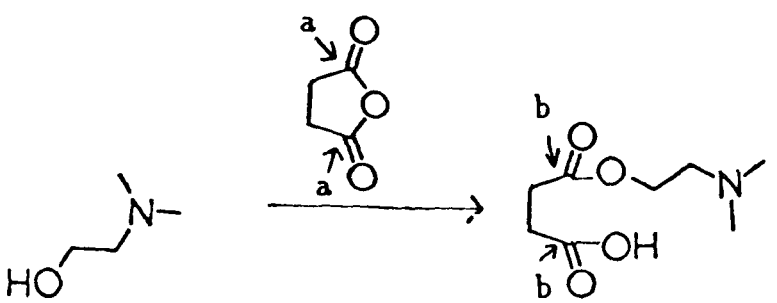

Figure 5.36

The region of the spectra between 35 and 60 ppm obtained at 1, 3 and 5 minutes after the mixing of succinic anhydride and N,N dimethyl ethanolamine.

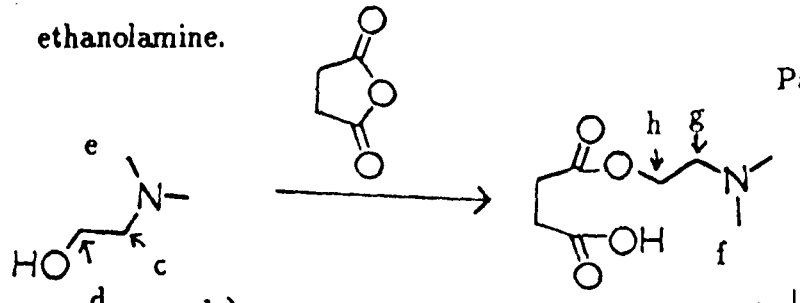

Parameters

Recycle delay = 3 seconds

AQ = 0.2 seconds

a).

b).

c).

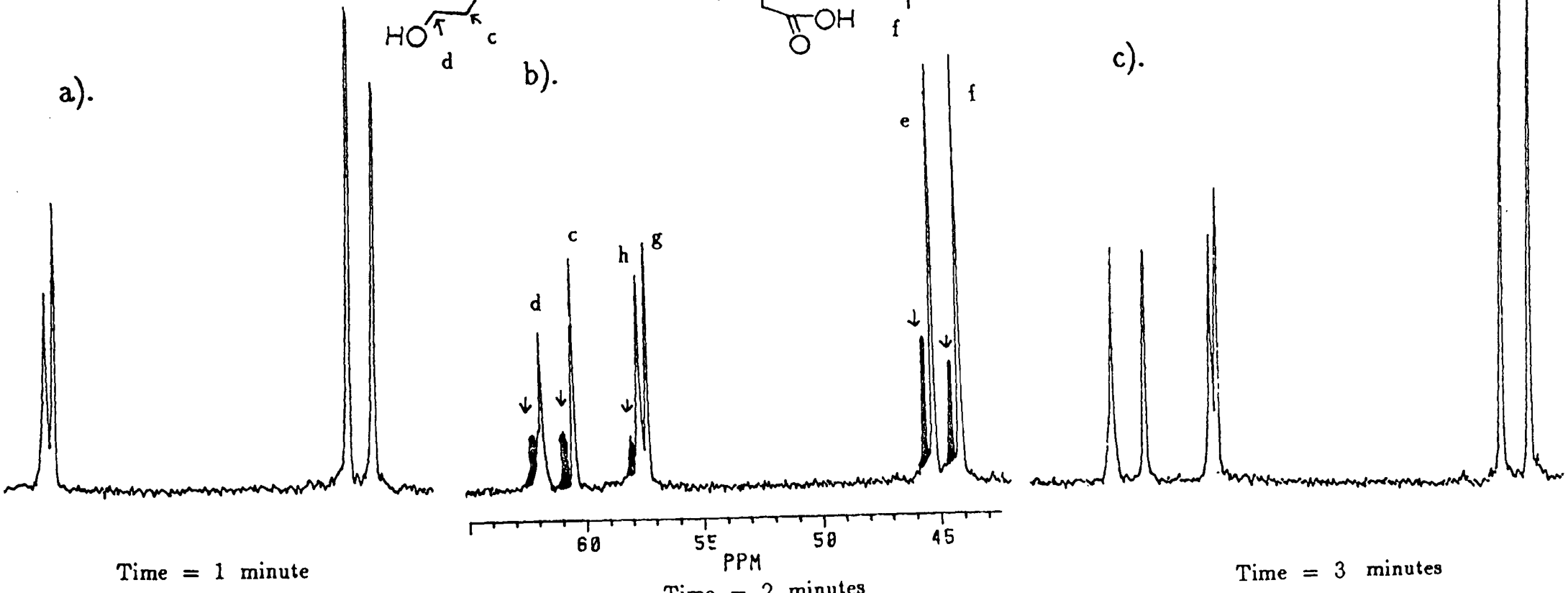

Time = 1 minute

Time = 2 minutes

Time = 3 minutes

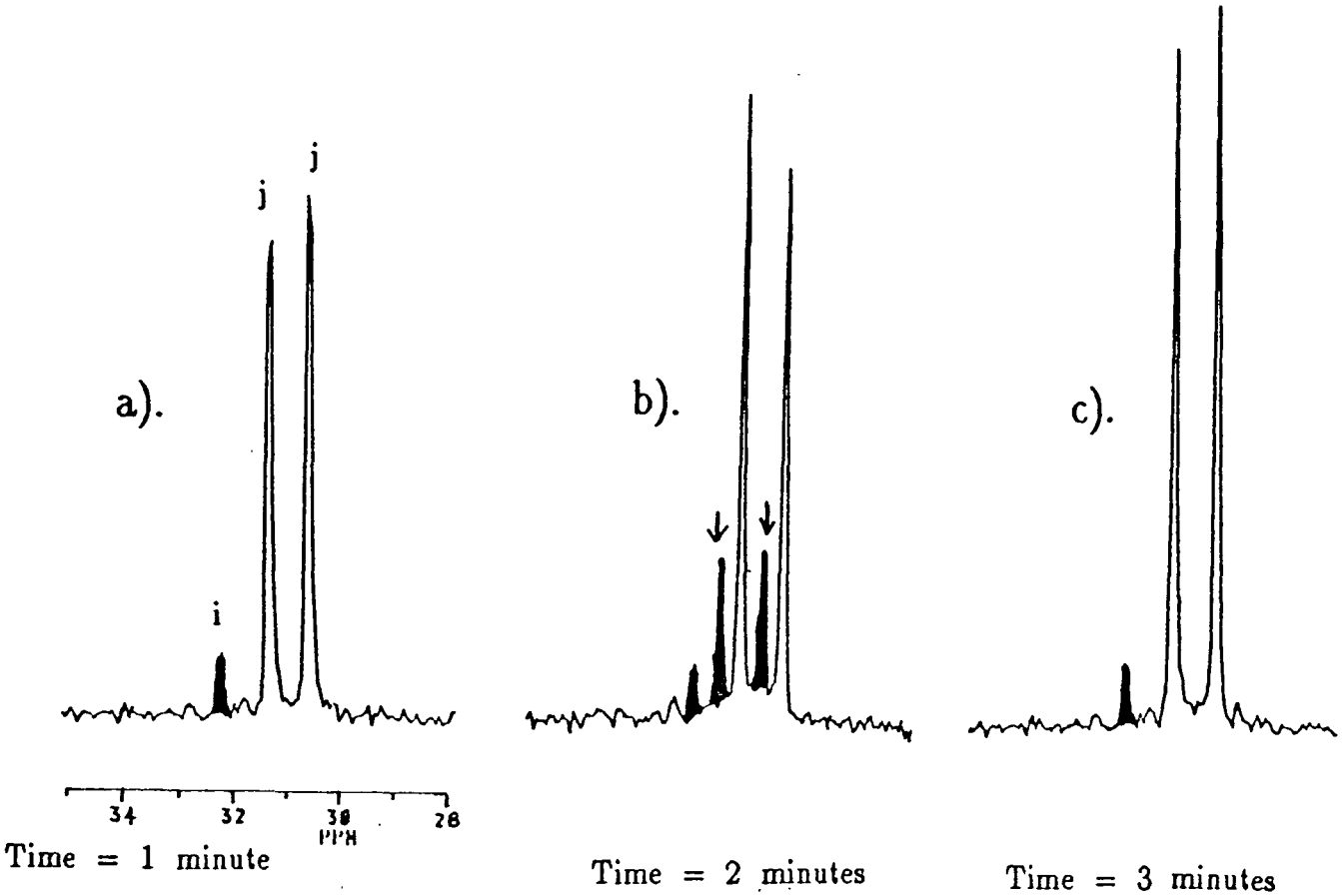

Time = 1 minute

Time = 2 minutes

Time = 3 minutes

Figure 5.37

The region of the spectra between 28 and 34 ppm obtained at 1, 3 and 5 minutes after the mixing of succinic anhydride and N,N dimethyl ethanolamine.

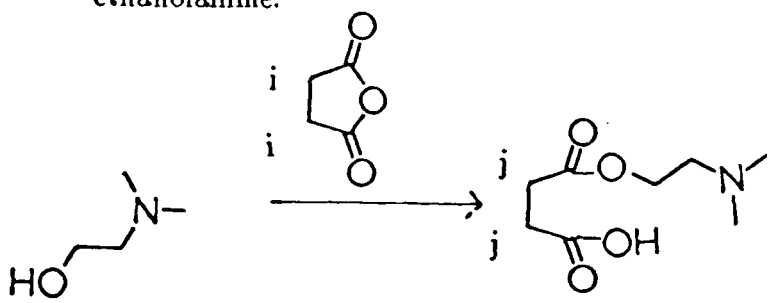

Figure 5.38

a). The salt formed from the reaction between succinic anhydride and N,N dimethyl ethanolamine.

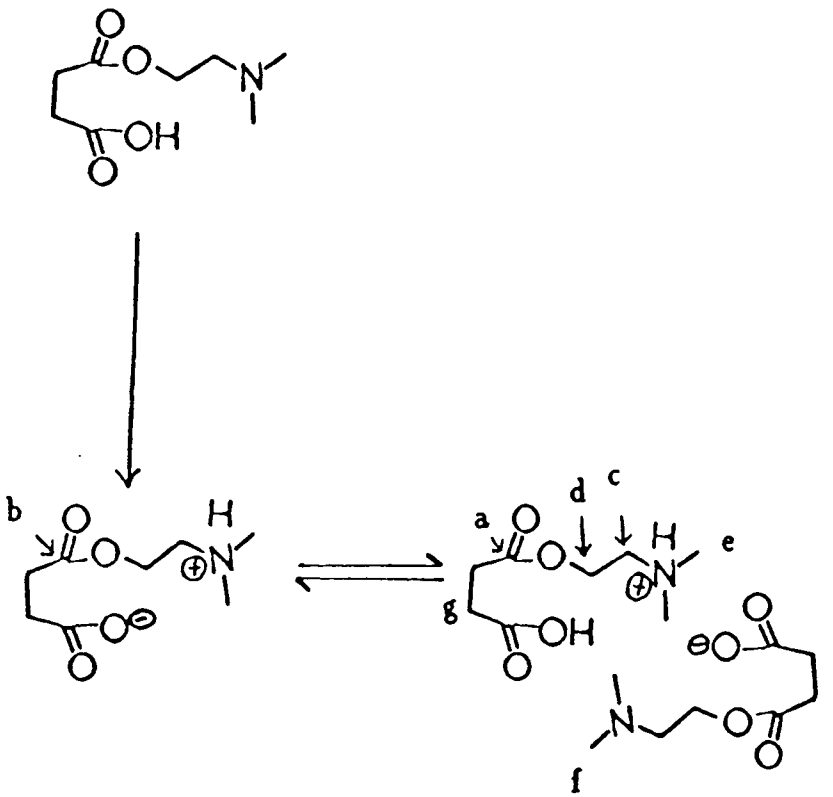

Figure 5.38

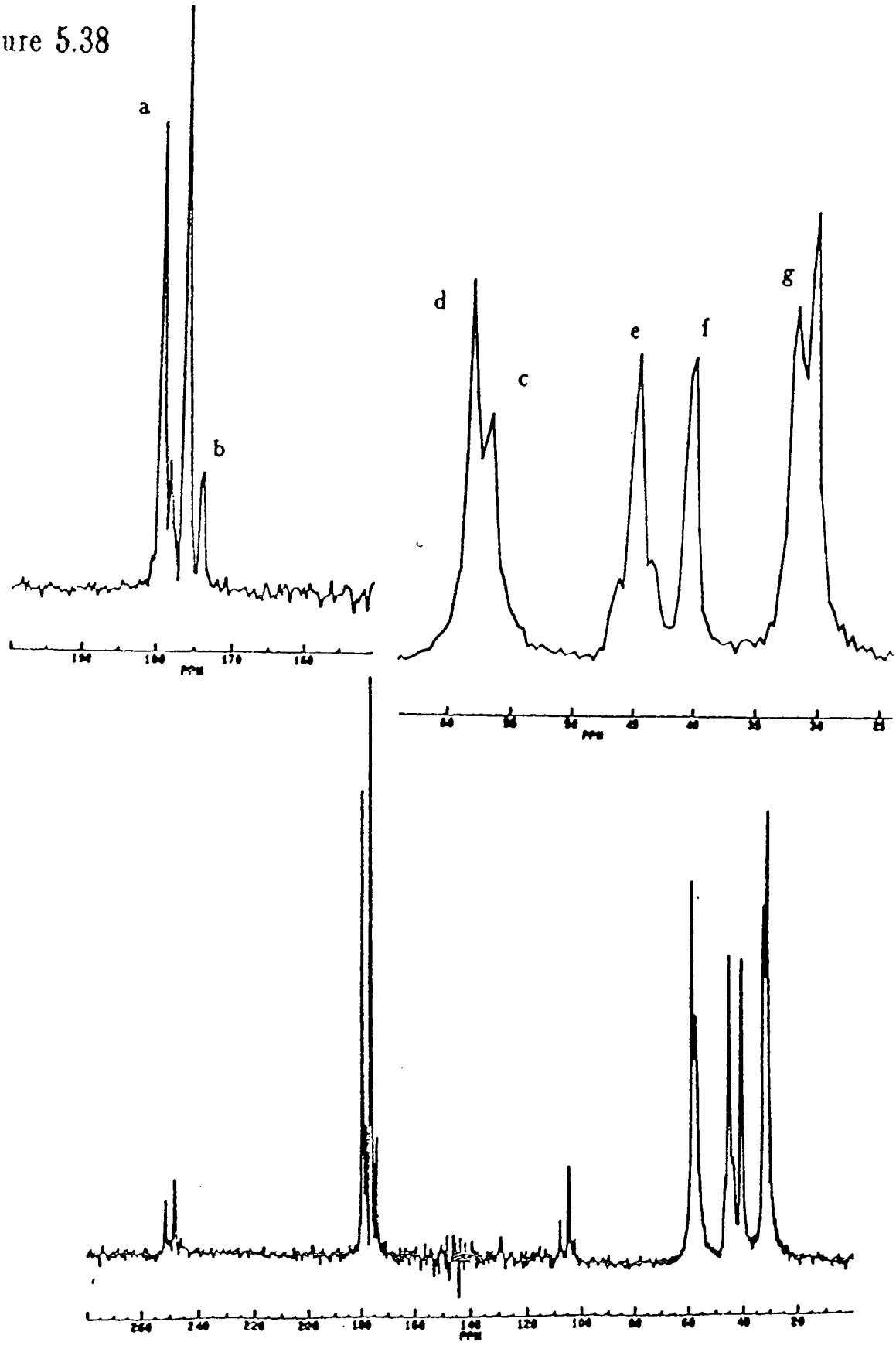

b). The ^{13}C CP NMR spectrum of the isolated salt.

in the region 28 to 34 ppm. The assignments are shown in the figure. Again two extra peaks are seen in the spectrum at 3 minutes since the start of the reaction. In the spectrum acquired at three minutes after the start of the reaction there is a second species formed, which subsequently disappears. It is thought that this species is the salt of the product, as shown in figure 5.38a. When the reaction is repeated but this time using acetone as the solvent, a large amount of salt precipitates out of solution. This salt has been isolated, and studied by ^{13}C cross–polarisation NMR. The ^{13}C CP NMR spectrum of the isolated salt is shown in figure 5.38b. There are two salt species present. The assignments are shown in the figure. Acetone is a less polar solvent than DMSO, thus the more polar salt species are less soluble in acetone.

5.5.2 Reaction between succinic anhydride and 4–(2–hydroxyethyl) morpholine

The reaction between succinic anhydride and 4–(2–hydroxyethyl) morpholine was studied in a similar way to the reaction between succinic anhydride and N,N dimethyl ethanolamine. Excess 4–(2–hydroxyethyl) morpholine was added at time zero to a solution of succinic anhydride dissolved in deuterated DMSO and the mixture was allowed to react in an NMR tube. The reaction was monitored by solution–state ^{13}C NMR.

The spectra in the region 170 to 175 ppm are shown together with assignments in figure 5.39. The loss of succinic anhydride as the reaction proceeds can clearly be seen. Several points of interest may be made. The time taken for the reaction to reach completion is much longer than for the reaction between succinic anhydride and N,N dimethyl ethanolamine.

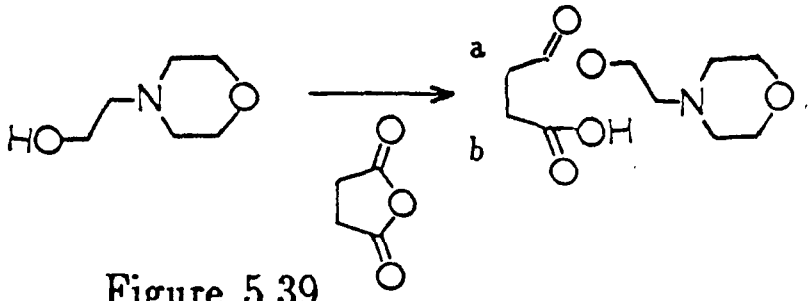

Parameters Recycle delay = 3 seconds

AQ = 0.2 seconds

Figure 5.39

The carbonyl region of the spectra obtained after the mixing of succinic anhydride and 4–(2–hydroxyethyl) morpholine.

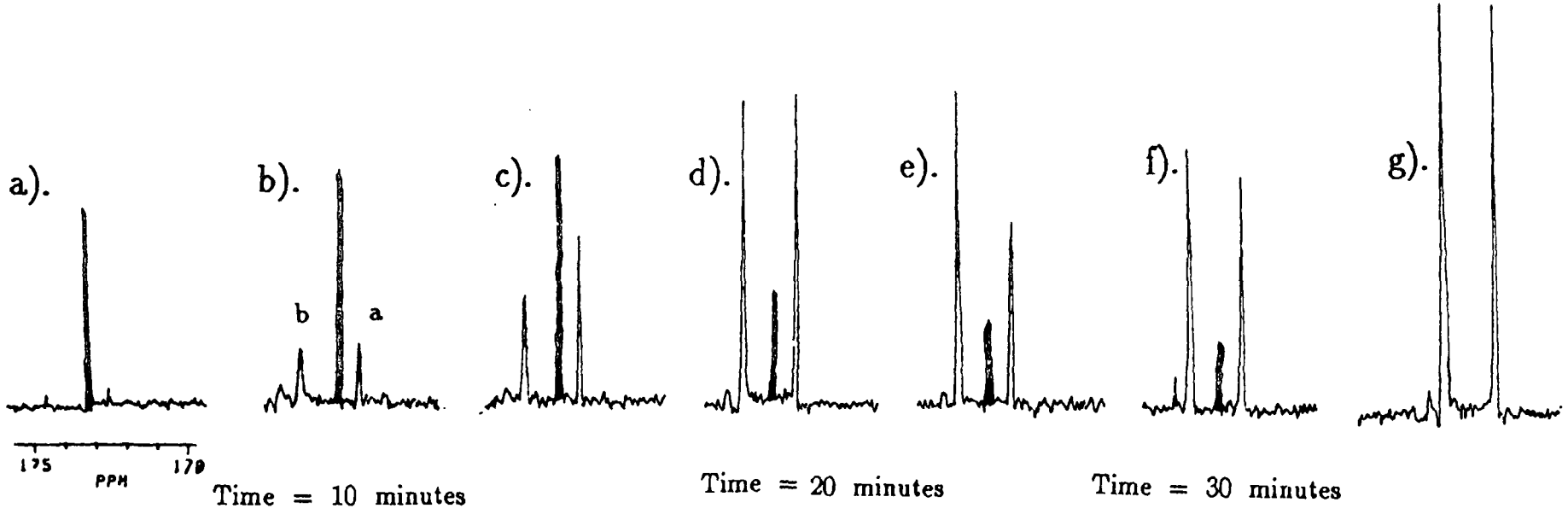

This is because the 4–(2–hydroxyethyl) morpholine is more sterically hindered than N,N dimethyl ethanolamine. 4–(2–hydroxyethyl) morpholine is also less basic than N,N dimethyl ethanolamine, causing the former to be less reactive with an anhydride. No evidence was found of the formation of salts as in the case of N,N dimethyl ethanolamine and succinic anhydride in either DMSO or acetone.

Overall the cross–linking reaction becomes much slower the less basic the amine and the more hindered the amine. Salt formation has been shown to take place in the reaction between succinic anhydride and N,N dimethyl ethanolamine, and conclusive evidence that the salt has two different structures has been shown.

Although such reactions are very simple compared to the cross–linking reaction between an acid anhydride copolymer and a triethanolamine–tipped polyester, the general trends shown by such reactions give an indication of what occurs in the cross–linking reaction between the two polymers.

CHAPTER 6

Degradation of acid anhydride/hydroxyl cross-linked systems.

6.1 Introduction

Both natural and synthetic polymers deteriorate as a result of conditions encountered during exposure. The changes in composition and structure lead to the degeneration of useful properties and, ultimately, to failure of the polymer. The cracking of rubber, the yellowing of cotton fabrics and the embrittlement of plastics are typical examples of polymer deterioration. These and similar changes occur under a wide variety of conditions, generally described as the exposure environment.

6.2 General aspects of polymer deterioration

Polymers vary widely in their vulnerability to deterioration when exposed to the same environment. These variations in stability are caused primarily by differences in chemical structure, but they also result from trace impurities in the polymer. Partially degraded molecules are a common impurity in polymers, and these modified molecules often initiate deterioration. Stability is also dependent on the physical structure or morphology of the polymer.

6.3 The exposure environment[1]

Both chemical reactants and energy sources contribute to the deterioration of polymeric materials. Although a wide variety of chemical reactants in the environment is responsible for polymer deterioration, oxygen is probably the most important. Most polymers react with oxygen under extreme conditions at combustion temperatures, and many oxidise extensively at much lower temperatures. Water ranks next to oxygen in importance as a chemical reactant in the exposure environment. Although its effect is most evident in the hydrolysis of condensation polymers, certain addition polymers are also vulnerable, and hydrolysis of side groups, for example, ester groups can adversely affect important properties. Hydrolysis of polymers is often catalysed by traces of acids or bases. This chapter is concerned with the hydrolysis of both the itaconic anhydride film and the maleic anhydride film.

For completeness, other methods of degradation are mentioned briefly. The absorption of several types of energy by polymers initiates or accelerates those chemical reactions responsible for deterioration. Various forms of radiation and mechanical stress contribute to polymer failure. Acceleration of deterioration by heat is a general phenomenon responsible for the degradation of polymers both in the presence and absence of chemical reactants. Ultraviolet radiation initiates the deterioration of many polymers, and mechanical stress also contributes to failure.

Long–term aging is the most important period of exposure. During this period the polymer is exposed to conditions of actual use. Deterioration is usually slow and can escape detection for long periods of

time. When visible effects become apparent, many polymers may already have failed for the application intended.

6.4 Hydrolytic degradation[2]

Moisture can have a deleterious effect on some types of polymer. Hydrolysis is a very important deteriorative process in modern polymer technology as many commercial materials incorporate hydrolysable linkages. These materials include polyesters, polyurethanes and polycarbonates. In each of these groups the hydrolysable group is almost invariably part of the main chain structure. Hence hydrolysis results in chain scission, leading to a rapid decrease in molecular weight and consequent rapid deterioration in the mechanical properties such as the tensile strength.

Polymers are much more resistant to hydrolysis than might be predicted from the behaviour of low molecular weight model compounds. This is not due to the inherent difference in stability of the hydrolysable linkages but to the fact that attack by the water is usually confined to the surface because of the hydrophobic nature of most organic polymers, and because of the subsequent low rate of diffusion of aqueous solutions into the polymer bulk. In the overall weathering process in many polymers there is no doubt that both the humidity and the presence of liquid water often play a significant role. It is usually difficult however to disentangle the effects of a large number of degradation mechanisms at work in typical outdoor exposures where the effects of sunlight and oxygen are paramount. There are some situations, however, in which there is no doubt that hydrolysis is the most important mechanism.

6.5 Acid anhydride/hydroxyl degradation studies[3]

The acid anhydride/hydroxyl cross–linked systems are intended for use as coatings for yachts. The cross–linked coatings must therefore be durable against various kinds of weathering. Throughout its lifetime, the coating must retain its colour and glossy appearance, be resistant to peeling and cracking, as well as maintain its physical and mechanical properties such as its strength and adhesion. The potential environment of a yacht paint is in humid, wet conditions such as are found in the mediterranean. In order to predict the durability of the acid anhydride/hydroxyl cross–linked systems under these conditions, accelerated tests were carried out on the films by Courtaulds Coatings. Although accelerated tests are not conclusive evidence for the prediction of the weathering of a coating in its intended environment, they are generally recognised as useful in so far as they indicate how the coating is likely to behave in long–term natural exposure tests. High humidity was identified as the most aggressive environment for the films. A series of experiments were carried out by Courtaulds Coatings to study the effect of high humidity on the films.

The films were prepared by mixing together stoichiometric amounts of the component polymer solutions. The mixture was degassed under vacuum. The films were drawn onto PTFE sheets to produce dry films between 150–200μm thick. The samples were cured for 24 hours in a dust–free environment at ambient temperature and humidity. The films were then exposed to an environment of 30% relative humidity at 25°C

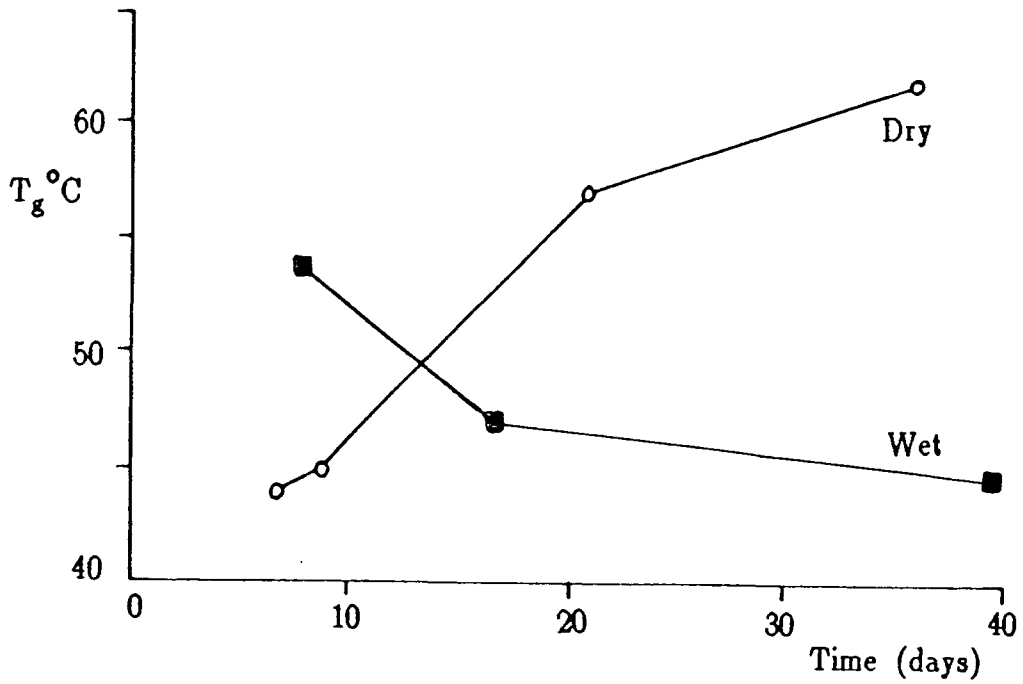

Figure 6.1

A comparison between the T_g of itaconic anhydride film which was subjected to 35°C/100% relative humidity and the T_g of itaconic anhydride film which was subjected to dry conditions only. Reproduced with permission from Courtaulds Coatings.

for 6 days, and the cure was allowed to continue. The cured films were placed in an environmental cabinet at 35°C and a relative humidity of 100%. These conditions attempted to simulate the environment which a yacht paint could be expected to be exposed to. The samples were removed at intervals to monitor the progress of the degradation. Both the itaconic and the maleic anhydride films showed evidence of irreversible degradation. The T_g of the itaconic anhydride film at 35°C/100% relative humidity was monitored as the degradation progressed, and was compared to the T_g of the sample of the same age, but which had not been exposed to the wet conditions. The results can be seen in figure 6.1. The clear film became white and opaque as degradation occurred, and a progressive lowering of the T_g was observed compared to the itaconic anhydride film which had undergone similar ageing in dry conditions.

Another method of monitoring the extent to which degradation has occurred is by measurement of the increasing sol fraction. The sol fraction is obtained by weighing a strip of degraded film of size 25×10×0.2mm. The strip was soaked in excess butan–2–one solvent for 5–6 hours. The solvent was then discarded, and the film soaked further in fresh solvent. The strip of film was then dried overnight at a slightly elevated temperature, and then reweighed. The ratio

$$\frac{\text{Weight of extracted material}}{\text{Weight of insoluble network polymer}}$$

is the sol:gel ratio.

The sol fraction increased as the age of the itaconic and maleic anhydride films kept at 35°C/100% relative humidity increased. The increasing sol fraction shows that hydrolysis of the network is taking

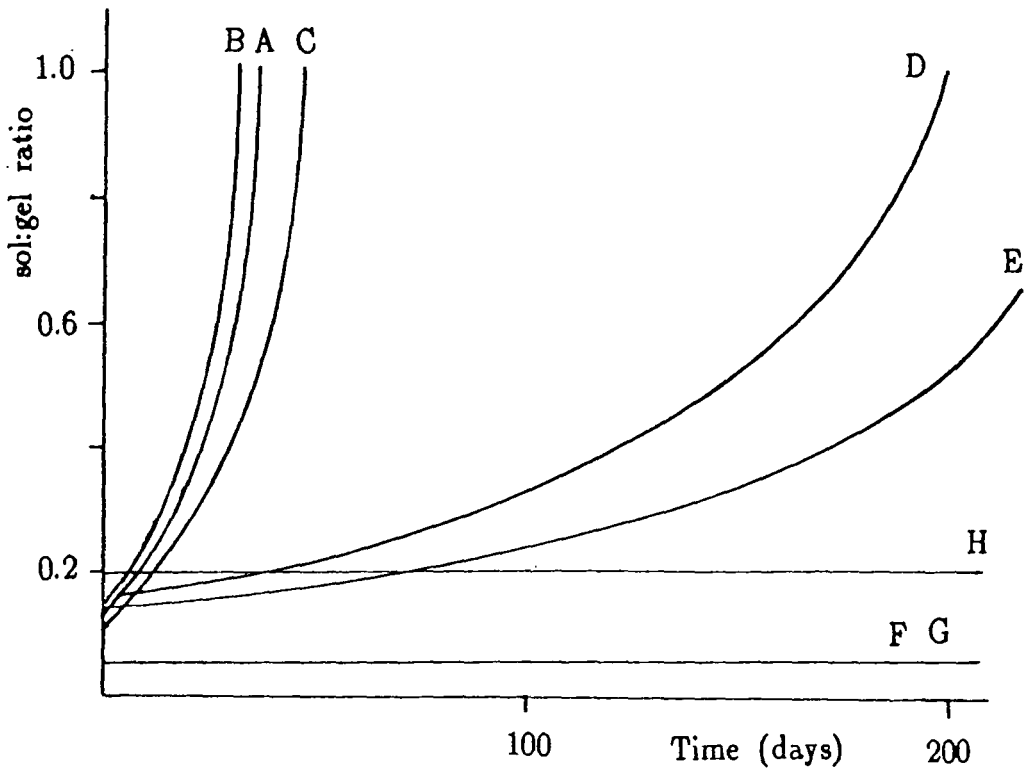

Figure 6.2

Sol/gel against age data for the itaconic anhydride films of the resins A to H. Reproduced with permission from Courtaulds Coatings.

Table 6.1

Resins A to H used as cross–linkers in figure 6.2

Key

A	Adipic polyester hydroxyamine
B	Adipic polyester hydroxyamine, 50% extended with triethanolamine
C	Azelaic polyester hydroxyamine
D	Cycloaliphatic polyester hydroxyamine
E	Hydrocarbon hydroxyamine
F,G	Aliphatic and aromatic linear polyesters cured with aliphatic triisocyanates
H	Proprietary system based on maleic copolymer and acrylic polyol.

Resins A to E are used to cross–link the itaconic anhydride copolymer.

place, and hence the measurement of the increasing sol fraction is a powerful technique for assessing the hydrolytic stability of the films. The degradation of a range of films was studied by the sol:gel method. The copolymer of itaconic anhydride, styrene and methyl methacrylate was cross–linked with a range of resins (A–H in table 6.1) where resin A is the most susceptible to water attack, and resin H the least. Figure 6.2 shows the sol/gel against age data for all of the itaconic anhydride films of the resins A to H. It can clearly be seen that the less hygroscopic the cross–linker resin, the less is the extent of degradation.

Although these data on hydrolytic ageing cannot identify the sites of degradation, a general trend in the rates of degradation may clearly be seen. The three cross–linkers A,B and C which have ester linkages along the main chain degrade at a much faster rate than cross–linkers D and E which have only hydrocarbons along the main chain. The itaconic anhydride films formed with cross–linkers H, F and G are not seen to degrade at all under conditions of 35°C and 100% relative humidity. All five resins A to E have a triethanolamine extension at the cross–link which is a possible cleavage site, whereas resins F, G and H are based on triisocyanates (F, G) and an acrylic polyol which do not have a triethanolamine cleavage site either at the cross–link or along the polymer chain.

Although these suggestions explain the observed relative rates of the various resins, the hydrolytic ageing data do not supply any concrete evidence to identify the actual sites of degradation. This was attempted through spectroscopic means.

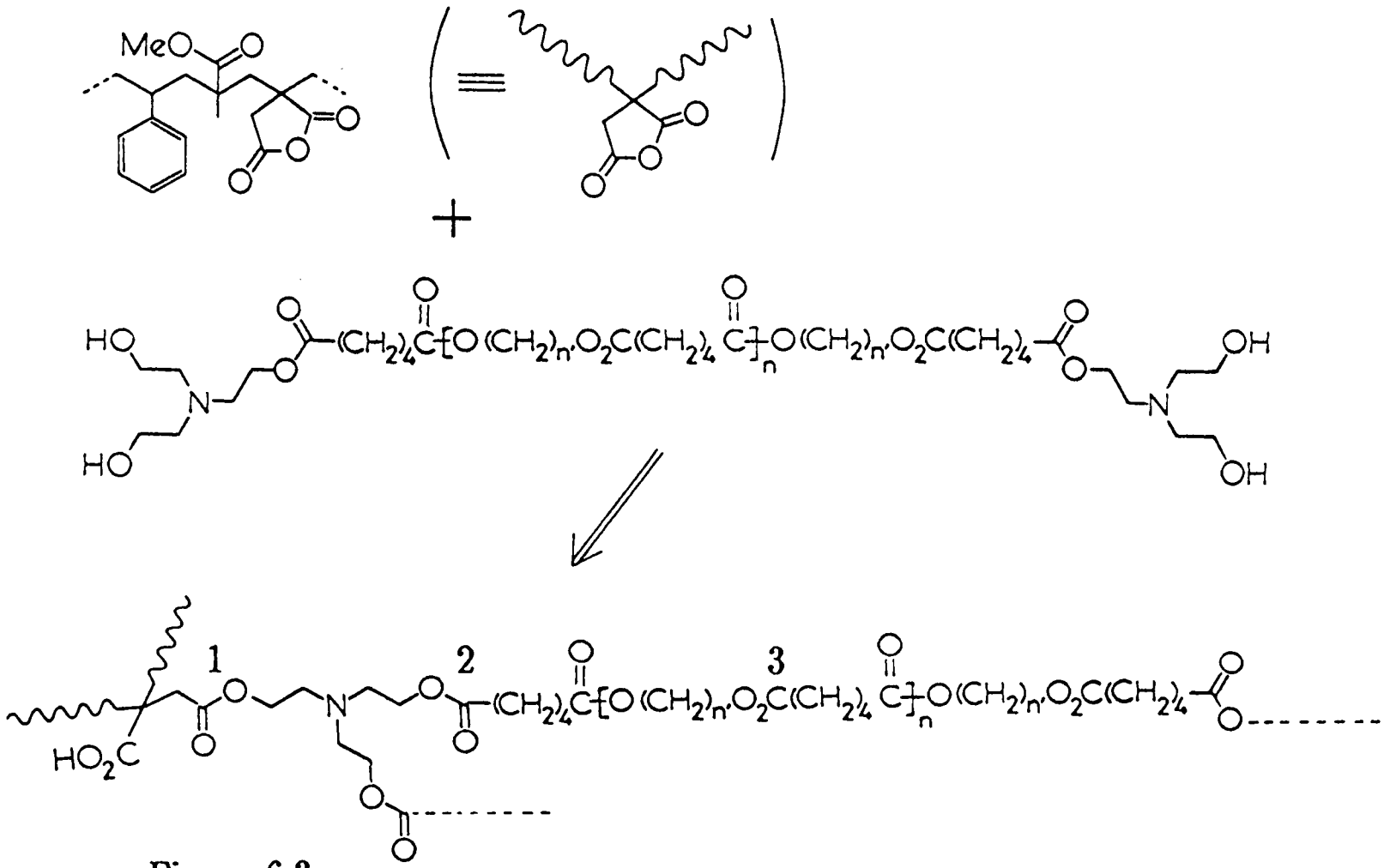

Figure 6.3

Possible sites of degradation in acid anhydride/hydroxyl systems.

6.6 Possible sites of degradation in acid anhydride/hydroxyl systems

Figure 6.3 shows the general structure of the itaconic anhydride film. There are three possible sites for hydrolysis to occur:

1. at the half–ester cross–link
2. at the ester linking the triethanolamine to the polyester backbone
3. at an ester linkage in the polyester backbone

Cleavage at position 1. would result in amine attached to the polyester unit, whereas cleavage at position 2. would leave amine–functional acrylic and acid–tipped polyester. Failure at position 3. would lead to polyester fragments.

There are two degradation models to consider.

6.6.1 Model A: cleavage only occurs at positions 1. and 2.

If cleavage were only to occur at the cross–links, it is reasonable to predict that scission of a few linkages would initially release polyester fragments of network only. As the degradation proceeds, scission takes place at more and more bonds. Therefore as hydrolysis continues, fragments containing copolymer as well as polyester are released. As even more cleavages take place, the fragments of copolymer and polyester break down into smaller fragments, until eventually the network is completely reverted back to molecules resembling the network precursors.

6.5.2 Model B: Cleavage occurs at all three positions

If cleavage were to occur along the backbone of the polyester chain as well as at the cross–link sites, then the prediction is that initially only polyester fragments of network will be released, with copolymer being released as the degradation proceeds for the same reason as in model A. If a scission occurs at position 3 in figure 6.3, then the ester linkage in the polyester chain which is next to the cleavage is more susceptible to attack than other ester linkages along the chain. This is known as the anchimeric effect, and is discussed in more detail later in the chapter. The net result towards the end of degradation will be that the network will contain intact copolymer chains together with fragmented polyester chains.

6.7 Characterisation and analysis of the sol product[4]

6.7.1 GPC

Sol extracts of the itaconic anhydride film with ageing periods ranging from just cured to 115 days showed progressive increases in apparent peak molecular weight as the age of the film increases. However the fragments expected from polyester cleavage are low molecular weight and highly functional. Such samples are at the limits of the range of the GPC apparatus, thus the results may only be treated as a guide.

6.7.2 NMR

Both ^{1}H and ^{13}C spectra of the sol fractions were obtained by

Courtaulds Coatings using a Bruker WP80 FTNMR spectrometer operating at 80MHz for protons and 20MHz for carbon. The spectra contained residues of both the acrylic and the polyester. However both the spectral resolution and the signal to noise were poor. The results were inconclusive; it was unclear if the polyester present was intact or in fragments.

6.7.3 HP liquid chromatography

Two major broad peaks were observed by HPLC. The first peak, and therefore the less polar of the two, is assigned to the polyester component in the sol. The second peak, which is more polar, contained acrylic. It could not be concluded, however, that the second peak did not contain some polyester residues.

6.8 Conclusions

From the evidence it is unclear exactly how the film degrades. The itaconic anhydride film samples are hydrolytically unstable resulting in the breakdown of either the polyester–triethanolamine linkage or the acrylic–triethanolamine cross–link, or both. No definite evidence from the sol fractions has been found which concludes beyond doubt that the ester linkages along the polyester backbone either do or do not hydrolyse. Although no precursor fragments of the polyester have been directly observed in the sol fractions, it is possible that these fragments could have been washed out of the film samples during the ageing process in the environmental cabinet. In order to complete the study of the

Table 6.2

Assignment of the peaks in the maleic anhydride film spectrum.

Peak/ppm	Assignment
173.5	C=O of MMA, cross–link, and polyester
143	Aromatic quaternary carbon of styrene
127.8	Aromatic C–H of styrene
63.1	O=C–O–CH_2 in polyester chain
51.3	CH_3O of MMA
45	Quaternary carbon of MMA
40–45	CH backbone carbons
41.5	CH of polystyrene
40.8	CH_2 'backbone' of copolymer
33.8	O–C(=O)–CH_2 in polyester chain
24.9	CH_2 'backbone' of polyester
19.6	CH_3 of MMA

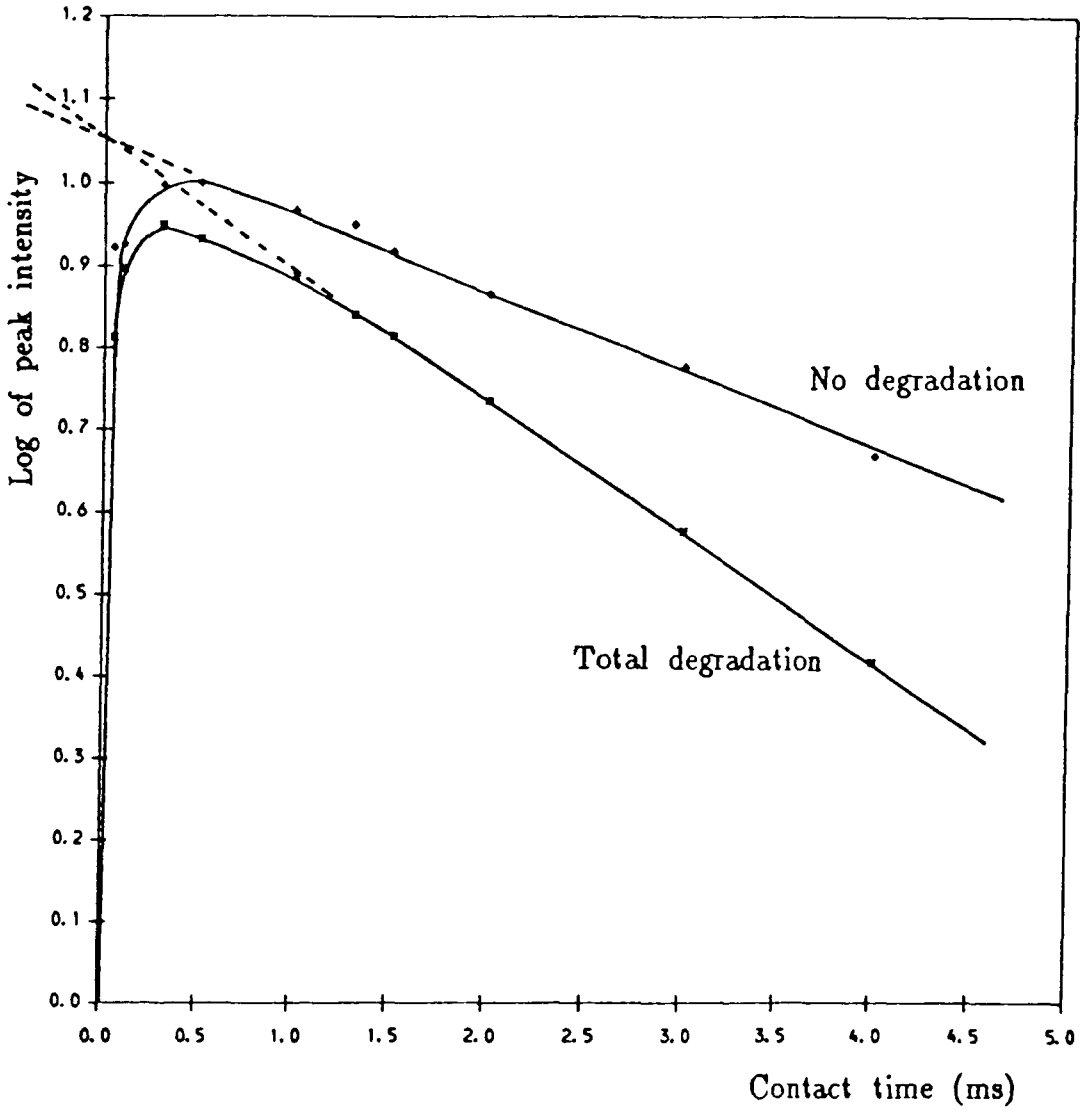

Figure 6.4

Plot of the log of the peak intensity against contact time for the copolymer peak at 40 ppm in the maleic anhydride film. The maleic anhydride film with no degradation is compared to the film with total degradation for contact times between 0.05 and 4 ms. The recycle delay was 6 seconds, the acquisition time was 26 ms and 1000 transients were acquired for each experiment.

degradation, the solid parts of the films were studied using solid–state ^{13}C MAS NMR. The intention was to study the solid fraction of the degraded films in order to clarify whether or not hydrolysis was occurring at the ester linkages along the polyester chains. The degradation of both the itaconic anhydride film and the maleic anhydride film was studied by solid–state NMR. Samples of the maleic anhydride film were prepared at four different stages of the degradation: no degradation (i.e. 1 week cure), 2 weeks degradation, 4 weeks degradation and total degradation (3 months degradation).

6.9 The degradation of the maleic anhydride film

During the curing reaction between the maleic anhydride, styrene and methyl methacrylate copolymer with the triethanolamine tipped polyester, the system converts from a liquid into a solid. Hence, if this process is reversed by hydrolysis, it is expected that the films would become less rigid as degradation progresses.

As the film degrades, any change in the absolute intensity of a particular peak may indicate a change in the chemical structure of the carbons which give rise to the peak. In order to study the change in intensity of the various carbons as the film degrades, variable contact time cross–polarisation experiments were carried out on the films at various stages in the degradation process.

Figure 6.4 shows the variable contact time intensities of the peak at 40 ppm (the CH_2 backbone of the copolymer). The assignments of the peaks for the maleic anhydride film are shown in table 6.2. The maleic

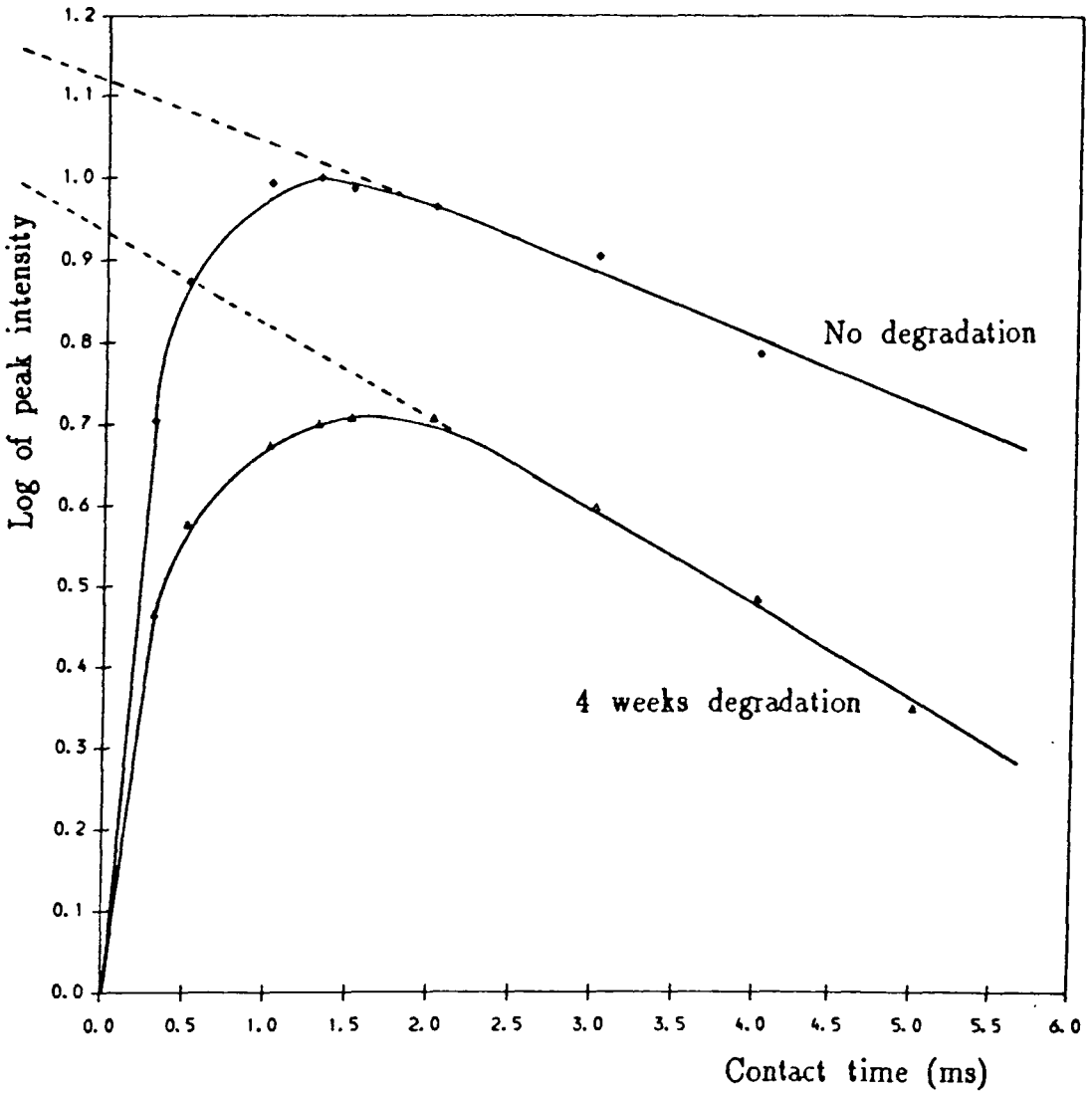

Figure 6.5

Plot of the log of the peak intensity against contact time for the polyester peak at 173 ppm in the maleic anhydride film. The maleic anhydride film with no degradation is compared to the film with 4 weeks degradation for contact times between 0.3 and 5 ms. The recycle delay was 6 seconds, the acquisition time was 26 ms and 1000 transients were acquired for each experiment.

Figure 6.6

Types of carbons in the polyester chain.

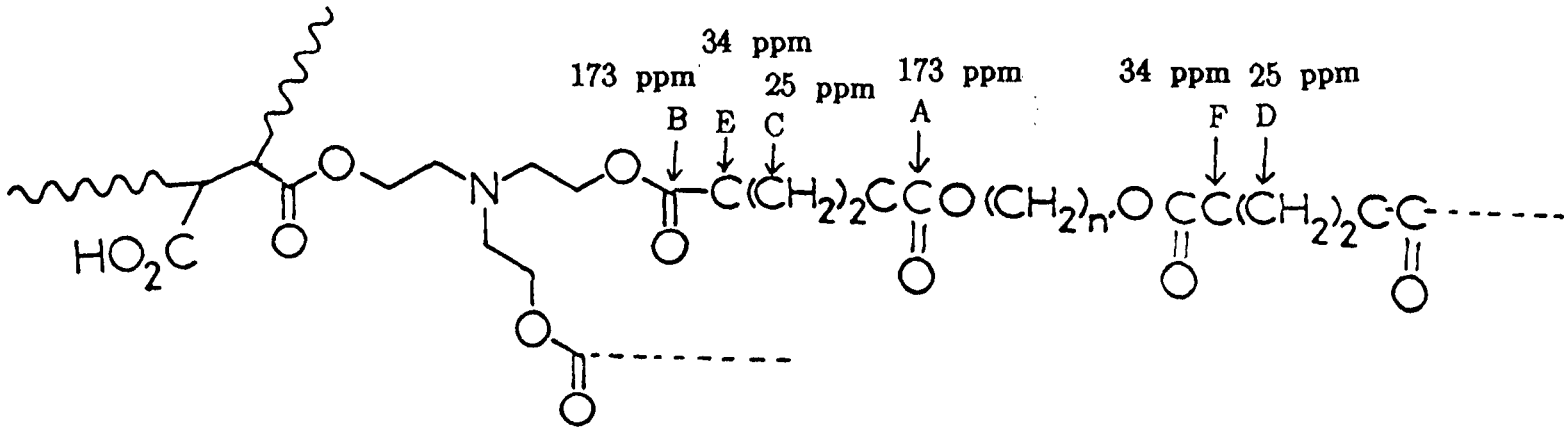

anhydride film with no degradation is compared to the film with total degradation for contact times between 0.05 and 4 ms. Extrapolating back to the intensity axis, it is found that the film without degradation and the film with total degradation both intercept the y axis at the same point. From this it may be concluded that the copolymer backbone remains intact during the degradation of the polymer film. Hence any degradation in the maleic anhydride film must be taking place either at the cross–links or along the polyester chain, or both.

A similar plot is shown in figure 6.5 for the peak at 173 ppm (the carbonyls in the polyester chain). Figure 6.5 compares the intensities of the maleic anhydride film with no degradation to the maleic anhydride film with 4 weeks degradation. A decrease in the intensity of 16% is seen for the film with 4 weeks degradation. There are two possible sites of degradation for the carbonyls in the polyester chain: the carbonyl at the ester linkages along the polyester chain (type A figure 6.6) and the carbonyl at the end of the polyester chain before the triethanolamine (type B figure 6.6). Assuming that only type B carbonyls cleave, and assuming that all such carbonyls cleave during the degradation, the maximum decrease in the intensity of the peak at 173 ppm may be calculated as 23%. Since this theoretical decrease in intensity is more than the experimental loss in intensity of the peak at 173 ppm, it is not possible to conclude from this whether only type B carbonyls are cleaved, or whether type A carbonyls are also hydrolysed. However, what it is possible to deduce is that some acid groups formed during the degradation of carbonyl groups type B give rise to a carbonyl peak at

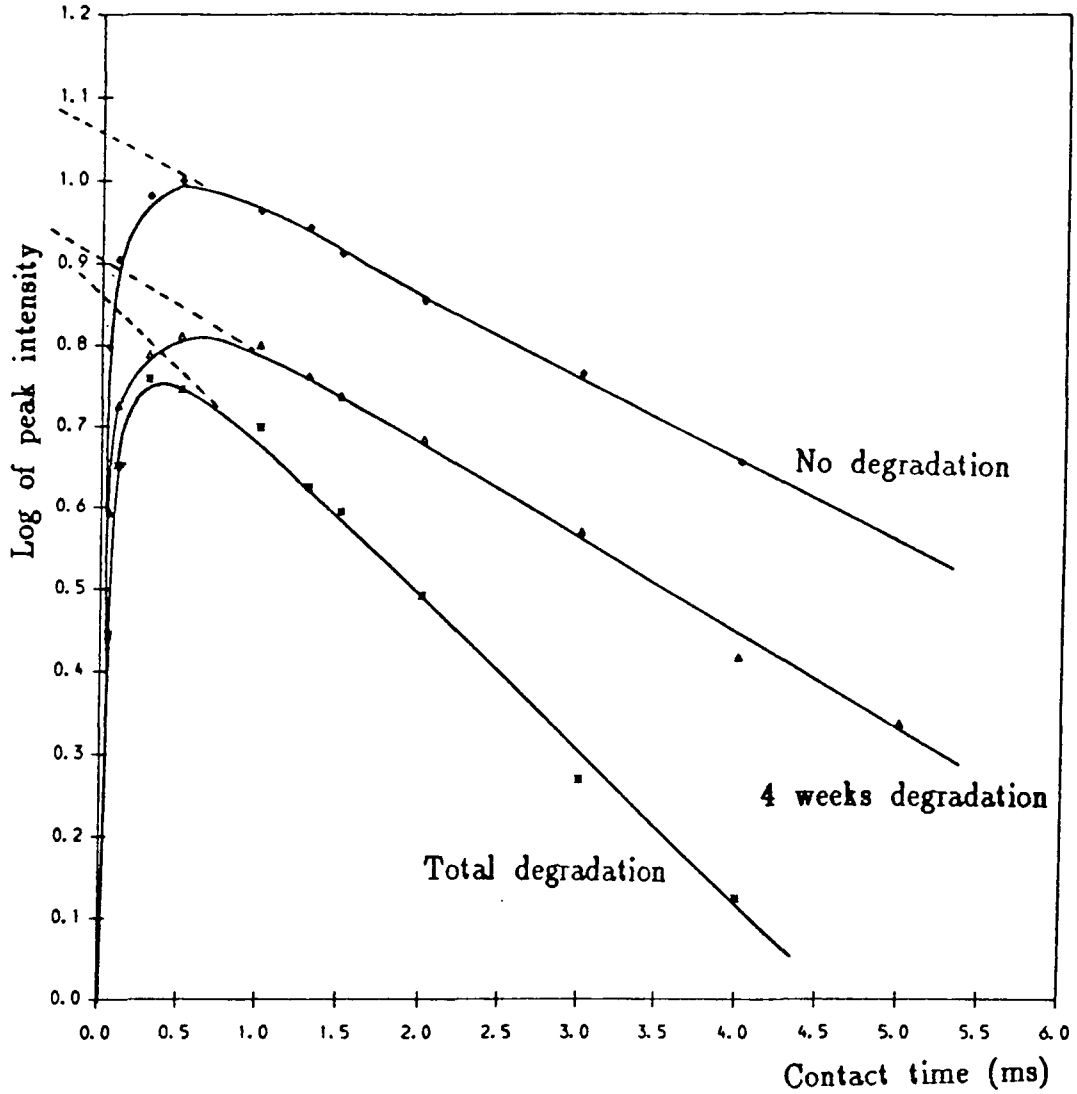

Figure 6.7

Plot of the log of the peak intensity against contact time for the polyester peak at 25 ppm in the maleic anhydride film. The maleic anhydride film with no degradation is compared to the film with 4 weeks degradation and with total degradation for contact times between 0.05 and 5 ms. The recycle delay was 6 seconds, the acquisition time was 26 ms and 1000 transients were acquired for each experiment.

Table 6.3

Values of T_{IS} and $T_{1\rho}$ for the maleic anhydride film.

$T_{1\rho}$	Peak			
Degradation	25 ppm	34 ppm	40 ppm	173 ppm
No deg.	9.67	8.92	10.07	11.29
2 weeks deg.	18.89	——	17.73	17.67
4 weeks deg.	10.98	9.51	12.81	9.85
Total deg.	4.54	——	6.422	5.81

T_{IS}	Peak			
Degradation	25 ppm	34 ppm	40 ppm	173 ppm
No deg.	0.063	0.056	0.054	0.425
2 weeks deg.	0.074	——	0.065	0.499
4 weeks deg.	0.060	0.057	0.054	0.443
Total deg.	0.078	——	0.057	0.402

Table 6.4

Assignment of the peaks in the itaconic anhydride film spectrum.

Peak/ppm	Assignment
173.5	C=O of MMA, cross–link, and polyester
144.8	Aromatic quaternary carbon of styrene
128.3	Aromatic C–H of styrene
63	O=C–O–CH_2 in polyester chain
49.6	CH_3O of MMA
45	Quaternary carbon of MMA
40–45	CH backbone carbons
41.5	CH of polystyrene
40.1	CH_2 'backbone' of copolymer
33.5	O–C(=O)–CH_2 in polyester chain
25	CH_2 'backbone' of polyester
19.8	CH_3 of MMA

177 ppm.

Figure 6.7 shows the variable contact time intensities of the peak at 25 ppm (the CH_2 backbone of the polyester). The plot compares the relative intensities of the 25 ppm peak of the films with no degradation, with 4 weeks degradation and with total degradation. Extrapolating back to the intensity axis as before, it can be seen that as the degradation progresses, the absolute intensity of the 25 ppm peak decreases consistently. There is a loss in intensity of 14% between the film with 4 weeks degradation and the film with no degradation, and a loss in intensity of 18% between the film with total degradation and the film with no degradation. It is of interest to determine whether this loss in intensity may be attributed to cleavage at the cross–link only (figure 6.6 position C), or whether there is a contribution to the decrease in intensity from cleavage at the ester positions along the chain (figure 6.6 position D). Calculations of the chemical shift have shown that degradation either at the cross–link or at the ester linkages along the polyester chain does not alter the chemical shift of the peak from 25 ppm. Therefore, any degradation which takes place either at the cross–link or at the ester linkage along the polyester chain should not result in a decrease in the absolute intensity of the fully degraded film compared to the film with no degradation. An explanation of why an 18% decrease in the absolute intensity is observed may be obtained through consideration of the effect on the overall intensity of the 25 ppm peak if the polyester chain were to degrade. If some or all of the ester linkages along the polyester chain are hydrolysed, then the polyester chain

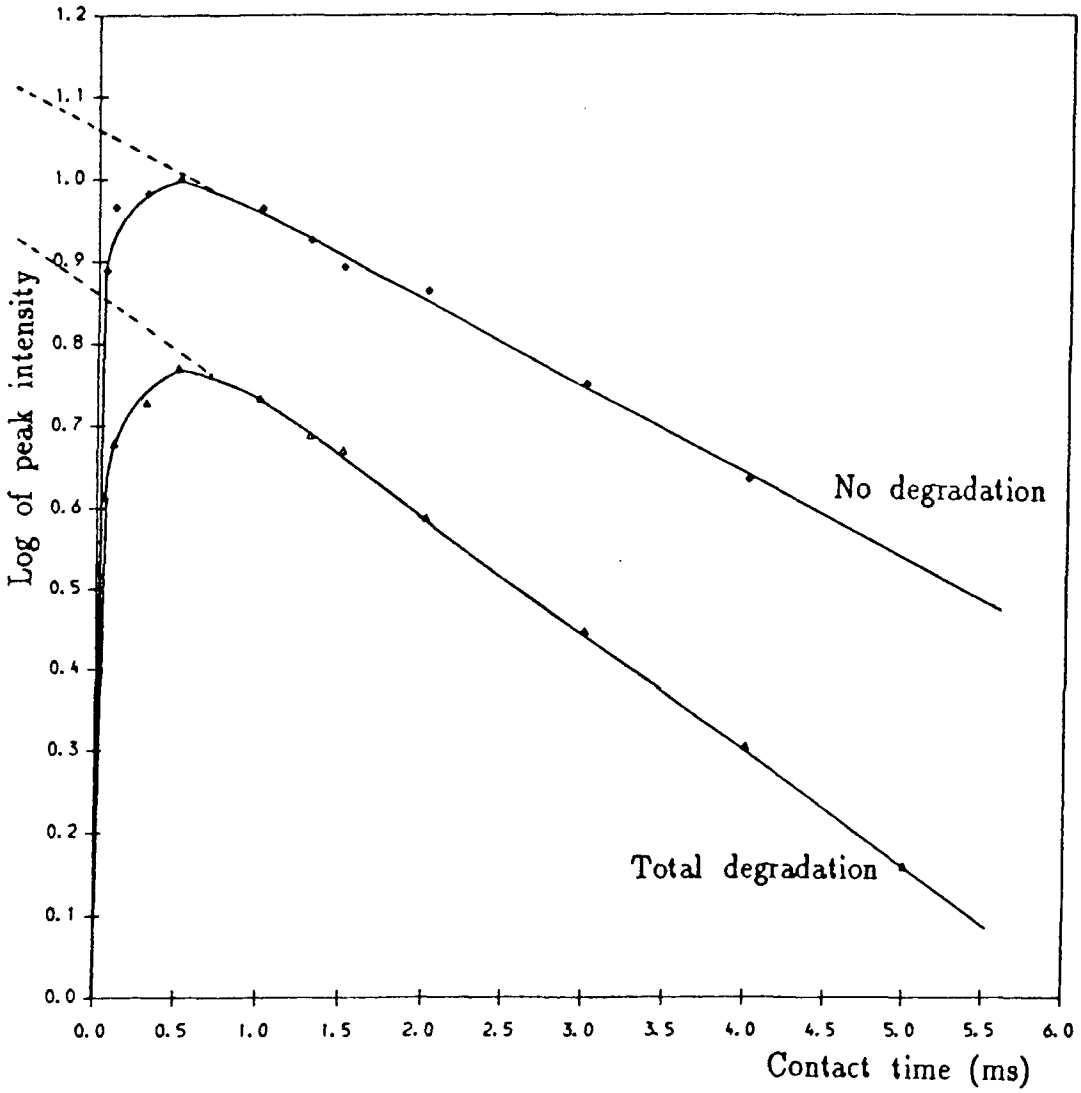

Figure 6.8

Plot of the log of the peak intensity against contact time for the polyester peak at 34 ppm in the maleic anhydride film. The maleic anhydride film with no degradation is compared to the film with total degradation for contact times between 0.05 and 5 ms. The recycle delay was 6 seconds, the acquisition time was 26 ms and 1000 transients were acquired for each experiment.

will break up into smaller fragments. The conditions in the environmental cabinet in which the maleic anhydride films were degraded were 35°C and 100% relative humidity. These conditions of continually dripping water wash any small fragments out of the film. Thus, when the absolute intensity of the totally degraded film is measured, a decrease in the absolute intensity of the 25 ppm peak is found. Therefore the decrease of 18% between the film with no degradation and the film with total degradation is partially due to the degradation of the ester linkages along the polyester chain.

The variable contact time intensities of the peak at 34 ppm (CH_2 next to the carbonyl) are shown in figure 6.8. The intensities of the maleic anhydride film with no degradation are compared with the maleic anhydride film with total degradation. Extrapolating back to the intensity axis, there is a loss in intensity of 18% between the film with no degradation and the film with total degradation. As in the case of the peak at 25 ppm, calculations of the chemical shifts have shown that degradation at either position E near the cross–link or position F along the polyester chain (see figure 6.6) does not alter the chemical shift of the 34 ppm peak. Therefore, for the same reason as in the case of the 25 ppm peak, the 18% loss in intensity must be due to degradation at the ester linkages along the polyester chain (position F figure 6.6).

Table 6.3 lists the values of T_{IS} and $T_{1\rho}$ obtained from the variable contact time plots (figures 6.4–5 and 6.7–8). Variable contact time measurements were also obtained for a maleic anhydride film with 2 weeks degradation, the values of T_{IS} and $T_{1\rho}$ of which are listed in table

6.3. It can be seen that the sample with 2 weeks degradation gave anomalous results which could not be explained. It is thought that the sample was at fault. However the experiment would have to be repeated to prove this. The anomalous plot of the maleic anhydride film with 2 weeks degradation has been omitted from figures 6.4–5 and 6.7–8 for this reason. However, because the maleic anhydride film with 2 weeks degradation has been left out of these plots, the conclusion that the ester linkage in the polyester backbone also cleaves during degradation must be treated with caution.

In order to obtain an understanding of the chemistry of the degradation process, spectra of the maleic anhydride film with no degradation are compared to spectra of the maleic anhydride film with total degradation. Figure 6.9a and b shows the carbonyl region of the ^{13}C CP MAS spectra of the maleic anhydride film with no degradation and with total degradation respectively. Figure 6.9a is dominated by the peak at 173 ppm. This is explained by the variable contact time measurements (figure 6.5). There is a new peak in figure 6.9b at 177 ppm. This corresponds to a carbonyl in the polyester chain which has been hydrolysed to a carboxylic acid as illustrated in figure 6.9c. The increase in intensity in figure 6.9b at about 180 ppm is attributed to the formation of more free carboxylic groups at the cross–link in the degraded sample compared to the maleic anhydride film with no degradation.

Figure 6.10a and b show the same spectra as figures 6.9, but this time the aliphatic region between 15 and 70 ppm is illustrated. The

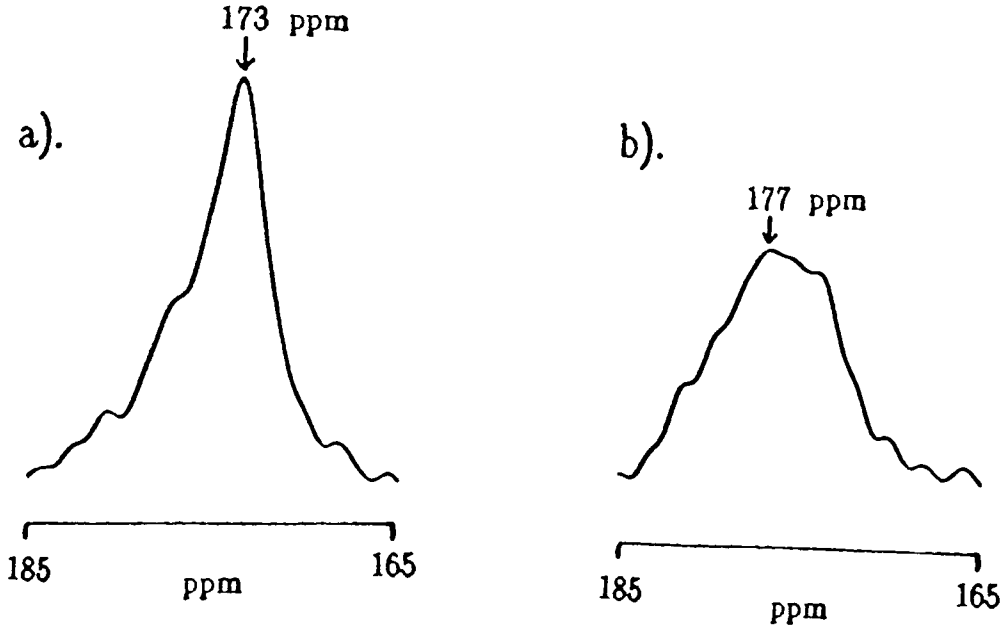

Figure 6.9

a). The carbonyl region of the ^{13}C cross–polarisation spectrum of the maleic anhydride film with no degradation.

b). The carbonyl region of the ^{13}C cross–polarisation spectrum of the maleic anhydride film with total degradation.

Recycle delay = 6 seconds
contact time = 1.5 ms
acquisition time = 26 ms
no. of transients = 1000

c).

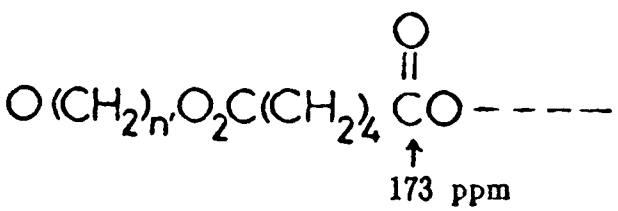

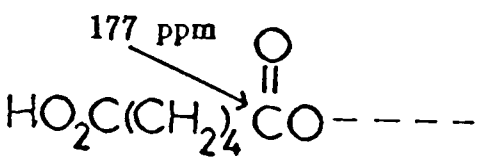

c). The new peak at 177 ppm corresponds to a carbonyl in the polyester chain which has been hydrolysed.

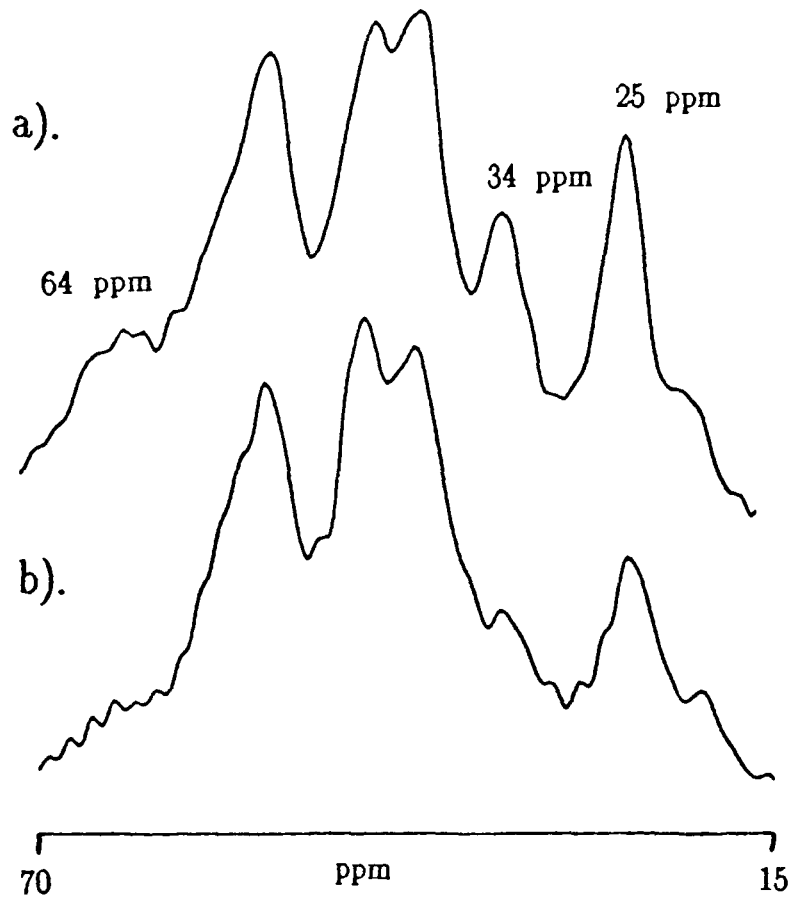

Figure 6.10

a). The aliphatic region of the ^{13}C cross–polarisation spectrum of the maleic anhydride film with no degradation.

b). The aliphatic region of the ^{13}C cross–polarisation spectrum of the maleic anhydride film with total degradation.

Recycle delay = 6 seconds
contact time = 1.5 ms
acquisition time = 26 ms
no. of transients = 1000

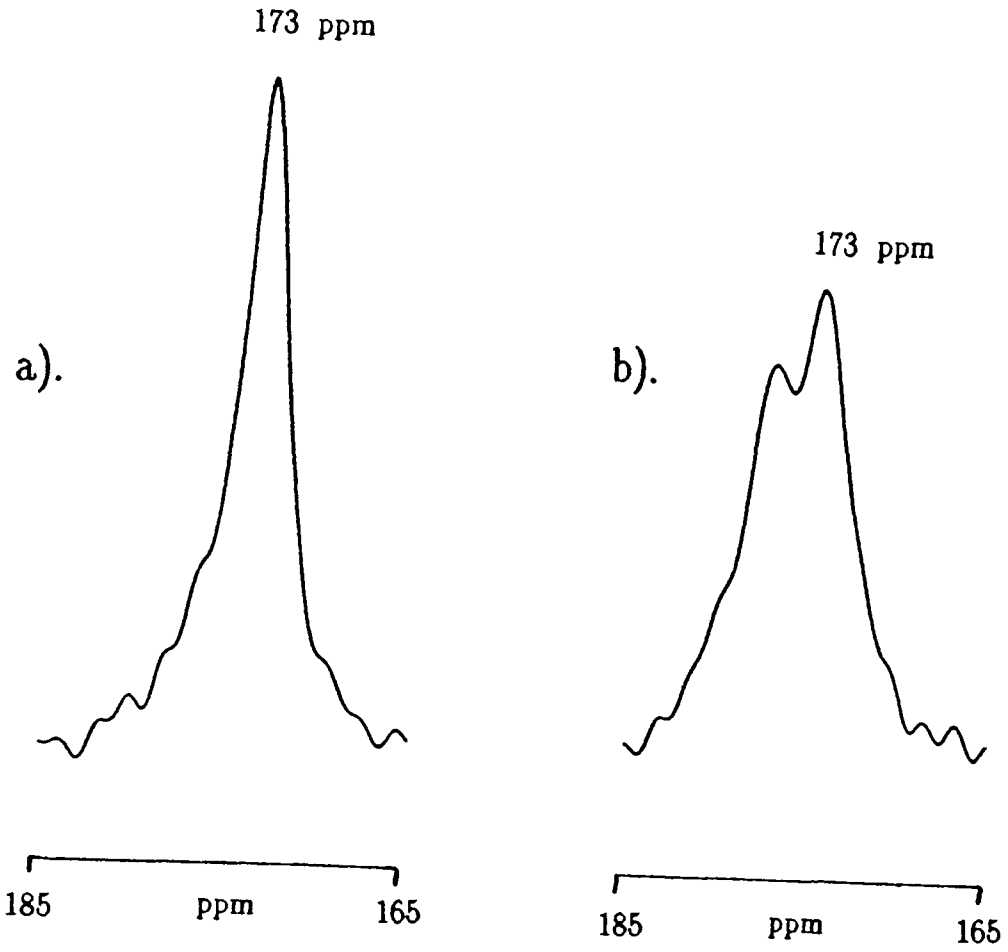

Figure 6.11

a). The carbonyl region of the ^{13}C single–pulse spectrum of the maleic anhydride film with no degradation.

b). The carbonyl region of the ^{13}C single–pulse spectrum of the maleic anhydride film with total degradation.

Recycle delay = 7 seconds

acquisition time = 26 ms

no. of transients = 3000

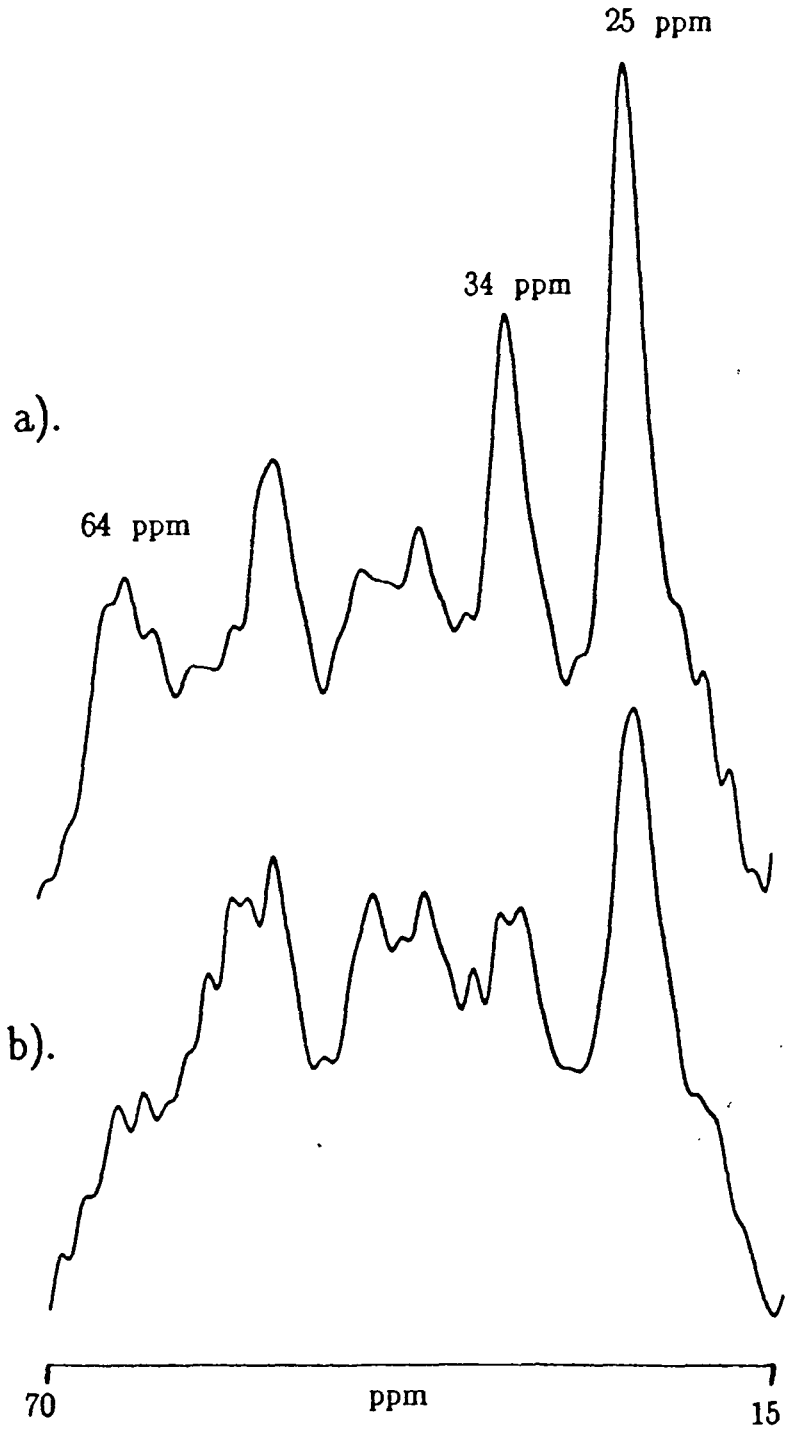

Figure 6.12

a). The aliphatic region of the ^{13}C single–pulse spectrum of the maleic anhydride film with no degradation.

b). The aliphatic region of the ^{13}C single–pulse spectrum of the maleic anhydride film with total degradation.

Recycle delay = 7 seconds

acquisition time = 26 ms

no. of transients = 3000

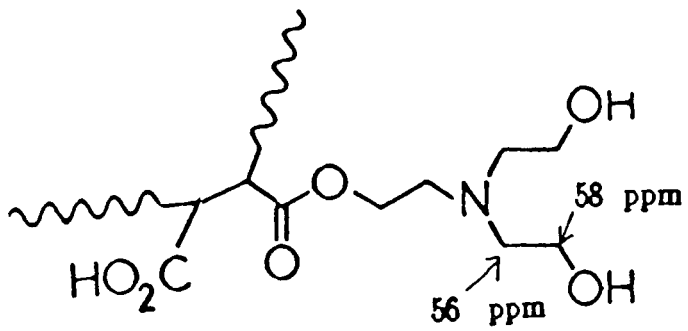

Figure 6.13

Predicted chemical shifts of the triethanolamine tip of the polyester.

peaks at 25 ppm and 34 ppm show a marked decrease in intensity in the fully degraded film compared to the maleic anhydride film with no degradation. Again, this is explained by the variable contact time measurements (figures 6.7 and 6.8).

Whereas the CP experiment enhances signals from the more rigid carbons, the single pulse experiment discriminates in favour of the more mobile carbons. The shorter the recycle time used, the more mobile is the region observed in the spectrum. Figure 6.11 shows the carbonyl regions of the single pulse spectra of the maleic anhydride film with no degradation (figure a), and the maleic anhydride film with total degradation (figure b). Figure 6.11a is dominated by the carbonyl peak of the polyester chain at 173 ppm. The intensity of the carbonyl at 173 ppm is greatly reduced in the case of the totally degraded film (figure 6.11b). This is direct evidence that the polyester chain hydrolyses. Again a shift is seen to higher ppm (179–181 ppm) in the totally degraded sample (figure 6.11b) compared to figure 6.11a, the film with no degradation. This is attributed to the formation of carboxylic acid groups in the film.

Figures 6.12a and b show the aliphatic regions (between 15 and 70 ppm) of the single pulse spectra of the maleic anhydride films with no degradation and with total degradation. There is a significant loss in intensity in the polyester peaks at 25, 34 and 64 ppm, the assignments of which are shown in Table 6.2. A decrease in the polyester resonances shows that degradation has taken place along the polyester chain.

There is one region of the spectrum of the totally degraded maleic

anhydride film (figure 6.12b) between 55–59 ppm where there is a significant increase in intensity. It is thought that this arises from the formation of free triethanolamine tips as the cross–links degrade. The two carbons of the triethanolamine tip have predicted chemical shifts of 56 ppm and 58 ppm as shown in figure 6.13. This is evidence that there is cleavage of the triethanolamine–polyester and/or the triethanolamine–copolymer ester linkages during hydrolysis, releasing free triethanolamine tipped fragments of polyester and copolymer with triethanolamine attached.

6.10 The degradation of the itaconic anhydride film

A study of the degradation similar to that of the maleic anhydride film has been made. In this work only two samples were studied: a sample of itaconic anhydride film with no degradation and a sample of itaconic anhydride film with total degradation (3 months degradation).

As in the case of the maleic anhydride film, variable contact time CP measurements were obtained for the itaconic anhydride films both with and without degradation. Figure 6.14 shows the variable contact time plot of the peak at 40 ppm (the CH_2 backbone of the copolymer) for the itaconic anhydride film with no degradation and with total degradation. The assignments of the peaks for the itaconic anhydride film are shown in Table 6.4. Extrapolating back to the intensity axis it can be seen that both the films with no degradation and with total degradation have the same absolute intensity. From this it may be concluded that the copolymer does not degrade.

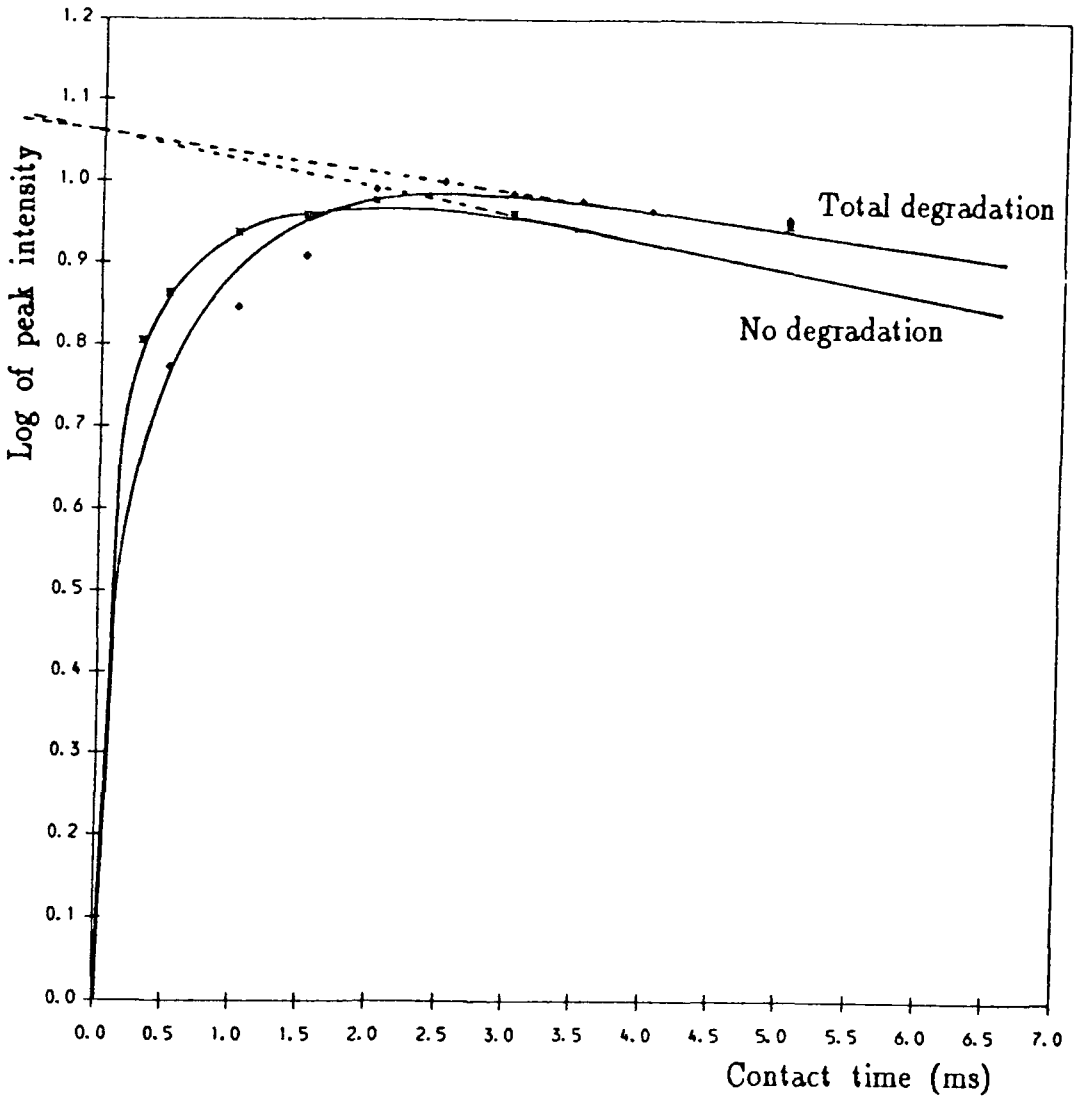

Figure 6.14

Plot of the log of the peak intensity against contact time for the copolymer peak at 40 ppm in the itaconic anhydride film. The itaconic anhydride film with no degradation is compared to the film with total degradation for contact times between 0.05 and 5 ms. The recycle delay was 6 seconds, the acquisition time was 26 ms and 1000 transients were acquired for each experiment.

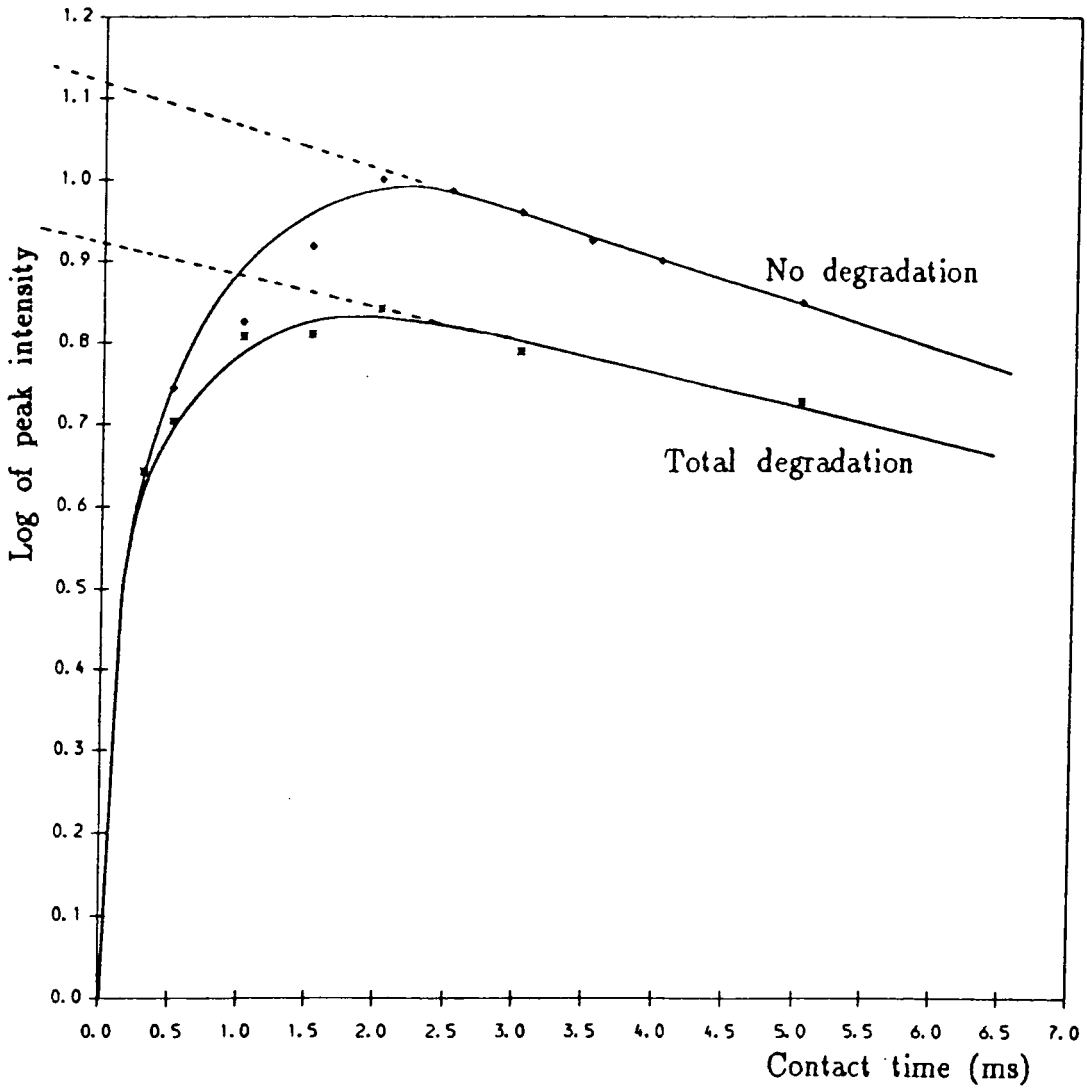

Figure 6.15

Plot of the log of the peak intensity against contact time for the polyester peak at 25 ppm in the itaconic anhydride film. The itaconic anhydride film with no degradation is compared to the film with total degradation for contact times between 0.3 and 5 ms. The recycle delay was 6 seconds, the acquisition time was 26 ms and 1000 transients were acquired for each experiment.

Table 6.5

Values of T_{IS} and $T_{I\rho}$ for the itaconic anhydride film.

$T_{I\rho}$	Peaks	
Degradation	25 ppm	40 ppm
No deg.	9.68	8.49
Total deg.	25.73	40.66

T_{IS}	Peaks	
Degradation	25 ppm	40 ppm
No deg.	0.063	0.054
Total deg.	0.393	0.364

A similar plot of the peak at 25 ppm (the CH_2 backbone of the polyester) for the itaconic anhydride film with no degradation and the itaconic anhydride film with total degradation is shown in figure 6.15. Extrapolating back to the intensity axis it can be seen that there is a loss in the intensity of the 25 ppm peak of 18% between the film with no degradation and the film with total degradation. As in the case of the maleic anhydride film, calculations of the chemical shifts have shown that degradation at either the cross–link or at the ester linkages along the polyester chain does not alter the chemical shift of the peak from 25 ppm, and hence the degradation of the itaconic anhydride film should not result in a loss of intensity of the peak at 25 ppm. This loss may be explained if hydrolysis were to take place along the polyester chain as well as at the cross–linkages. Some polyester chains hydrolyse into fragments which are washed out of the film in the environmental cabinet. Table 6.5 lists the values of T_{IS} and $T_{1\rho}$ obtained from the variable contact time plots (figures 6.14–6.15).

The chemical changes which take place during degradation of the itaconic anhydride film may be understood by comparing the spectra of the itaconic anhydride film with no degradation to the spectra of the film with total degradation.

Figure 6.16a and b show the carbonyl region of the carbon CP MAS spectra of the itaconic anhydride film with no degradation and total degradation respectively. The spectrum of the film with no degradation is dominated by the peak at 173 ppm (the carbonyls in the polyester chain). But figure 6.16b, the spectrum of the itaconic anhydride film with

total degradation, shows a decrease in the intensity of the peak at 173 ppm. As has been discussed for the maleic anhydride film, this decrease could arise from either the degradation of the cross–link only, or the degradation of both the cross–linkages and the ester linkages in the polyester chain. In figure 6.16b there is an increase in the intensity of peaks to a higher ppm. This is attributed to the formation of more free carboxylic acid groups in the totally degraded sample compared to the itaconic anhydride film with no degradation.

Figures 6.17a and b illustrates the aliphatic regions of the same spectra as in figure 6.16a and b. The aliphatic region between 10 and 70 ppm is shown of the ^{13}C CP spectra of the itaconic anhydride film with no degradation (figure a) and the itaconic anhydride film with total degradation (figure b). The polyester peaks at 25 ppm and 34 ppm in figure b, the assignments of which are shown in Table 6.4, show a marked decrease in intensity relative to the copolymer peaks in the spectrum b, compared to the same two peaks in the case with no degradation (figure a). Again this indicates that degradation is taking place either at the cross–links or both at the cross–links and at the ester positions along the polyester chain.

The single pulse excitation experiment discriminates in favour of the mobile carbons. Single pulse spectra of the itaconic anhydride film with no degradation and with total degradation were obtained with a recycle time of 7 seconds. At this recycle time the polyester peaks have reached equilibrium, and therefore the intensities of the polyester peaks in the single pulse spectra of the films with no degradation and total

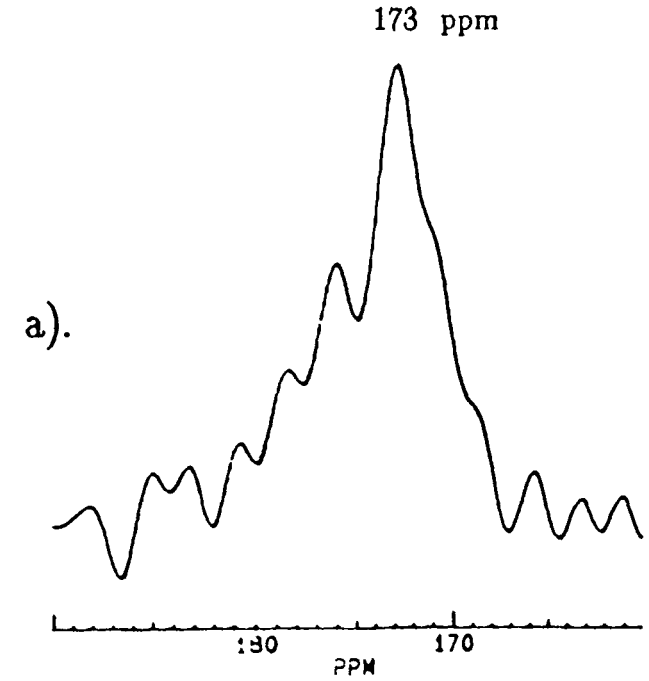

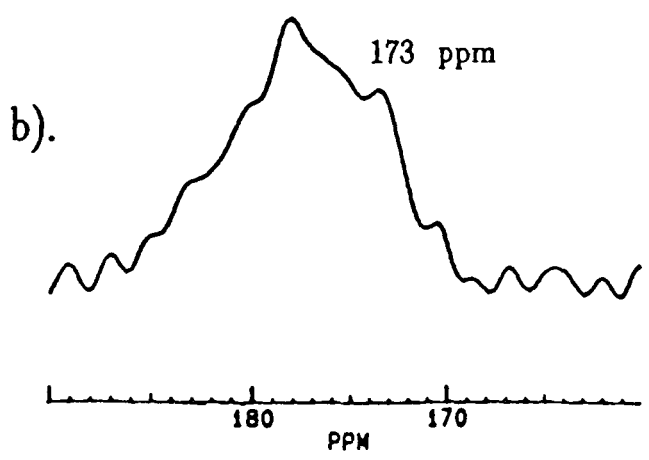

Figure 6.16

a). The carbonyl region of the ^{13}C cross–polarisation spectrum of the itaconic anhydride film with no degradation.

b). The carbonyl region of the ^{13}C cross–polarisation spectrum of the itaconic anhydride film with total degradation.

Recycle delay = 6 seconds
contact time = 1.5 ms
acquisition time = 26 ms
no. of transients = 1000

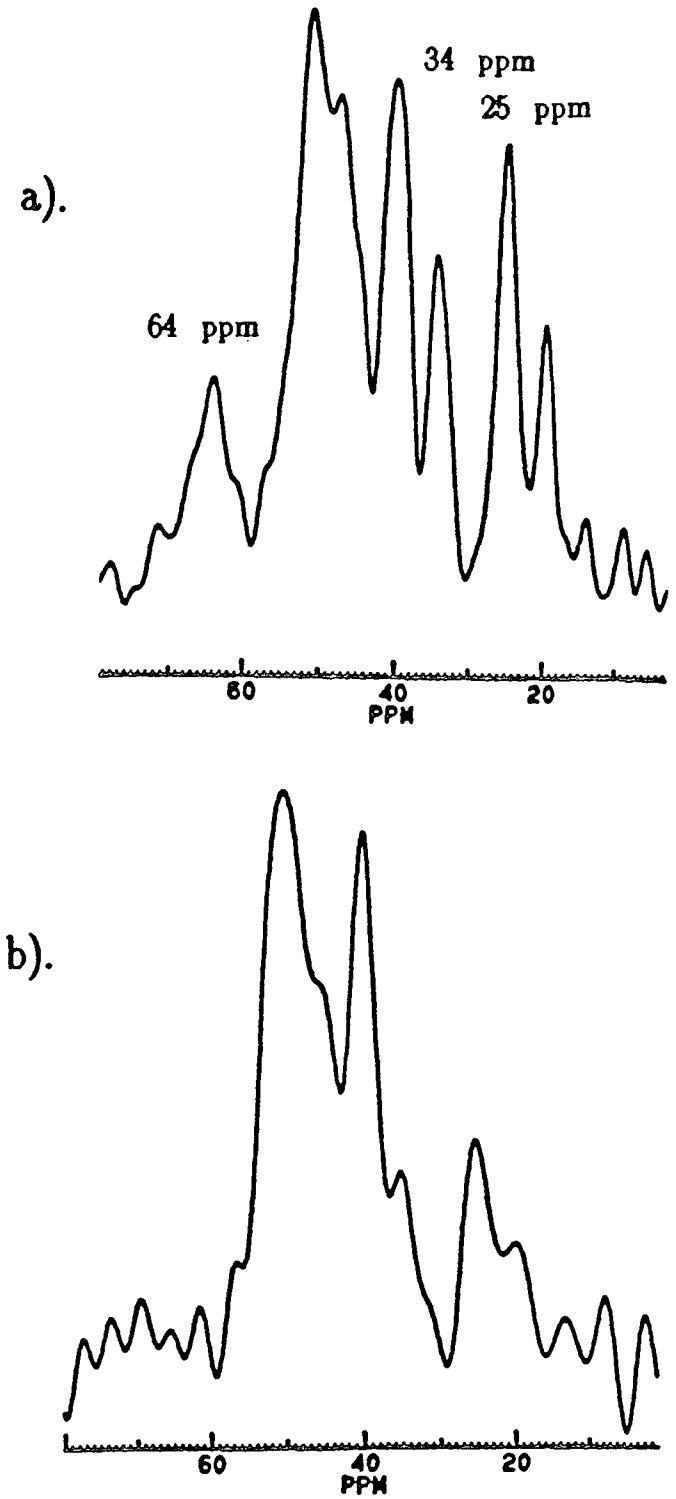

Figure 6.17

a). The aliphatic region of the ^{13}C cross–polarisation spectrum of the itaconic anhydride film with no degradation..

b). The aliphatic region of the ^{13}C cross–polarisation spectrum of the itaconic anhydride film with total degradation.

Recycle delay = 6 seconds

contact time = 1.5 ms

acquisition time = 26 ms

no. of transients = 1000

degradation may be compared quantitatively. Figures 6.18a and b show the carbonyl regions of the single pulse excitation spectra of the non–degraded sample and the totally degraded sample respectively. The carbonyl peak (173 ppm) is greatly reduced in intensity in the film with total degradation compared to the film with no degradation. It is not possible to conclude from this peak alone whether the degradation is taking place only at the cross–link positions, or whether the ester linkages along the polyester chain are also hydrolysed to cause this reduction in the peak at 173 ppm. In figure 6.18b there is a shift to higher ppm (179–181 ppm) compared to figure 6.18a, which is attributed to the formation of free carboxylic acid groups during the degradation of the itaconic anhydride film. There is intensity in the region of 171 ppm in figure 6.18a. This is the predicted position of the peak due to the ester of itaconic anhydride in the cross–link. This intensity is not present in the spectrum of the totally degraded film (figure b), possibly indicating cleavage of the cross–link (see figure 6.18c).

The aliphatic regions (10–70 ppm) of the same single pulse spectra are shown in figure 6.19a and b. There is a significant loss in intensity in the polyester peaks at 25, 34 and 64 ppm. The assignment of the peaks are shown in Table 6.4. Calculations show that there is no change in chemical shift between the non–degraded carbons giving rise to the peaks at these positions, and the same carbons when they are degraded. Thus, any loss in intensity of these peaks must be due to the hydrolysis of the polyester chain, where some of the small fragments formed are washed out of the film while it is degrading in the environmental

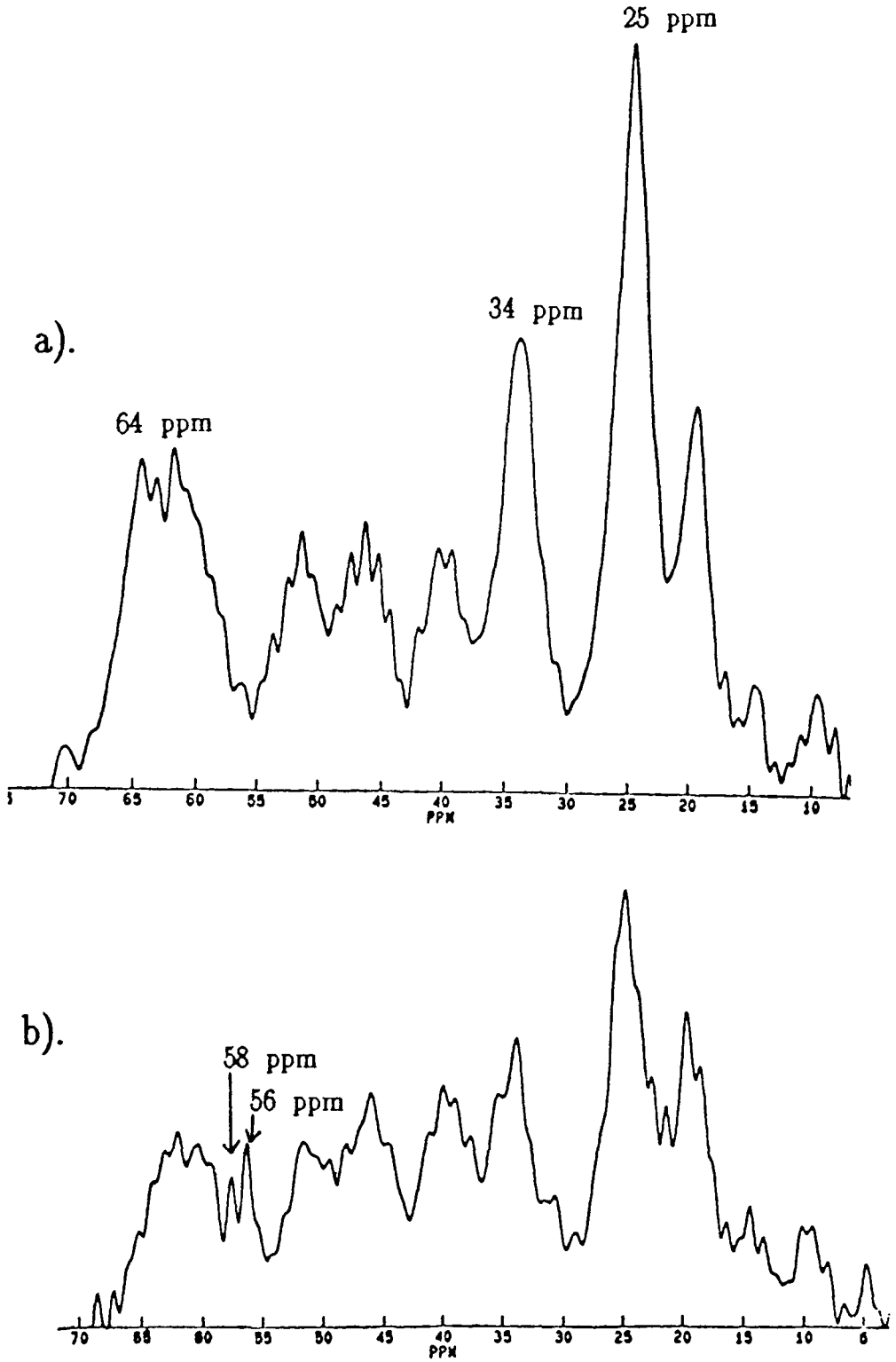

Figure 6.19

a). The aliphatic region of the ^{13}C single–pulse spectrum of the itaconic anhydride film with no degradation.

b). The aliphatic region of the ^{13}C single–pulse spectrum of the itaconic anhydride film with total degradation.

Recycle delay = 7 seconds

acquisition time = 26 ms

no. of transients = 3000

cabinet. There is one region between 55 ppm and 59 ppm in which the intensity increases notably in the fully degraded case (figure 6.19b) compared to the film with no degradation (figure a). One possibility is that this intensity arises from the triethanolamine tip after cleavage has taken place at the cross–link. It is probable that there is cleavage of the triethanolamine–polyester and triethanolamine–copolymer ester linkages during hydrolysis, releasing copolymer with triethanolamine attached and triethanolamine tipped fragments of polyester (figure 6.19c).

6.11 Conclusions from solid–state NMR study

From solid–state ^{13}C MAS NMR there is conclusive evidence that cleavage occurs in all three positions predicted in figure 6.3. The acrylic copolymer does not degrade, but merely unzips from the polyester. There is, however, cleavage at some of the ester linkages along the polyester chain. Variable contact time measurements show that the polyester chains undergo 18% degradation of the ester linkages along the backbone of the polyester chains. Not all the cross–links are cleaved. There is concrete evidence that some of the polyester remains intact and cross–linked, even in films which are considered to be totally degraded.

6.12 The anchimeric effect[5]

The anchimeric effect is the most likely cause of the breakdown of the polyester backbone during the degradation studies. The anchimeric effect is the intramolecular catalytic action on a particular site by a neighbouring group or atom on the same molecule.

In ester hydrolysis, a hydroxyl or carboxylate ion situated on the same molecule and close to the ester group promotes attack by the nucleophile, water. This provides more pressure on the alcohol to be released, and so results in an accelerated rate of hydrolysis. The effect only operates strongly over short distances. As the separation between assisting group and reaction site increases, the rate of hydrolysis decreases rapidly.

Equations representing the anchimeric effect are shown in figure 6.20.

There are two important parameters which directly affect how good a resistance a polyester has to hydrolysis.

1. The steric factor. The more sterically–hindered the polyester, the greater is its resistance to hydrolysis.
2. The anchimeric effect. For a polyester to have a good resistance to hydrolysis, the diol and diacid precursors must contain at least four linear carbons between the functional groups.

Both ethylene glycol and butane 1,4 diol, when incorporated in a polyester, have a poor resistance to hydrolysis due to the anchimeric effect. Increasing the number of linear carbon atoms between the diol components of the polyester should go some way towards stabilising the films from hydrolysis attack. However, hydrolysis would still take place at the cross–link positions. It is believed that the nitrogen atom positioned β to the cross–link atom aids the hydrolysis of the cross–link by the reversal of the mechanism by which it catalyses the formation of the

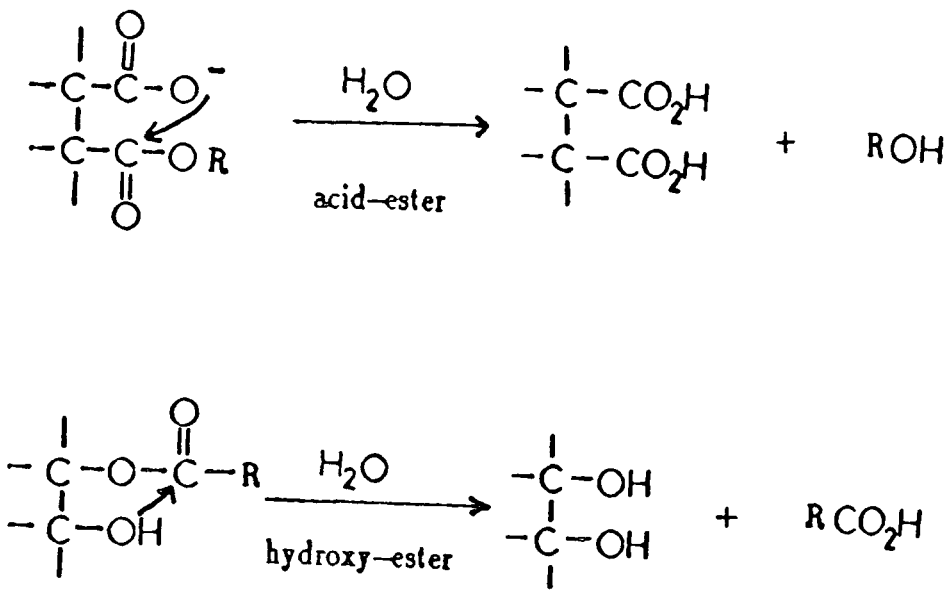

Figure 6.20

Equations representing the anchimeric effect in ester hydrolysis.

cross–link. From the degradation studies undertaken, it is clear that the polyester component of the two–pack film system needs to be completely modified. The polyester should be replaced by a long chain without any hydrolysable linkage along the backbone, and the ester cross–link replaced by some linkage which is more resistant to water attack.

CHAPTER 7

Solid–state nuclear Overhauser effects in cross–linked polymers

7.1 Introduction

Carbon 13 NMR spectroscopy can be used to investigate molecular conformation and molecular motion[1]. Those NMR parameters, from which information about the motion of molecules in the solution state may be obtained (i.e. spin–lattice relaxation times and nuclear Overhauser enhancements), may also be acquired for solids from dipolar–decoupled ^{13}C NMR spectra[2]. In this chapter we concentrate on the nuclear Overhauser effect, and the prediction of the behaviour of the carbon spins when subjected to various pulse sequences.

Irradiation at the proton frequency in solid state ^{13}C MAS NMR spectroscopy allows the observation of carbon resonances without effect from (^{13}C,^{1}H) dipolar couplings. However the ^{13}C equilibrium magnetisation is changed from a Boltzmann distribution by the interaction of the ^{1}H and ^{13}C dipoles when the proton resonances are saturated with a radiofrequency field[3]. This results in the nuclear Overhauser effect (NOE).

Although the nuclear Overhauser effect is very commonly observed and discussed for solutions, it is rarely reported in the case of solids. Most spectra of solids are obtained using cross–polarisation so that the question of a NOE does not arise. However, in some cases where the solid is very mobile, simple MAS spectra without cross–polarisation can

be obtained which may have nuclear Overhauser enhancements. The nuclear Overhauser effect in the solid state does not appear to have been discussed in detail.

Equations describing the behaviour of macroscopic magnetisation have been derived by Solomon through consideration of population changes[3]. Abragam has also described a related theory in density matrix notation[4]. The treatment used by Solomon is the more easily understood, hence Solomon's theory has been used here in the study of transient Overhauser effects in the solid state.

Consider an ensemble of N spins, $I \equiv {}^{13}C = \frac{1}{2}$ and $S \equiv {}^{1}H = \frac{1}{2}$

Four eigenstates of the spins can be defined by the following relations:

$$\hat{I}_z|\alpha\rangle = +\tfrac{1}{2}|\alpha\rangle \qquad \hat{S}_z|\alpha\rangle = +\tfrac{1}{2}|\alpha\rangle$$

$$\hat{I}_z|\beta\rangle = -\tfrac{1}{2}|\beta\rangle \qquad \hat{S}_z|\beta\rangle = -\tfrac{1}{2}|\beta\rangle$$

Hence, the unperturbed eigenstates for C–H spin pairs are $|\alpha\rangle|\alpha\rangle$, $|\beta\rangle|\alpha\rangle$, $|\alpha\rangle|\beta\rangle$ and $|\beta\rangle|\beta\rangle$. These eigenstates have occupation numbers $N_{\alpha\alpha}$, $N_{\beta\alpha}$, $N_{\alpha\beta}$ and $N_{\beta\beta}$ respectively.

When these coupled spins are placed in a magnetic field of intensity B_0, the energy levels are split as shown in figure 7.1.

If an RF field with a frequency equal to the Larmor frequency of the proton spins is applied to these spins, transitions will be induced between the energy levels. The number of transitions, say $\alpha\alpha \rightarrow \beta\beta$ will be proportional to $N_{\alpha\alpha}$, the population of the $\alpha\alpha$ state; the number of transitions $\beta\alpha \rightarrow \beta\beta$ will similarly be proportional to $N_{\beta\alpha}$, the population of the $\beta\alpha$ state. Initially the lower energy level will have a larger population so that the number of upward transitions will exceed the number of

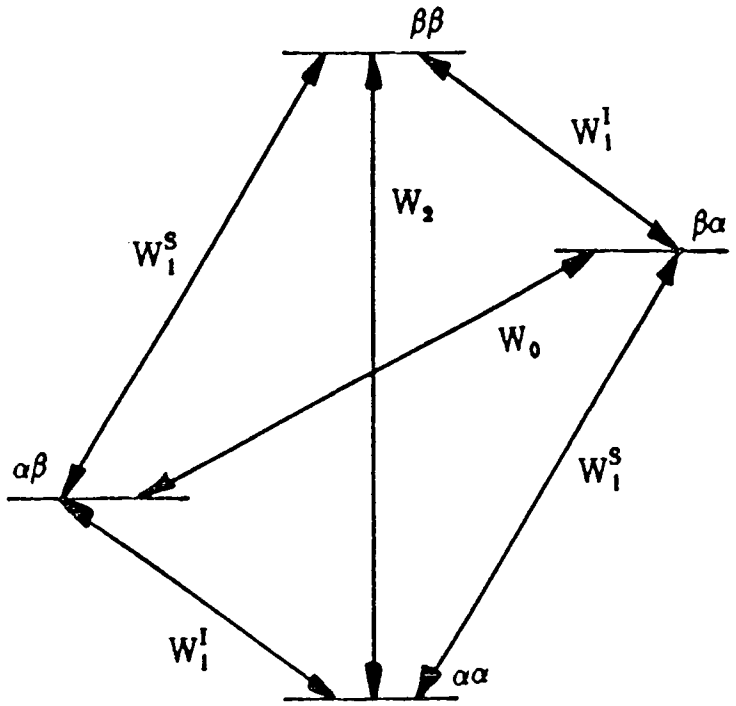

Figure 7.1

The energy level diagram for a coupled C–H spin system placed in a magnetic field.

downward transitions. If the RF field is strong, this process results in saturation. When the energy levels are saturated, the populations of the two energy levels become equal, and the absorption of RF energy will cease. A mechanism exists for these populations to return to equilibrium. The mechanism by which nuclear spins return to equilibrium is called spin–lattice relaxation. A quantity W may be defined as the probability per unit time that a transition will occur between any two states due to spin relaxation.

The description of the spin–lattice relaxation in figure 7.1 requires four transition probabilities:

W_1^I The single quantum transition probability that spin I will go from α to β (or β to α) while the state of spin S remains unchanged.

W_1^S The single quantum transition probability for spin S when the state of spin I remains unchanged.

W_2 The two quantum transition probability for the two spins to relax simultaneously in the same direction, i.e. $\alpha\alpha \rightarrow \beta\beta$ or $\beta\beta \rightarrow \alpha\alpha$.

W_0 The zero quantum transition probability for a mutual spin flip, $\alpha\beta \rightarrow \beta\alpha$ or $\beta\alpha \rightarrow \alpha\beta$.

7.2 The nuclear Overhauser effect

7.2.1 Definition

The nuclear Overhauser enhancement is the fractional change in the integrated NMR absorption intensity of a nuclear spin when the NMR absorption of another spin is saturated[5]. The spins may be either chemically–shifted homonuclear or heteronuclear spins. In the solid–state,

only heteronuclear Overhauser effects are possible due to spin diffusion between proton spins. In order to understand how the nuclear Overhauser effect arises, it is necessary to consider the population changes which occur when a spin is saturated. Figure 7.2 (a–c) shows schematically how the populations of the I–S coupled spin systems change when the S spins are saturated.

Figure 7.2a shows the population levels (not the energy levels) of the coupled I–S spin system at equilibrium. Let the excess population of levels 2 and 3 at equilibrium be $\delta-\Delta$ and $-\delta+\Delta$ respectively. The excess population of level 1 will be $-\delta-\Delta$, and the population of level 4 will be $\delta+\Delta$.

The NMR resonance of spin S will consist of two transitions, 1→2 and 3→4, both of the same frequency. Likewise the resonance of spin I will have two components, the 1→3 and 2→4 transitions.

Figure 7.2b shows how the populations of these four levels change when the S spins are saturated. If a strong RF field is applied at the resonance frequency of the S spins, then the S spins will become saturated. The result is that the energy levels become equally populated. i.e. $P_1=P_2$ and $P_3=P_4$.

There is a limiting condition on these population levels that the total number of spins must remain unchanged. These population changes do not result in any change in the I spin resonance absorption energy. Thus at the stage shown in figure 7.2b there is no enhancement of the carbon signal.

Figure 7.2c shows how the spin–lattice transition probabilities W

Figure 7.2

Excess populations

A Population level diagram to show the nuclear Overhauser effect.

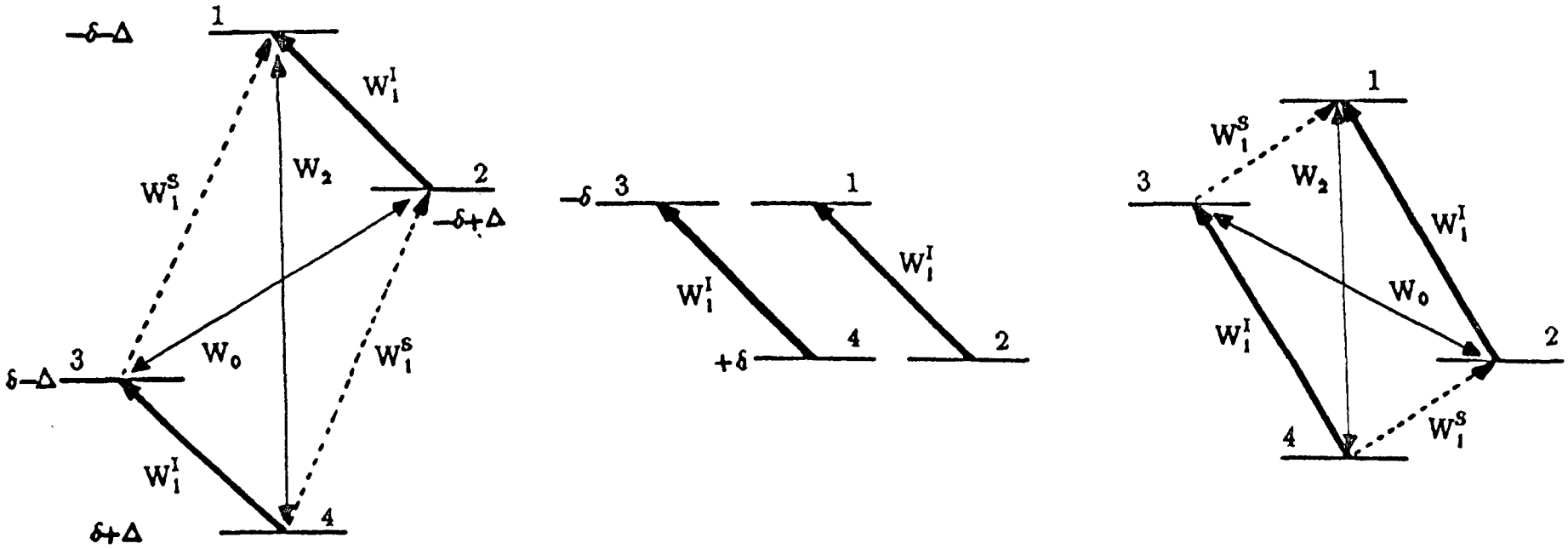

a). Equilibrium situation

b). After saturation of the protons.

c). W_0 and W_2 attempt to restore equilibrium.

W_2–simultaneous jump of ^1H and ^{13}C spins.

⇡ = ^1H

⇑ = ^{13}C

Figure 7.3

Pulse sequence for the measurement of the heteronuclear NOE enhancement in the solution state.

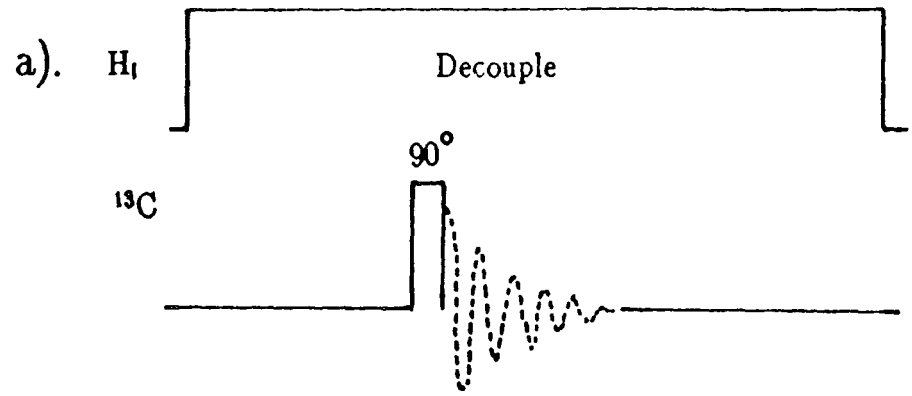

a). Pulse sequence to obtain ^{13}C spectrum with NOE.

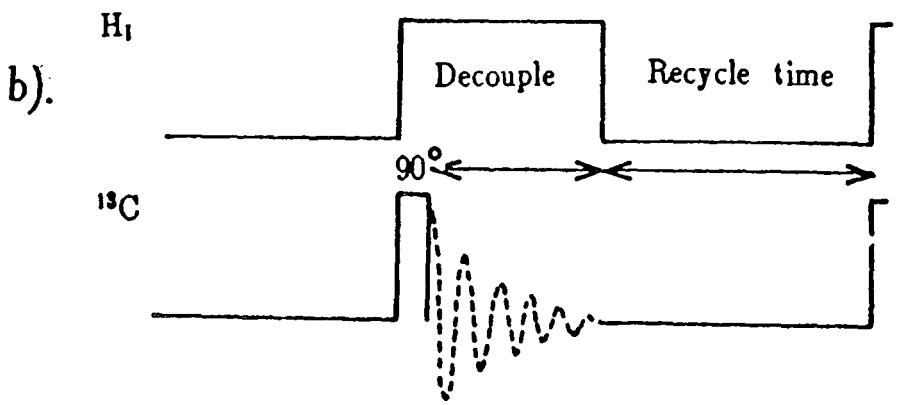

b). Pulse sequence to obtain ^{13}C spectrum without NOE.

must be taken into account to explain the nuclear Overhauser effect. Figure 7.2b is not an equilibrium situation. The population difference P_4–P_1 in figure 7.2b is less than the equilibrium value P_4^0–P_1^0 = 2δ+2Δ. The effect of W_2 will be to attempt to re–establish equilibrium by increasing P_4 and decreasing P_1. Therefore the effect of W_2 is to increase the intensity of the I spin resonance. The effect of W_0 will be to increase P_2 and decrease P_3 to attempt to restore equilibrium. W_0 has an overall effect of decreasing the intensity of the NMR resonance of spin I. In reality all the transition probabilities are simultaneously effective, and the resulting enhancement of spin I arises from a compromise between transition probabilities W_2 and W_0. The amount by which the carbon signal is increased is an important value in NMR spectroscopy. The ways in which the nuclear Overhauser enhancement factors are measured are described in the following section.

7.3 Techniques for the measurement of NOE's

7.3.1 Solution–state NOE: The gated–decoupling method

In order to measure a heteronuclear NOE enhancement it is required to saturate the S spins whilst observing the I spins; and then compare the intensities obtained with their equilibrium values. This is done very simply by integrating resonances with and without a period of presaturation.

In order to obtain a decoupled ^{13}C spectrum with the NOE it is necessary to saturate the proton resonances during the delay period between pulses. In the solution state this is easily done by leaving the

proton decoupler on continuously throughout the experiment. The pulse sequence is shown in figure 7.3a. Figure 7.3b shows the pulse sequence used to obtain a decoupled spectrum without the NOE in the solution state. The recycle delay, t_d, must be long enough to allow the carbon spins to reach their equilibrium value. T_d must usually be at least 9 times the longest carbon T_1. The NOE enhancement factors (NOEF) are readily obtained by comparing the intensities of peaks between spectra with and without the NOE.

7.3.2 Solid–state NOE

In the case of solids, it is not feasible to leave the proton decoupler on for long periods of time since the decoupling power necessary for work on solids is an order of magnitude larger than that of the solution case. The duty cycle of pulse experiments must be kept low. A new pulse sequence has been devised which overcomes this problem. The new pulse sequence to obtain a decoupled solid–state spectrum with NOE is shown in figure 7.4a. A spin $I=\frac{1}{2}$ case is saturated when the populations of the two energy levels are equal. This situation occurs when the magnetisation is tilted into the *xy* plane. Therefore a succession of 90° pulses at the proton frequency during the recycle delay saturates the proton spins. The new pulse sequence (figure 7.4a) consists of such a saturation chain of 90° pulses at the proton frequency followed by carbon observation. A 5 μs 90° proton pulse was applied every 1ms during the saturation chain.

A spectrum without the NOE may be obtained using the pulse

Figure 7.4

Pulse sequence for the measurement of the heteronuclear NOE enhancement in the solid state.

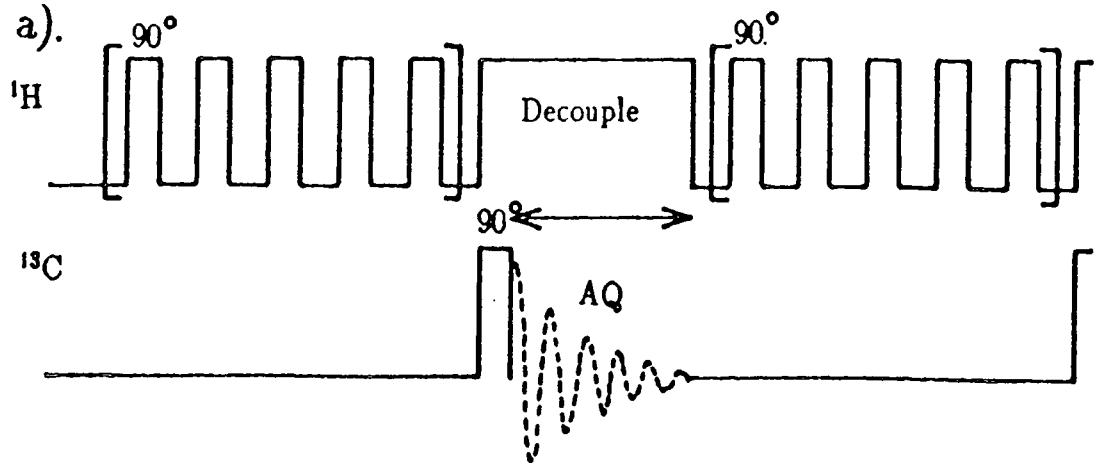

a). Pulse sequence to obtain ^{13}C spectrum with NOE.

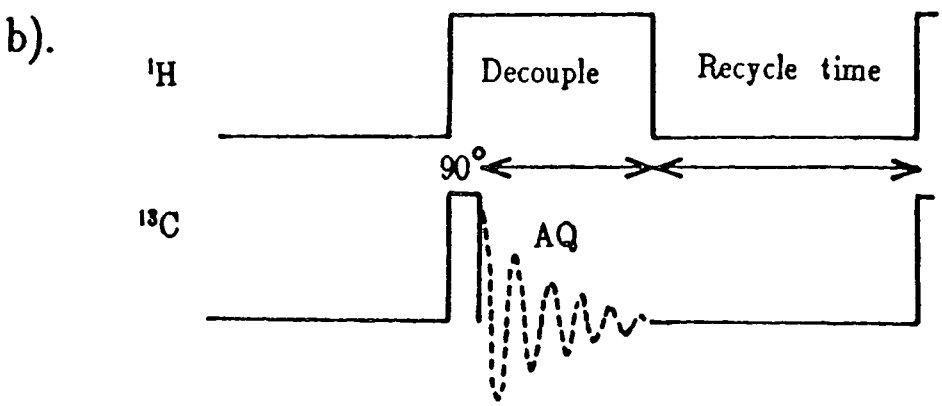

b). Pulse sequence to obtain ^{13}C spectrum without NOE.

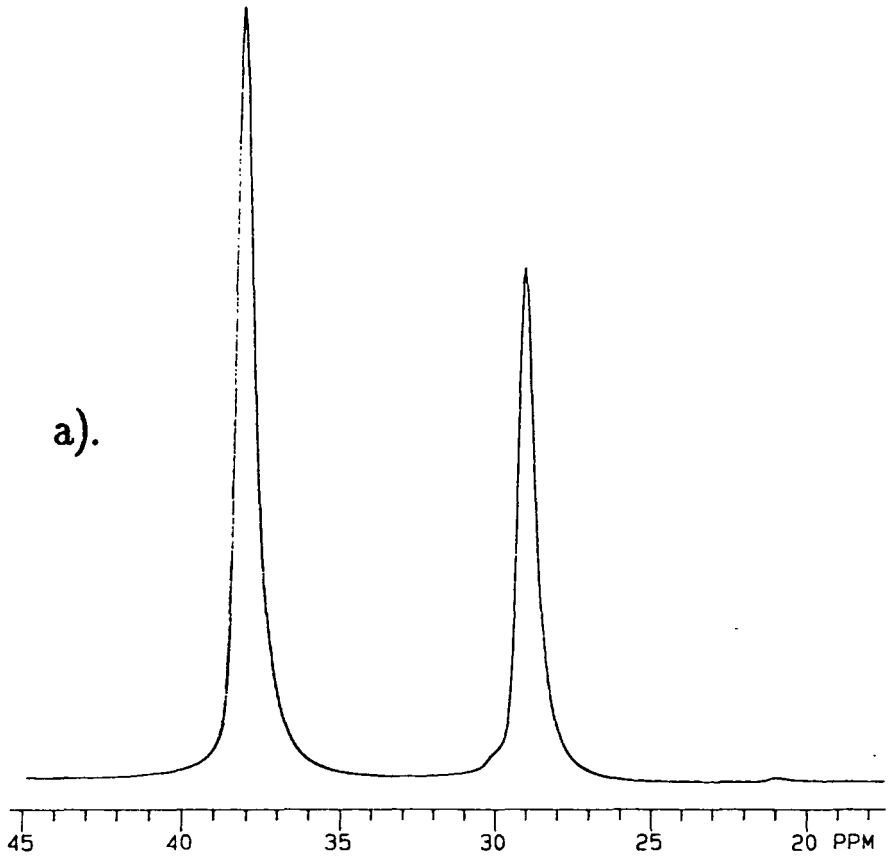

Figure 7.5

a). Solid–state decoupled ^{13}C spectrum of adamantane with NOE

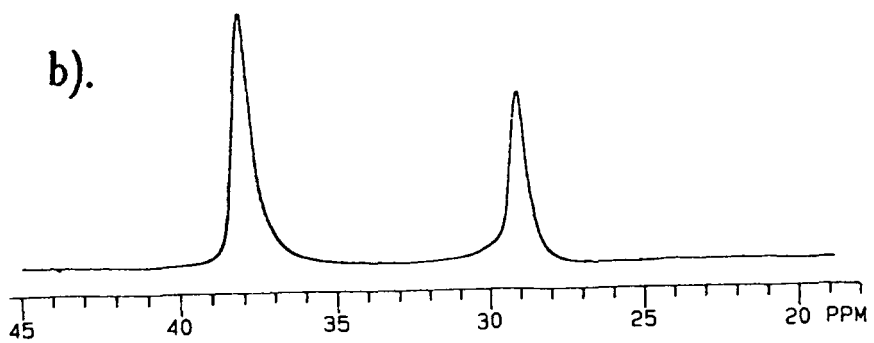

b). Solid–state decoupled spectrum of adamantane without NOE.

Recycle time = 30 seconds

Acquisition time = 99 ms

no. of transients = 16

program shown in figure 7.4b (the gated–decoupler method), as for solution–state studies. However for solids a high–power decoupler is used. Provided the recycle delay is long enough, turning off the decoupler during the delay allows the nuclei to relax to an equilibrium Boltzmann distribution at the time of the observation pulse. Again, the recycle delay should normally be about nine times the longest T_1.

The ratio of peak intensities in the spectrum with NOE to those in the spectrum obtained using the gated decoupler method gives the NOE enhancement factors. Ideally a pulse program which interleaves between the pulse programs in figures 7.4a and 7.4b may be used. This would minimise possible errors due to sample heating.

The pulse sequences in figures 7.4a and 7.4b were tested on adamantane. Figure 7.5a shows the solid state decoupled spectrum of adamantane with NOE, and figure 7.5b shows the decoupled spectrum of adamantane without NOE. Comparison between the intensities of the peaks in each spectrum gives η, the NOE factor. These are tabulated and compared with the solution state values in Table 7.1. It can be seen that there is a very good agreement between the η values measured in the solid state using the new pulse sequence, and in the solution state by conventional methods. The relaxation in adamantane is dominated by the dipolar mechanism, hence the nuclear Overhauser enhancement factor is the theoretical maximum for each peak within the experimental error. Spins whose relaxation is not dominated by the dipolar mechanism have reduced values of the NOEF.

The pulse sequences in figures 7.4a and 7.4b have been applied on

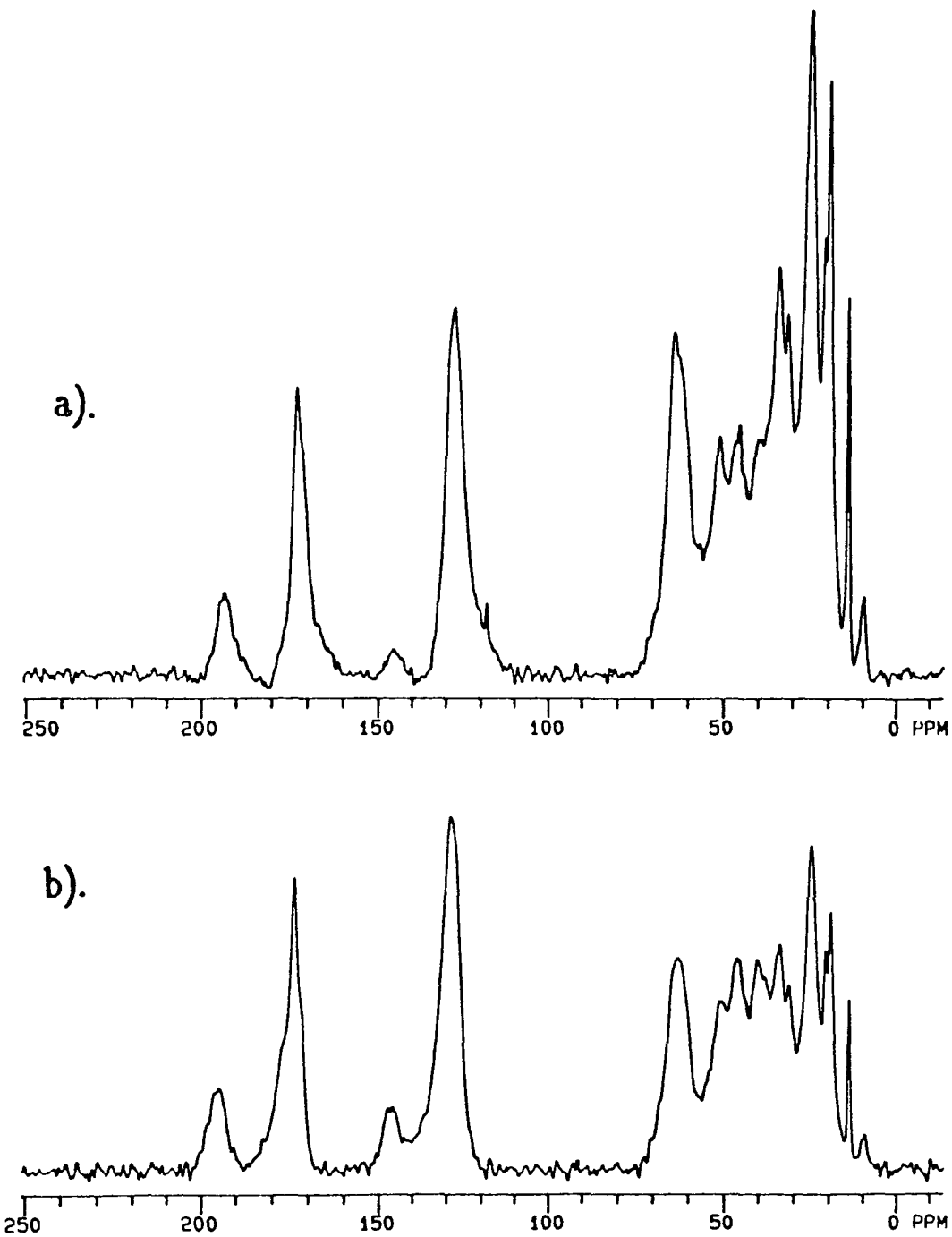

Figure 7.6

a). Solid–state decoupled ^{13}C spectrum of the itaconic anhydride film with NOE.

b). Solid–state decoupled ^{13}C spectrum of the itaconic anhydride film without NOE.

Recycle time = 7 seconds

Acquisition time = 26 ms

no. of transients = 1000

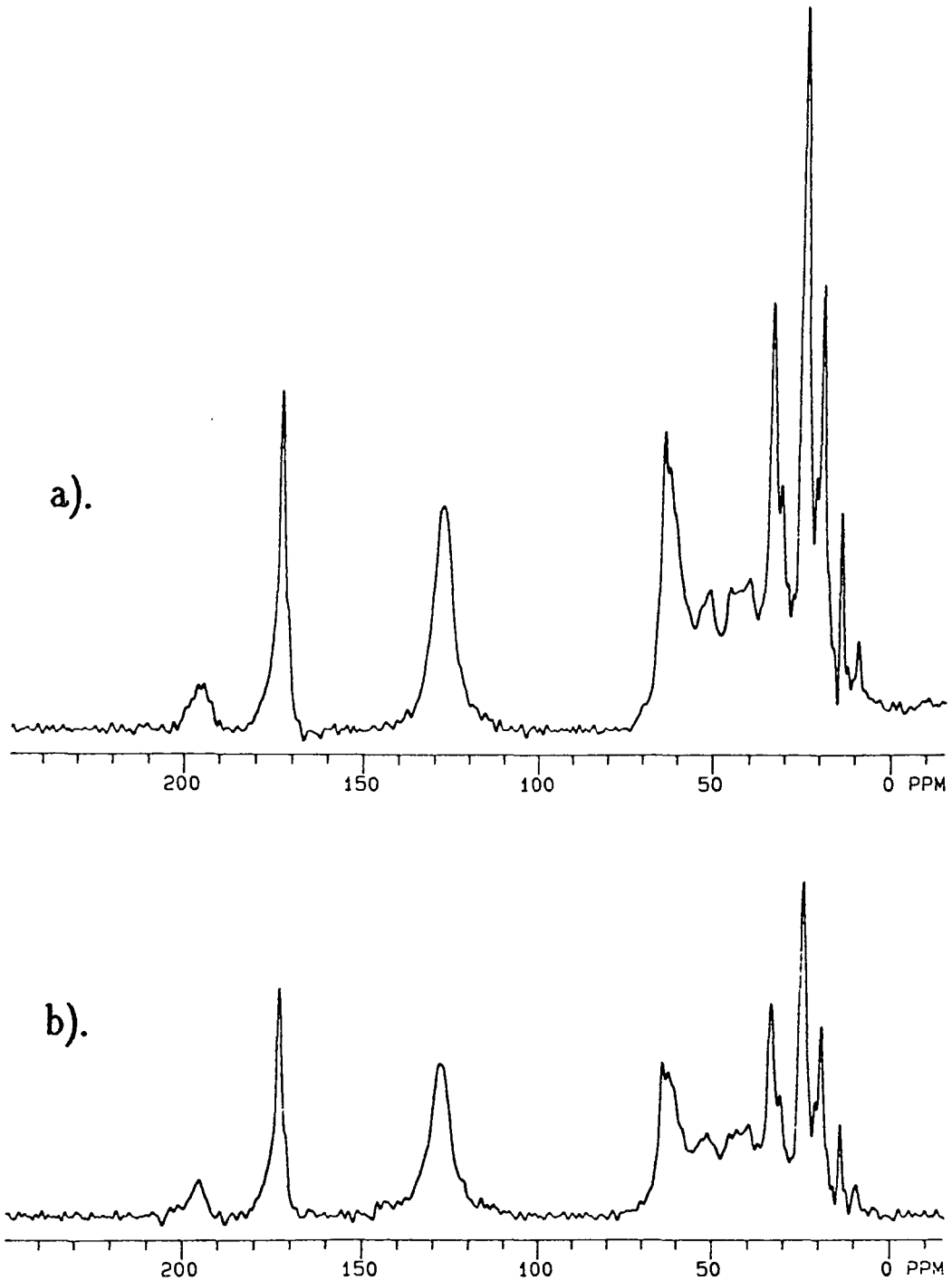

Figure 7.7

a). Solid–state decoupled ^{13}C spectrum of the maleic anhydride film with NOE.

b). Solid–state decoupled ^{13}C spectrum of the maleic anhydride film without NOE.

Recycle time = 7 seconds

Acquisition time = 26 ms

no. of transients = 1000

Table 7.1

The NOE factors for adamantane in both the solution and solid states.

	Adamantane NOE Peak	
	29.4 ppm	38.4 ppm
Solution	1.970	1.979
Solid	1.874	1.859

Table 7.2

Nuclear Overhauser enhancements for the itaconic anhydride film.

Peak/ppm	η	Assignment
19	1.14	CH_3 of MMA
25	1.24	CH_2 'backbone'
34	1.06	O–C(=O)–CH_2
64	0.86	O=C–OCH_2

Table 7.3

Nuclear Overhauser enhancements for the maleic anhydride film.

Peak/ppm	η	Assignment
19	1.21	CH_3 of MMA
25	1.36	CH_2 'backbone'
34	0.97	O–C(=O)–CH_2
64	0.82	O=C–OCH_2

both the itaconic anhydride film and the maleic anhydride film. The spectra with and without the NOE for the itaconic anhydride film are shown in figures 7.6a and 7.6b respectively, and similar spectra for the maleic anhydride film are shown in figure 7.7a and 7.7b. Values of η for peaks which show the Overhauser enhancement are shown in Tables 7.2 and 7.3 for the itaconic anhydride and the maleic anhydride films respectively.

In the solution state, each carbon is coupled to a proton or protons either directly bonded to it or in its immediate environment. Thus the nuclear Overhauser enhancement factor has been used to obtain information about C–H bond lengths and structure.

However, in the solid state, the ^1H–^1H dipolar interactions are very strong. Each proton spin is strongly coupled to other proton spins. The protons usually have a single T_1 value due to spin diffusion. A carbon spin is coupled very strongly to its attached protons. These protons are also strongly coupled to other protons nearby. The result is that a carbon spin in the solid–state is strongly coupled to nearby protons, and is coupled to a lesser extent to the more distant protons. This makes the steady–state NOE values less specific in the solid–state. It is therefore generally not possible to use solid–state nuclear Overhauser enhancements to obtain C–H bondlengths and structural information.

7.4 Effects of inadequate pulse delays[6,7]

As has been described in the last section, a spectrum without the NOE may be obtained using the pulse sequence shown in figure 7.4b (the

gated decoupler method) as for solution state studies. Provided the recycle delay t_d is long enough, turning off the decoupler during the delay allows the nuclei to relax to an equilibrium Boltzmann distribution at the time of the observation pulse[6,8]. However, if the recycle delay is reduced, and the nuclei are not allowed to reach thermal equilibrium, then the value of the nuclear Overhauser enhancement factor is affected[6].

Figure 7.8 compares a plot of intensities of the peak at 25 ppm for the itaconic anhydride film obtained with NOE by varying the saturation time using the pulse sequence in figure 7.4a with a plot of intensities of the peak at 25 ppm obtained with transient Overhauser effects by varying the recycle time using the SPE pulse sequence (figure 7.4b). Comparison between these two intensities for each recycle time gives a plot of NOE against recycle time for the peak at 25ppm, as shown in figure 7.9. If an inadequate pulse delay is used in the SPE pulse sequence (figure7.4b) then a reduced value of the nuclear Overhauser enhancement is observed. It is of the greatest importance, therefore, when measuring NOE enhancements that the recycle delay is long enough to allow the nuclei to return to thermal equilibrium.

7.5 Transient Overhauser effects

In transient NMR experiments, the populations of the spin states are disturbed from their equilibrium or steady–state values and the decay of the system to a new steady–state is observed[6,9]. The perturbation may be effected by two main methods.

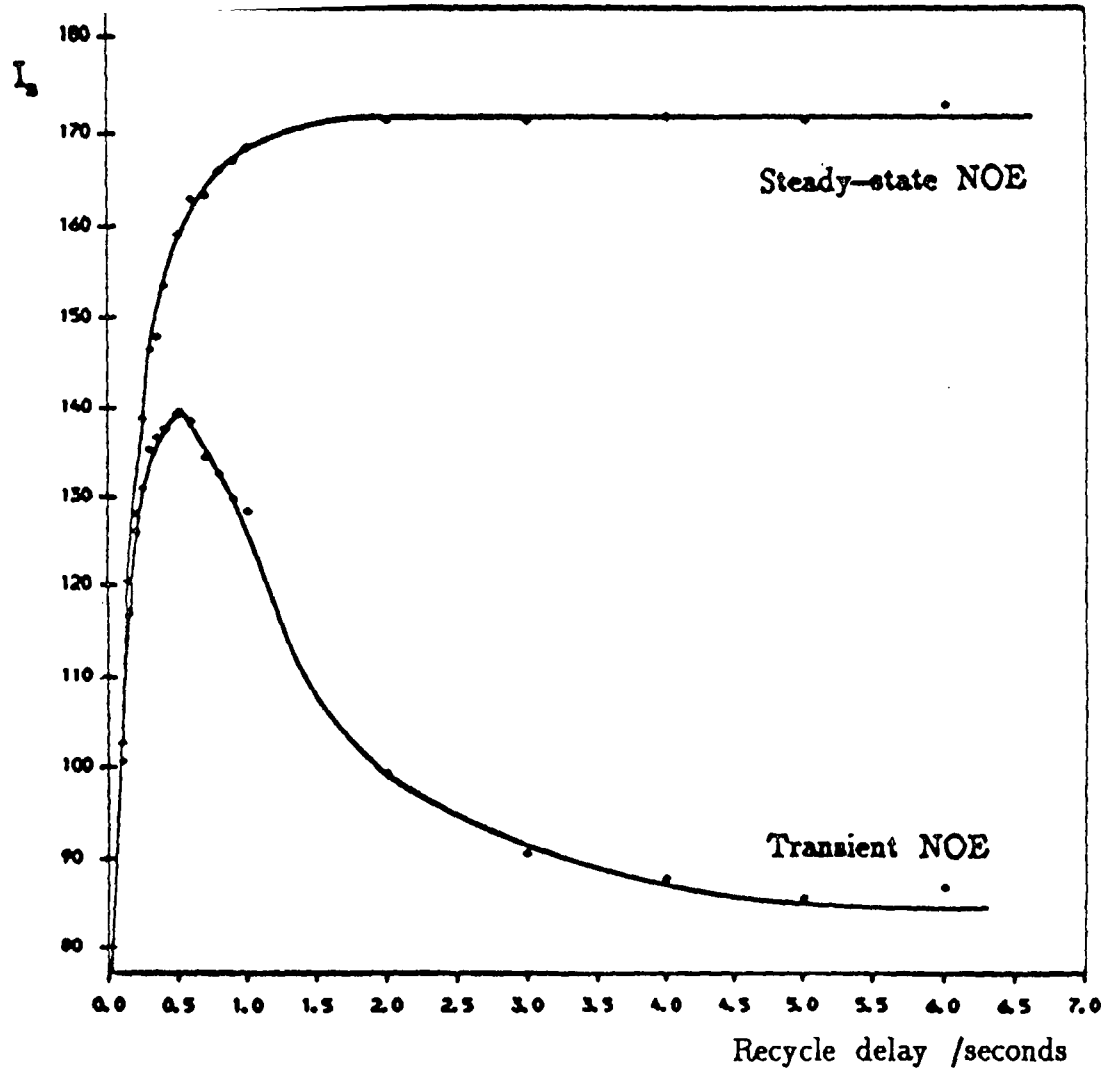

Figure 7.8

A comparison of the intensities of the peak at 25 ppm for the itaconic anhydride film obtained a). with steady–state NOE and b). with transient nuclear Overhauser effects.

AQ = 26 ms

NT = 1000

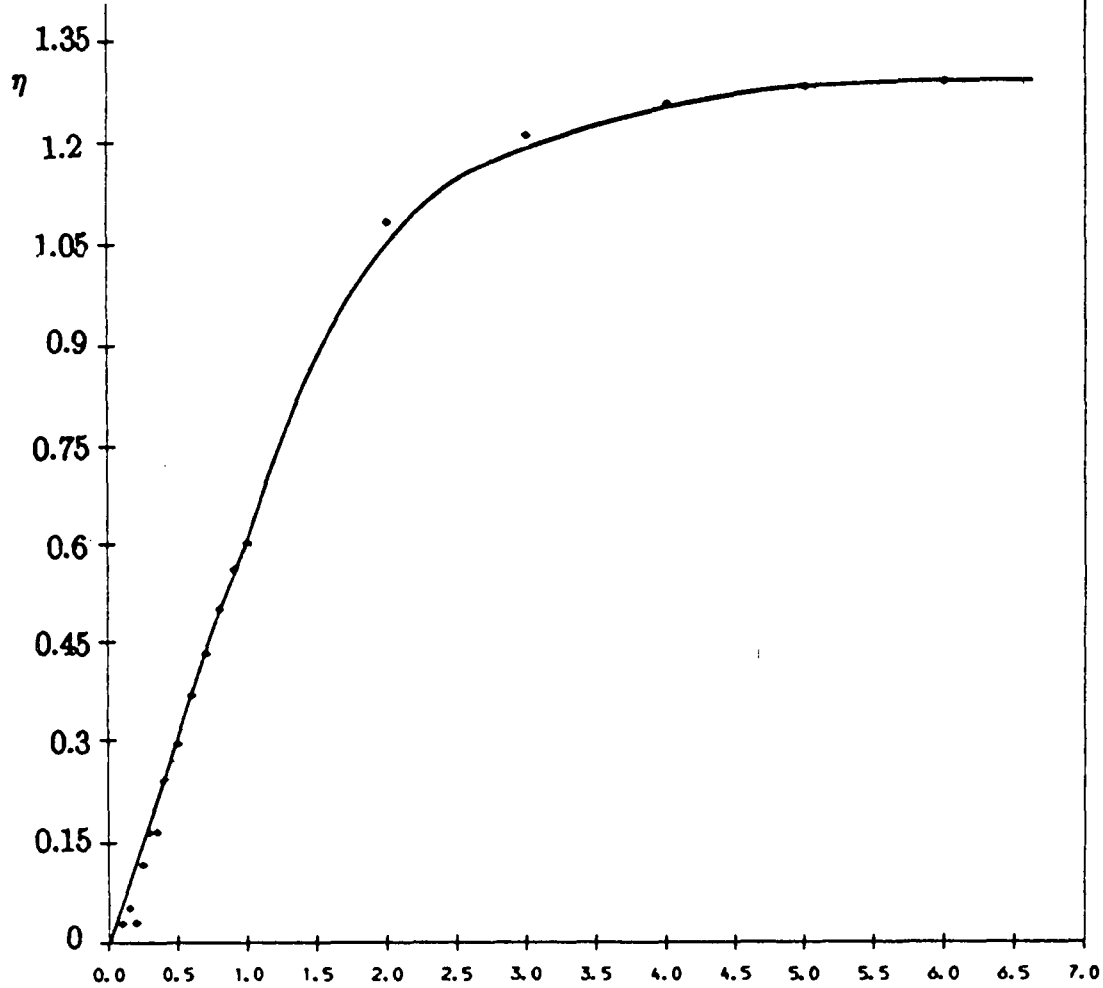

Figure 7.9

The apparent nuclear Overhauser enhancement factor obtained for the peak at 25 ppm for the itaconic anhydride film when inadequate recycle delays are used.

AQ = 26 ms

NT = 1000

1. by applying a strong RF field at the resonance frequency of one of the spins
2. by removing a saturating field from a spin

The behaviour of a spin system under the various possible treatments is the subject of the rest of this chapter.

Consider a two spin system $I \equiv {}^{13}C = \frac{1}{2}$ and $S \equiv {}^{1}H = \frac{1}{2}$. It is assumed that the only mutual interaction is the (I,S) dipole–dipole interaction, but relaxation of both nuclei by other mechanisms is not excluded.

The relaxation of the C–H coupled spin system has been described by Solomon[3] by a pair of simultaneous differential equations.

$$\frac{d}{dt}(\langle I_z\rangle - I_0) = -(\langle I_z\rangle - I_0)/T_1^{II} - (\langle S_z\rangle - S_0)/T_1^{IS} \qquad (7.1a)$$

$$\frac{d}{dt}(\langle S_z\rangle - S_0) = -(\langle I_z\rangle - I_0)/T_1^{IS} - (\langle S_z\rangle - S_0)/T_1^{SS} \qquad (7.1b)$$

The general solution is of the form

$$\langle I_z\rangle = I_0 + C_1\exp(-\lambda_1 t) + C_2\exp(-\lambda_2 t) \qquad (7.2a)$$

$$\langle S_z\rangle = S_0+(\lambda_1-1/T_1^{II})C_1T_1^{IS}\exp(-\lambda_1 t)+(\lambda_2-1/T_1^{II})C_2T_1^{IS}\exp(-\lambda_2 t) \qquad (7.2b)$$

where C_1 and C_2 are constants, and λ_1 and λ_2 are roots of the characteristic equation.

$$\lambda = \frac{1}{2T_1^{II}}\left[(x+1) \pm \left[(x-1)^2+4\left[\frac{\eta\gamma_I}{\gamma_S}\right]^2\right]^{\frac{1}{2}}\right] \qquad (7.3)$$

where $x = \dfrac{T_1^{II}}{T_1^{SS}}$ (7.4)

Both T_1^{II} and T_1^{SS} are easily measured. T_1^{II} is simply the carbon T_1 value, and similarly, T_1^{SS} is the proton T_1 value. T_1^{IS}, the cross–relaxation rate, may be expressed in terms of the NOEF, η by

$$T_1^{IS} = \frac{T_1^{II}}{\eta}\left[\frac{\gamma_I}{\gamma_S}\right] \qquad (7.5)$$

In order to obtain values for the constants C_1 and C_2, the equations must be solved under specific limiting conditions which depend upon the pulse sequence applied to the spins.

Two transient experiments are covered in this thesis.

7.6 The single pulse excitation experiment[9]

The pulse sequence for the single pulse excitation (SPE) experiment is shown in figure 7.10. In order to obtain an expression for the carbon magnetisation at any instance in the recycle delay, the calculation must be split into two stages.

7.6.1 Stage 1

Stage one calculates the growth of I_z between t=0 and $t=t_{aq}$, the end of the acquisition time. A 90° pulse is applied to spin I, followed by an acquisition period t_{aq} during which the spins are decoupled. If an infinitely powerful RF is assumed, then the initial conditions of the spins at time t=0 are

$$\langle I_z\rangle(0)=0 \qquad (7.6a)$$

and

$$\langle S_z\rangle(0)=0 \qquad (7.6b)$$

The proton spins are kept saturated between times t=0 and $t=t_{aq}$, thus we have another limiting condition; that the S magnetisation is zero throughout stage 1.

$$\text{i.e. } \langle S_z\rangle(0)=\langle S_z\rangle(t)=0 \qquad (7.6c)$$

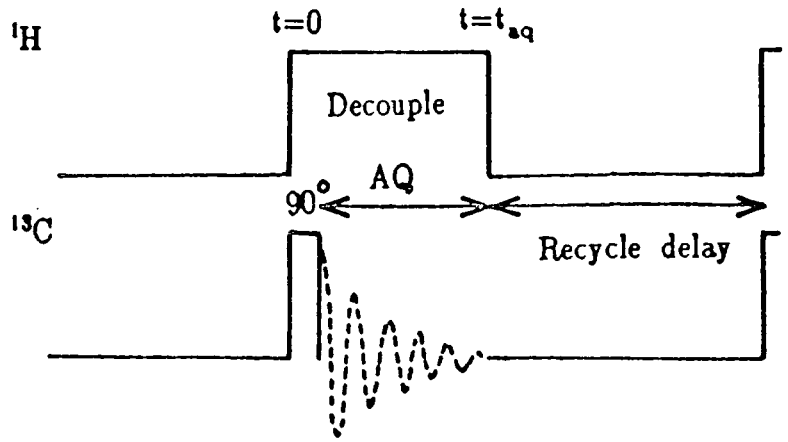

Figure 7.10

The pulse sequence for the single–pulse–excitation experiment.

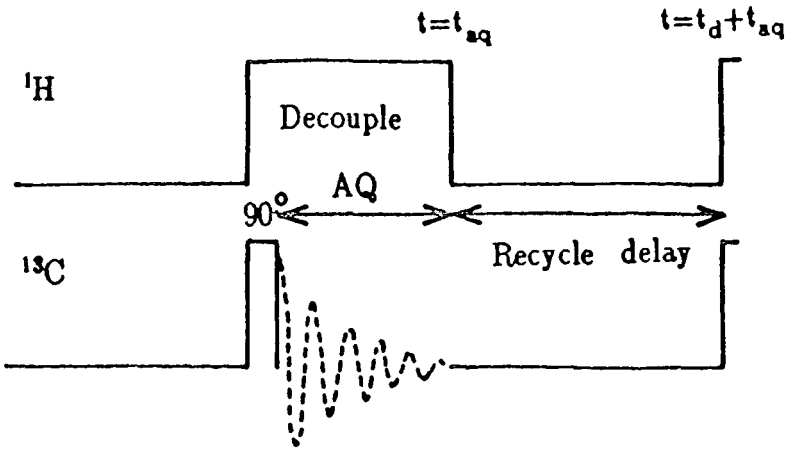

Figure 7.11

The pulse sequence for the single–pulse–excitation experiment. The second stage of the calculation considers the development of I_x between $t=t_{aq}$ and $t=t_d+t_{aq}$.

Substituting these conditions into equations 7.2a and 7.2b leads to values for the constants C_1 and C_2, and hence an expression for the carbon intensity at the end of the acquisition time.

$$\langle I_z\rangle(t_{aq}) = \left[\frac{S_0 T_1^{II}}{T_1^{IS}} + I_0\right]\left[1 - \exp\left[-\frac{t_{aq}}{T_1^{II}}\right]\right] \qquad (7.7)$$

7.6.2 Stage 2

Stage 2 of the calculation considers the development of the carbon magnetisation between time $t=t_{aq}$ and the end of the recycle time $t=t_d+t_{aq}$ as shown in figure 7.11.

The following calculation considers the time dependence of $\langle I_z\rangle$ after releasing $\langle S_z\rangle$ from saturation.

The initial conditions are now $\langle S_z\rangle(t_{aq})=0$ (7.8a)

and $\langle I_z\rangle(t_{aq}) = \left[\frac{S_0 T_1^{II}}{T_1^{IS}} + I_0\right]\left[1 - \exp\left[-\frac{t_{aq}}{T_1^{II}}\right]\right]$ (7.8b)

The expectation value of the carbon magnetisation at the end of the recycle delay, $\langle I_z\rangle(t_{aq}+t_d)$, will be given by the solution of the Solomon equations under these boundary conditions.

As before, expressions for the constants C_1 and C_2 are found, and these constants are then substituted in equation 7.2a to yield:

$$\frac{\langle I_z\rangle(t_{aq}+t_d)-I_0}{I_0} = A$$

where

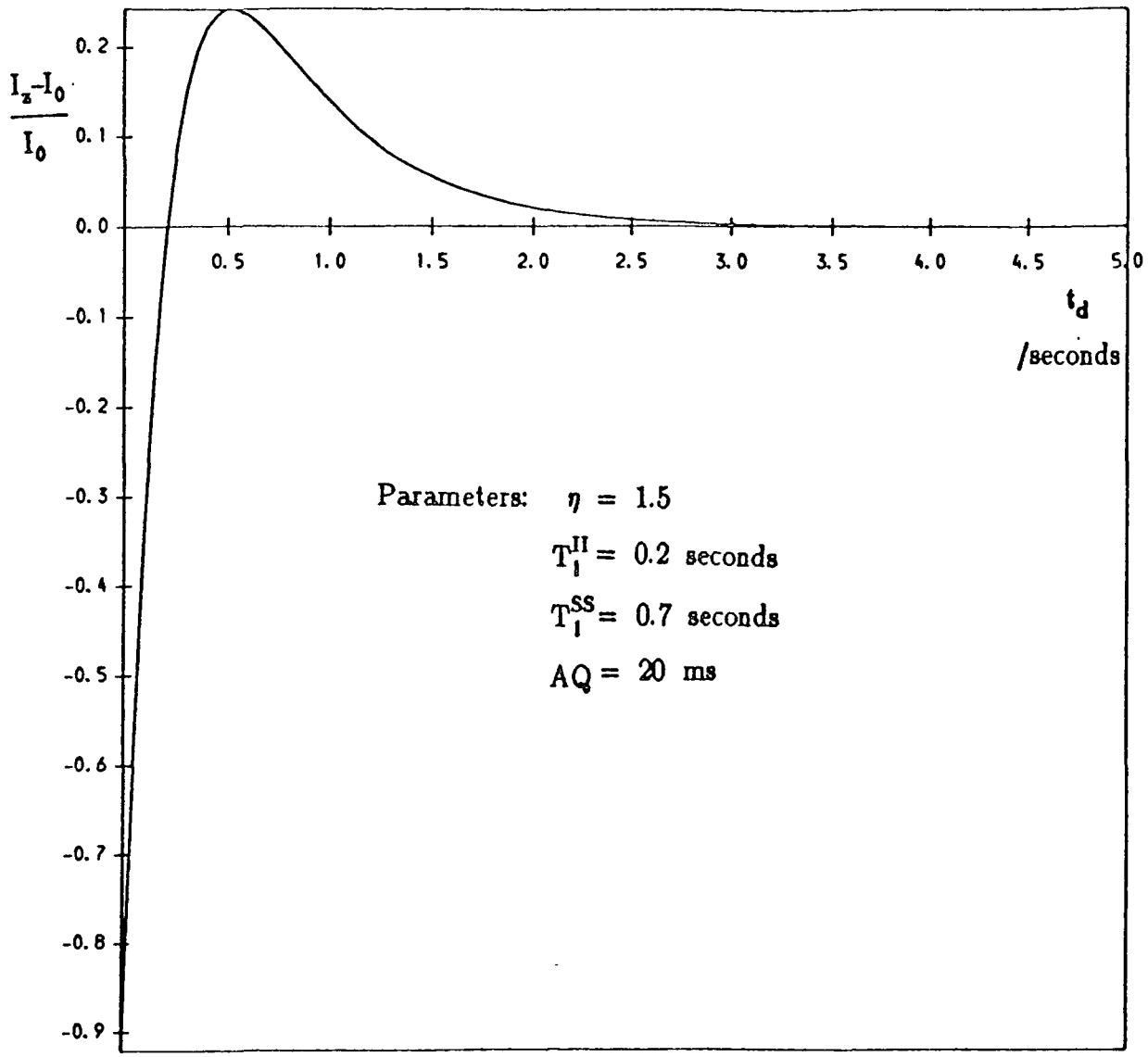

Figure 7.12a

A typical simulation of the carbon intensity observed during the recycle delay in the single–pulse experiment.

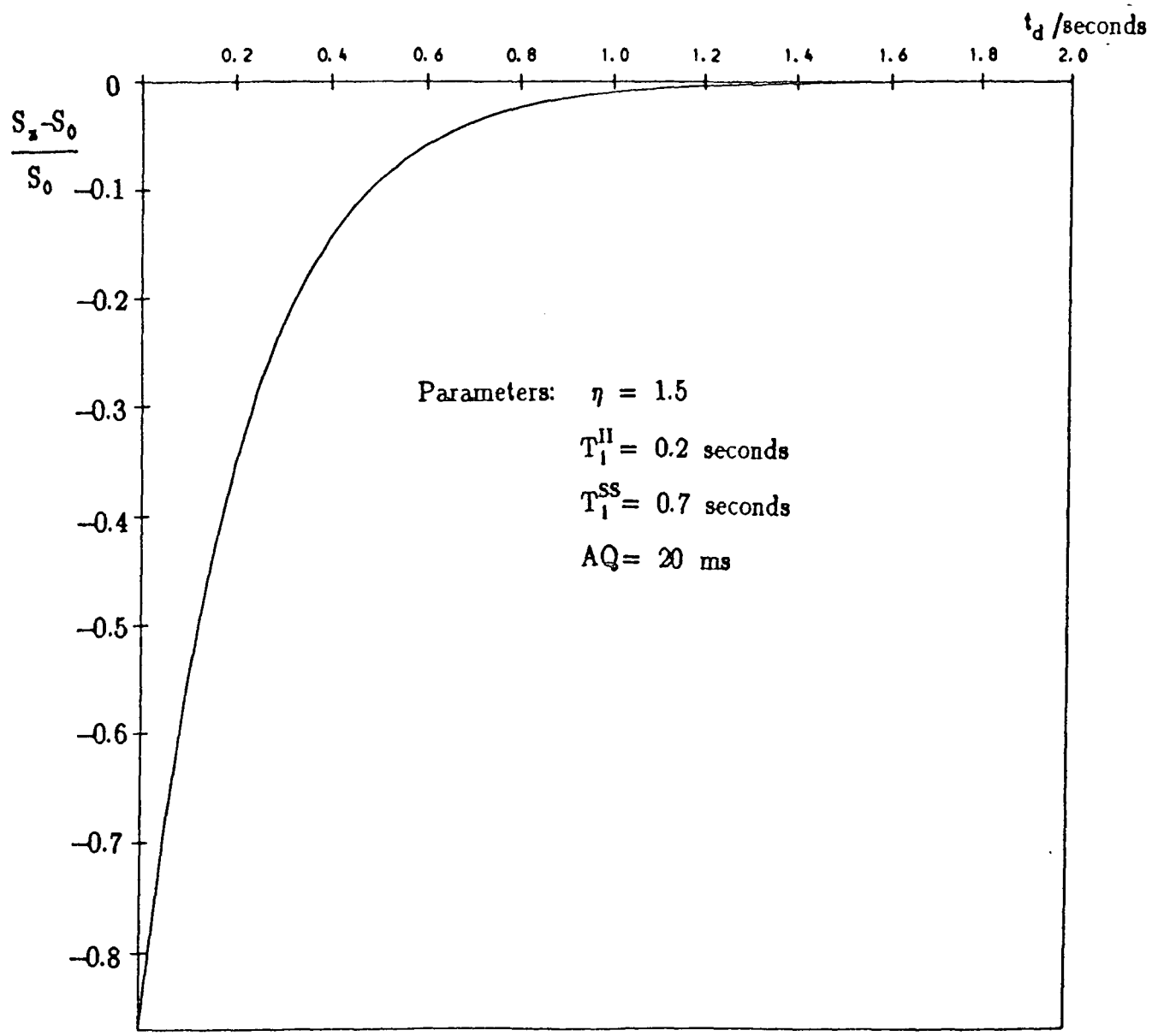

Figure 7.12b

A typical simulation of the proton intensity during the recycle delay in the single–pulse experiment.

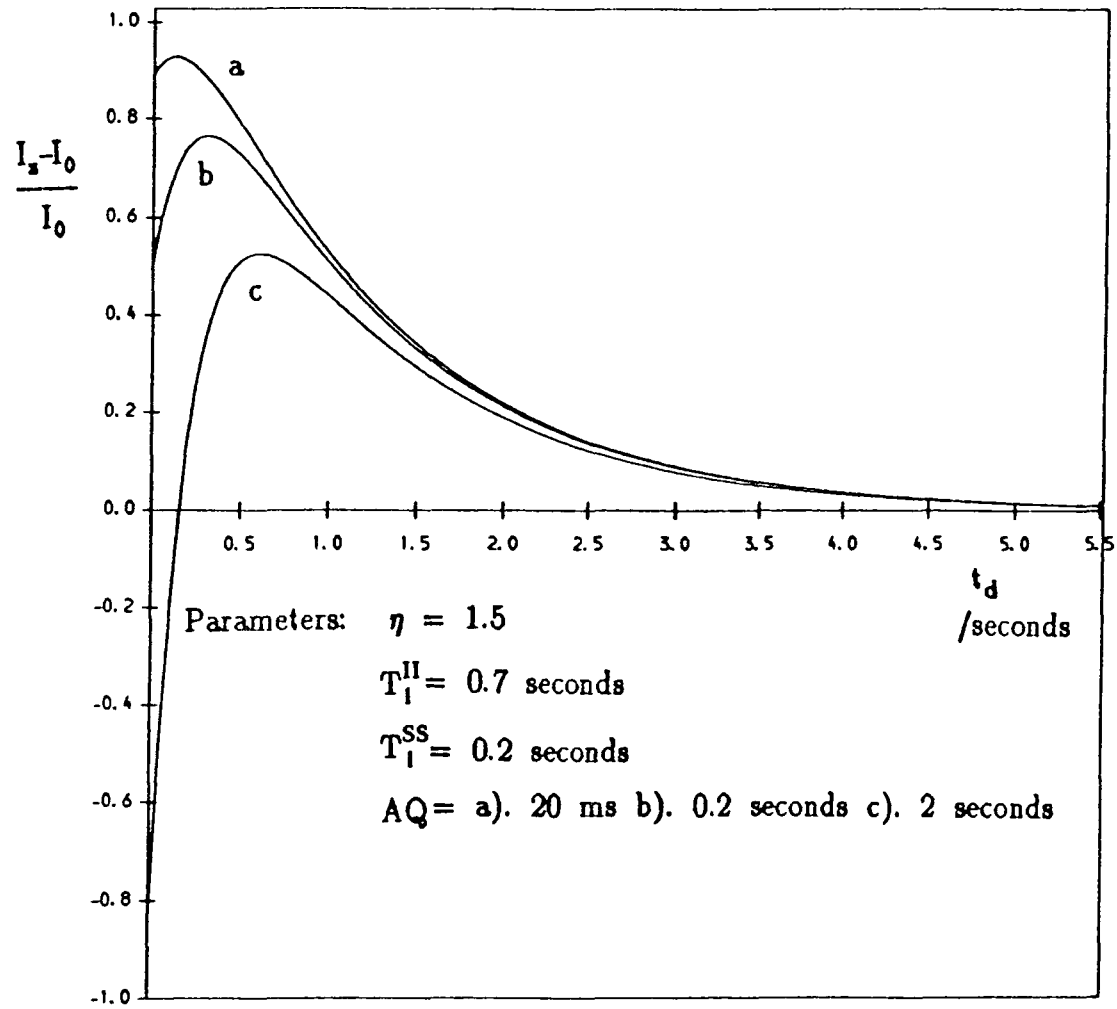

Figure 7.13

A simulation to illustrate how varying the acquisition time alters the observed carbon magnetisation.

$$A = \frac{\exp(-t_{aq}/T_1^{II})}{T_1^{II}(\lambda_2-\lambda_1)}\left[(\eta+1)\left[(\lambda_1 T_1^{II}-1)\exp(-\lambda_2 t_d) - (\lambda_2 T_1^{II}-1)\exp(-\lambda_1 t_d)\right]\right]$$

$$+\frac{\eta(\lambda_2\exp(-\lambda_1 t_d)-\lambda_1\exp(-\lambda_2 t_d))}{(\lambda_2 - \lambda_1)} \qquad (7.9)$$

$$\text{where } \lambda_1,\lambda_2 = \frac{1}{2T_1^{II}}\left[x+1 \pm \left[(x-1)^2+ 4\left[\frac{\eta\gamma_I}{\gamma_S}\right]^2\right]^{\frac{1}{2}}\right] \qquad (7.10)$$

$$\text{and } x = \frac{T_1^{II}}{T_1^{SS}} \qquad (7.10a)$$

The pulse sequence is then repeated.

A simulation program has been written using equation 7.9 to predict the behaviour of the carbon intensity during the recycle delay. The computer program can be found in Appendix A. Figure 7.12a shows a typical simulation of the carbon intensity using realistic parameter values for the variables. Figure 7.12b shows a theoretical simulation of how the proton magnetisation varies under the same conditions. From equation 7.9 it can be seen that several parameters affect the carbon intensity at a particular point in the recycle delay. One of these is t_{aq}, the duration of the high–power decoupling, which effects the build–up of the NOE[10]. Therefore the acquisition time is an experimental parameter which must be taken into account in order to obtain a correct simulation of the carbon intensity. Figure 7.13 demonstrates how varying the acquisition time alters the observed carbon magnetisation.

Once the carbon magnetisation during the recycle delay is predicted theoretically, it is necessary to compare the theory with experiment. Signal from the first few transients of the experiment is rejected to

Figure 7.14

The single–pulse–excitation spectra obtained for the itaconic anhydride film. The recycle delay ranged between 0.02 and 5 seconds. The acquisition time was 20 ms, and 1000 transients were acquired for each spectrum.

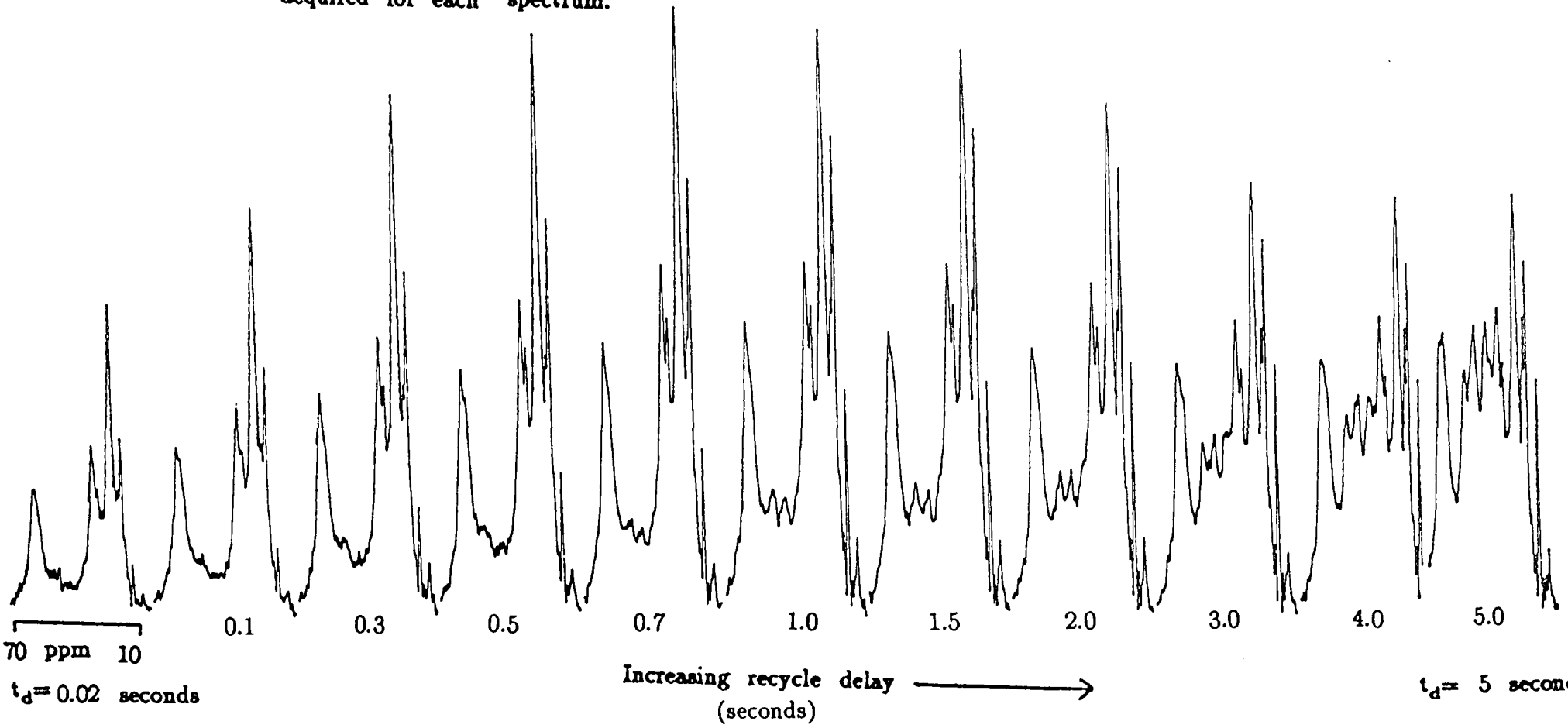

enable a steady–state situation to occur before the data is acquired. The signal accumulated is proportional to the macroscopic magnetisation M_z^I, and hence to the expectation value of the carbon intensity $\langle I_z \rangle (t_{aq}+t_d)$.

$$\frac{M_z^I}{M_0} = \frac{\langle I_z \rangle (t_{aq}+t_d)}{I_0} \qquad (7.11)$$

The SPE experiment was repeated several times on the itaconic anhydride film, each time with a different recycle delay (t_d). The signal intensities of the spectra obtained after Fourier transformation of the FIDs represent the magnetisations at the time of the 90° ^{13}C pulse. Therefore it is possible to trace the time development of the magnetisation (i.e. the transient NOE) by varying the recycle delay of the gated decoupler experiment. In this way the growth of the carbon magnetisation towards equilibrium was monitored. The SPE spectra obtained for the itaconic anhydride film are shown in figure 7.14. In general, the lower the recycle time, the more mobile are the peaks which are observed in the spectrum. Thus only polyester peaks are apparent in the spectra with low recycle time.

Simulations have been made of the carbon intensity for each of the four peaks at 19, 25, 34 and 64ppm which show transient nuclear Overhauser effects. These simulations are compared to the experimental intensities in figures 7.15–18 for the itaconic anhydride film. The assignments of the peaks and their relevant parameters are shown in Table 7.4. The Overhauser enhancement, η, was measured using the saturation method described in section 7.3.2 (figure 7.4a). T_1^{II}, the carbon T_1 was measured using the MOST pulse sequence as described in chapter

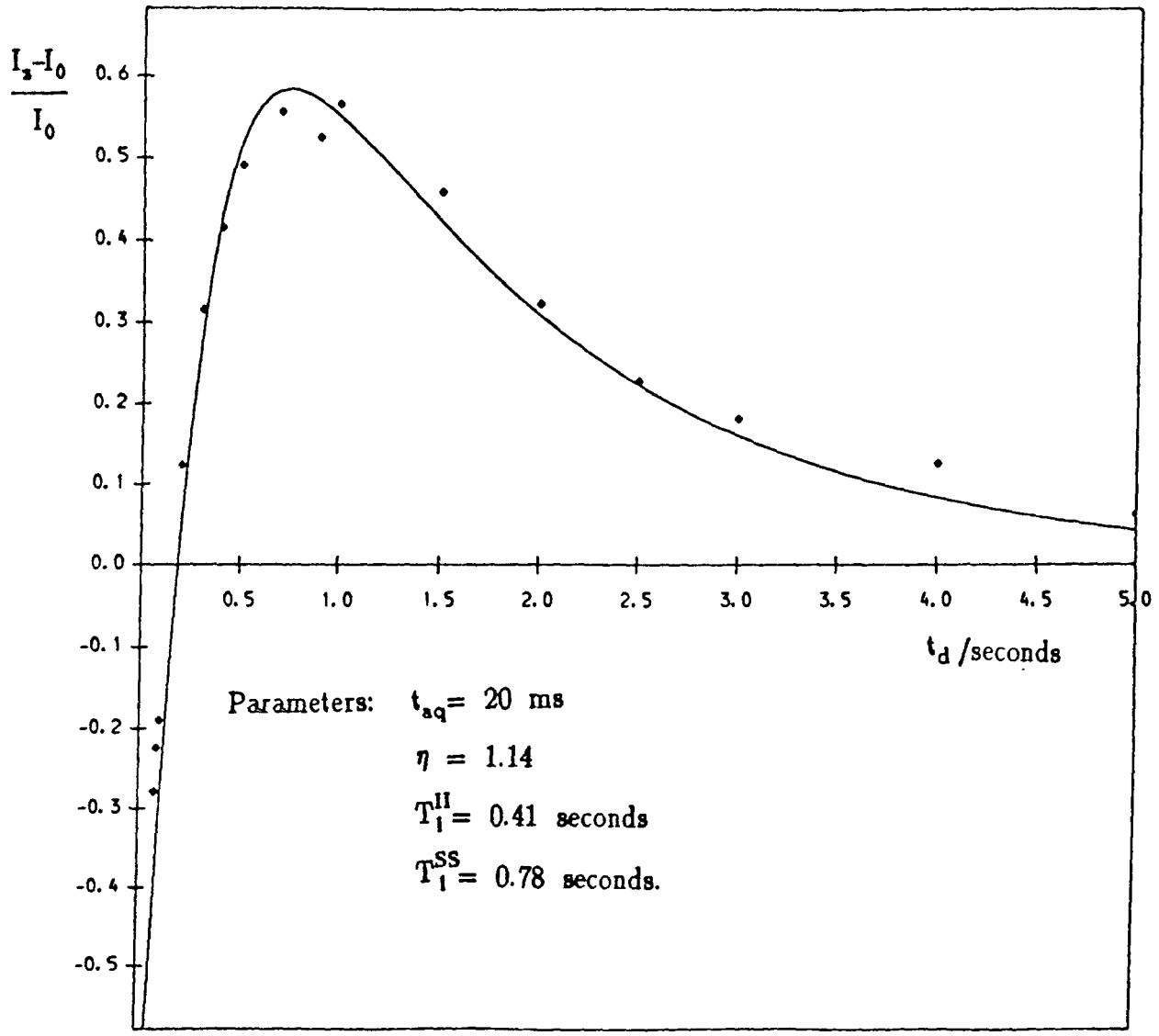

Figure 7.15

A comparison between the theoretical SPE simulation and the experimental intensities for the peak at 19 ppm in the itaconic anhydride film.

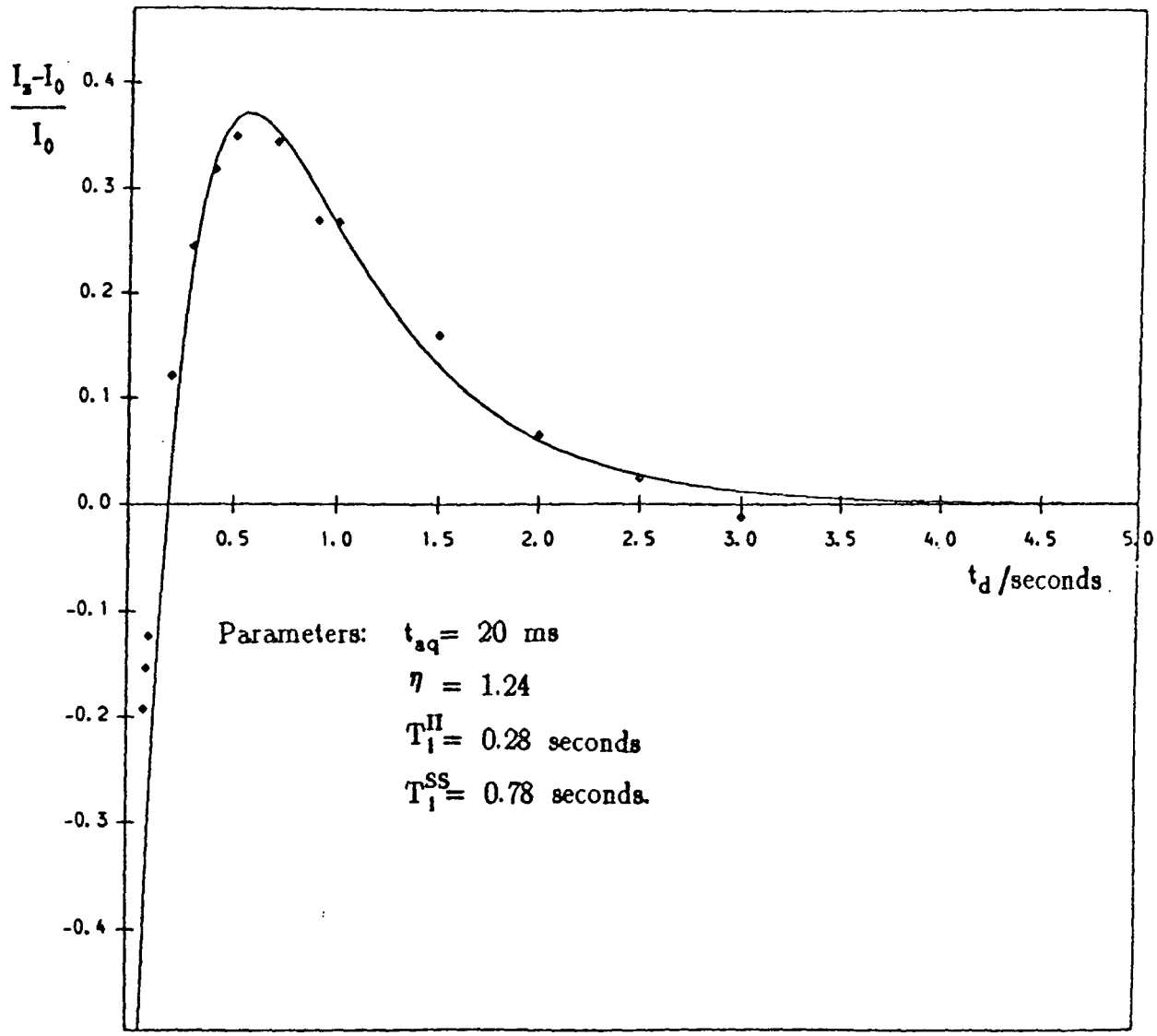

Figure 7.16

A comparison between the theoretical SPE simulation and the experimental intensities for the peak at 25 ppm in the itaconic anhydride film.

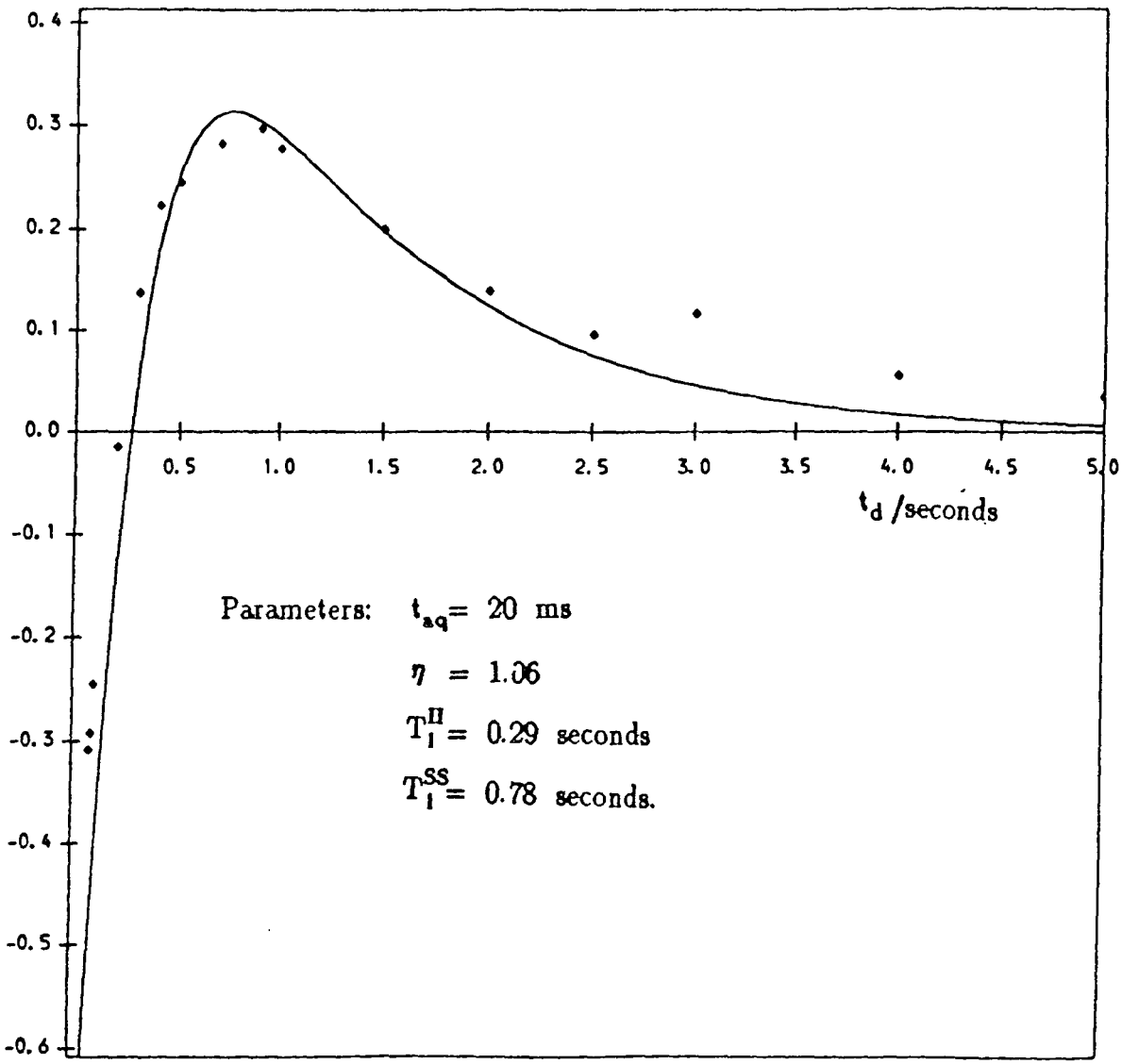

Figure 7.17

A comparison between the theoretical SPE simulation and the experimental intensities for the peak at 34 ppm in the itaconic anhydride film.

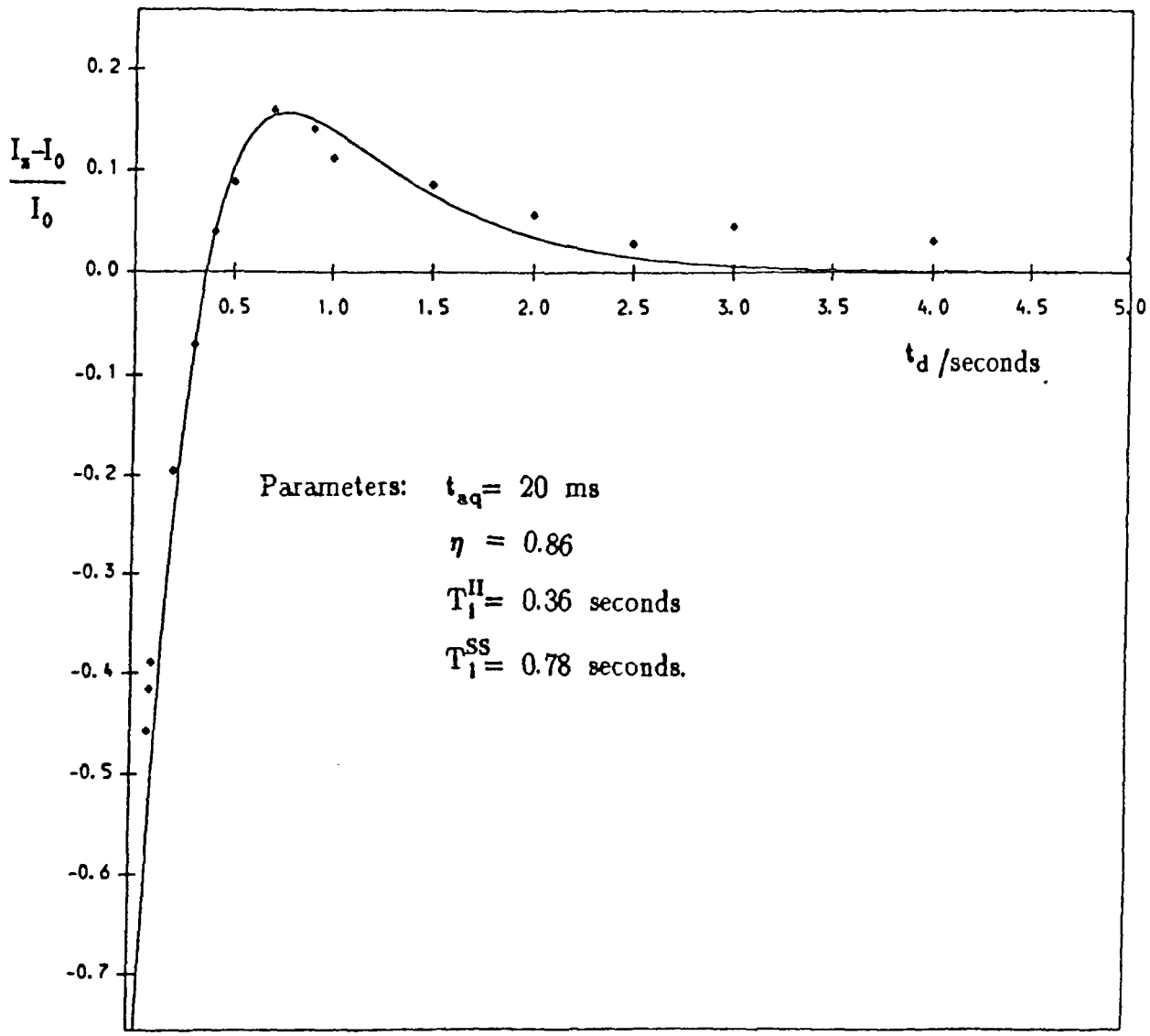

Figure 7.18

A comparison between the theoretical SPE simulation and the experimental intensities for the peak at 64 ppm in the itaconic anhydride film.

Table 7.4

Parameters for the simulation of the SPE carbon intensity of the itaconic anhydride film.

Peak/ppm	η	T_1^{II}/seconds	Assignment
19	1.14	0.41	CH_3 of MMA
25	1.24	0.28	CH_2 'backbone'
34	1.06	0.29	O–C(=O)–CH_2
64	0.86	0.36	O=C–OCH_2

Table 7.5

Parameters for the simulation of the SPE carbon intensity of the maleic anhydride film.

Peak/ppm	η	T_1^{II}/seconds	Assignment
19	1.21	0.32	CH_3 of MMA
25	1.24	0.23	CH_2 'backbone'
34	1.06	0.29	O–C(=O)–CH_2
64	0.86	0.34	O=C–OCH_2

Five. T_1^{SS}, the proton T_1, assumed to be single exponential, was measured by the saturation recovery method. T_1^{II} is also assumed to be single exponential. As discussed in chapter Five, the carbon T_1's of the polyester peaks have two components, the shorter component arising from the carbons of the more mobile polyester, either uncross–linked, or cross–linked at only one end of the polyester chain, and the longer component arising from the carbons of the more rigid polyester cross–linked at both ends of the polyester chain. The more mobile a particular carbon atom, the more likely it is to show NOE effects. The assumption was made that only the more mobile carbons in the polyester chain contributed to the observed transient Overhauser effects. Therefore only the short component of the carbon T_1 has been taken into account in the simulations (Figures 7.15–18). Initially the simulations are an excellent fit to the experimental data. However at longer recycle times (4 seconds onwards), the measured experimental carbon intensity is greater than the theoretical prediction. At short recycle times (< 3 seconds) the longer ^{13}C T_1 component has a negligible effect on the measured carbon intensity. However, as the recycle time is increased, the longer component of the carbon T_1 has a larger contribution to the measured carbon intensity. The effect of the longer ^{13}C T_1 component has been neglected in the theoretical simulations, hence, at longer recycle times, the theoretical simulation deviates from the experimental data.

The single pulse excitation experiments were also repeated on the maleic anhydride film, again each time with a different recycle delay. The SPE spectra are shown in figure 7.19. Figures 7.20–23 show the four

Figure 7.19

The single-pulse-excitation spectra obtained for the maleic anhydride film. The recycle delay ranged between 0.02 and 5 seconds. The acquisition time was 20 ms, and 1000 transients were acquired for each spectrum.

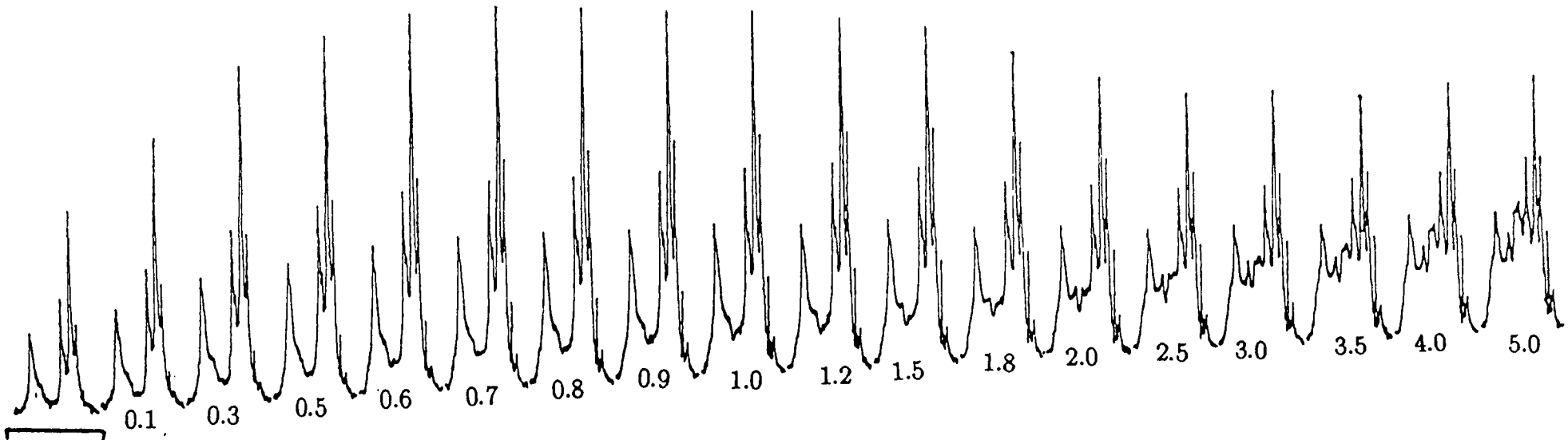

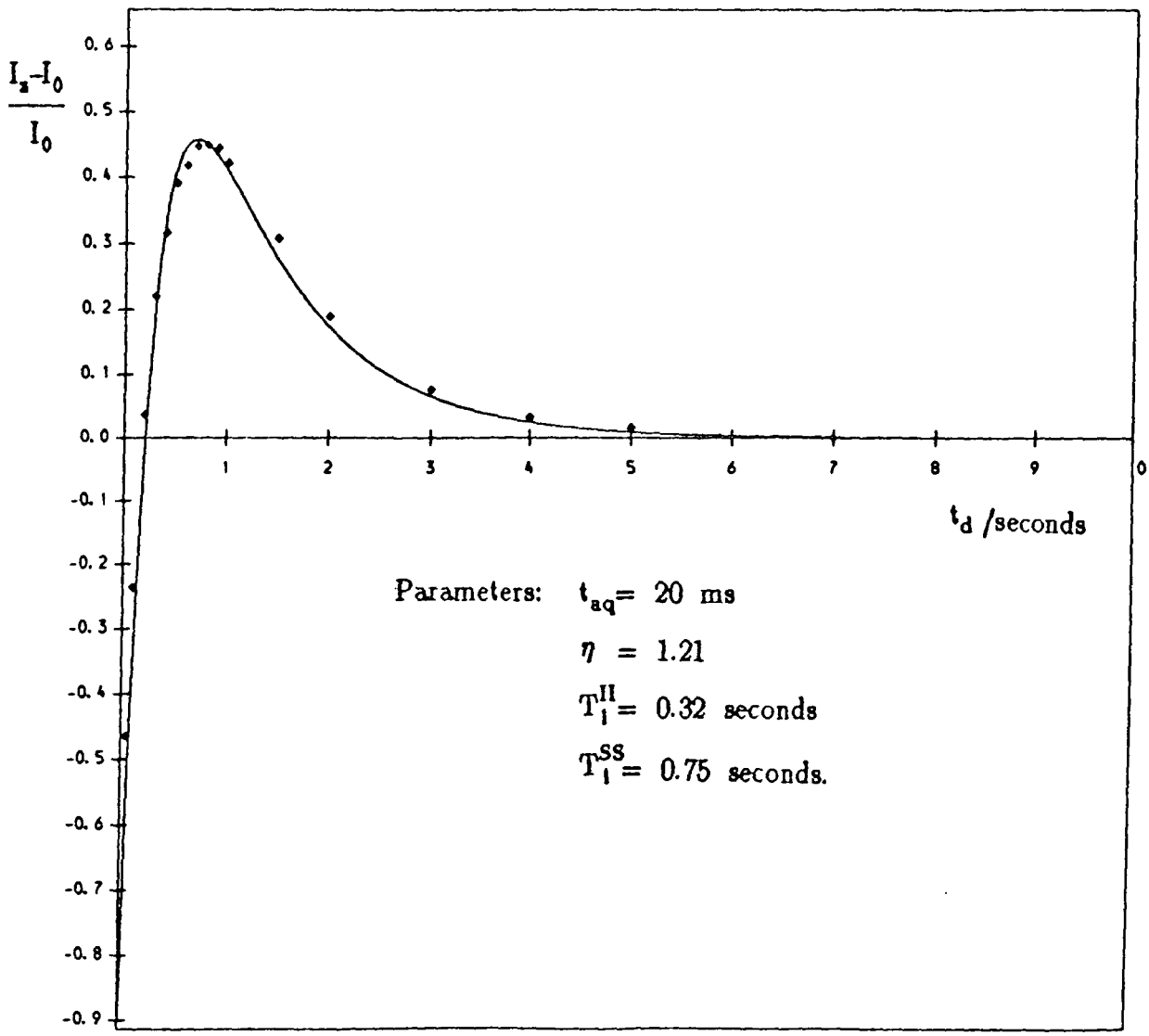

Figure 7.20

A comparison between the theoretical SPE simulation and the experimental intensities for the peak at 19 ppm in the maleic anhydride film.

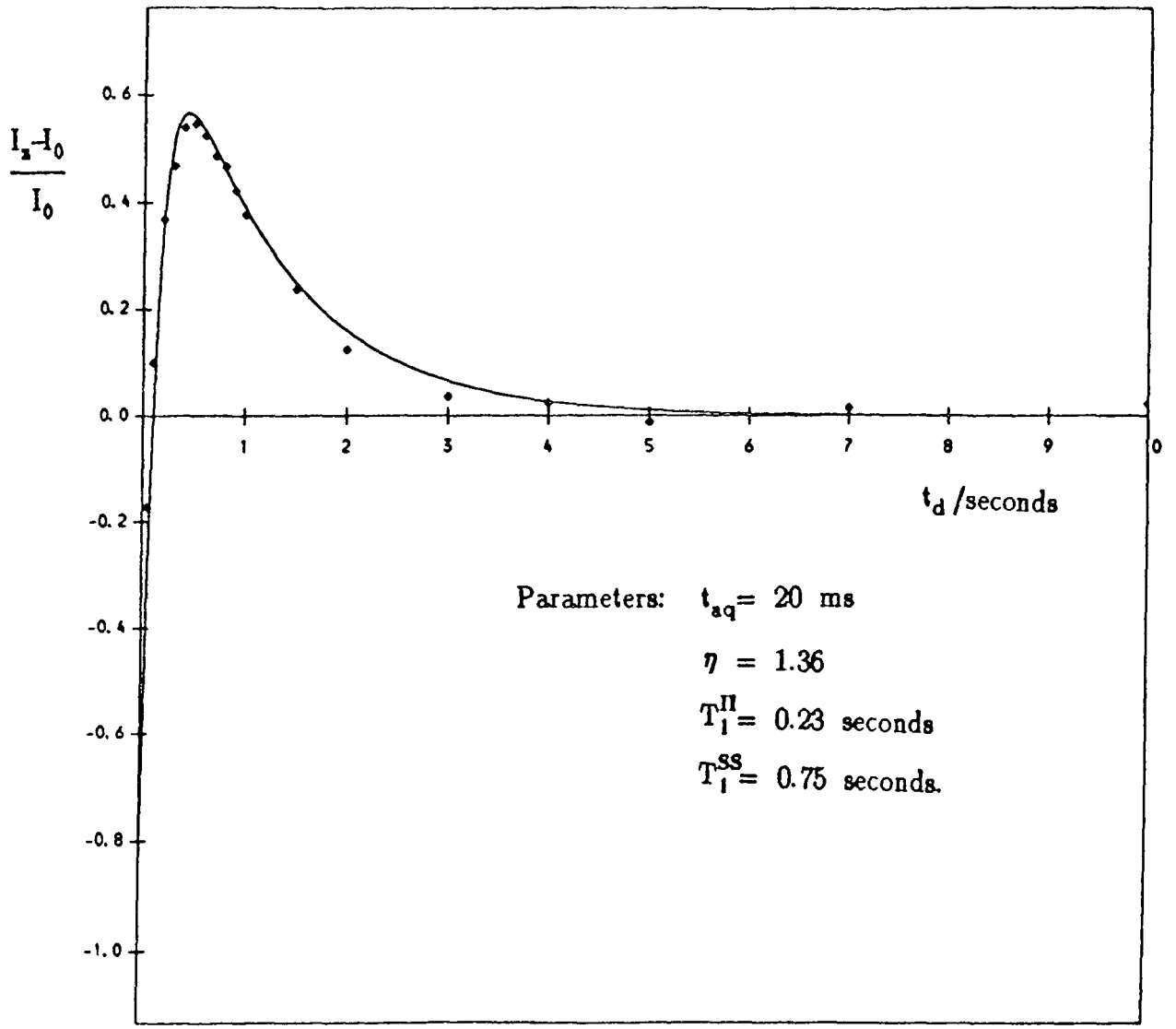

Figure 7.21

A comparison between the theoretical SPE simulation and the experimental intensities for the peak at 25 ppm in the maleic anhydride film.

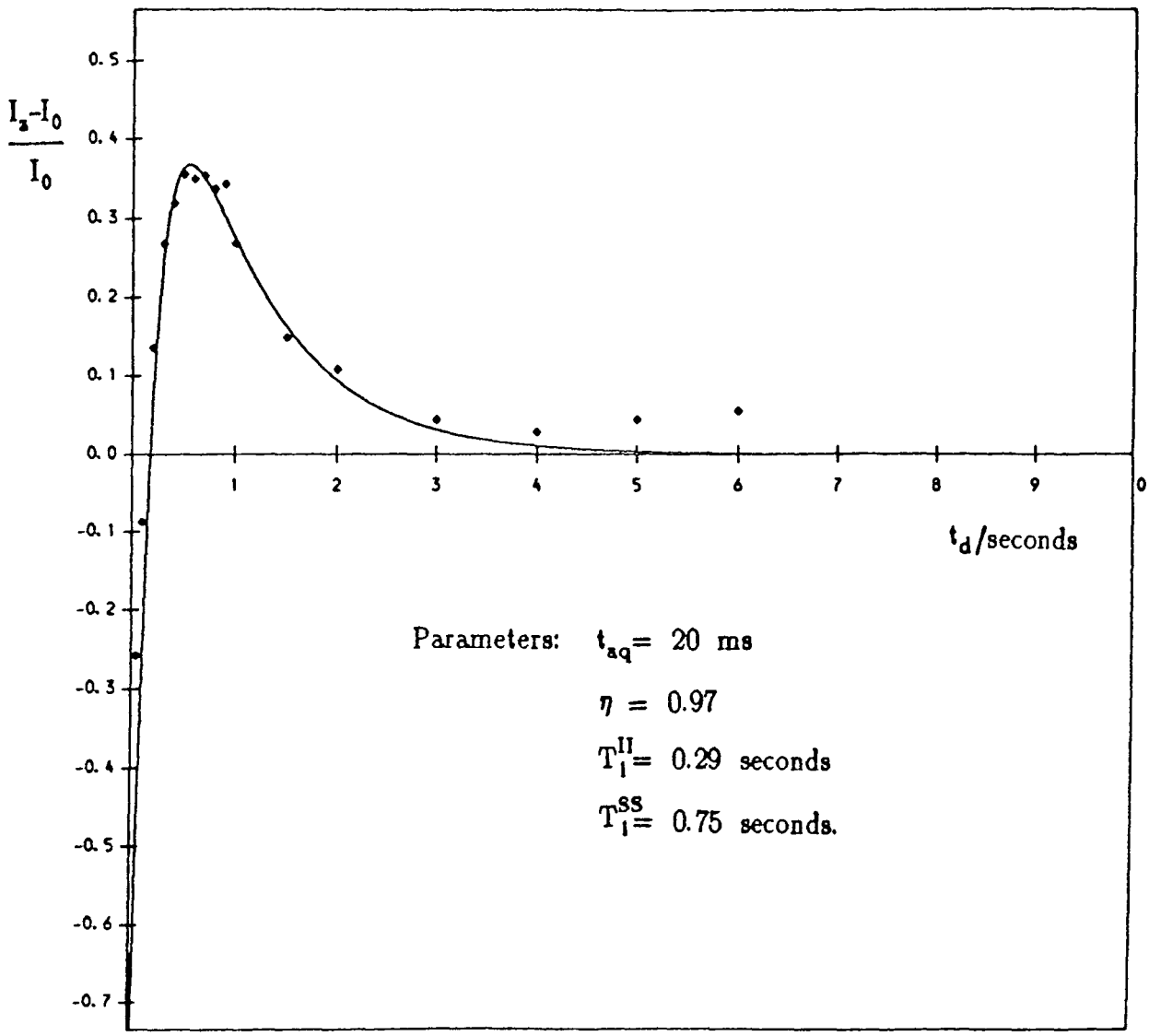

Figure 7.22

A comparison between the theoretical SPE simulation and the experimental intensities for the peak at 34 ppm in the maleic anhydride film.

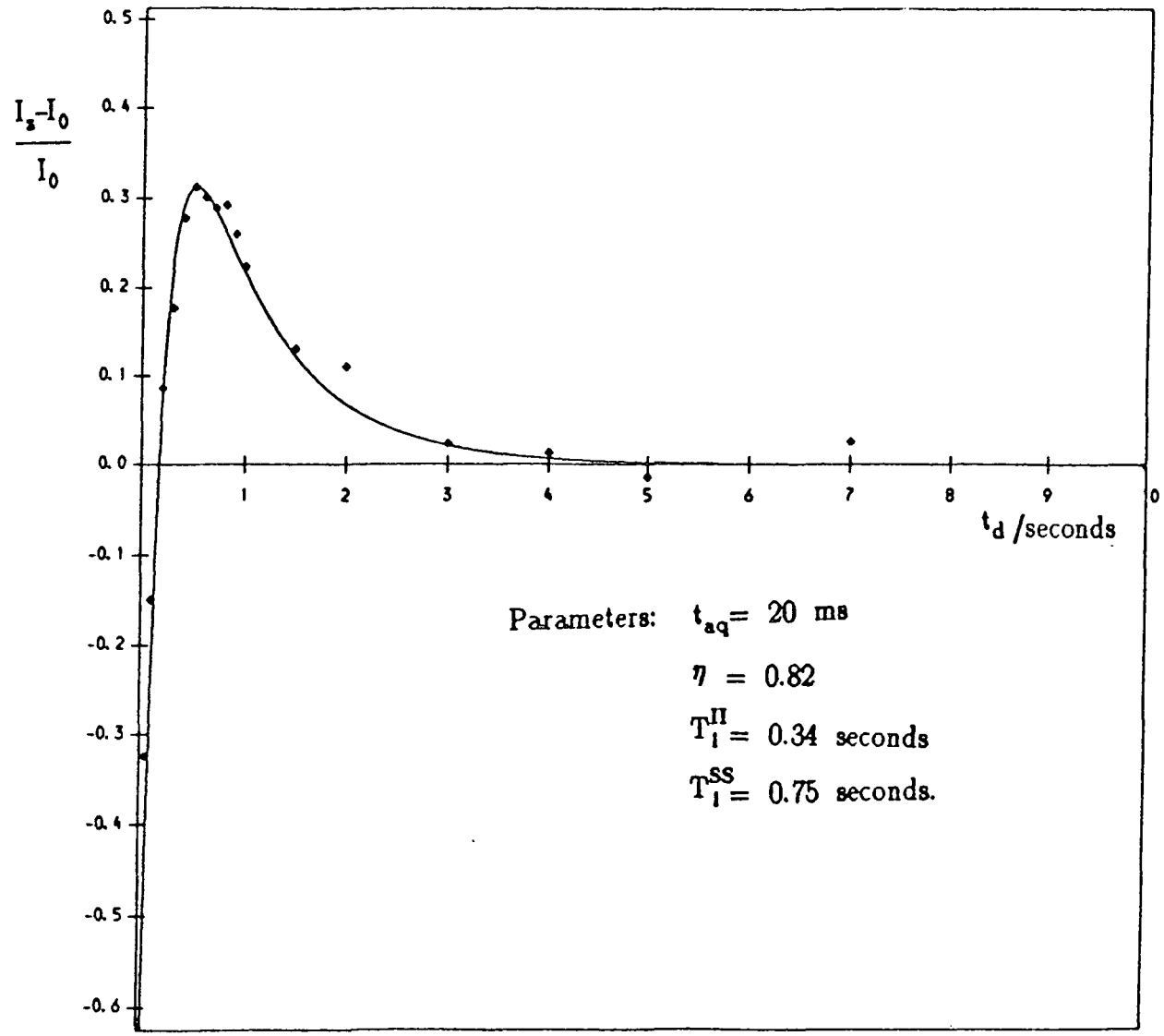

Figure 7.23

A comparison between the theoretical SPE simulation and the experimental intensities for the peak at 64 ppm in the maleic anhydride film.

peaks in the maleic anhydride film spectra with nuclear Overhauser enhancements. The assignments of the peaks and the relevant parameters are shown in Table 7.5.

From figs 7.15–18 and 7.20–23 it may be seen that the simulations produce an excellent fit to the experimental spectra in spite of the fact that many complexities (such as anisotropy of the relevant motion and the direct effects of spin diffusion) have been ignored.

The practical conclusion from the gated–decoupler MAS experiment in the solid–state without cross–polarisation is that for mobile systems, in order to measure correct resonance intensities, the proton decoupler must be gated off for a long time. Spectra obtained at shorter recycle times will not yield correct relative intensities between carbons in any one spectrum since the NOE will vary from one carbon to another. Thus care must be taken when using the gated–decoupler experiment for quantitative measurements.

7.7 A second transient experiment: INV1H[9]

The pulse sequence for the INV1H experiment is shown in figure 7.24. The experiment consists of a 180° pulse at the proton frequency followed by a delay τ during which the proton spin systems are allowed to evolve. The intensity of the carbon magnetisation during the delay τ is monitored by a carbon 90° read pulse followed by carbon acquisition and dipolar decoupling. A recycle delay of at least $5\times T_1^{II}$ is used to allow full recovery to the Boltzmann distributions.

An expression for the carbon magnetisation at any instance during

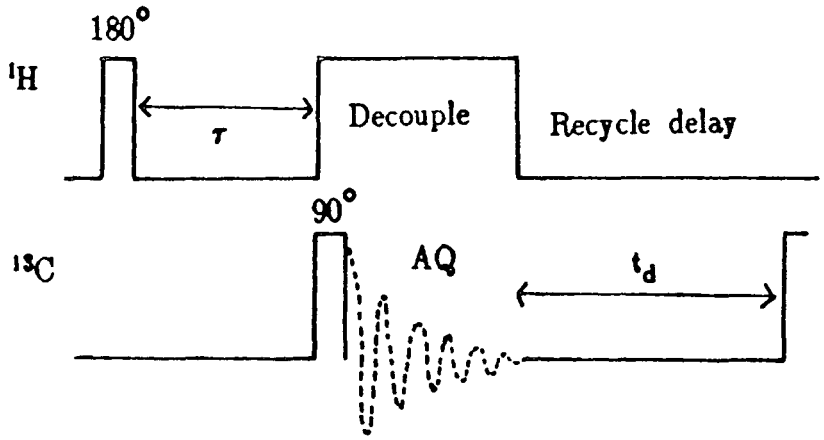

Figure 7.24

The pulse sequence for the INV1H experiment.

the delay τ may be obtained in a similar way as for the SPE transient experiment. However the calculation for the INV1H experiment has only one step.

7.7.1 Calculation of I_z

The aim of the experiment is to monitor the time dependence of the carbon spins after the inversion of the proton magnetisation. The only part of the pulse sequence which needs to be considered theoretically is from the 180° proton pulse until the end of the delay τ. (Figure 7.24)

If t=0 is immediately after the 180° proton pulse, then the initial conditions of the spins at time t=0 are

$$\langle I_z \rangle(0) = +I_0 \qquad (7.12a)$$

and

$$\langle S_z \rangle(0) = -S_0 \qquad (7.12b)$$

Substituting these conditions into equations 7.2a and 7.2b leads to values for the constants C_1 and C_2, and hence an expression for the carbon intensity at the end of the delay period τ.

$$\frac{\langle I_z \rangle_\tau - I_0}{I_0} = \frac{2T_1^{II}}{\eta(\lambda_2 - \lambda_1)}\left[\exp(-\lambda_1\tau) - \exp(-\lambda_2\tau)\right] \qquad (7.13)$$

As in the previous SPE experiment, the theoretical simulation is compared to experimental data. The INV1H experiment was repeated several times on a sample of itaconic anhydride film, each time varying the value of the delay τ. The recycle delay is kept constant at 5s throughout the experiments. All three of the mobile polyester peaks and the CH_3 copolymer peak reach equilibrium by 5 seconds. The spectra obtained for the itaconic anhydride film are shown in figure 7.25. As

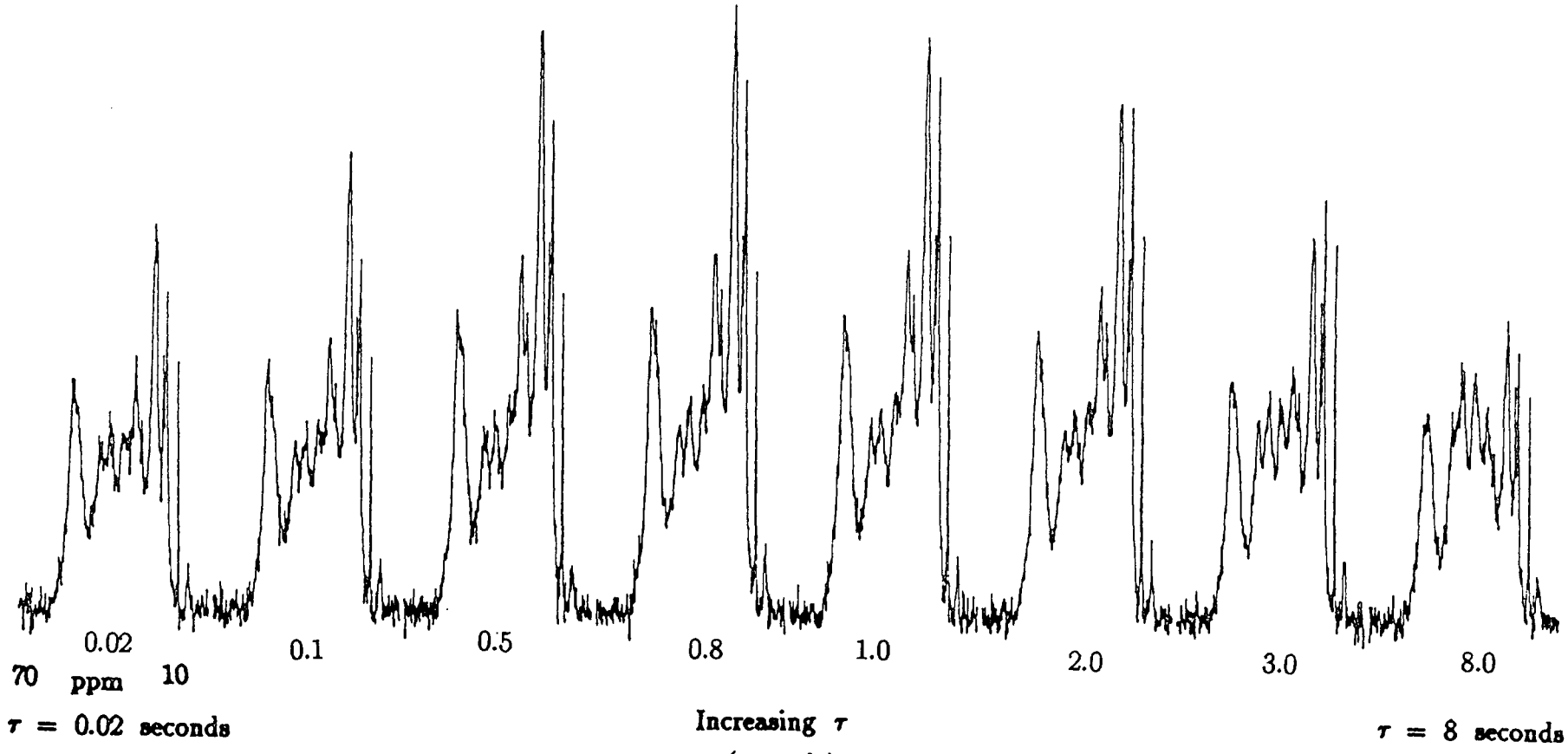

Figure 7.25

The INV1H spectra obtained for the itaconic anhydride film. The delay τ ranged between 0.02 and 8 seconds. The acquisition time was 20 ms, and 1000 transients were acquired for each spectrum.

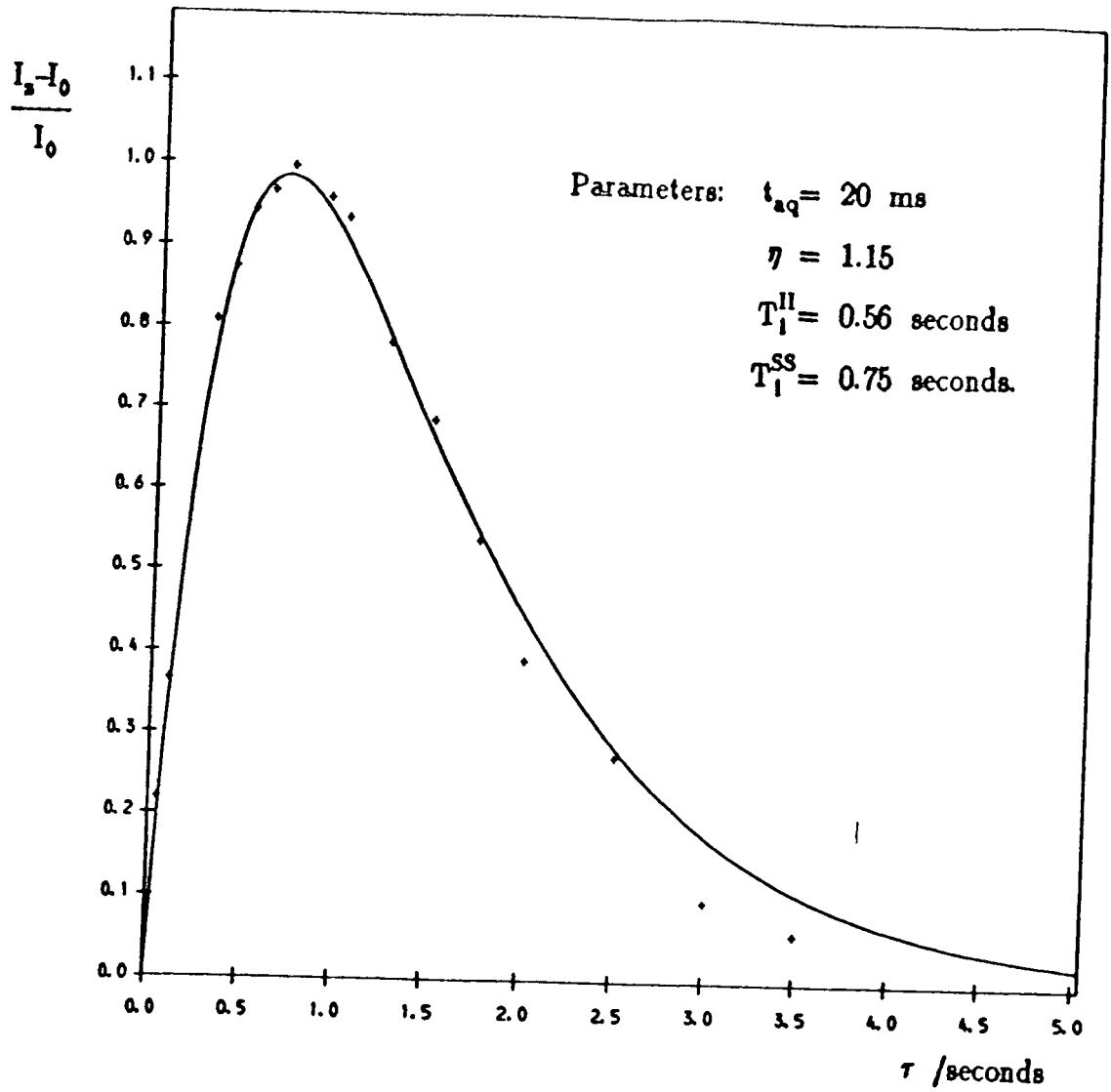

Figure 7.26

A comparison between the theoretical INV1H simulation and the experimental intensities for the peak at 19 ppm in the itaconic anhydride film.

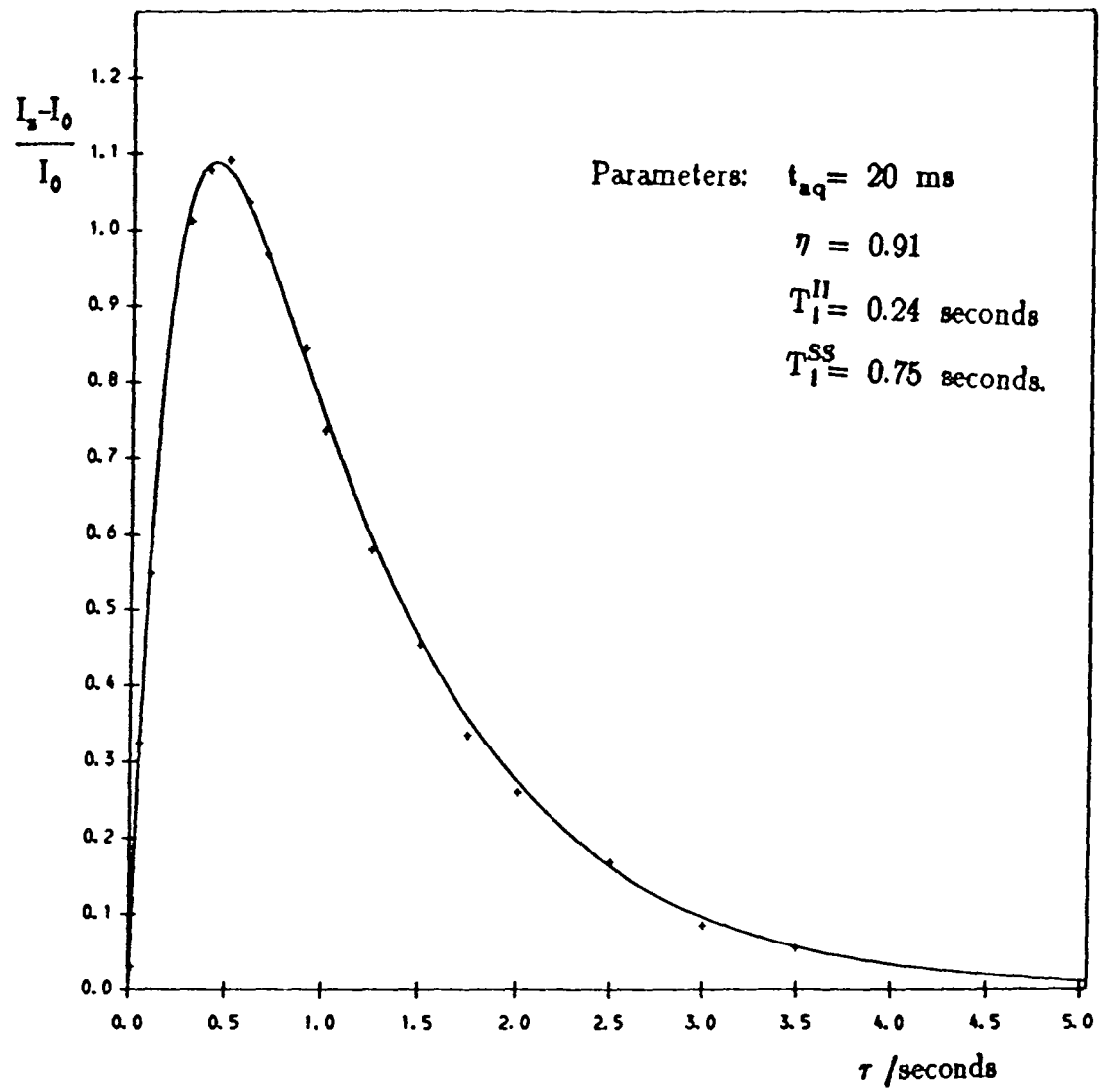

Figure 7.27

A comparison between the theoretical INV1H simulation and the experimental intensities for the peak at 25 ppm in the itaconic anhydride film.

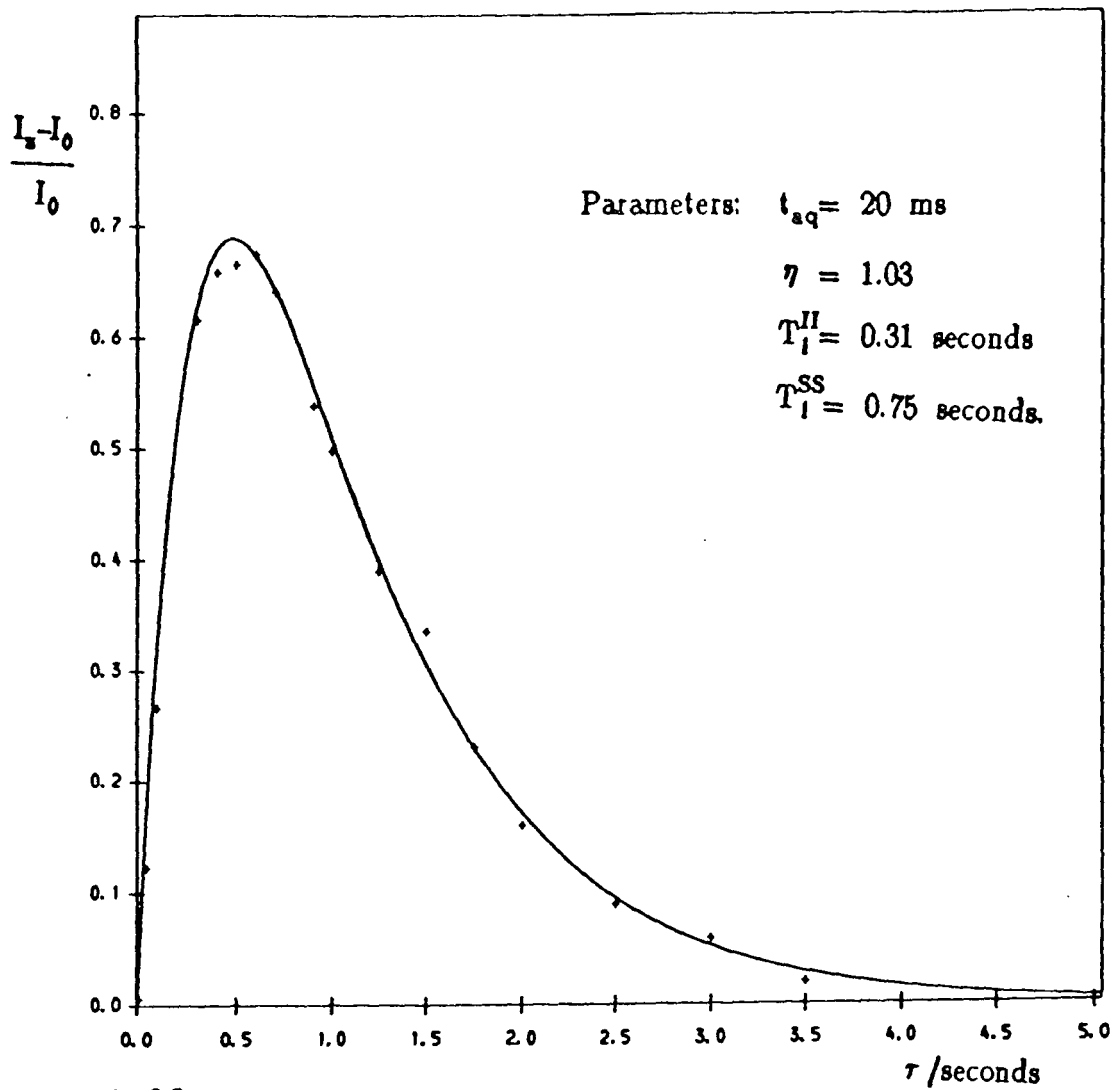

Figure 7.28

A comparison between the theoretical INV1H simulation and the experimental intensities for the peak at 34 ppm in the itaconic anhydride film.

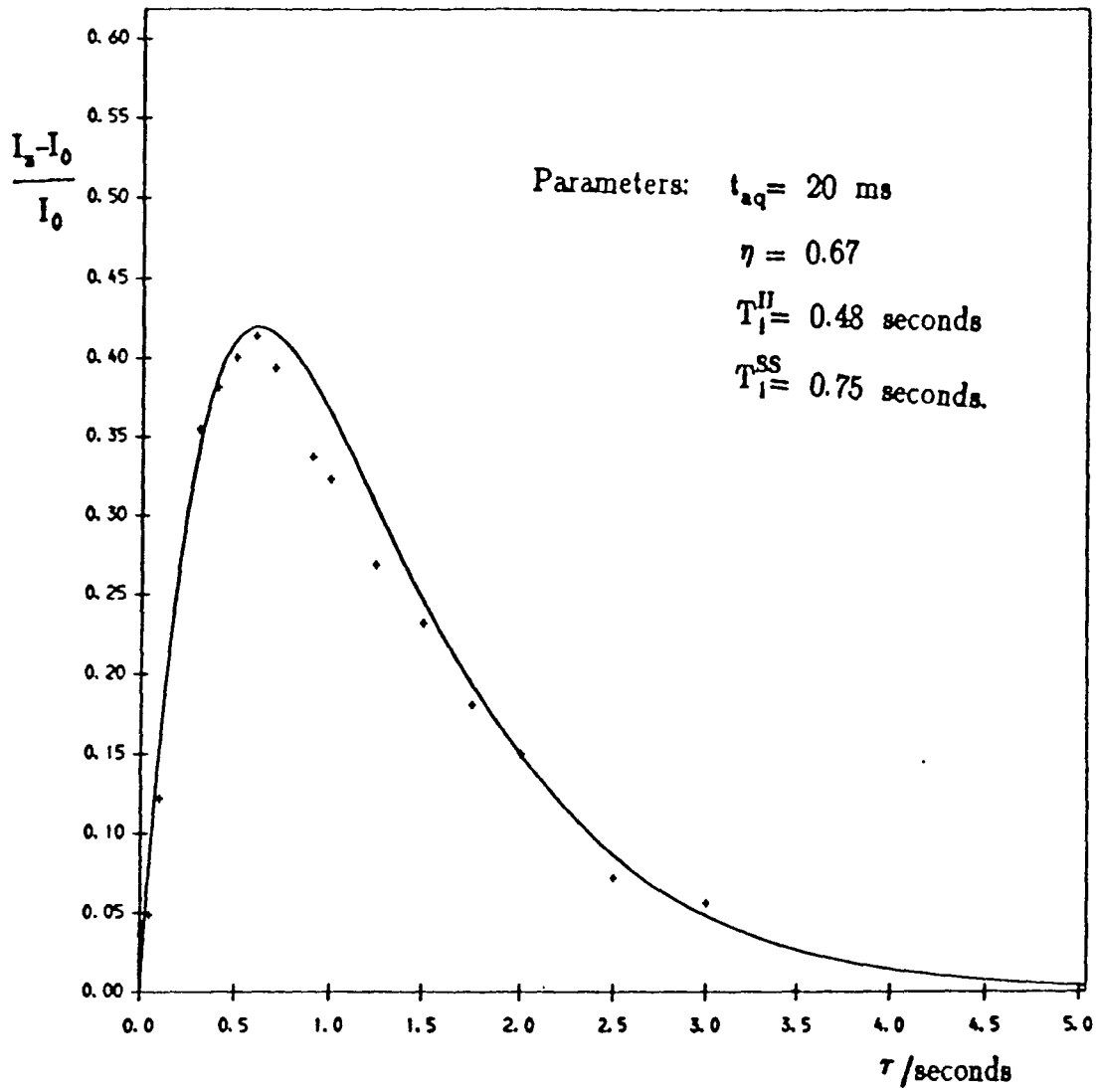

Figure 7.29

A comparison between the theoretical INV1H simulation and the experimental intensities for the peak at 64 ppm in the itaconic anhydride film.

Figure 7.30

The INV1H spectra obtained for the maleic anhydride film. The delay τ ranged between 0.02 and 8 seconds. The acquisition time was 20 ms, and 1000 transients were acquired for each spectrum.

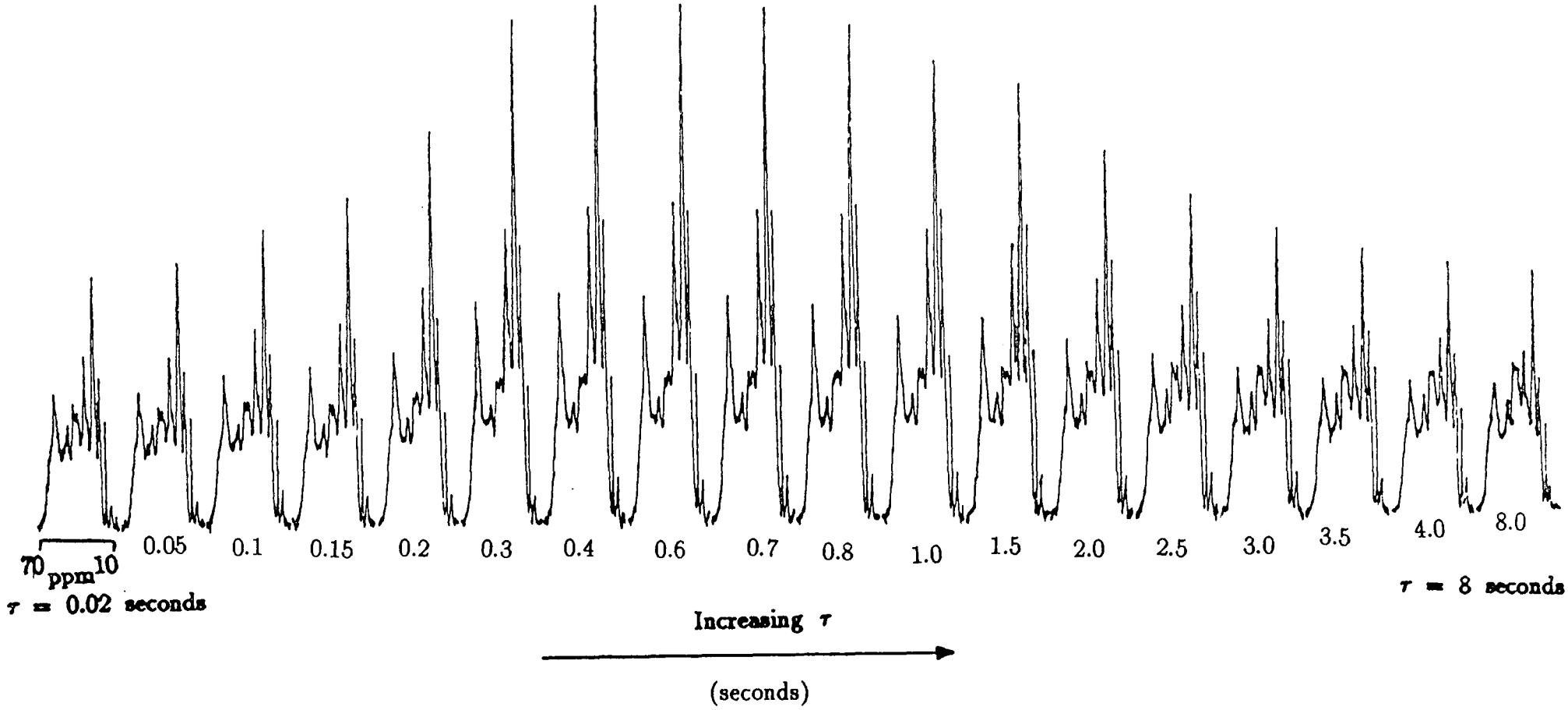

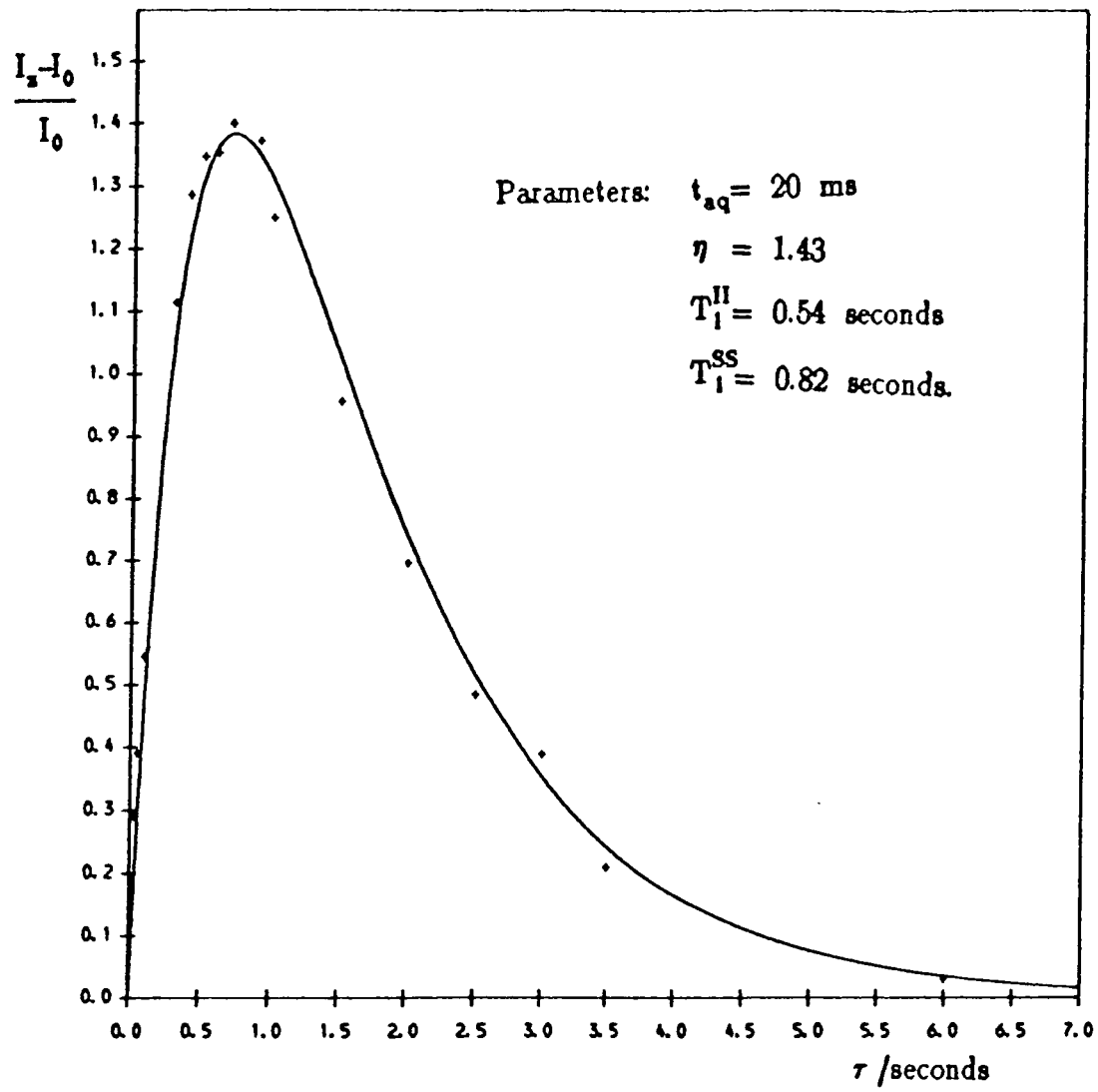

Figure 7.31

A comparison between the theoretical INV1H simulation and the experimental intensities for the peak at 19 ppm in the maleic anhydride film.

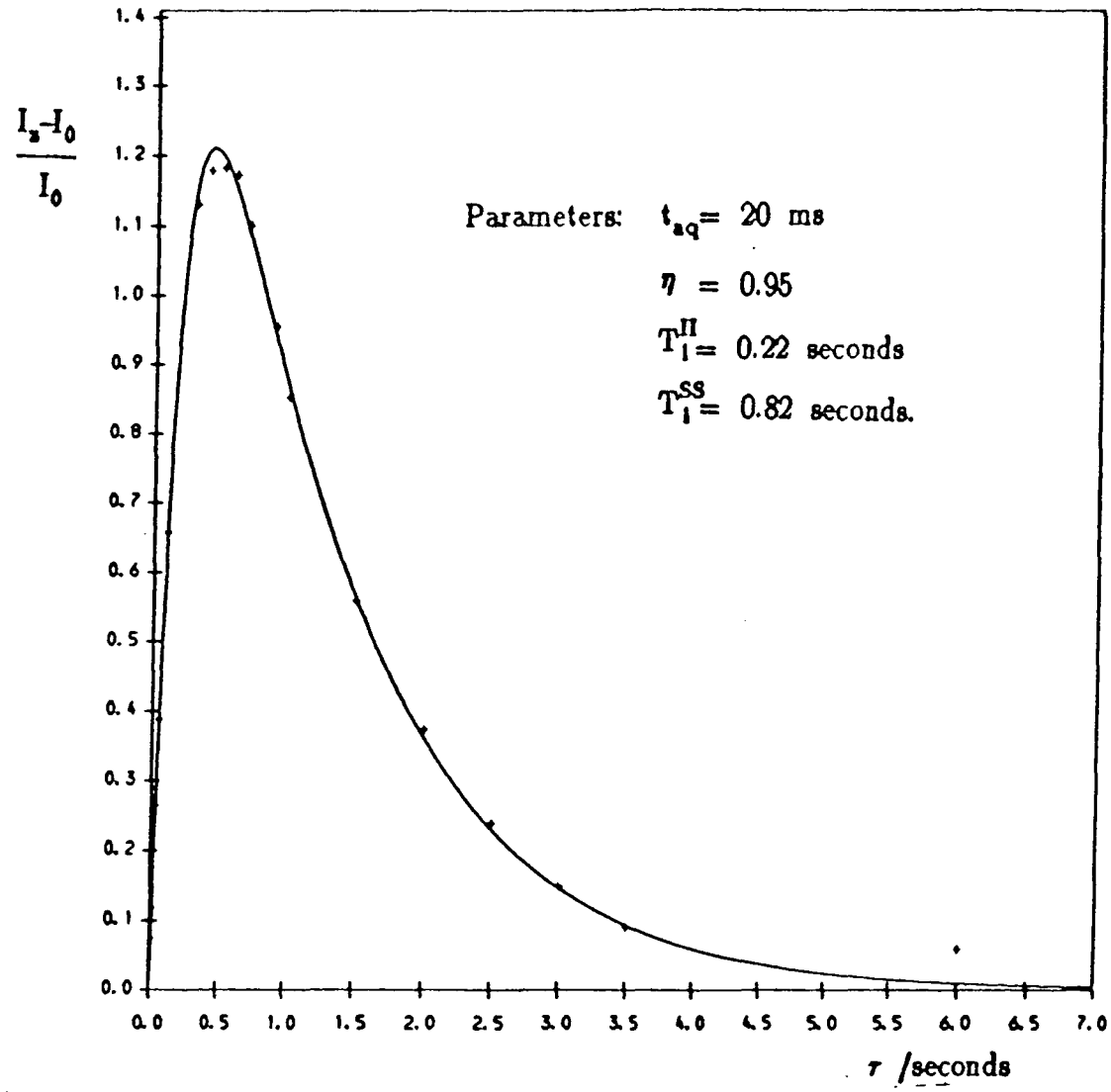

Figure 7.32

A comparison between the theoretical INV1H simulation and the experimental intensities for the peak at 25 ppm in the maleic anhydride film.

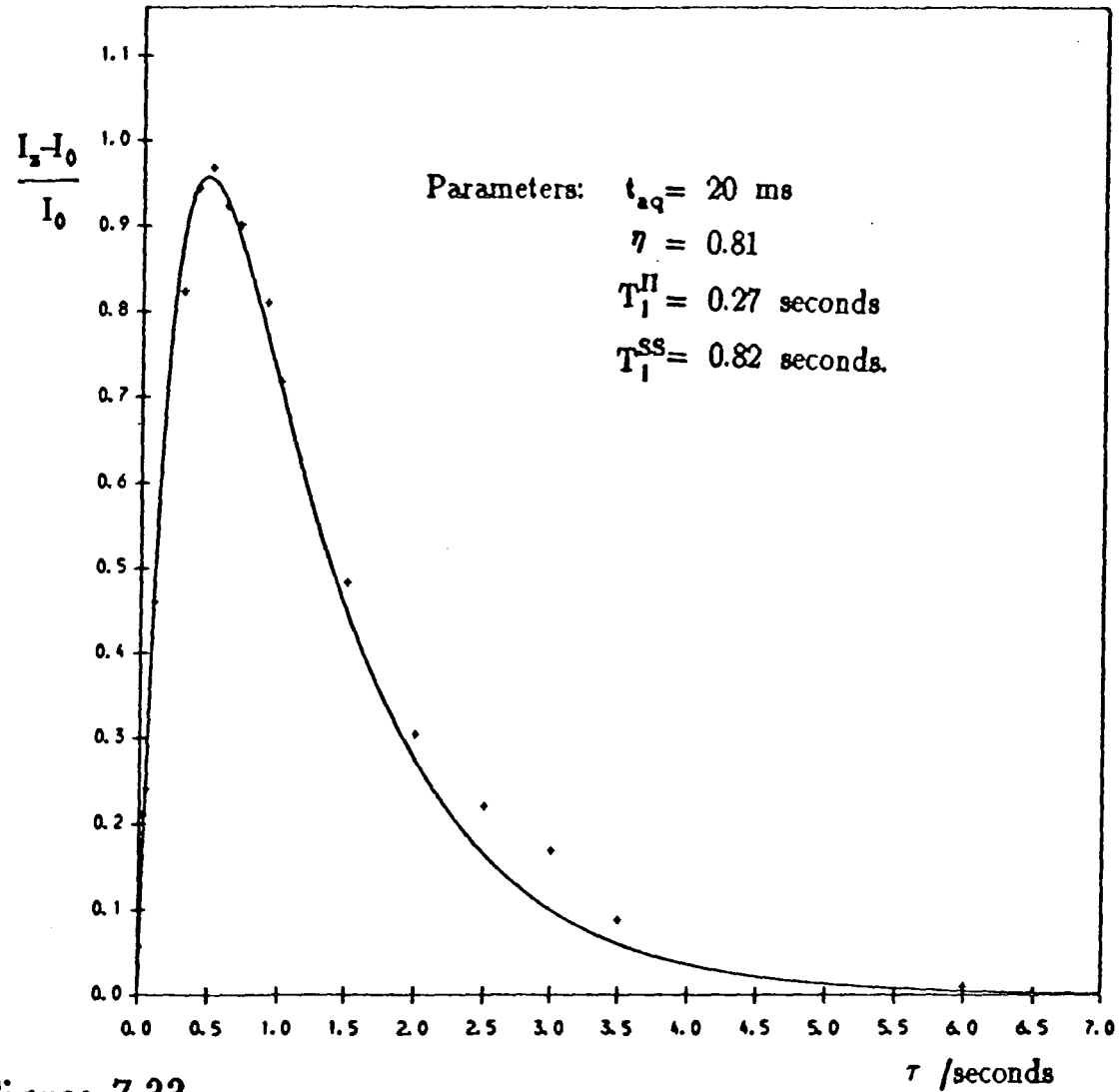

Figure 7.33

A comparison between the theoretical INV1H simulation and the experimental intensities for the peak at 34 ppm in the maleic anhydride film.

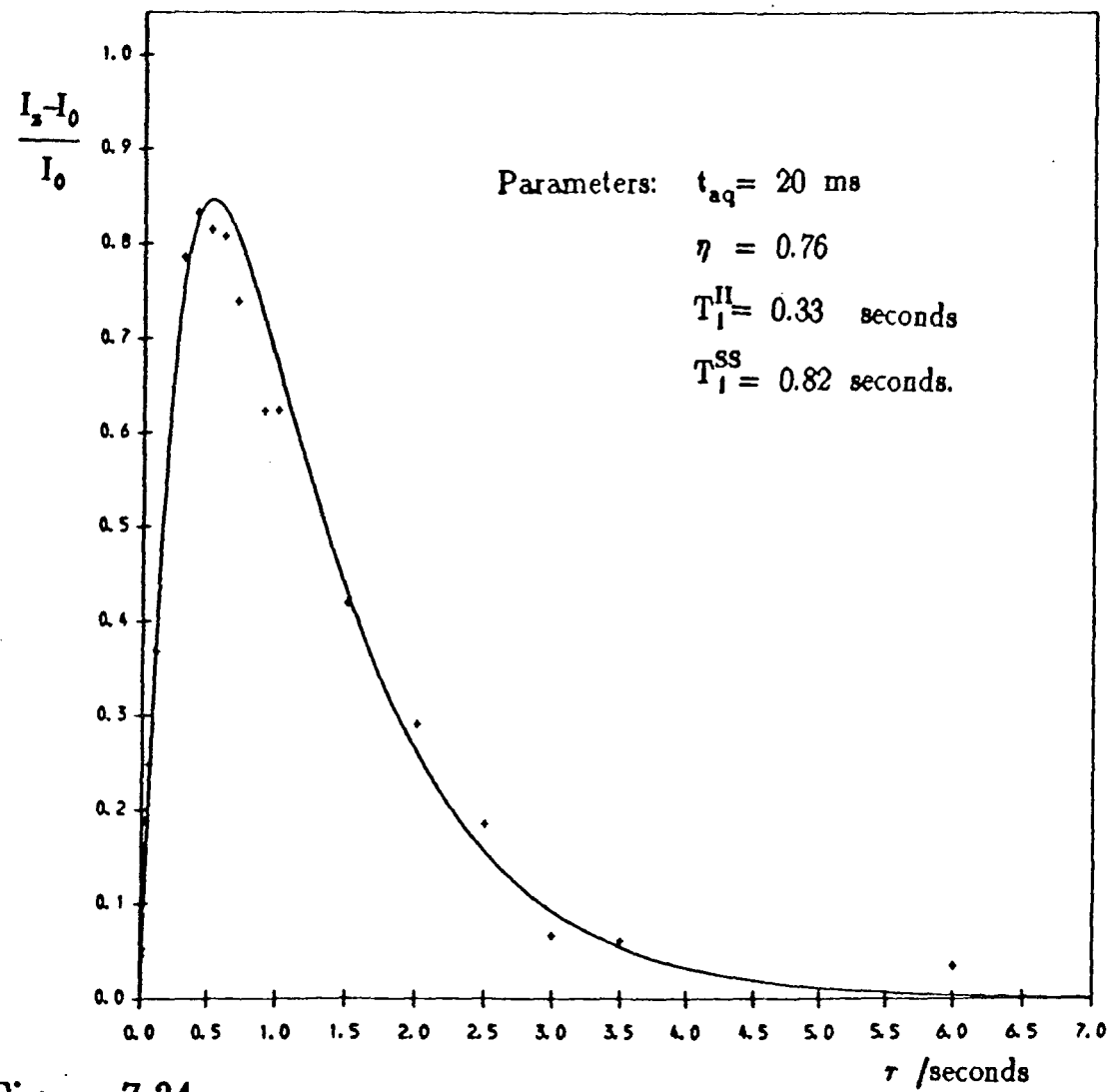

Figure 7.34

A comparison between the theoretical INV1H simulation and the experimental intensities for the peak at 64 ppm in the maleic anhydride film.

before, plots of the theoretical simulation compared to the experimental data are shown in figures 7.26–29. Similar spectra and plots are shown for the maleic anhydride film in figure 7.30 and figures 7.31–34 respectively. The values of η, T_1^{II} and T_1^{SS} were measured in the same way as for the SPE experiment. Again T_1^{II}, the carbon T_1, is two–component. However in this experiment the longer ^{13}C T_1 component does not have such a noticeable effect on the measured ^{13}C intensities at longer τ delays. This is because the carbon signal does not start from the saturation situation but from equilibrium. Thus any effect on the carbon magnetisation due to the long ^{13}C component is negligible.

The systems studied are unusual in that some of the carbon T_1 values in question are smaller than the proton T_1 value, T_1^{SS}. The proton T_1 value is increased by the averaging effect of spin diffusion, while the carbon T_1 values are small due to the mobility of the polyester chains and the lack of spin diffusion because of the low natural abundance of ^{13}C. In order to observe transient nuclear Overhauser effects in the solid state it is necessary that there are carbons in mobile positions. In general, the more mobile a carbon, the shorter is its T_1 value. The NOE decay occurs as soon as the dipolar decoupling is removed. The strength of the transient Overhauser effect is dependent upon competition between the decay of the NOE and the growth of signal due to the carbon T_1. If T_1^{II} is long, then the NOE will decay before enough signal is present, and no transient NOE effects will be observed. (Figure 7.35a). However if T_1 is short, then the carbon signal due to the T_1 will have grown significantly before the NOE starts to decay, and transient NOE effects

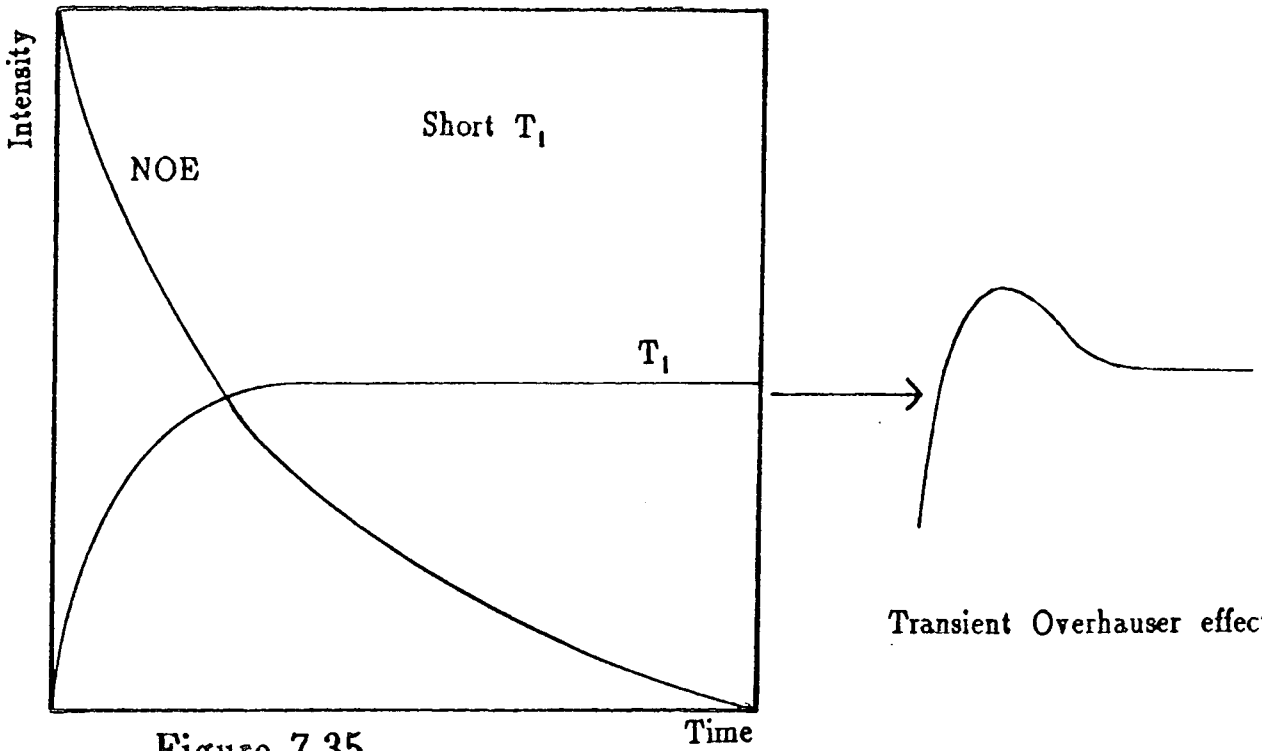

Figure 7.35

The strength of the transient Overhauser effect is dependent upon competition between the decay of the NOE and the growth of signal due to the carbon T_1.

a). If T_1 is short, then signal is present before the NOE fully decays. Hence transient nuclear Overhauser effects will be observed.

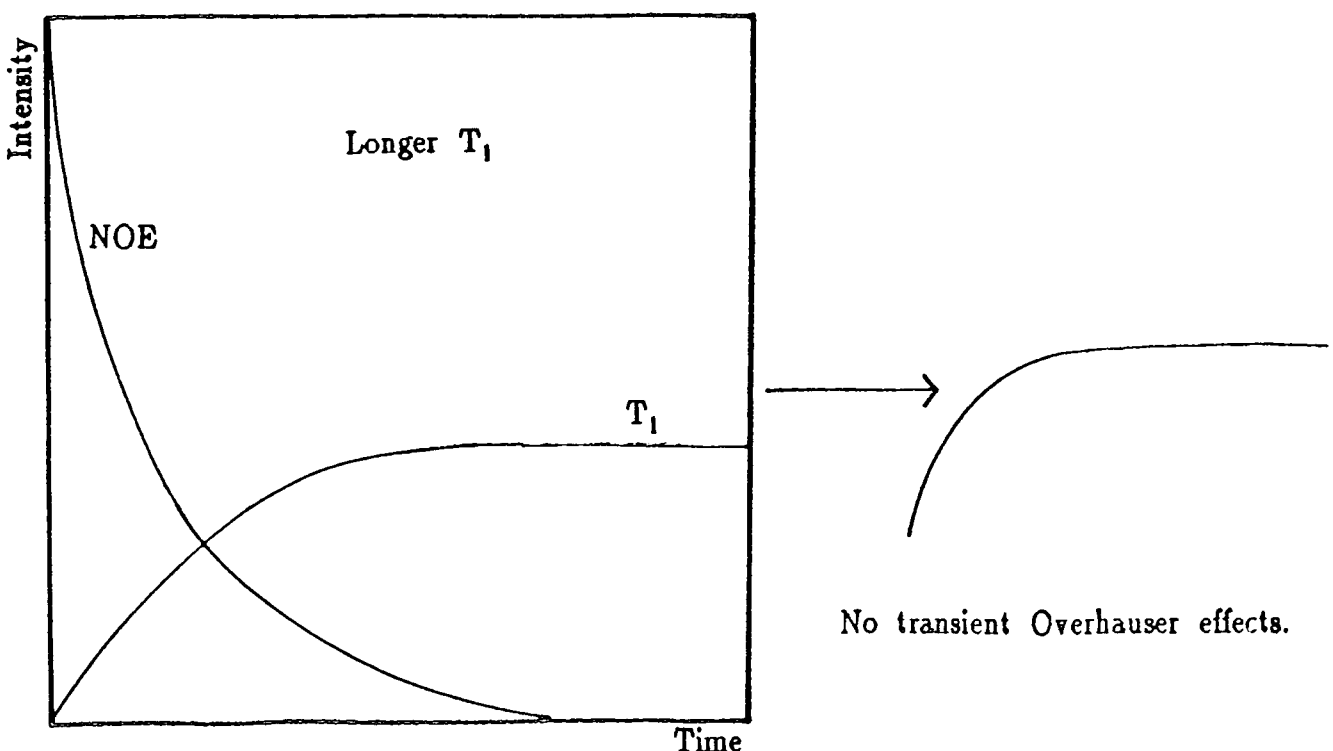

b). If T_1 is longer, then the NOE will decay before enough signal is present. Thus no transient Overhauser effects will be observed.

will be observed (figure 7.35b).

The treatment of carbon spins in this chapter is also applicable to other nuclei, independent of the sign of the Overhauser enhancement. In principle, nuclei such as ^{29}Si should show negative transient Overhauser effects. However no suitable sample which contains silicon has been found as yet. The ^{29}Si T_1 values of the silicon compounds tested to date have been too long for transient NOE effects to be present.

CHAPTER 8

Solid–state heteronuclear NOESY

8.1 Molecular motion

One of the most important properties of the NMR method is its sensitivity to the various types of molecular motions. Both the relaxation processes T_1 and T_2 occur by the interaction of the nuclear spin system with fluctuating local magnetic fields. These fields are generated, for example, by other spins in the system, and their fluctuations are governed by the motion of the molecules or molecular fragments. If the locally induced magnetic fields have components at the appropriate Larmor frequency, they can interact and cause spin relaxation. The larger such a component, the quicker relaxation can occur. The power available from the fluctuations in the local fields at a particular frequency (ω) can be expressed in terms of the spectral density $J(\omega)$.

$$J(\omega) = \int_{-\infty}^{+\infty} G(\tau)\exp(-i\omega\tau)d\tau \qquad (8.1)$$

where $G(\tau)$ is the autocorrelation function.

Molecular motion may be divided into two types: isotropic and anisotropic. Isotropic motions are described by a one–parameter correlation function which averages the interactions to zero. The motion is considered anisotropic when its correlation function splits into at least two different time scales and can be described by at least two characteristic times.

Various models such as the Hall–Helfand,[1] Viovy–Monnerie[2] and

Figure 8.1

The ^{13}C solution–state spectrum of $^{13}C_2$–enriched polyester. The recycle delay was 3 seconds, the acquisition time 1.2 seconds and 256 transients were acquired.

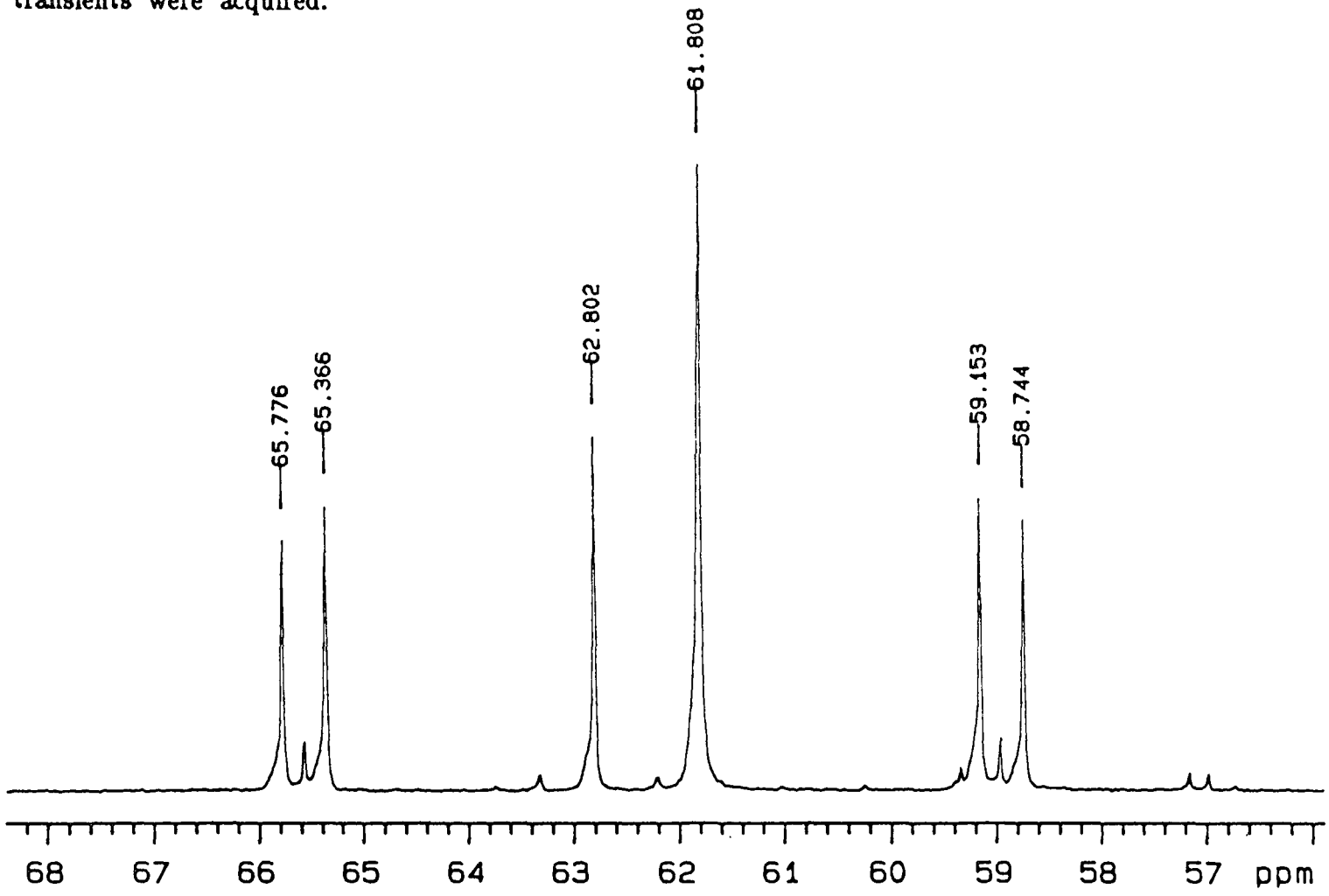

Figure 8.2

The assignments of the peaks in the spectrum shown in figure 8.1

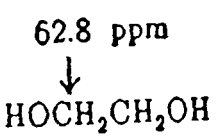

Free ethylene glycol

Jones–Stockmayer[3] models have been proposed to describe the motion observed in bulk polymers. Originally the intention in the present work was to measure ^{13}C T_1 values and NOE enhancement factors for the itaconic anhydride film, which was ^{13}C–enriched at the ethylene glycol position, at different temperatures, and then to compare these data to those obtained using the models in an attempt to describe the motion undergone by the polyester chain in the itaconic anhydride film.

8.2 Assignment of ^{13}C–enriched polyester

The synthesis of the itaconic anhydride film enriched with $^{13}C_2$ at the ethylene glycol positions in the polyester chain is described in detail in Chapter Four. The solution–state spectrum of the ^{13}C–enriched polyester after tipping with triethanolamine, but before the cross–linking with a copolymer is shown in figure 8.1. There appear to be two approximately equivalent ^{13}C carbons and two coupled ^{13}C carbons with different environments. The peak at 61.8 ppm is due to the enriched ethylene glycol incorporated in an approximately symmetrical position in the polyester chain. The pair of doublets originate from polyester chains with ethylene glycol tips. The assignments of the peaks are shown in figure 8.2. It is believed that the peak at 62.8 ppm arises from unreacted free ethylene glycol.[4] The assignments were made by comparing the carbon shifts observed with the shifts predicted from the ^{13}C NMR Chemical Shift Handbook.[5]

Figure 8.3

Single–pulse–excitation spectra of the $^{13}C_2$–enriched itaconic anhydride film between 300 K and 355 K without nuclear Overhauser effects.

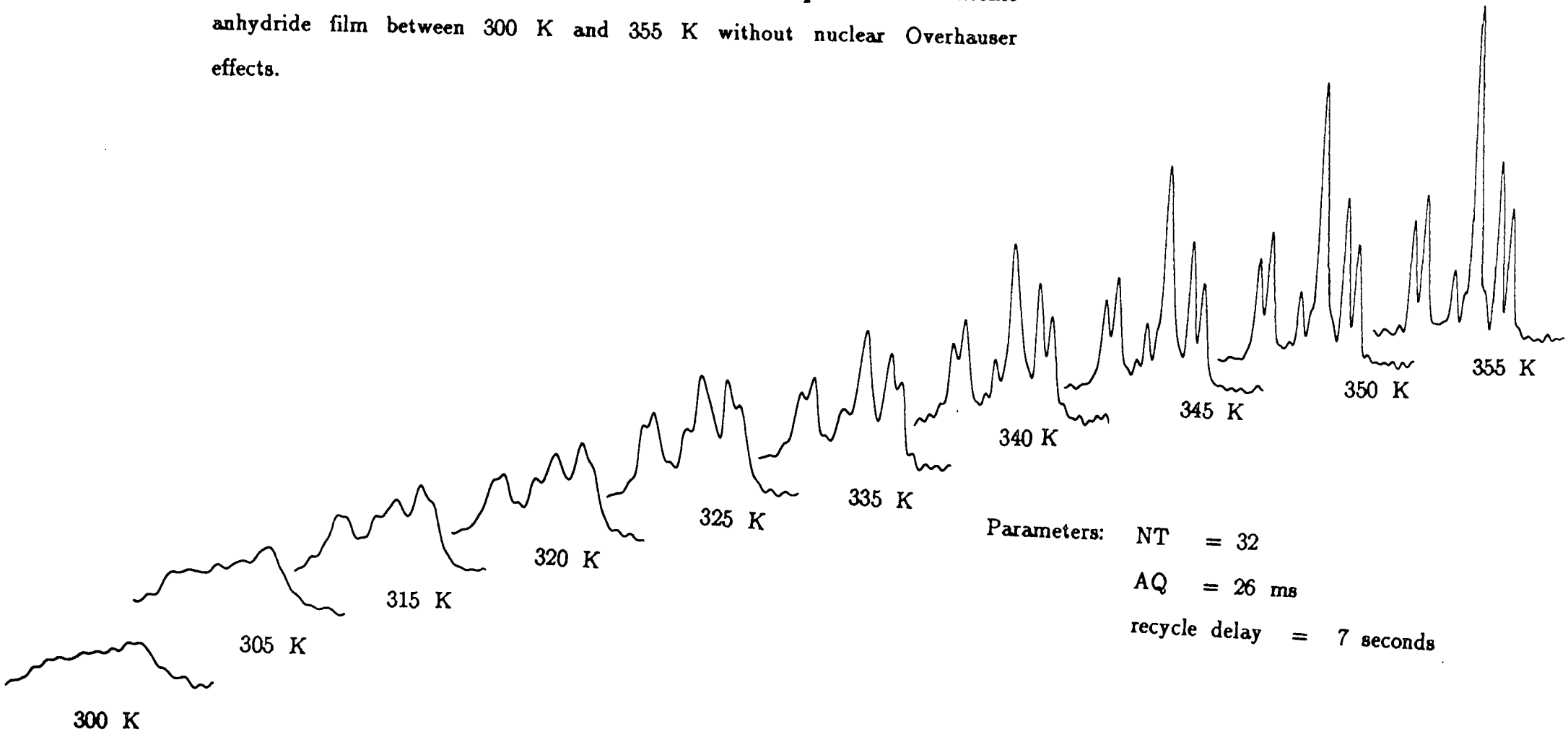

Figure 8.4

Spectra of the $^{13}C_2$–enriched itaconic anhydride film between 300 K and 355 K with nuclear Overhauser enhancements.

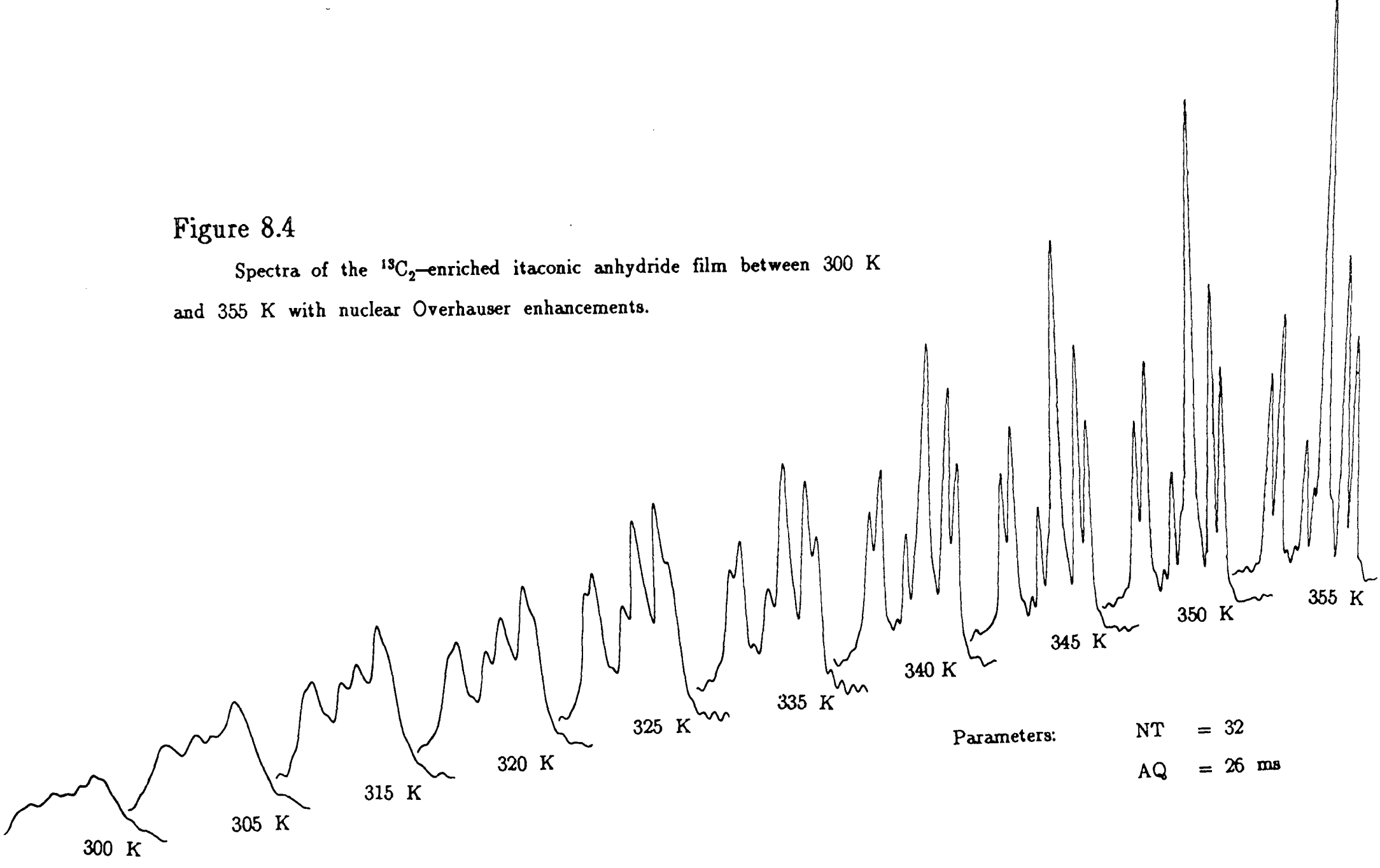

8.3 Measurements of solid–state NOEF

Solid–state spectra were obtained for the ^{13}C–enriched itaconic anhydride film both without and with the nuclear Overhauser enhancement for temperatures between 300 K and 355 K. These spectra are shown in figures 8.3 and 8.4 respectively. Unfortunately, at temperatures between 300 and 345K the carbon peaks were not sufficiently resolved to allow measurement of the NOEF for the peaks. The temperature range over which the NOEF measurements could be obtained was too narrow to attempt to use any of the models to describe the motion of the ethylene glycol units in the polyester chain. For similar reasons it was also not possible to obtain ^{13}C T_1 measurements over a wide–enough range to describe the motion of the polyester chains in the itaconic anhydride film.

8.4 Solid–state NOE

Fundamentals of the theory of the nuclear Overhauser effect were established in 1955 by Solomon.[6] Since that time an increasing number of chemical applications have appeared in the literature, and studies of spin–lattice relaxation[7] and NOE[8,9,10] have proved to be direct and powerful methods of structure elucidation in the solution–state. The work presented in this thesis has attempted to take the concept of the nuclear Overhauser effect one stage further into the solid–state.

The one–dimensional NOE experiments described in Chapter Seven suffer from one major drawback. Spin diffusion between the protons in the polymer film is efficient. Therefore, calculations of the C–H bond

Figure 8.5

The two–dimensional NOESY pulse sequence.

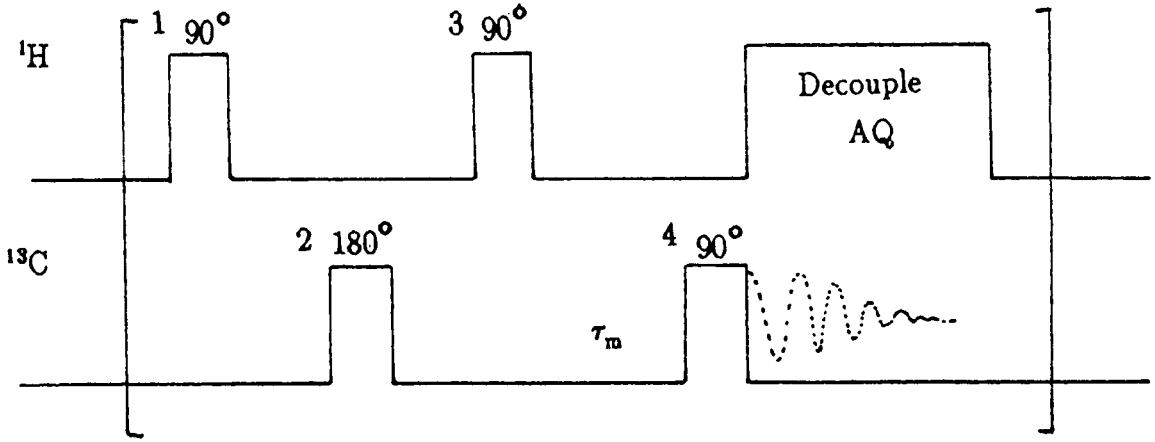

1	X Y –X –Y –X –Y X Y X Y –X –Y –X –Y X Y
2	Y
3	X Y –X –Y X Y –X –Y Y –X –Y X Y –X –Y X
4	X
RLS	X X X X –X –X –X –X Y Y Y Y –Y –Y –Y –Y

length from the one–dimensional NOE experiments would not yield an accurate answer. In order to obtain structural information in the solid–state, the strong ^1H–^1H dipolar interactions must be suppressed. This can be achieved either by the use of multiple pulse sequences or by raising the temperature. The remainder of this chapter is concerned with the study of the heteronuclear NOESY experiment in the solid–state. The advantages of the two–dimensional technique are apparent in the study of macromolecules where spin diffusion is efficient, making the conventional steady–state NOE less specific.[11] The heteronuclear NOESY experiment has been applied extensively in the solution–state. However due to the nature of the experiment, applications of the heteronuclear NOESY experiment are limited in the solid–state.

8.5 The solid–state NOESY experiment

The two–dimensional heteronuclear NOE experiment (NOESY) pulse sequence is shown in figure 8.5.[12,13,14] The sequence involves three successive 90° ^1H pulses. The first 90° ^1H pulse creates transverse magnetisation. During the evolution period, t_1, the various magnetisation components precess with their characteristic precession frequency in the *xy* plane and are frequency–labelled. A 180° carbon pulse is applied in the middle of the evolution period t_1 to remove scalar and dipolar interactions between ^1H and ^{13}C nuclei. Thus, at the end of the t_1 period the ^1H spins are only frequency–labelled. After the second proton 90° pulse, cross–relaxation leads to incoherent magnetisation transfer during the mixing time τ_m. The signal is recorded after the mixing time as a

function of t_2. A recycle time of at least $5\times T_1$ is required to enable the system to reach equilibrium before each sequence. A two–dimensional Fourier transformation of the data matrix $S(t_1,t_2)$ then produces the desired frequency–domain spectrum. The appearance of a cross–peak at frequencies ω_1 and ω_2 in the 2D spectrum indicates that a cross–relaxation process during the mixing period has transferred magnetisation components of frequency ω_1 to a transition of frequency ω_2. The pulse sequence used, together with phases of the pulses and the receiver are shown in Figure 8.5. This phase cycling eliminates artifacts and axial peaks, and it ensures the quadrature detection in the F_1 dimension.

Before applying the NOESY pulse sequence to the itaconic anhydride film with $^{13}C_2$ enrichment at the ethylene glycol position, the proton spectrum of the sample had to be obtained to determine the extent to which the ^1H–^1H dipolar interactions were averaged. As illustrated in section 8.3, the resolution of the single–pulse carbon spectrum is poor below 345K. The chosen temperature for the solid–state NOESY experiment was 363K. Proton single–pulse and CRAMPS spectra were acquired at a temperature of 363K in order to assess the extent of averaging of the ^1H–^1H dipolar interactions. The proton single–pulse spectrum obtained is shown in figure 8.6. It is clear that the ^1H–^1H dipolar interactions are sufficiently averaged by molecular motion that some fine structure is visible. The CRAMPS spectrum obtained did not yield any better resolution. It was therefore deemed unnecessary to apply homonuclear decoupling techniques during the t_1 delay, or to synchronise

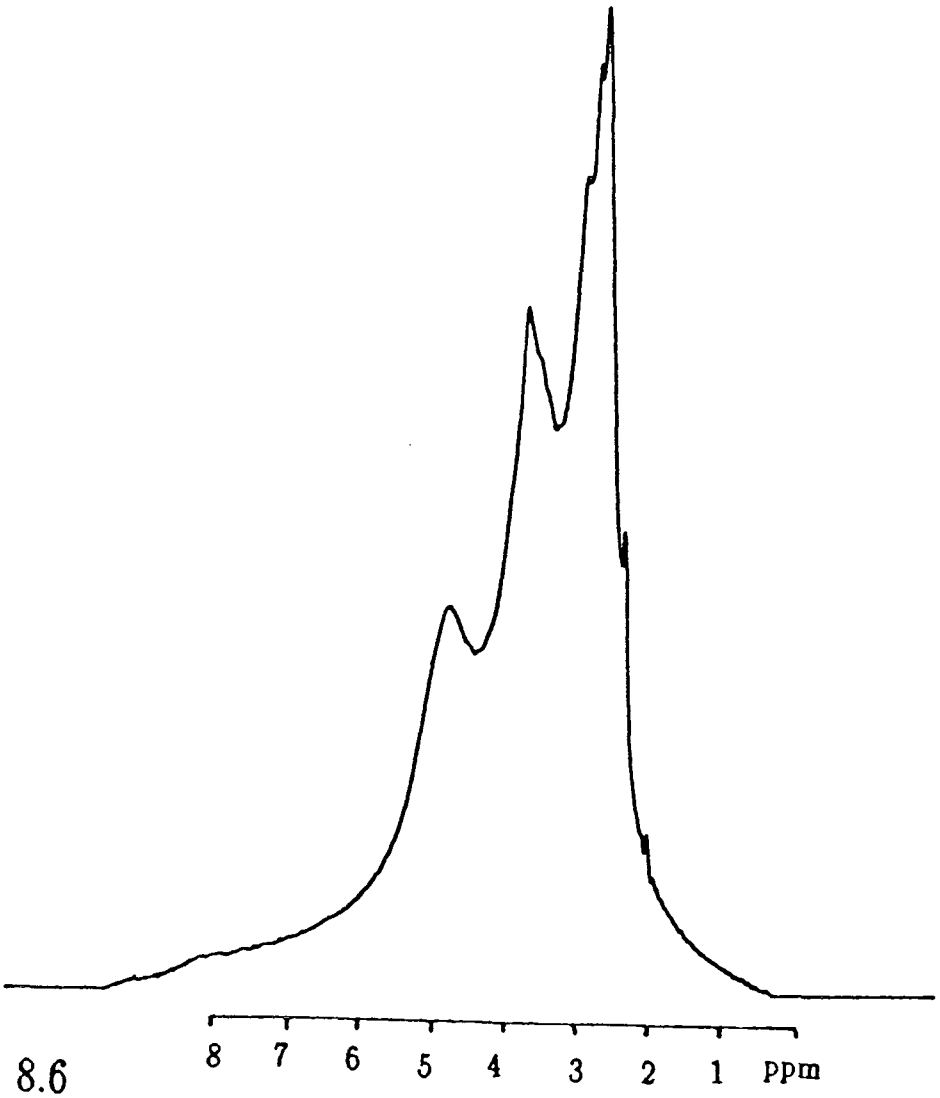

Figure 8.6

The proton single–pulse spectrum of the $^{13}C_2$–enriched itaconic anhydride film obtained at 363 K.

Parameters: NT = 32

AQ = 128 ms

Recycle time = 5 seconds

the rotor rotation during delays t_1 and τ_m.

The solid–state NOESY spectrum obtained is shown in figure 8.7. and the cross–sections of the proton spectra at each of the carbon peaks are shown in figure 8.8. The main advantage of the 2D NOESY experiment over the 1D NOE experiments is that it can clearly be seen between which protons and carbons cross–relaxation takes place. The proton projection shows only protons which undergo cross–relaxation to the ^{13}C–enriched carbons. The doublet at 58.7 and 59.1 ppm arises from the CH_2 next to the OH group in the polyester chains which are tipped with an ethylene glycol unit. The cross–section of the proton spectrum at this ^{13}C doublet shows two main proton peaks at 4.31 and 3.88 ppm as well as other smaller peaks. The peak at 3.88 ppm corresponds to the protons on the CH_2 next to the OH group, and the proton peak at 4.31 ppm corresponds to the protons on the adjacent CH_2 group. The other smaller proton peaks arise from cross–relaxation between the carbon and the other protons in the polyester chain. The doublet at 65.7 and 65.3 ppm corresponds to the CH_2 group positioned β to the OH in the terminal ethylene glycol unit. The cross–sections of the proton spectra again show two main peaks at 4.31 and 3.88 ppm as well as other smaller proton peaks. The assignments of these proton peaks is already given. Therefore, both types of protons in the terminal ethylene glycol unit have cross–relaxation to both carbons, causing nuclear Overhauser enhancement of these carbons. The carbon peak at 61.8 ppm arises from ethylene glycol which has been incorporated in the polyester chain in an approximately symmetrical position between two adipic acid groups. The

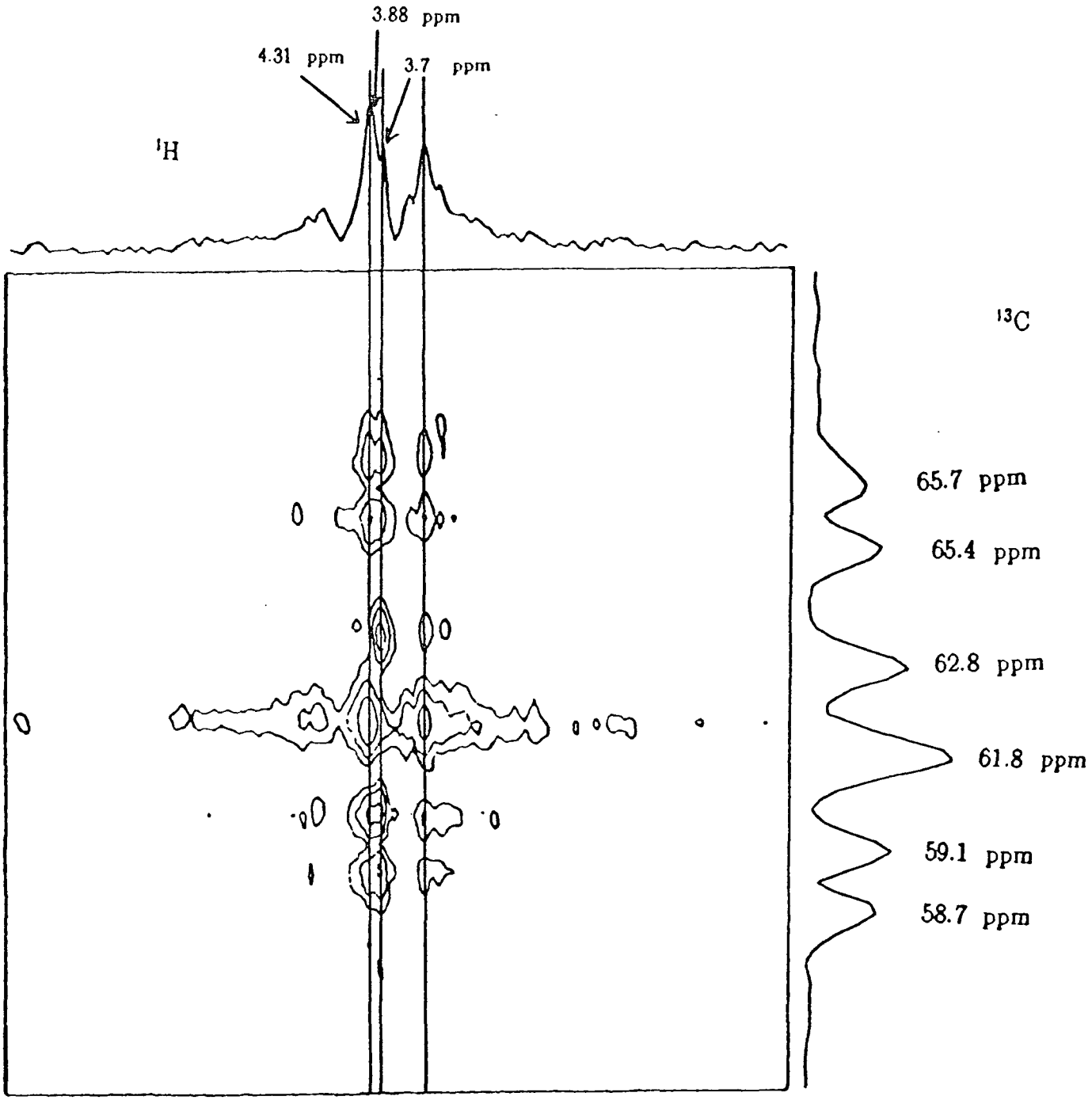

Figure 8.7

The solid–state NOESY spectrum of $^{13}C_2$–enriched itaconic annydride film.

Parameters: AQ = 128 ms
t_1 = 64 μs
Recycle delay = 2 seconds
NT = 500
τ_m = 0.3 seconds

Figure 8.8

Cross–sections of the proton spectra in the NOESY spectrum of $^{13}C_2$–enriched itaconic anhydride film.

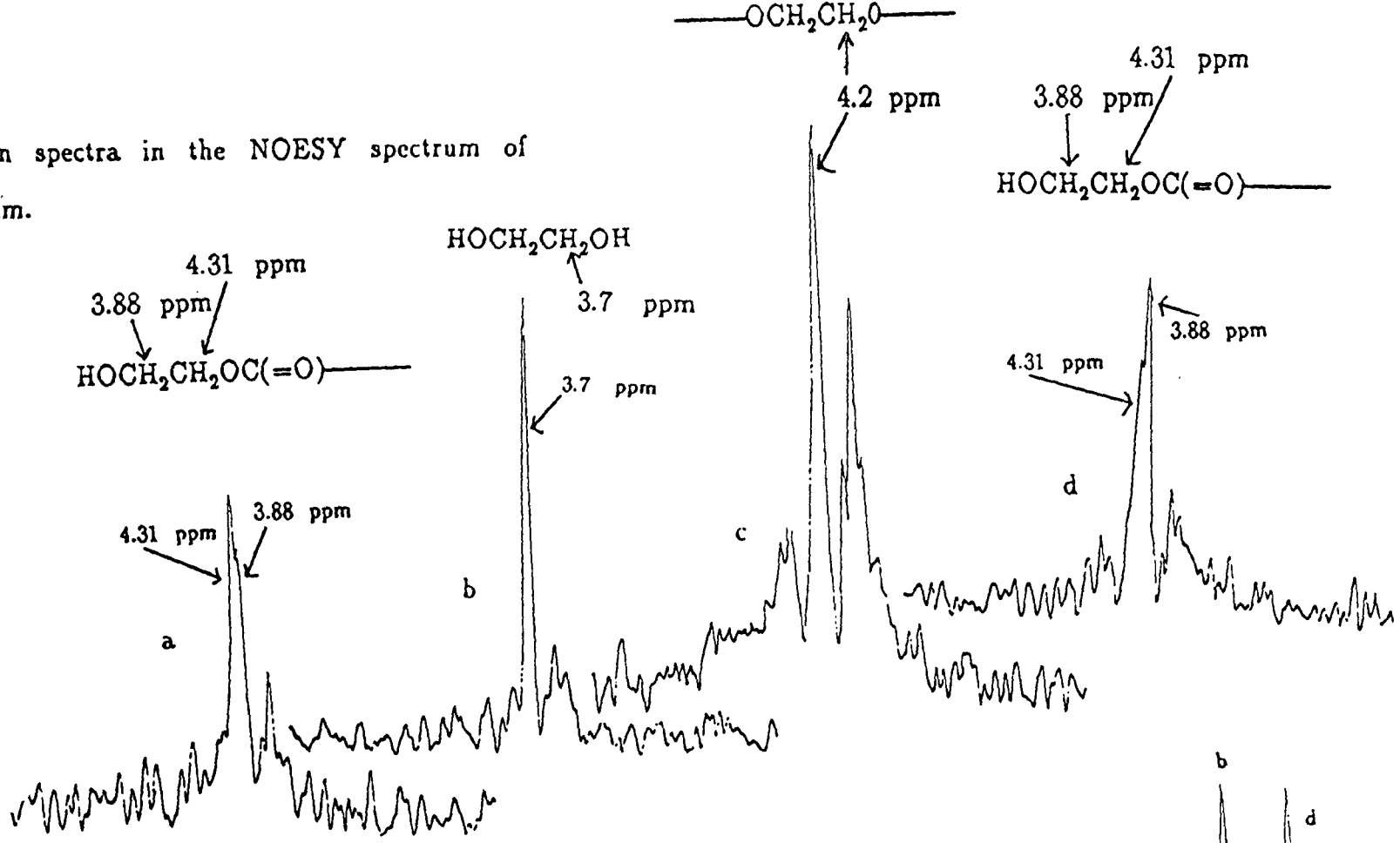

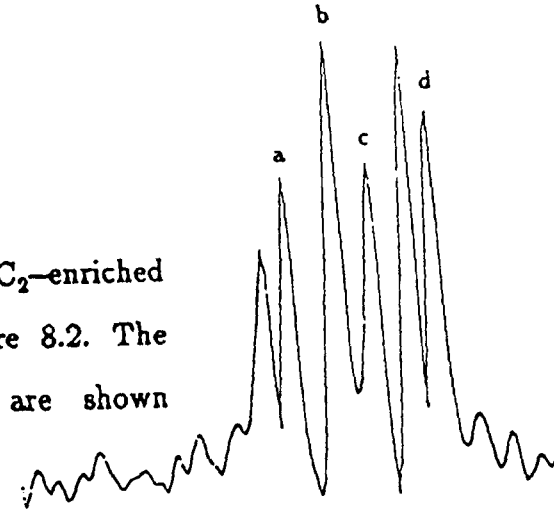

The ^{13}C projection from the solid–state NOESY spectrum of $^{13}C_2$–enriched ethylene glycol. The carbon peaks a to d are assigned in figure 8.2. The proton cross–sections corresponding to these carbon peaks are shown above.

corresponding proton spectrum for this peak shows that all the protons in the polyester chain undergo cross–relaxation to the carbon at 61.8 ppm, with the strongest cross–relaxation arising from the protons which are directly bonded to the carbons. In the solid state, the ^{1}H–^{1}H dipolar interactions are very strong. Each proton spin is strongly coupled to other proton spins nearby. The protons usually have a single T_1 value due to spin diffusion. The result is that a carbon spin in the solid state is strongly coupled to nearby protons, and is coupled to a lesser extent to the more distant protons. It is therefore not a surprising observation that the enriched ethylene glycol carbons, when incorporated in the polyester chain, are coupled by varying extents to all the protons in the polyester chain. The peak at 62.8 ppm is believed to arise from free unreacted ethylene glycol in the system.[4] The corresponding proton spectrum contains a peak at 3.7 ppm which is consistent with the chemical shift of the protons in ethylene glycol.

The heteronuclear NOESY experiment in the solid–state is unlikely to be able to produce the extent of information and applications which arise from the NOESY experiment in the solution–state. This is because of the problem of obtaining good resolution in the proton spectrum. There are several criteria which must be met before a sample is suitable for the solid–state heteronuclear NOESY experiment.

1. The sample must have suitable nuclei which possess a short T_1
2. The proton spectrum must have reasonable resolution either from molecular motion or by the use of CRAMPS
3. The sample must have good signal–to–noise. This often means that enrichment is necessary.

CHAPTER 9

Conclusions

9.1 Conclusions

In this thesis a number of ^{13}C solid–state NMR techniques have been demonstrated which yield information concerning the structure and the variation in the regional mobilities of the cross–linked films. The work in this thesis has relied on two main pulse sequences: the cross–polarisation experiment and the single–pulse–excitation experiment. The theoretical aspects of the cross–polarisation experiment have been discussed in Chapter Three.

In Chapter Five, peaks in the spectra of the copolymers and the cross–linked films used in this thesis are assigned. The films were found to contain polyester chains of two different mobilities. The two mobilities were distinguishable on account of the fact that the polyester carbons had a two–component carbon T_1. A new pulse sequence (MOST) was presented which can be used to measure the carbon T_1's of the mobile polyester chains specifically. It was proposed that the more rigid polyester chains with the longer carbon T_1 were polyester chains which are cross–linked at both ends, thus having a restricted mobility, and that the more mobile polyester chains were polyester chains which were cross–linked at only one end, or totally uncross–linked. The carbon T_1 of the rigid polyester chains could be distinguished from those of the mobile polyester chains by using the T1CP pulse sequence. The cross–polarisation

technique works best for rigid protonated carbons, and therefore the carbon T_1 values of the rigid polyester chains may be specifically measured by the T1CP pulse sequence.

At room temperature the cross–polarisation relaxation characteristics of the copolymer and the polyester peaks are too similar to be distinguished by variable contact time measurements. However, variable temperature studies have shown that at 80°C the cross–polarisation relaxation characteristics of the copolymer and polyester peaks are sufficiently dissimilar from each other to allow CP spectra of the copolymer and the polyester parts of the film to be observed separately.

The kinetics of the cross–linking reaction between the itaconic anhydride copolymer and the triethanolamine tipped polyester was studied by monitoring the proton T_1 as a function of curing time. It was found that the reaction was mainly over by 180 hours into the cure. Spin diffusion was found to have an effect on the populations. To complement this data it would be interesting to make a similar study which monitors the proton $T_{1\rho}$ as a function of curing time.

Chapter Six was concerned with the hydrolytic stability of the films. The final application of the cross–linked films was to be as a paint for yachts. Therefore it is of the utmost importance that the cross–linked films are stable in wet environments. It was shown that the cross–linked films degraded in wet conditions. Failure was pin–pointed at the cross–link sites and at some of the ester cross–links along the polyester chain. Breakdown of ester linkages along the polyester chain was believed to take place via the anchiomeric effect. Further research is

necessary to find a suitable cross–linker which does not have hydrolysable bonds along the backbone chain, and which does not form cross–links which are susceptible to attack by water.

In Chapter Seven the first published work on the transient nuclear Overhauser effect in the solid–state was presented. The theory behind the transient NOE was discussed for both the single pulse experiment and the INV1H pulse sequence. Comparison between the theoretical simulation and the experimental data shows that the theory is a good model for the cross–linked films. It would be of interest to apply this theory to another nucleus which shows a negative Overhauser enhancement, for example ^{29}Si. However it is not easy to find suitable samples for solid–state transient NOE measurements. As yet no suitable ^{29}Si solid–state sample has been found. The ^{29}Si T_1 values have always been too long for transient NOE effects to be present.

Finally, in Chapter Eight the results of the first solid–state heteronuclear NOESY experiment are presented. The 2D experiment was obtained using a sample of itaconic anhydride film which was ^{13}C–enriched at the ethylene glycol position. The experiment showed that individual types of proton could be pin–pointed as providing cross–relaxation to a particular type of carbon. By using such an experiment it should be possible to obtain solid–state structural correlation for carbons and protons between which relaxation occurs.

To summarise, solid–state NMR has proved to be a powerful tool which may be used to gain a new insight into the structure and mobility of cross–linked polymers. Solid–state NMR was able to provide valuable

information on the degradation of the cross–linked films which was not provided by any of the other techniques used in the analysis. Lastly, transient nuclear Overhauser effects in the solid–state have been observed. The theory behind such effects was established, and simulations of the model gave excellent agreement with experiment. A solid–state heteronuclear NOESY experiment has been achieved, thus opening the doors for structural determination in the solid–state via the nuclear Overhauser effect.

REFERENCES

CHAPTER 2

1. Potter W.G., "Epoxide Resins", Butterworth & Co Ltd., London (1970).
2. "Comprehensive polymer science", 6 ch.6 Pergamon Press plc, Oxford (1989).
3. Lenz R.W., "Organic Chemistry of Synthetic High Polymers", Wiley–Interscience (1967).
4. Flory P.J., "Principles of Polymer Chemistry", Cornell University Press (1953).
5. "Introduction to Polymer Science and Technology", Wiley–Interscience (1977).
6. Sakolov L.B., "Synthesis of Polymers by Polycondensation", Israel Program for scientific Translations, Jerusalem ch.1 (1968).
7. Carothers W.H., Chem. Revs., 8 353 (1931).
8. "Comprehensive Polymer Science", 3 ch.8., Pergamon Press plc, Oxford (1989).
9. Carothers W.H., Trans. Farad. Soc., 32 39 (1936).
10. Flory P.J., J. Am. Chem. Soc., 63 3083 (1941).
11. Flory P.J., Chem. Revs., 39 137 (1946).
12. Stockmayer W.H., J. Chem Phys. 11 45 (1943).
13. "Comprehensive Polymer Science", 2 ch.9, Pergamon Press plc, Oxford (1989).

CHAPTER 3

1. Stern O., Gerlach W., Ann. Physik 74 673 (1924).
2. Shaw D., "Fourier Transform NMR Spectroscopy", Elsevier, Amsterdam, (2nd edition) (1984).
3. Gerstein B.C., Dybowski C.R., "Transient Techniques in NMR of Solids", Academic Press Inc., (1985).
4. Abragam A., "The Principles of Nuclear Magnetism", Clarendon, Oxford (1961).
5. Solomon I., Phys. Rev., 99 559 (1955).
6. Harris R.K., "Nuclear Magnetic resonance Spectroscopy", Longman Scientific and Technical, (1986).
7. Haeberlen U., "High Resolution NMR in Solids. Selective Averaging", Academic Press, New York, (1976).
8. Slichter C.P., "Principles of Magnetic Resonance", Springer–Verlag, (1978).
9. Komoroski R.A., "High Resolution NMR Spectroscopy of Synthetic Polymers in Bulk", VCH publishers Inc., Florida, (1986).
10. Fedotov V.D., Schneider H., "Structure and Dynamics of Bulk Polymers by NMR Methods", Springer–Verlag (1989).
11. Andrew E.R., Farnell L.F., Firth M., Gledhill T.D., J. Magn. Reson., 1 27 (1969).
12. Diehl P., Fluck E., Kosfeld R., "High Resolution Spectroscopy in Solids", Springer–Verlag (1976).
13. Stejskal E.O., Schaefer J., J. Magn. Reson., 18 560 (1975).

14. Tangenfeldt J., Haeberlen U., J. Magn. Reson., 36 453 (1979).

CHAPTER 4

1. Bruker Spectrospin Ltd., "Pulse NMR Spectrometer CXP user's manual."
2. Pines A., Gibby M.G., Waugh J.S., J. Chem. Phys 59 569 (1973).
3. Opella S.J., Frey D.M.H., J.A.C.S. 101 5855 (1979).
4. Torchia D.A., J. Magn. Reson. 30 613 (1978).
5. European Patent no. 0048128 (1984).
6. Decroix J.C., Bouvier J.M., Roussel R., Nicco A., Brunceau E.M., J. Polymer Sci. Symposium 52 299 (1975).
7. European Patent no. 0048120 (1984).
8. European Patent no. 0259172 (1987).

CHAPTER 5

1. Opella S.J., Frey D.M.H., J. Am Chem. Soc., 101 5855 (1979).
2. Bremser W., Franke B., Wagner H., "Chemical Shift ranges in Carbon–13 NMR Spectroscopy", Verlag Chemie Weinheim (1982).
3. Noggle J.H., Schirmer R.E., "The Nuclear Overhauser Effect", Academic Press, New York (1971).
4. Torchia D.A., J. Magn. Reson., 30 613 (1978).
5. Solomon I., Phys. Rev., 99 559 (1955).
6. Larsen D.W., Strange J.M., J. Polym. Sci. Phys. Ed., 11 65 (1973).
7. Larsen D.W., Strange J.M., J. Polym. Sci. Phys. Ed., 11 449 (1973).

CHAPTER 6

1. "Polymer Stabilization", Ed. Hawkins W.L., Wiley–Interscience New York (1972).
2. "Polymer Stabilisation and Degradation", Ed. Klemchuk P.P., ACS Symposium Series 280, A.C.S. Publishers, Washington d.c. (1985).
3. Marrion A.R., Port A.B., "New Chemistry and Technology in the Development o Isocyanate–free Paint Systems", RSC Congress Belfast, (April 1990). In Press.
4. Courtaulds Coatings Internal Report.
5. Turpin E.T., J. Paint Technology, 47 40 (1975).

CHAPTER 7

1. Komoroski A., Peat I.R., Levy G.C., "Topics in Carbon–13 NMR Spectroscopy" 2 Ed. G.C. Levy, Wiley, New York (1976).
2. Torchia D.A., Vanderhart D.L., "Topics in Carbon–13 NMR Spectroscopy" 3 Ed. G.C. Levy, Wiley, New York (1979).
3. Solomon I., Phys. Rev. 99 559 (1955).
4. Abragam A., "The Principles of Nuclear Magnetism", O.U.P. London (1961).
5. Kuhlmann K., Grant D.M., Harris R.K., J. Chem. Phys. 52 3439 (1970).
6. Opella S.J., Nelson D.J., Jardotzky O., J. Chem Phys. 64 2533 (1976).
7. Jelinski L.W., Sullivan C.E., Torchia D.A., J. Magn. Reson. 41 133 (1980).
8. Harris R.K., Newman R.H., J. Magn. Reson. 24 449 (1976).
9. Noggle J.H., Schirmer R.E., "The Nuclear Overhauser Effect", Academic Press, New York. (1971).
10. Lyerla J.R., Levy G.C., "Topics in Carbon–13 NMR Spectroscopy" 1 G.C. Levy Ed., Wiley New York (1974).

CHAPTER 8

1. Hall C.K., Helfand E., J. Chem. Phys. 77 3275 (1982).
2. Viovy J.L., Monnerie L., Brochon J.C., Macromolecules 16 1845 (1983).
3. Jones A.A., Stockmayer W.H., J. Polym. Sci. Phys. Ed. 15 847 (1975).
4. Breitmaier E.,Haas G., Voelter W., "Atlas of Carbon–13 NMR Data", Heyden, Rheine (1979).
5. Bremser W., Franke B., Wagner H., "Chemical Shift ranges in Carbon–13 NMR Spectroscopy", Verlag Chemie Weinheim (1982).
6. Solomon I., Phys. Rev. 99 559 (1955).
7. Vold R.L., Waugh J.S., Klein M.P., Phelps D.E., J. Chem. Phys. 48 3831 (1968).
8. Kuhlmann K.F., Grant D.M., J. Am. Chem. Soc. 90 7355 (1968).
9. Kuhlmann K.F., Grant D.M., Harris R.K., J. Chem. Phys. 52 3439 (1970).
10. Noggle J.H., Schirmer R.E., "The Nuclear Overhauser Effect", Academic Press, New York (1971).
11. Kumar A., Wagner G., Ernst R.R., Wüthrich K., J. Am. Chem. Soc. 103 3654 (1981).
12. Rinaldi P.L., J. Am. Chem. Soc. 105 5167 (1983).
13. Yu C., Levy G.C., J. Am. Chem. Soc. 105 6994 (1983).
14. Yu C., Levy G.C., J. Am. Chem. Soc. 106 6533 (1984).

APPENDIX A

COMPUTER PROGRAMS

SPEPLT: A program to simulate the carbon intensity in the single–pulse–excitation experiment.

```
      PROGRAM SPEPLT
      REAL IZ(6000,20), T(6000), IZMIN, IZMAX, LAMBD1, LAMBD2
      REAL TOBS(20), IZOBS(20), IZOMAX
      READ (5,*) TAC0, DTAC, NAC, T1II, T1SS, ETA, GAMMAI, GAMMAS, TD1,
     1     TSTEP
      X = T1II / T1SS
      A = (X - 1) ** 2
      B = ((GAMMAI*ETA)/GAMMAS) ** 2
      C = X + 1 + SQRT(A + 4*B)
      D = X + 1 - SQRT(A + 4*B)
      LAMBD1 = C / (2*T1II)
      LAMBD2 = D / (2*T1II)
      ALPHA = (LAMBD2 - LAMBD1) * T1II
      ALPHA1 = (1 + ETA) / (ALPHA)
      TAC = TAC0
      IZMIN = 1.E6
      IZMAX = -1.E6
      DO 40 KK = 1, NAC
        ALPHA2 = (EXP(-TAC/T1II)*ALPHA1)
        DO 10 I = 1, 6000
          TD = (I - 1) * TSTEP
          T(I) = TD
          POWER1 = EXP(-LAMBD1*TD)
          POWER2 = EXP(-LAMBD2*TD)
          A1 = (LAMBD1*T1II - 1.0) * POWER2
          A2 = (LAMBD2*T1II - 1.0) * POWER1
          B1 = LAMBD2 * POWER1 - LAMBD1 * POWER2
          IZ(I,KK) = (ALPHA2*(A1 - A2)) + ((ETA*B1)/(LAMBD2 - LAMBD1))
          IND = I
          IF (TD .GE. TD1) GO TO 20
   10   CONTINUE
   20   CONTINUE
        DO 30 I = 1, IND
          IF (IZ(I,KK) .LT. IZMIN) IZMIN = IZ(I,KK)
          IF (IZ(I,KK) .GT. IZMAX) IZMAX = IZ(I,KK)
   30   CONTINUE
        TAC = TAC + DTAC
   40 CONTINUE
      READ (7,*) NOBS
      DO 50 I = 1, NOBS
        READ (7,*) TOBS(I), IZOBS(I)
   50 CONTINUE
      DO 60 I = 1, NOBS
        IZOBS(I) = (IZOBS(I) - IZOBS(NOBS)) / IZOBS(NOBS)
        IF (IZOBS(I) .GT. IZMAX) IZMAX = IZOBS(I)
   60 CONTINUE
      IF (IZMAX .NE. 0) IZMIN = -1
      IZMAX = IZMAX+0.1
      CALL PAPER(1)
      CALL PSPACE(0.1, 0.9, 0.1, 0.9)
      CALL MAP(0.0, T(IND), IZMIN, IZMAX)
      CALL BORDER
      CALL AXES
      DO 70 KK = 1, NAC
        CALL PTJOIN(T, IZ(1,KK), 1, IND, 0)
        CALL PTPLOT(TOBS, IZOBS, 1, NOBS, 252)
   70 CONTINUE
      CALL GREND
      END
```

INVER: A program to simulate the proton intensity in the single–pulse–excitation experiment.

```
      PROGRAM INVER
      REAL IZ(5000),T(5000),IZMIN,IZMAX,LAMBD1,LAMBD2 ,INT(18),TIME(18)
      REAL IINF
      READ(5,*) T1II,T1SS,ETA,GAMMAI,GAMMAS,TAU1,TSTEP,IINF
             DO 50 I = 1, 18
                   READ(7,*) INT(I),TIME(I)
50            CONTINUE
              CONTINUE
      WRITE(6,*) TIME(10),INT(10)
             DO 60 I = 1, 18
                   INT(I) = (INT(I) - IINF)/IINF
60           CONTINUE
      X = T1II / T1SS
      A = (X-1)**2
      B = ((ETA * GAMMAI) / GAMMAS)**2
      C = X+1 + SQRT(A + 4*B)
      D = X+1 - SQRT(A + 4*B)
      LAMBD1 = C / (2*T1II)
      LAMBD2 = D / (2*T1II)
      ALPHA = (2 * ETA) / T1II
      ALPHA1 = ALPHA / (LAMBD2-LAMBD1)
      IZMIN = 1.E6
      IZMAX = -1.E6
             DO 100 I = 1, 1000
                   TAU = (I-1) * TSTEP
                   T(I) = TAU
                   POWER1 = EXP(-LAMBD1*TAU)
                   POWER2 = EXP(-LAMBD2*TAU)
                   IZ(I) = ALPHA1 * (POWER1 - POWER2)
                   IND = I
                   IF (TAU .GE. TAU1) GO TO 200
100          CONTINUE
200          CONTINUE
             DO 300 I = 1, IND
                   IF (IZ(I) .LT. IZMIN) IZMIN = IZ(I)
                   IF (IZ(I) .GT. IZMAX) IZMAX = IZ(I)
300          CONTINUE
      IZMAX = IZMAX + 0.2
      CALL PAPER(1)
      CALL PSPACE(0.1,0.9,0.1,0.9)
      CALL MAP(0.0,T(IND),IZMIN,IZMAX)
      CALL BORDER
      CALL AXES
            CALL PTJOIN(T,IZ(1),1,IND,0)
      CALL PTPLOT(TIME,INT,1,18,232)
      CALL GREND
      END
```

INV1H: A program to simulate the carbon intensity in the INV1H experiment.

```
      PROGRAM INV1H
      REAL SZ(5000),T(5000),SZMIN,SZMAX,LAMBD1,LAMBD2
      READ(5,*) T1II,T1SS,ETA,GAMMAI,GAMMAS,TAU1,TSTEP
      X = T1II / T1SS
      A = (X-1)**2
      B = ((ETA * GAMMAI) / GAMMAS)**2
      C = X+1 + SQRT(A + 4*B)
      D = X+1 - SQRT(A + 4*B)
      LAMBD1 = C / (2*T1II)
      LAMBD2 = D / (2*T1II)
      ALPHA = 2 / (LAMBD2-LAMBD1)
      ALPHA1 = (LAMBD1-(1/T1II))
      ALPHA2 = (LAMBD2-(1/T1II))
      SZMIN = 1.E6
      SZMAX = -1.E6
            DO 100 I = 1, 5000
                  TAU = (I-1) * TSTEP
                  T(I) = TAU
                  POWER1 = EXP(-LAMBD1*TAU)
                  POWER2 = EXP(-LAMBD2*TAU)
                  SZ(I) = (ALPHA1 * POWER1) - (ALPHA2 * POWER2)
                  SZ(I) = ALPHA * SZ(I)
                  IND = I
                  IF (TAU .GE. TAU1) GO TO 200
100         CONTINUE
200         CONTINUE
            DO 300 I = 1, IND
                  IF (SZ(I) .LT. SZMIN) SZMIN = SZ(I)
                  IF (SZ(I) .GT. SZMAX) SZMAX = SZ(I)
300         CONTINUE
      SZMAX = 0
      CALL PAPER(1)
      CALL PSPACE(0.1,0.9,0.1,0.9)
      CALL MAP(0.0,T(IND),SZMIN,SZMAX)
      CALL BORDER
      CALL ANNOTP(1,0)
      CALL AXES
            CALL PTJOIN(T,SZ(1),1,IND,0)
      CALL GREND
      END
```

APPENDIX B

LECTURES, COLLOQUIA AND SEMINARS BETWEEN 1/8/87 AND 31/7/90.

UNIVERSITY OF DURHAM

Board of Studies in Chemistry

COLLOQUIA, LECTURES AND SEMINARS GIVEN BY INVITED SPEAKERS 1ST AUGUST 1987 to 31st JULY 1988

BIRCHALL, Prof. D. (I.C.I. Advanced Materials) Environmental Chemistry of Aluminium	25th April 1988
BORER, Dr. K. (University of Durham Industrial Research Labs.) The Brighton Bomb - A Forensic Science View	18th February 1988
BOSSONS, L. (Durham Chemistry Teachers' Centre) GCSE Practical Assessment	16th March 1988
BUTLER, Dr. A.R. (University of St. Andrews) Chinese Alchemy	5th November 1987
CAIRNS-SMITH, Dr. A. (Glasgow University) Clay Minerals and the Origin of Life	28th January 1988
DAVIDSON, Dr. J. (Herriot-Watt University) Metal Promoted Oligomerisation Reactions of Alkynes	November 1987
GRADUATE CHEMISTS (Northeast Polytechnics and Universities) R.S.C. Graduate Symposium	19th April 1988
GRAHAM, Prof. W.A.G. (University of Alberta, Canada) Rhodium and Iridium Complexes in the Activation of Carbon-Hydrogen Bonds	3rd March 1988
GRAY, Prof. G.W. (University of Hull) Liquid Crystals and their Applications	22nd October 1987
HARTSHORN, Prof. M.P. (University of Canterbury, New Zealand) Aspects of Ipso-Nitration	7th April 1988
HOWARD, Dr. J. (I.C.I. Wilton) Chemistry of Non-Equilibrium Processes	3rd December 1987
JONES, Dr. M.E. (Durham Chemistry Teachers' Centre) GCSE Chemistry Post-mortem	29th June 1988
JONES, Dr. M.E. (Durham Chemistry Teachers' Centre) GCE Chemistry A Level Post-mortem	6th July 1988
KOCH, Prof. H.F. (Ithaca College, U.S.A.) Does the E2 Mechanism Occur in Solution?	7th March 1988
LACEY, Mr. (Durham Chemistry Teachers' Centre) Double Award Science	9th February 1988

LUDMAN, Dr. C.J. (Durham University) Explosives	10th December 1987
McDONALD, Dr. W.A. (I.C.I. Wilton) Liquid Crystal Polymers	11th May 1988
MAJORAL, Prof. J.-P. (Université Paul Sabatier) Stabilisation by Complexation of Short-Lived Phosphorus Species	8th June 1988
MAPLETOFT, Mrs. M. (Durham Chemistry Teachers' Centre) Salters' Chemistry	4th November 1987
NIETO DE CASTRO, Prof. C.A. (University of Lisbon and Imperial College) Transport Properties of Non-Polar Fluids	18th April 1988
OLAH, Prof. G.A. (University of Southern California) New Aspects of Hydrocarbon Chemistry)	29th June, 1988
PALMER, Dr. F. (University of Nottingham) Luminescence (Demonstration Lecture)	21st January 1988
PINES, Prof. A. (University of California, Berkeley, U.S.A.) Some Magnetic Moments	28th April 1988
RICHARDSON, Dr. R. (University of Bristol) X-Ray Diffraction from Spread Monolayers	27th April 1988
ROBERTS, Mrs. E. (SATRO Officer for Sunderland) Talk - Durham Chemistry Teachers' Centre - "Links Between Industry and Schools"	13th April 1988
ROBINSON, Dr. J.A. (University of Southampton) Aspects of Antibiotic Biosynthesis	27th April 1988
ROSE van Mrs. S. (Geological Museum) Chemistry of Volcanoes	29th October 1987
SAMMES, Prof. P.G. (Smith, Kline and French) Chemical Aspects of Drug Development	19th December 1987
SEEBACH, Prof. D. (E.T.H. Zurich) From Synthetic Methods to Mechanistic Insight	12th November 1987
SODEAU, Dr. J. (University of East Anglia) Durham Chemistry Teachers' Centre Lecture: "Spray Cans, Smog and Society"	11th May 1988
SWART, Mr. R.M. (I.C.I.) The Interaction of Chemicals with Lipid Bilayers	16th December 1987
TURNER, Prof. J.J. (University of Nottingham) Catching Organometallic Intermediates	11th February 1988
UNDERHILL, Prof. A. (University of Bangor) Molecular Electronics	25th February 1988
WILLIAMS, Dr. D.H. (University of Cambridge) Molecular Recognition	26th November 1987
WINTER, Dr. M.J. (University of Sheffield) Pyrotechnics (Demonstration Lecture)	15th October 1987

UNIVERSITY OF DURHAM

Board of Studies in Chemistry

COLLOQUIA, LECTURES AND SEMINARS GIVEN BY INVITED SPEAKERS
1ST AUGUST 1988 to 31st JULY 1989

ASHMAN, Mr. A. (Durham Chemistry Teachers' Centre) The Chemical Aspects of the National Curriculum	3rd May, 1989
AVEYARD, Dr. R. (University of Hull) Surfactants at your Surface	15th March, 1989
AYLETT, Prof. B.J. (Queen Mary College, London) Silicon-Based Chips:- The Chemist's Contribution	16th February, 1989
BALDWIN, Prof. J.E. (Oxford University) Recent Advances in the Bioorganic Chemistry of Penicillin Biosynthesis	9th February, 1989
BALDWIN & WALKER, Drs. R.R. & R.W. (Hull University) Combustion: Some Burning Problems	24th November, 1988
BOLLEN, Mr. F. (Durham Chemistry Teachers' Centre) Lecture about the use of SATIS in the classroom	18th October, 1988
BUTLER, Dr. A.R. (St. Andrews University) Cancer in Linxiam: The Chemical Dimension	15th February, 1989
CADOGAN, Prof. J.I.G. (British Petroleum) From Pure Science to Profit	10th November, 1988
CASEY, Dr. M. (University of Salford) Sulphoxides in Stereoselective Synthesis	20th April, 1989
CRESSEY & WATERS, Mr. D. & T. (Durham Chemistry Teachers' Centre) GCSE Chemistry 1988: "A Coroner's Report"	1st February, 1989
CRICH, Dr. D. (University College London) Some Novel Uses of Free Radicals in Organic Synthesis	27th April, 1989
DINGWALL, Dr. J. (Ciba Geigy) Phosphorus-containing Amino Acids: Biologically Active Natural and Unnatural Products	18th October, 1988
ERRINGTON, Dr. R.J. (University of Newcastle-upon-Tyne) Polymetalate Assembly in Organic Solvents	1st March, 1989
FREY, Dr. J. (Southampton University) Spectroscopy of the Reaction Path: Photodissociation Raman Spectra of NOCl	11th May, 1989
GRADUATE CHEMISTS, (Polytechs and Universities in North East England) R.S.C. Symposium for presentation of papers by postgraduate students	12th April, 1989

HALL, Prof. L.D. (Addenbrooke's Hospital, Cambridge) — 2nd February, 1989
NMR - A Window to the Human Body

HARDGROVE, Dr. G. (St. Olaf College, U.S.A.) — December, 1988
Polymers in the Physical Chemistry Laboratory

HARWOOD, Dr. L. (Oxford University) — 25th January, 1988
Synthetic Approaches to Phorbols Via Intramolecular Furan Diels-Alder Reactions: Chemistry under Pressure

JÄGER, Dr. C. (Friedrich-Schiller University GDR) — 9th December, 1988
NMR Investigations of Fast Ion Conductors of the NASICON Type

JENNINGS, Prof. R.R. (Warwick University) — 26th January, 1989
Chemistry of the Masses

JOHNSON, Dr. B.F.G. (Cambridge University) — 23rd February, 1989
The Binary Carbonyls

JONES, Dr. M.E. (Durham Chemistry Teachers' Centre) — 14th June, 1989
Discussion Session on the National Curriculum

JONES, Dr. M.E. (Durham Chemistry Teachers' Centre) — 28th June, 1989
GCSE and A Level Chemistry 1989

LUDMAN, Dr. C.J. (Durham University) — 18th October, 1988
The Energetics of Explosives

MACDOUGALL, Dr. G. (Edinburgh University) — 22nd February, 1989
Vibrational Spectroscopy of Model Catalytic Systems

MARKO, Dr. I. (Sheffield University) — 9th March, 1989
Catalytic Asymmetric Osmylation of Olefins

McLAUCHLAN, Dr. K.A. (University of Oxford) — 16th November, 1988
The Effect of Magnetic Fields on Chemical Reactions

MOODY, Dr. C.J. (Imperial College) — 17th May, 1989
Reactive Intermediates in Heterocyclic Synthesis

MORTIMER, Dr. C. (Durham Chemistry Teachers' Centre) — 14th December, 1988
The Hindenberg Disaster - an Excuse for Some Experiments

NICHOLLS, Dr. D. (Durham Chemistry Teachers' Centre) — 11th July, 1989
Demo. "Liquid Air"

PAETZOLD, Prof. P. (Aachen) — 23rd May, 1989
Iminoboranes XB≡NR: Inorganic Acetylenes?

PAGE, Dr. P.C.B. (University of Liverpool) — 3rd May, 1989
Stereocontrol of Organic Reactions Using 1,3-dithiane-1-oxides

POLA, Prof. J. (Czechoslovak Academy of Sciences) — 15th June, 1989
Carbon Dioxide Laser Induced Chemical Reactions - New Pathways in Gas-Phase Chemistry

REES, Prof. C.W. (Imperial College London) — 27th October, 1988
Some Very Heterocyclic Compounds

REVELL, Mr. P. (Durham Chemistry Teachers' Centre) — 14th March, 1989
Implementing Broad and Balanced Science 11-16

SCHMUTZLER, Prof. R. (Technische Universitat Braunschweig) — 6th October, 1988
Fluorophosphines Revisited - New Contributions to an Old Theme

SCHROCK, Prof. R.R. (M.I.T.) — 13th February, 1989
Recent Advances in Living Metathesis

SINGH, Dr. G. (Teesside Polytechnic) — 9th November, 1988
Towards Third Generation Anti-Leukaemics

SNAITH, Dr. R. (Cambridge University) — 1st December, 1988
Egyptian Mummies: What, Where, Why and How?

STIBR, Dr. R. (Czechoslovak Academy of Sciences) — 16th May, 1989
Recent Developments in the Chemistry of Intermediate-Sited Carboranes

VON RAGUE SCHLEYER, Prof. P. (Universitat Erlangen Nurnberg) — 21st October, 1988
The Fruitful Interplay Between Calculational and Experimental Chemistry

WELLS, Prof. P.B. (Hull University) — 10th May, 1989
Catalyst Characterisation and Activity

UNIVERSITY OF DURHAM

Board of Studies in Chemistry

COLLOQUIA, LECTURES AND SEMINARS GIVEN BY INVITED SPEAKERS 1ST AUGUST 1989 TO 31ST JULY 1990

ASHMAN, Mr. A. (Durham Chemistry Teachers' Centre) — 11th October, 1989
The National Curriculum - an update

BADYAL, Dr. J.P.S. (Durham University) — 1st November, 1989
Breakthoughs in Heterogeneous Catalysis

BECHER, Dr. J. (Odense University) — 13th November, 1989
Synthesis of New Macrocylic Systems using Heterocyclic Building Blocks

BERCAW, Prof. J.E. (California Institute of Technology) — 10th November, 1989
Synthetic and Mechanistic Approaches to Ziegler-natta Polymerization of Olefins

BLEASDALE, Dr. C. (Newcastle University) — 21st February, 1990
The Mode of Action of some Anti-tumour Agents

BOLLEN, Mr. F.(Formerly Science Advisor, Newcastle LEA) — 27th March, 1990
Whats's New in Satis, 16-19

BOWMAN, Prof. J.M. (Emory University) — 23rd March, 1990
Fitting Experiment with Theory in Ar-OH

BUTLER, Dr. A. (St. Andrews University) — 7th December, 1989
The Discovery of Penicillin: Facts and Fancies

CAMPBELL, Mr. W.A. (Durham Chemistry Teachers' Centre) — 12th September, 1989
Industrial catalysis - some ideas for the National Curriculum

CHADWICK, Dr. P. (Dept. of Physics, Durham University) — 24th January, 1990
Recent Theories of the Universe (with Reference to National Curriculum Attainment Target 16)

CHEETHAM, Dr. A.K. (Oxford University) — 8th March, 1990
Chemistry of Zeolite Cages

CLARK, Prof. D.T. (ICI Wilton) — 22nd February, 1990
Spatially Resolved Chemistry (using Natures's Paradigm in the Advanced Materials Arena)

COLE-HAMILTON, Prof. D.J. (St. Andrews University) — 29th November, 1989
New Polymers from Homogeneous Catalysis

CROMBIE, Prof. L. (Nottingham University) — 15th February, 1990
The Chemistry of Cannabis and Khat

DYER, Dr. U. (Glaxo) — 31st January, 1990
Synthesis and Conformation of C-Glycosides

FLORIANI, Prof. C. (University of Lausanne, Switzerland) — 25th October, 1989
Molecular Aggregates - A Bridge between homogeneous and Heterogeneous Systems

GERMAN, Prof. L.S. (USSR Academy of Sciences - Moscow) — 9th July, 1990
New Syntheses in Fluoroaliphatic Chemistry: Recent Advances in the Chemistry of Fluorinated Oxiranes

GRAHAM, Dr. D. (B.P. Reserch Centre) — 4th December, 1989
How Proteins Absorb to Interfaces

GREENWOOD, Prof. N.N. (University of Leeds) — 9th November, 1989
Novel Cluster Geometries in Metalloborane Chemistry

HOLLOWAY, Prof. J.H. (University of Leicester) — 1st February, 1990
Noble Gas Chemistry

HUGHES, Dr. M.N. (King's College, London) — 30th November, 1989
A Bug's Eye View of the Periodic Table

HUISGEN, Prof. R. (Universität München) — 15th December, 1989
Recent Mechanistic Studies of [2+2] Additions

IDDON, Dr. B. (Univeristy of Salford) — 15th December, 1989
Schools' Christmas Lecture - The Magic of Chemistry

JONES, Dr. M.E. (Durham Chemistry Teachers' Centre) — 3rd July, 1990
The Chemistry A Level 1990

JONES, Dr. M.E. (Durham Chemistry Teachers' Centre) — 21st November 1989
GCSE and Dual Award Science as a starting point for A level Chemistry - how suitable are they?

JOHNSON, Dr. G.A.L. (Durham Chemistry Teachers' Centre) — 8th February, 1990
Some aspects of local Geology in the National Science Curriculum (attainment target 9)

KLINOWSKI, Dr. J. (Cambridge University) — 13th December 1989
Solid State NMR Studies of Zeolite Catalysts

LANCASTER, Rev. R. (Kimbolton Fireworks) — 8th February, 1990
Fireworks - Principles and Practice

LUNAZZI, Prof. L. (University of Bologna) — 12th February, 1990
Application of Dynamic NMR to the Study of Conformational Enantiomerism

PALMER, Dr. F. (Nottingham University) — 17th October, 1989
Thunder and Lightning

PARKER, Dr. D. (Durham University) — 16th November, 1989
Macrocycles, Drugs and Rock 'n' roll

PERUTZ, Dr. R.N. (York University) — 24th January, 1990
Plotting the Course of C-H Activations with Organometallics

PLATONOV, Prof. V.E. (USSR Academy of Sciences - Novosibirsk) — 9th July, 1990
Polyfluoroindanes: Synthesis and Transformation

POWELL, Dr. R.L. (ICI) — 6th December, 1989
The Development of CFC Replacements

POWIS, Dr. I. (Nottingham University) — 21st March, 1990
Spinning off in a huff: Photodissociation of Methyl Iodide

RICHARDS, Mr. C. (Health and Safety Executive, Newcastle) — 28th February, 1990
Safety in School Science Laboratories and COSHH

ROZHKOV, Prof. I.N. (USSR Academy of Sciences - Moscow) — 9th July, 1990
Reactivity of Perfluoroalkyl Bromides

STODDART, Dr. J.F. (Sheffield University) — 1st March, 1990
Molecular Lego

SUTTON, Prof. D. (Simon Fraser University, Vancouver B.C.) — 14th February, 1990
Synthesis and Applications of Dinitrogen and Diazo Compounds of Rhenium and Iridium

THOMAS, Dr. R.K. (Oxford University) — 28th February, 1990
Neutron Reflectometry from Surfaces

THOMPSON, Dr. D.P. (Newcastle University) — 7th February, 1990
The role of Nitrogen in Extending Silicate Crystal Chemistry